University of Southern Queensland

NUMERICAL ANALYSIS OF LIGHT TRANSMISSION IN DUAL-CORE WAVEGUIDES

A Thesis submitted by

Joshua McKeiver, BSc

For the award of

Master of Science (Research)

2023

ABSTRACT

We use a pseudo-spectral Fast Fourier Transform method on MATLAB to study solitary wave solutions for fractional, coupled non-linear Schrödinger equations and find novel stability boundaries associated with solution symmetry within the fractional derivative order. From the bifurcation diagram we find soliton stability corresponding to symmetry, and other curious dynamics such as, symmetry breaking, non-stationary, and bright / dark pulses, and potentially new conditions to support symmetry making dynamics. We explore fractional derivatives of order $\alpha \in (1, 2]$, and display the results for consideration.

CERTIFICATION OF THESIS

I Joshua McKeiver declare that the MSCR Thesis entitled Numerical analysis of light transmission in dual-core waveguides is not more than 40,000 words in length including quotes and exclusive of tables, figures, appendices, bibliography, references, and footnotes. The thesis contains no material that has been submitted previously, in whole or in part, for the award of any other academic degree or diploma. Except where otherwise indicated, this thesis is my own work.

Date: 12th January 2023

Endorsed by:

Associate Professor Dmitry Strunin

Principal Supervisor

Professor Yury Stepanyants

Associate Supervisor

Student and supervisors' signatures of endorsement are held at the University.

ACKNOWLEDGEMENTS

This thesis would have been impossible without the support, guidance, patience, understanding, encouragement, and still more patience of Associate Professor Dmitry Strunin. Thank you, Dmitry: I will always be grateful for your willingness to take me on as a student and thereby introducing me to the amazing world of mathematical physics. I would also like to thank Professor Yuri Stepanyants for guidance and assistance when required. Thank you, Yury, for your encouragement.

I want to thank the University of Southern Queensland Destination Australia, and QTAC Rural and Regional Enterprise scholarships for financial assistance. This research has been supported by the Australian Government Research Training Program Scholarship.

I want to thank my beautiful wife, Jessie. I would not be here without your support and encouragement by putting up with me all these years. I will always be grateful for you. I would also like to thank my children, Charlie, and Marieke, who supported me by understanding that I needed time to study, for years. Thank you for being so wonderful and patient, I could not have done this without you. Finally, I want to thank my mum: a ne’er do well high school drop-out who pursued a tertiary education as a mature aged student. Demonstrating that higher education is possible no matter where you come from or what people say about your potential. I hope one day I approach the example you set for me as a parent. Thank you for your support, guidance, and encouragement over the past 36 years so far.

Thank you all. I would like to acknowledge this thesis represents the combined effort of everyone listed here. I truly appreciate and am humbled by all your support.

TABLE OF CONTENTS

LIST OF TABLES

LIST OF FIGURES

CHAPTER 1 INTRODUCTION

The study of waves have been of interest to mathematicians and physicists for thousands of years: Pythagoras experimented with vibrating strings in the sixth century BC, while Galileo is said to have initiated the modern study of waves in the sixteenth century AD [1]. Throughout this time, our mathematical sophistication and hence our level of understanding of mechanical and mathematical nuances of waves has developed further, particularly since the application of calculus and study of partial differential equations (PDEs), fractional differential equations (FDEs), and diffusion equations, as part of academic research.

Our understanding of waves has evolved from vibrating strings and the study of acoustics and soundwaves to much more complex phenomena. The family of Schrödinger equations and nonlinear Schrödinger equations (NLSEs) are a set of PDEs which have been employed to model a very wide range of natural behaviours, such as optical (light wave) waveguide research with applications in optical fibre networks supporting the internet [2-8]. Furthermore, NLSEs are used to model phenomena in plasma physics [6, 9-11], condensed matter physics [12-14] and quantum physics [6, 9, 10, 12, 15, 16]. An important area of research with respect to NLSEs is finding conditions that support solitary waves: more specifically, solitary wave stability boundaries within these systems.

Solitons are a type of wave first studied and published in 1845 by John Scott Russell [17]. In his published work, Scott Russell reported observing stable water waves travelling along a canal, which maintained their shape and speed for as long as Scott Russell could follow them (approximately one or two miles) before losing sight of the wave [17]. The creation of highly stable waves resistant to perturbations, and their stability boundaries are of interest due to various optical applications such as improved optical fibre transmission rates, with immediate benefits for communication networks [7, 11].

Commensurate with the progression of wave research, so too did the paradigm of Physics shift from ‘classical’ to ‘modern’ studies with the development of relativity and Quantum Mechanics [18]. Relativity describes the geometry of space and time: for example, using the geometry of a well to describe the effect of gravity [19]. Quantum Mechanics may be succinctly described as the probability of observing a particle in space: for example, the probability of observing an electron in the vicinity of a proton. The probabilistic description of a particle is derived from the wave-particle duality of quantum scale objects [19].

For a more sophisticated understanding of the significance of Schrödinger equations, and by extension fractional NLSEs, it is necessary to first understand how complex analysis and physics coalesce in the study of mathematical physics.

1.1 Quantum mechanical motivation

The unreasonable effectiveness of mathematics has provided a firm foundation which has allowed all sciences to flourish. To this end, and to demonstrate the importance of mathematical research in NLSEs, we will discuss the physical dilemma which led Erwin Schrödinger to develop the wave equations governing the wave-particle duality proposed by de Broglie [19].

Research from de Broglie suggested wave-particle duality applied to electrons as well as photons, thereby equating the energy of a particle to the energy (E) of a wave, proportional to its frequency using the following model:

$$E = hf \tag{1.1}$$

where f is the frequency and h is Planck's constant. We need to understand h = λp, where λ represents wavelength, and p is the momentum of a particle. From classical physics, we know p = mv, where m is the mass of the particle, and v is the velocity of the particle (where $v = \dot{x}$, the first time derivative of the position of the particle). Now we may rewrite (1.1) as follows:

$$E = f\lambda mv. \tag{1.2}$$

Now, we see de Broglie's assertion builds on Einstein's concept of mass energy equivalence. We recall the speed of a wave c = fλ, and if we assume the velocity in (1.2) is the speed of light, c, then v = c. Thus, we arrive at Einstein's famous mass, energy equivalency (without momentum terms):

$$E = mc^2. \tag{1.3}$$

The problem here is that we have a wave (since c = fλ), but at the time, a governing wave equation did not exist to describe how this light wave solution behaved in a medium: physicists had a solution to a wave equation without the wave equation problem.

We may consider a simplified solution to this problem by studying the classical heat equation: an example which serves as a straightforward demonstration of how quantum mechanics and complex analysis complement each other to provide useful results. We see the heat diffusion equation below:

$$u_t = u_{xx} \quad (1.4)$$

where u_t denotes the first partial derivative of the wave solution u with respect to time $u_t = \frac{\partial u}{\partial t}$, and u_{xx} denotes the second partial derivative with respect to space, $u_{xx} = \frac{\partial^2 u}{\partial x^2}$. We must understand the heat equation is not a suitable solution for relativistic particles, as heat travels relatively slowly as compared to light, and the solution is not Lorentz invariant [19]. Equation (1.4) may be generalised to the n^{th} dimension using the Laplacian operator Δ, but in Physics this is restricted to spatial Cartesian coordinates (x, y, z):

$$u_t = \Delta u. \quad (1.5)$$

To solve this problem (1.4), we take a commonly used mathematical method taught in undergraduate studies: simplify the problem. Therefore, we assume a solution of the form of a plane wave in time, choose one space dimension, x, and take an educated guess for the solution. By ansatz (or by understanding the derivative of an exponential function returns the original function itself), we try the plane-wave solution:

$$u(x,t) = Ae^{(kx-\omega t)}. \quad (1.6)$$

Since the argument of the exponent must be non-dimensional, we include the constants k and ω. By dimensional analysis, we take k to be the wavenumber, and ω to be the wave frequency. To ensure compatibility with the potential wave solution (1.1), we will assume $k = \frac{2\pi}{\lambda}$, and omega becomes the angular frequency $\omega = 2\pi f$.

To solve equation (1.5) in one space dimension, we begin taking derivatives of equation (1.6):

$$\begin{aligned} u_t &= -\omega Ae^{(kx-\omega t)} \\ u_{xx} &= k^2 Ae^{(kx-\omega t)} \end{aligned} \quad (1.7)$$

and substituting the derivatives into equation (1.4) yields the following result:

$$-\omega A e^{(kx-\omega t)} = k^2 A e^{(kx-\omega t)}. \tag{1.8}$$

For (1.8) to be true for E, we need to draw once again from Physics to provide guidance to motivate the Schrödinger wave equation. Therefore, we consider equation (1.8) describes the energy of a closed system.

The Hamiltonian (H) is an operator acting on E, which describes the total energy of a system in the following way: H = T + V. Classical Physics dictates T= $\frac{mv^2}{2}$ is the kinetic energy, and V(x,t) is given as the potential energy, which, as its classical counterpart, implies V(x,t) is a forcing term (we may assume V(x,t) = mgh, where 'g' is the force of gravity acting on an object with mass 'm' with some spatial displacement, height 'h', interchangeable with x), which has a firm foundation in classical physics. As H acts as an operator on the energy E (recall we are considering the energy of a wave), H provides a first order, nonlinear, heterogeneous differential equation $E = \frac{m\dot{x}^2}{2} + mgx$.

From our solution u, we may substitute the spatial and angular frequency k and ω by considering the de Broglie wavelength $\lambda = \frac{h}{p}$ and the quantisation of angular momentum $\hbar = \frac{h}{2\pi}$. For compatibility with equation (1.1) we assumed k = $\frac{2\pi}{\lambda} \Rightarrow k = \frac{2\pi p}{h} = \frac{p}{\hbar}$, so momentum p = kħ (momentum depends on the wavenumber), and we assumed ω = 2πf, f = $\frac{\omega}{2\pi}$. This means we can substitute ω and k^2 in (1.7) with the following:

$$\omega = 2\pi f, \qquad k^2 = \frac{p^2}{\hbar^2}.$$

Now we proceed with the Hamiltonian, where we recall previously $T = \frac{mv^2}{2} = \frac{p^2}{2m}$. Since de Broglie proved E = hf, which is the total energy of a particle, and $T = \frac{p^2}{2m}$, then using Hamiltonian operators on our wave solution with E = hf as the total energy of a particle, we find with H = T + V, (1.4) becomes

$$(hf)u(x,t) = \left(\frac{p^2}{2m}\right)u(x,t) + V(x,t) \tag{1.9}$$

If we choose to take the natural response of the system, we set the forcing term V(x,t) = 0, then we reduce (1.9) as follows:

$$\left(\frac{h\omega}{2\pi}\right)u(x,t) = \left(\frac{(k\hbar)^2}{2m}\right)u(x,t)$$

$$\hbar\omega u(x,t) = \left(\frac{k^2\hbar^2}{2m}\right)u(x,t)$$

$$\hbar\omega u(x,t) = k^2\left(\frac{\hbar^2}{2m}\right)u(x,t) \tag{1.10}$$

Now we take (1.4), and our solution (1.6), and substitute:

$$\hbar u_t = \frac{\hbar^2}{2m}u_{xx}. \tag{1.11}$$

Substituting our solutions from (1.7), (1.11) becomes

$$\hbar(-\omega Ae^{(kx-\omega t)}) = \frac{\hbar^2}{2m}(k^2Ae^{(kx-\omega t)}). \tag{1.12}$$

For (1.12) to be true, the left-hand side and right-hand side must share the same sign, therefore, we draw from complex analysis and choose a complex plane solution. That is, we include $i^2 = -1$, an ‘impossible’, imaginary number. Now, our solution in (1.6) becomes

$$u(x,t) = Ae^{i(kx-\omega t)}. \tag{1.13}$$

Then taking derivatives with the new solution:

$$\begin{aligned} u_t &= -i\omega Ae^{i(kx-\omega t)} \\ u_{xx} &= -k^2 Ae^{i(kx-\omega t)} \end{aligned} \tag{1.14}$$

For the wave equation to be true with our new complex valued solution (1.13), we need to make the wave equation complex, so (1.11) takes the form of a Schrödinger equation:

$$i\hbar u_t = -\frac{\hbar^2}{2m} u_{xx}. \tag{1.15}$$

Substituting the complex solution into our linear, time-dependent Schrödinger equation (1.15) and omitting the forcing term $V(x,t)$, we see the natural response of the system:

$$(i\hbar) - i\omega Ae^{i(kx-\omega t)} = \left(-\frac{\hbar^2}{2m}\right) - k^2 Ae^{i(kx-\omega t)}$$

$$\hbar\omega = \left(\frac{\hbar^2}{2m}\right) k^2, \tag{1.16}$$

If we rearrange this equation, we see a harmonic oscillator and we can determine the angular frequency as a function of mass of the particle and the wavenumber of the system:

$$\omega = \left(\frac{\hbar}{2m}\right)k^2,$$

or alternatively, the spatial frequency as a function of angular frequency and mass:

$$k = \sqrt{\frac{2m\omega}{\hbar}}.$$

We see that the plane wave solution we solved, based on the heat equation contains mass. It is this fact, in part, that motivates the study of solitons as an analogue for a wave/particle duality, hence the term ‘soliton’ implies the name of a particle. This example serves to demonstrate the culmination of mathematics and physics in NLSEs, and how such equations may be used to explore physical solutions and applications of real-world problems. This also shows how complex analysis with ‘imaginary’ numbers are used to describe real-world phenomena.

From this example used to guide our motivation for research into NLSEs, we can see how complex analysis, wave mechanics, and classical physics have come together to galvanise the study of modern physics and provide a foundation on which modern science, and specifically mathematical physics has thrived: therein lies the significance of NLSE research.

Development in mathematics has promoted growth in the family of Schrödinger equations, formally known as dispersive equations (if friction and dissipation are zero), to include relativistic particles and coupled systems used to model real phenomena. Such recent developments bring us to the point of this research: to numerically analyse soliton solutions to coupled time-dependent, one dimensional, fractional, cubic NLSEs of the form

$$
\begin{aligned}
&i\mathrm{u}_{1_t} + (1/2)\mathrm{u}_{1_\alpha} + |\mathrm{u}_1|^2\mathrm{u}_1 + \mathrm{u}_2 = 0 \\
&i\mathrm{u}_{2_t} + (1/2)\mathrm{u}_{2_\alpha} + |\mathrm{u}_2|^2\mathrm{u}_2 + \mathrm{u}_1 = 0,
\end{aligned}
\tag{1.17}
$$

where $\alpha \in (1, 2]$ denotes the order of the fractional derivative. Let us consider (1.17) in more detail. For simplicity, we normalise the physical constants used from our simplified Schrödinger equation example (1.15) (effectively setting $\hbar = 1$) and treat this system as a mathematical problem only. If we consider an uncoupled system consisting of one wave, u, where u is the wave solution to this equation (therefore, u_1 and u_2 are solutions to (1.17), referred to as the 'solution pair'), it follows that $\mathrm{u_t}$ is the group velocity of the wave u, and typically, $\mathrm{u_{xx}}$ denotes the group velocity dispersion [20, 21]. In our research we seek to explore fractional solutions. That is, we replace the second space derivative $\mathrm{u_{xx}}$, with u_α, where $\alpha \in (1, 2]$. The nonlinear cubic term in (1.17) includes the modulus squared, which, given a complex valued plane-wave solution (as we derived earlier in the chapter in equation 1.13), returns a real value, in this case:

$$
\begin{aligned}
|\mathrm{e}^{i\theta}|^2 &= |\cos\theta + i\sin\theta|^2 \\
&= \left(\sqrt[2]{\cos^2\theta + \sin^2\theta}\right)^2 \\
&= 1
\end{aligned}
$$

In physics, and specifically quantum particle theory, if the solution u is the probability amplitude, the modulus squared, $|\mathrm{u}_1|^2$, is understood to be the probability of finding a particle, known as the probability density function (PDF), in this case it equals one [19, 22]. This makes sense because we have restricted the particle to exist within polar domain space θ. Therefore, the probability of finding the particle on θ is one (because we have restricted its existence to θ only). If we restrict ourselves to the mathematical approach, then from classical wave theory, or wave mechanics, $|u_1|^2$ is understood to be the energy density (ED), and it equals one from the identity given above [22]. Here, it is useful to note how θ acts as a coefficient for i in the exponent. Its equivalent application as the argument for sin and cos means θ may serve as a complex valued phase constant represented as μ.

Arriving at this wave equation via the Hamiltonian (1.15), we can once again borrow from physics. Since the Hamiltonian operates on the wave equation, then its solution u(x,t) may now be known as the eigenfunction, which describes a state of definite energy: it is a stationary state where the PDF does not change in time. In other words, if the solution function is an eigenvalue, the solution u(x,t) may be represented as a soliton, and the soliton contains information on the energy of the system, therefore it may be interchangeable with the mathematical term ED.

The coupling terms (the last terms on the left-hand side in (1.17)) in this system mean our waves are interacting with each other: the state of one wave influences the state of the other wave, acting as a forcing term for the other wave. Physically, this has been demonstrated via thorough research in laboratory experiments and mathematical treatment by Driben and Malomed [23]. Driben and Malomed investigated light waves in a waveguide coupled by the tunnelling of light, accounting for gain and loss, and Kerr nonlinearity in the waveguide medium [23]. Their research is significant because the system they studied represents a Parity-Time (**PT**) Symmetric System when setting gain and loss equal to each other. A **PT** Symmetric System should not make physical sense, yet further supports the Quantum Mechanical interpretation of NLSEs and serves to prove how ‘impossibilities’ be it mathematical, or physical, can be proven true and exist with useful purpose.

1.1.1 PT Symmetric Systems

To understand symmetries in the context of NLSE research, we must discuss Quantum Mechanics and relativity in more detail. As we described earlier in this chapter in terms of the PDF, Quantum Mechanics may be succinctly described as the probability of observing a particle in space. This probabilistic description of a particle is derived from the wave particle duality of quantum scale objects [19]. Relativity describes the geometry of space and time: for example, using the geometry of a well to describe the behaviour of an object under the force of gravity: there are useful demonstrations available online where heavy objects are placed on trampoline mats, and smaller objects can be shown to ‘orbit’ the larger object proportional to both objects’ respective mass and velocities, and therefore the geometry of the trampoline surface (see [24] for an example) [19].

Symmetries are a phenomenon found in both quantum mechanics and relativity. In the **PT** Symmetric System sense, symmetry is not restricted to geometry, but also includes time. Mathematically speaking, a discrete symmetry in quantum mechanics is called Hermiticity, while continuous symmetry exists as Special Relativity [18].

Combining these concepts, a point in space-time must exist in $\mathbb{R}$ and is represented by the vector (x, y, z, t) in Cartesian coordinates (where x, y, and z denote orthogonally mutual dimensions in space, and t represents a point in time, acting as a fourth dimension). The Poincaré group expresses special relativity and is ten dimensional. The Poincaré group consists of the following:

Four translations: $[x + a,\ y + b,\ z + c,\ t + d]$, where a, b, c, and d $\in \mathbb{R}$.

Three rotations:

$$R_x(\theta) = \begin{bmatrix} 1 & 0 & 0 \\ 0 & \cos\theta & -\sin\theta \\ 0 & \sin\theta & \cos\theta \end{bmatrix}, R_y(\theta) = \begin{bmatrix} \cos\theta & 0 & \sin\theta \\ 0 & 1 & 0 \\ -\sin\theta & 0 & \cos\theta \end{bmatrix}, R_z(\theta) = \begin{bmatrix} \cos\theta & -\sin\theta & 0 \\ \sin\theta & \cos\theta & 0 \\ 0 & 0 & 1 \end{bmatrix},$$

where $\theta \in n\pi$, $n \in \mathbb{Z}$, and

three velocity boosts: $\frac{d}{dt}[x, y, z]$ [18].

The Poincare group is significant because it contains symmetries which should not be found in nature; parity (**P**) changes the sign of spatial coordinates $(x, y, z, t) \rightarrow (-x, -y, -z, t)$, changing the handedness of space; whereas time reversal (**T**) changes the sign (the direction) of time $(x, y, z, t) \rightarrow (x, y, z, -t)$ [18]. Therefore, **PT** operators are excluded from the geometrical symmetry of nature, forming the subset contained within the Poincaré group, the Proper Orthochronous Lorentz group [18].

Including **PT** operators, and thereby including complex matrices within the Proper Orthochronous Lorentz group results in **PT** symmetry, specifically, combined **P** and **T** symmetry [18]. From above, since $\mathbf{P}(x, y, z, t) \rightarrow (-x, -y, -z, t)$, and $\mathbf{T}(x, y, z, t) \rightarrow (x, y, z, -t)$, then $\mathbf{PT}(x, y, z, t) \rightarrow (-x, -y, -z, -t)$.

Applying **PT** symmetry to Quantum Mechanics and the numerical analysis of light transmission in dual-core waveguides, we understand **PT** Symmetric Systems have complex potentials which may be considered as a system interacting with its environment [18]. That is, the **PT** Symmetric System is susceptible to gain and loss, where **PT** symmetry means gain equals loss. Driben and Malomed demonstrated what should otherwise be a physical impossibility by showing both mathematically (with numerical solutions to coupled NLSEs) and in physical optical experiments that **PT** Symmetric Systems and solutions exist.

Given the remarkable and unreasonable utility of NLSEs, which we demonstrated earlier in the chapter, physicists and mathematicians continue development and research in NLSEs and their solutions. The combination of complex analysis with Quantum Physics extends Quantum Mechanics into the complex domain, and allows for such research areas as NLSE solutions and **PT** Symmetric Systems: praised as one of the top ten physics discoveries in the past ten years at the time of writing [25].

Mathematically speaking, extending Quantum Mechanics into the complex domain is useful, as this transformation allows scientists to rely on complex analysis to solve problems which may otherwise be difficult to solve with real analysis. Transforming the domain from $\mathbb{R} \to \mathbb{C}$ means we lose the ordering property associated with real analysis, therefore the concept of 'stability' does not make sense with complex analysis, and real, unstable physical systems can be shown to be stable in the complex domain [26].

1.2 Fractional order Fast Fourier Transform

So where do fractional order derivatives come from? Returning to mathematics and the scope of this research, we analysed various solutions to coupled NLSEs of the fractional variety. The concept of fractional calculus is almost as old as conventional calculus with integer order derivatives. However, considering conventional calculus has proven useful in the sciences so far, comparatively little research has been conducted in the field of fractional calculus: in fact, fractional calculus may be defined by numerous and distinct ways [27].

Integer derivatives are introduced very early in the careers of mathematicians conceptually as the value of the slope of a function f(x) at a given point, ‘x’. That is, the rate of change between a function and its variable. So, if we plot displacement of a particle f(t) in metres on the vertical y-axis, at a given time ‘t’ in seconds on the horizontal t-axis, the derivative in this case is $\frac{df(t)}{dt} = \frac{dy}{dt}$ which is the change in displacement over time, and in this instance has a value of metres per second, known colloquially as speed, or more appropriately, instantaneous velocity. So we learn the first derivative of displacement in time is velocity, and the derivative of velocity in time is acceleration and if we continue in this fashion after acceleration the third, fourth, fifth and sixth derivatives of displacement over time yield jerk, snap, crackle and pop (you will feel ‘jerk’ when changing direction while sitting in a vehicle navigating a corner, mid-turn, or perhaps you avoid childish games so you do not fall victim to the biggest jerk in the neighbourhood during a game of tug-of-war) [19, 28].

If the first derivative of displacement over time has the physical interpretation of velocity, and the second derivative of displacement over time has the physical interpretation of acceleration, what about fractional values between one and two? What does it physically mean to take a fractional derivative such as 1.4, 1.9, or indeed any quotient such that a, b $\in \mathbb{R}$, where $\frac{a}{b} = \alpha$ and for the scope of this research, $\alpha \in (1, 2]$?

When evaluating means to calculate fractional derivatives, we can see some properties which are distinct from conventional derivatives, such as nonlocal, memory properties, and the need to solve such problems almost exclusively using numerical methods (see appendix A1) [29]. Furthermore, what does it mean to take a fractional derivative of a coupled NLSE? In physical terms, since we are taking fractional values of the space derivative perhaps this means we will explore memory properties of group velocity dispersion, and how this affects soliton stability.

FDEs may be categorised into space, time, or space/time FDEs, and may be applied to model various natural phenomena, including, in our case, light waves [29]. FDEs generally require a considerable amount of computational power, especially when considering finite difference methods. However, solving FDEs can be significantly easier using Fast Fourier Transform (FFT) methods: the number of calculations can be reduced from $O(N^2)$ to $O(N\log N)$ [29, 30].

FDEs have been shown to model natural phenomena more accurately than integer calculus in some cases, with demonstrated applications in semiconductor research, hydrogeology, finance and other areas [29]. The significance of this research is to explore solitary wave stability boundaries in fractional, coupled NLSEs used to model light in a dual-core waveguides.

Recently, some papers have sought to raise attention to applications of FDEs, spanning across fields such as physics, control problems, signal and image processing, mechanics and dynamic systems, environmental science, and economics [31, 32]. Most of these fields make use of the memory properties of FDEs: to properly describe friction processes in physics, or to preserve textures in image processing, and analyse economic processes based on memory [31]. While within physics the accepted view is that fractional calculus applied to quantum mechanics is still in its infancy [33], the fact remains fractional order Fourier transform and its application to quantum mechanics is the title of an article published by Namias in 1980 [34], and is perhaps indicative of the relatively little research attention fractional calculus in quantum mechanics has received: fractional calculus is not in its infancy due to age, rather this is a neglected field of mathematical physics which requires more research.

1.3 Solitary waves

We have previously described how solitons are a wave/particle solution to NLSEs that say something of the energy of a system, but they still lack a rigorous definition. Loosely described, solitons are a subset of solitary waves that conserve their shape and behaviour over time, and after perturbations and collisions with other solitons (except for a phase shift) [21, 35]. After accounting for nonlinear effects, it is possible to derive soliton solutions resistant to self-similar blow-up [21].

After normalising physical constants, we can analyse the coupled, fractional Schrödinger equation (1.17) term by term for a better understanding in terms of soliton behaviour. If we take the first equation from our coupled system in (1.17), we see four terms on the left-hand side:

$$i\mathrm{u}_{1_t} + (1/2)\mathrm{u}_{1_\alpha} + |\mathrm{u}_1|^2\mathrm{u}_1 + \mathrm{u}_2 = 0.$$

If u(x,t) is a complex plane-wave soliton solution, then the first term of this wave equation, the first time derivative ($i\mathrm{u}_{1_t}$), represents the group velocity of our wave solution. The group velocity describes the velocity of the wave packet, or solution wave envelope (the ‘inner’ wave envelope is made up smaller ‘surface’ waves or phases moving at the phase velocity) [19]. The fractional order term to the $\alpha = 2$ space derivative represents dispersion, that is, different elements of the wave solution travelling at different velocities, dependent on frequency: dispersion is evident when a rock is thrown in a pond, and waves travelling at different velocities result in ripples spreading out over the pond, this spreading out of waves (and by extension, wave envelopes) is dispersion [20, 21]. The nonlinear term, (which may include the coefficient $\mu > 0$ for the focusing case, and $\mu < 0$ is the defocussing case) as explained earlier, is the ED (since we are dealing with complex variables, the ED equals one), which leaves the original solution u_1, and the solution to the second equation, u_2, making the equation coupled [21, 36]. To summarize, the coupled NLSEs contain the group velocity of the solution, the dispersion of the solution, the solution itself, and coupling term which is the solution to the other half of NLSE system.

1.4 Research motivation

Equipped with this knowledge of NLSEs and mathematics, where does this research fit in the field of mathematical physics? We wish to explore the propagation and stability boundaries of novel soliton modes such as bright and dark solitons using a Fast Fourier Transform (FFT) method executed on MATLAB. The significance of this research lies in the analysis of these equations using fractional derivative analysis, discovering fractional stability boundaries related to solution symmetry, and of course, contributing to our understanding of NLSEs by sharing any other curious results and dynamics, where we hope to find results consistent with other fractional NLSE research [36-39].

This area of research should contribute to the field of mathematics by sharing fractional derivative values and the fractional derivative effect on solitons. The research could contribute to our understanding of coupled NLSEs, or the applications of coupled NLSEs. Primarily, this research is focussed on numerical analysis of coupled NLSEs and finding soliton stability boundaries in terms of fractional derivative values: a relatively new research area.

CHAPTER 2 METHODS

Numerical analysis and experiments were conducted using MATLAB (R2022b) running a FFT program modified for coupled, fractional NLSEs (the code is available in Appendix B) to find stable solutions for the fractional NLSE (1.17) [30, 36]. Since we concern ourselves with stationary solitons, we employ regular, periodic boundary conditions, [8, 11, 12, 22, 40-42]. The MATLAB script was run until system failure to determine computational memory limits, then the script was corrected to determine the time at which the solutions became numerically unstable and 'blew up'. This ensured the MATLAB script was optimised to reduce numerical and memory error while ensuring experiments were run for a sufficiently long time to verify soliton stability.

Once the MATLAB program was written, we set about finding numerical stability boundaries. During this time, the experiment limits were determined, and solution plotting and data collection programs were written to efficiently manage the data output.

2.1 Code validation

In this section we discuss and explain various plots used to describe the numerical solutions. Since we run numerical experiments on light waves, waterfall plots, such as in Figure 2.1 show the evolution of the light wave in three dimensions: two in space (wavelength and amplitude), and one in time to show the evolution of the solution. The heatmap (shown in Figure 2.2) displays the same information as the waterfall plot, but in two dimensions. The heatmap shows the wavelength of the soliton on and x-axis, over time on the y-axis, and uses colour to denote the amplitude dimension of the wave over time (hence the name, ‘heatmap’: a ‘hotter’, ‘brighter’ colour denotes a higher value amplitude, whereas a ‘cold’ or ‘dark’ colour denotes a lower value amplitude).

Figure 2.1 exemplifies an accumulation of numerical errors contributing to ‘blow-up’ from approximately time ‘t’ = 800, for what appears to be an otherwise stable soliton. It is important to note that one ‘t’ does not correspond to one second ‘s’. Since the experiments simulate the transmission of light, we observe that time $1t \ll 1s$, hence we use the term ‘t’ to denote the evolution of the solution over time and not the fundamental unit seconds ‘s’. Additionally, the units to denote space ‘x’ do not correspond to the fundamental unit metres ‘m’. Since we are dealing with the electromagnetic spectrum, if we restrict the light pulses to the visible spectrum, the plots would be in the order of nanometres. Therefore, to optimise experiment results, we conducted numerical experiments up to t = 750 on a space ‘x’ large enough to depict the behaviour of the light pulse and to capture the wavelength of the light pulse to observe behaviour and stability.

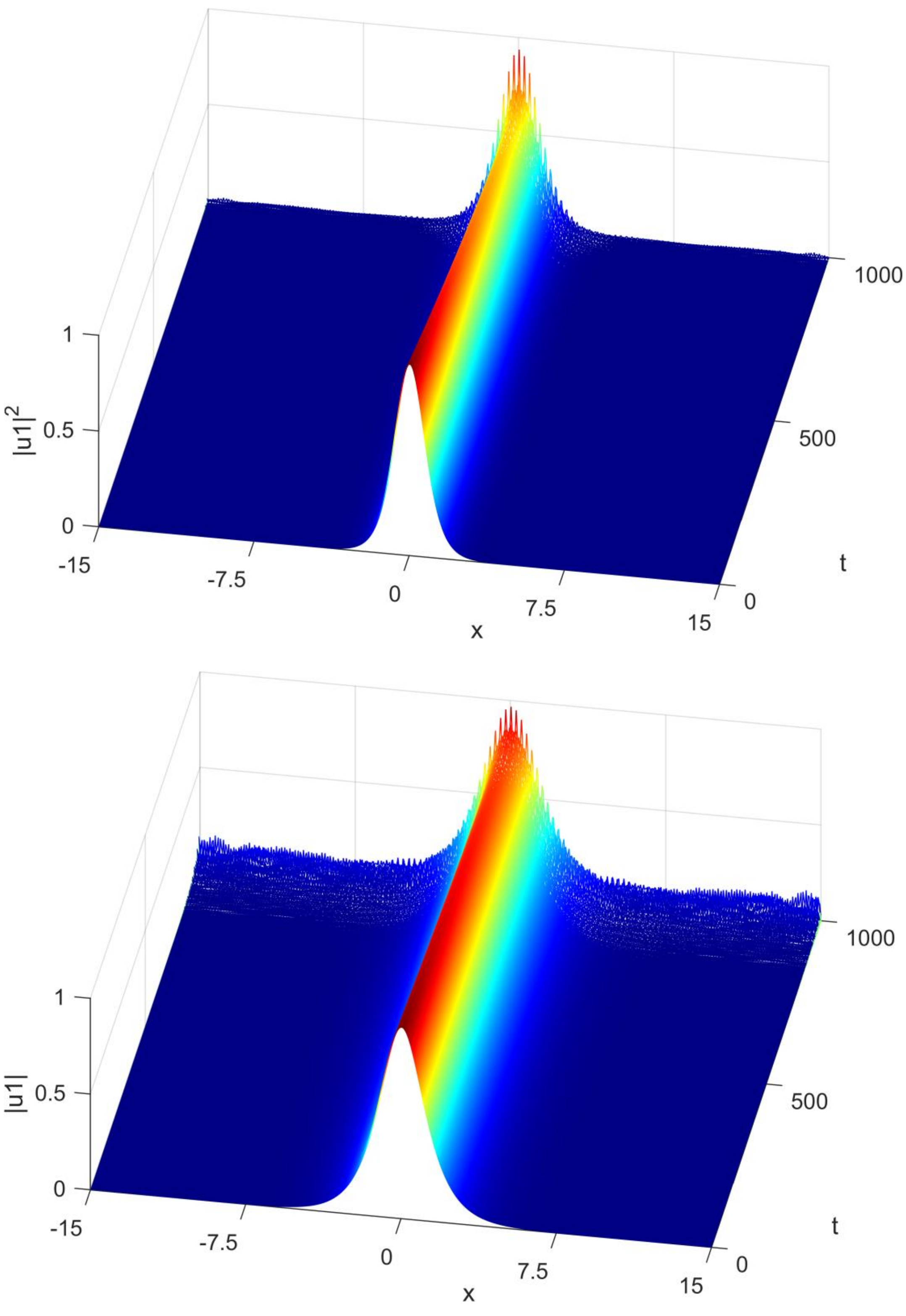

Figure 2.1 ED (top) and its solution (bottom) show numerical instability resulting in ‘blow up’, present as spikes and dispersion when $t > 800$.

2.2 Results and analysis

To determine stability of results as objectively as possible, MATLAB programs output the following plots which are discussed and explained in detail in this section.

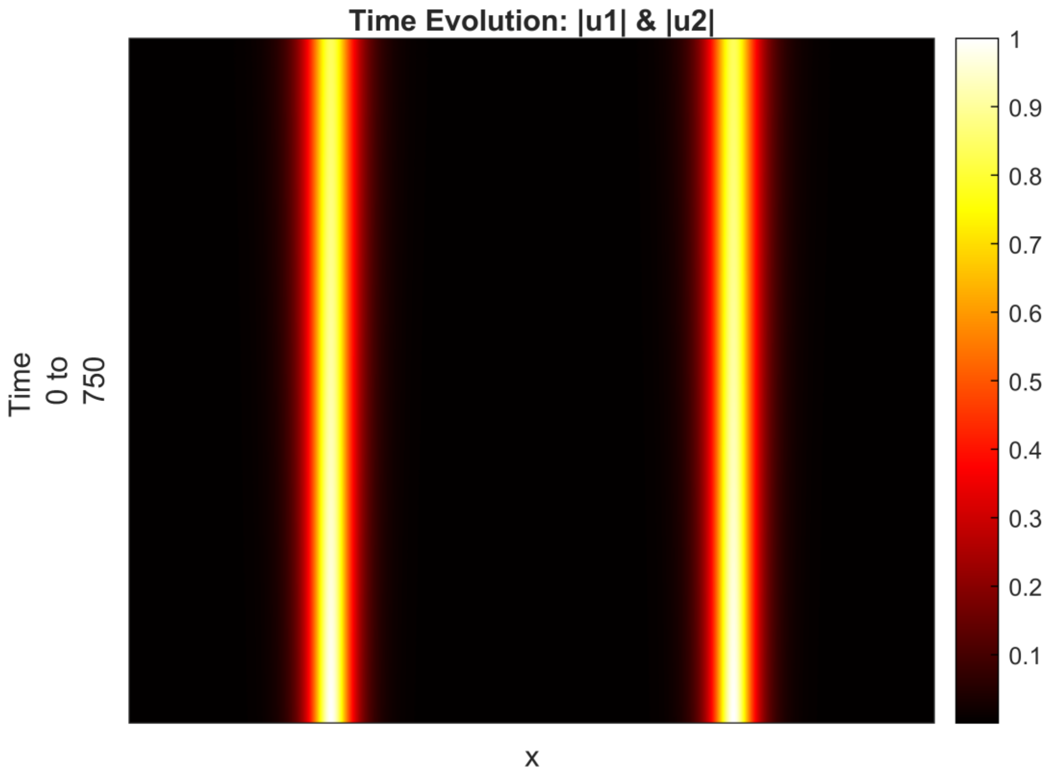

Figure 2.2 Side by side heatmap of coupled, stable, symmetric soliton solution pair.

Since we analyse coupled nonlinear solutions, we examine how pairs of solitons interact. If a soliton is stable and symmetric, it will appear to behave as the solitons do in Figure 2.2. If the solitons are stable and asymmetric, we would expect one soliton to be bright, and the other soliton to be significantly more dark, as in the Figure 2.3, where the bright solution corresponds to an amplitude of approximately two, which is higher than its counterpart which has an amplitude of approximately one: hence, the solutions are asymmetric. Therefore, heatmaps are a common method of evaluating soliton behaviour, where colour is used to denote the height of the solution against the field. In Figure 2.2, the colour black corresponds to a height of zero – the solution field surface - while the colour white corresponds to a height of one, describing the shape of the solution as it evolves over time (the colours scale according to the maximum amplitude of the solution, therefore white does not always correspond to an amplitude of one) [3, 7, 8, 11, 12, 15, 35, 36, 43]. However, we must rely on other figures to assist with asymmetric stability assessment. The side-by-side heatmap will clearly show oscillations for the large peak amplitude values, but not for smaller asymmetric peak amplitudes which may appear as noise, or the heatmap may simply obfuscate oscillations or dispersion in the system due to our inability to distinguish between finer, darker colour grades.

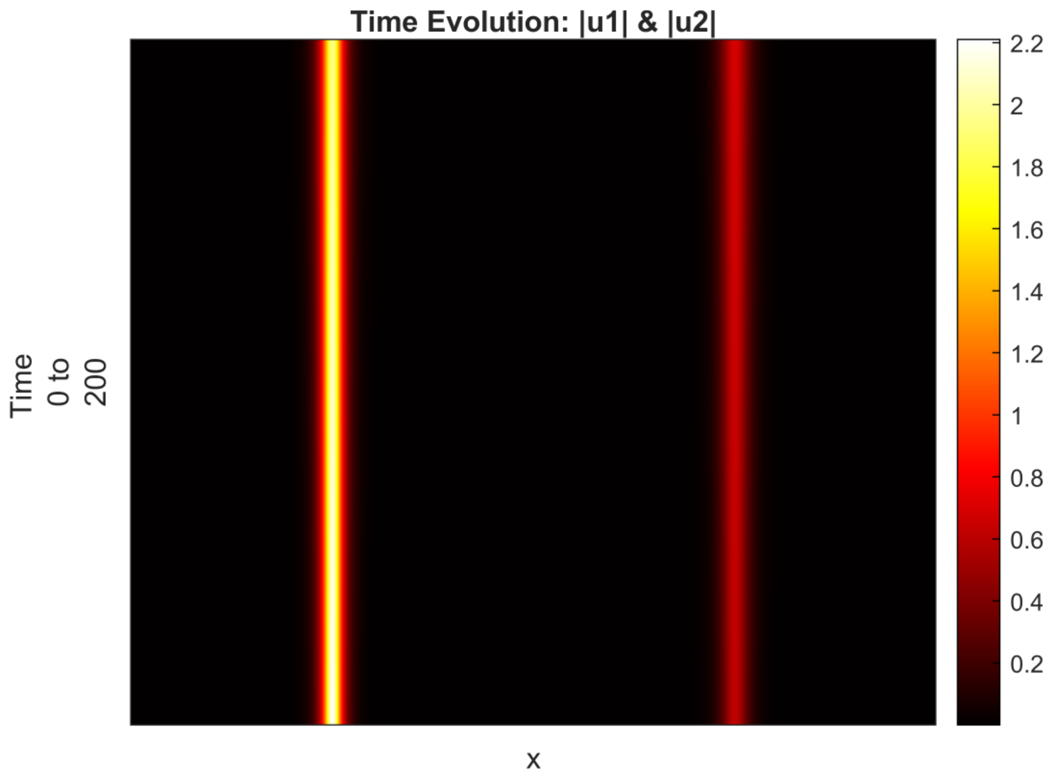

Figure 2.3 Side by side heatmap of stable, asymmetric soliton solution pair.

Solitons for this form of coupled NLSE such as (1.17) consist of combinations of decaying oscillations and permanent ‘wave’ solutions, so it is not always possible to observe a soliton solution that consists only of the permanent wave solutions after the oscillations have decayed [44, 45]. Considering the soliton solutions are a system evolving in time, we may say the oscillations and decay correspond to transient behaviour of the system, whereas permanent wave solutions correspond to the steady-state. Therefore, since the experiments are restricted to 750t, we can expect some of our solutions to oscillate and decay over time but still be classified as stable, since the experiment may not allow sufficient time to observe steady-state behaviour [45].

Since the peak amplitude of the soliton solutions we observe in our experiments generally decrease over time, we consider a soliton stable if it has minimal, low-frequency oscillations, minimal dispersion, and conserves its behaviour. Considering we are testing soliton stability by perturbing the wave equation, soliton stability is somewhat subjective, and because we are exploring stability in terms of fractional derivative values, we will take a soliton as stable when it is sufficiently well-behaved [44]. We provide evidence to support our conclusions which are open to debate and discussion.

The experiments have been conducted with a spatial width of ±15x, to a time of 750t as a standard for showing solution stability. Using experiment time is a commonly accepted approach to show soliton stability and has been used extensively in mathematical research of solitons [21, 23, 36, 46, 47]. However, soliton stability requires some knowledge of the perturbation and the intended application, this implies stability also depends on previous knowledge of the system, and not simply how long a solution conserves behaviour. Therefore, running an experiment for a sufficiently long time should not be the only determinant of stability. So, we consider a system stable if it has low frequency oscillations and low frequency dispersion relative to the experiment length, 750t [44]. Experiments may run to other times, such as 200t, or 1000t to allow for closer scrutiny of dispersive and radiative effects as appropriate.

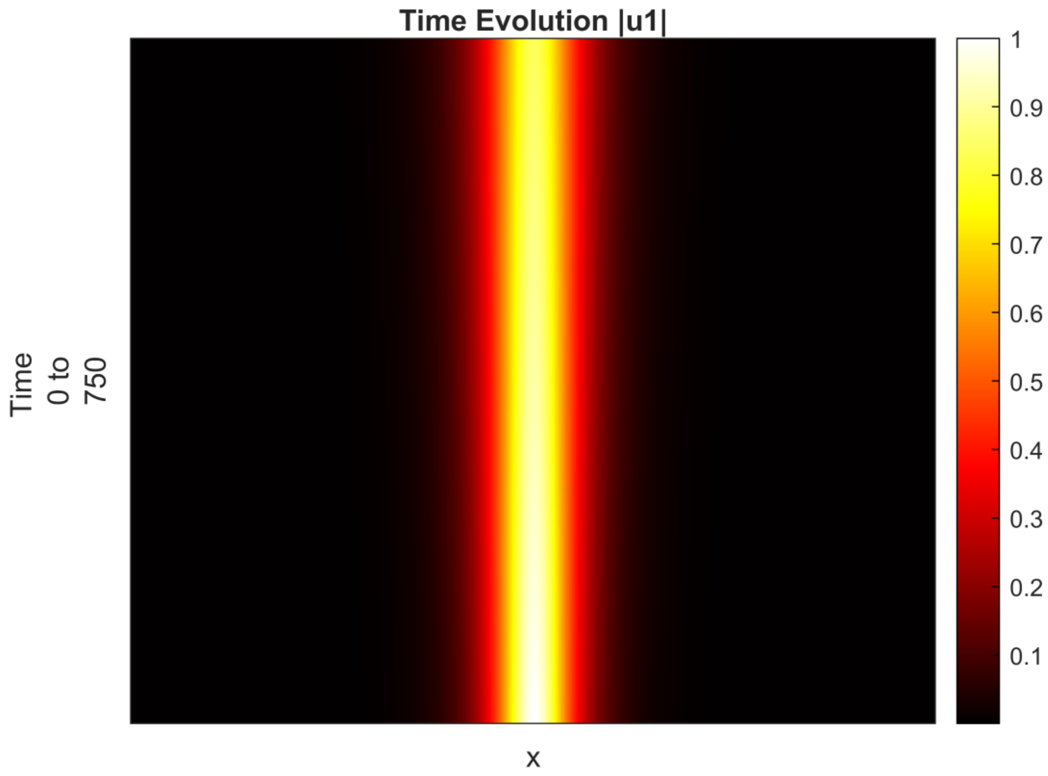

Figure 2.4 A closer view of the soliton u_1 allowing for a more detailed inspection of dispersion or oscillation effects.

Figure 2.4 offers improved scrutiny of soliton behaviour by showing a single solution: allowing dispersion and oscillation effects to be more obvious and easily identifiable for the absolute value of the solution u_1, i.e. $|u_1|$. Figure 2.5 extends on this line of reasoning, however this plot displays the ED, or the absolute value of the solution squared, i.e. $|u_1|^2$ for the same period of time. The ED will further amplify oscillations, and also serves to capture the ED in and of itself, so we see how energy is distributed throughout the solution field.

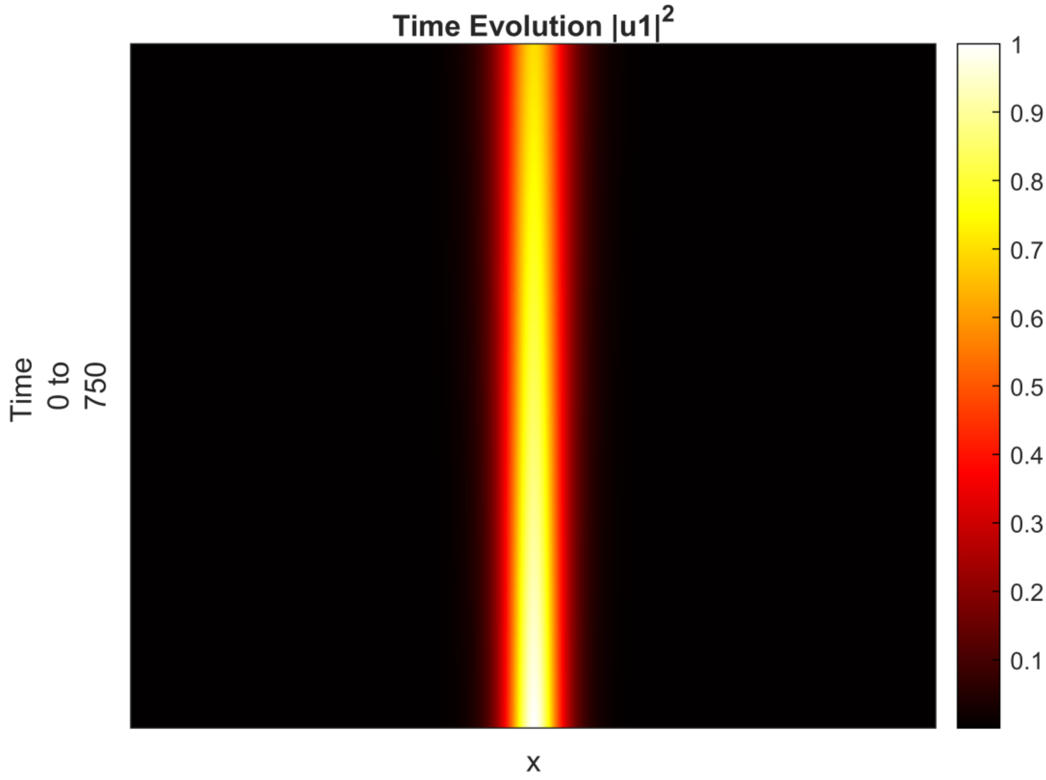

Figure 2.5 ED of the soliton u_1 from figure 2.4.

Since soliton studies find applications in a range of fields, we clarify the term 'ED' may be interchanged with 'intensity' in optics, or physically with the 'PDF', which is interpreted as the probability of finding a particle in given space, hence it is customary to display solutions in this manner as the ED, intensity, or PDF, and we understand these terms are interchangeable depending on the field of research [19, 41, 48, 49].

Waterfall plots of the solitons offer an alternative view from which we can see in detail the behaviour of the soliton peak amplitude and oscillations over the course of the experiment. The waterfall plot will also allow dispersion in the field to be visible due to the stark contrast of the plot of the solution field against the white background. Like the heatmap, the waterfall plot is also a common method to display soliton solutions [3, 9, 23, 35, 47, 50-53]. In Figure 2.6, we see a side-by-side comparison of a solution u_2 with its corresponding ED, where we note the behaviour of the solution compresses when depicted as the ED.

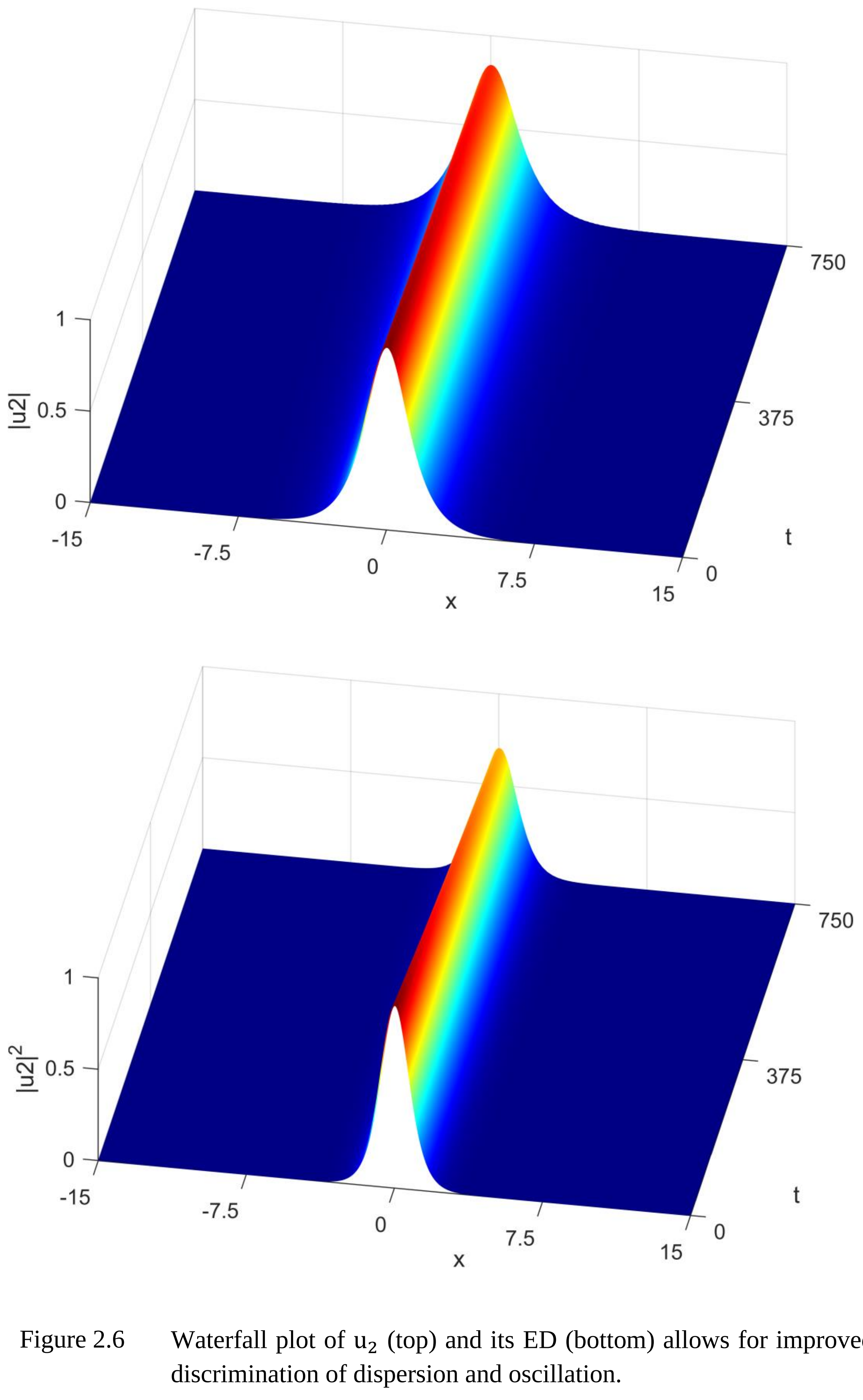

Figure 2.6 Waterfall plot of u_2 (top) and its ED (bottom) allows for improved discrimination of dispersion and oscillation.

To shift the analysis of the soliton stability away from qualitative to a more quantitative assessment, we collected other information such as peak amplitude evolution as in Figure 2.7 (where $|u_{1_{max}}|$ denotes the peak, or maximum amplitude of $|u_1|$ at each time step), phase portraits (such as Figure 2.11) of the gradient of both the peak amplitude and centre of mass and direction fields of the gradient of the peak amplitude and centre of mass during the experimental process. These methods are appropriate and have been used to support confirmation of stability regions in other studies of nonlinear processes [3, 8, 10, 31, 41, 44, 46, 54-57].

Since the gradient is determined from the peak amplitude and the centre of mass of the numerical solutions, we do not rely on phase and direction fields as 'true' phase and direction fields, rather quasi-phase, and quasi-direction fields, used to inform an assessment. The phase portraits and direction fields are not used to definitively identify stable nodes, be the basis of a claim a solution is indeed self-supporting or to definitively justify a result. The phase portraits and direction fields are used as part of a mathematician's analytical toolkit to help discern the goings-on of a solution [44].

The peak amplitude evolution captures the value of the maximum amplitude at each timepoint and summarises the behaviour of the solution over the course of the experiment: otherwise referred to as a time-series analysis of the peak amplitude [56, 58]. Figure 2.7 shows the peak amplitude of a stable solution pair since it appears linear, or at least shows little sign of oscillations.

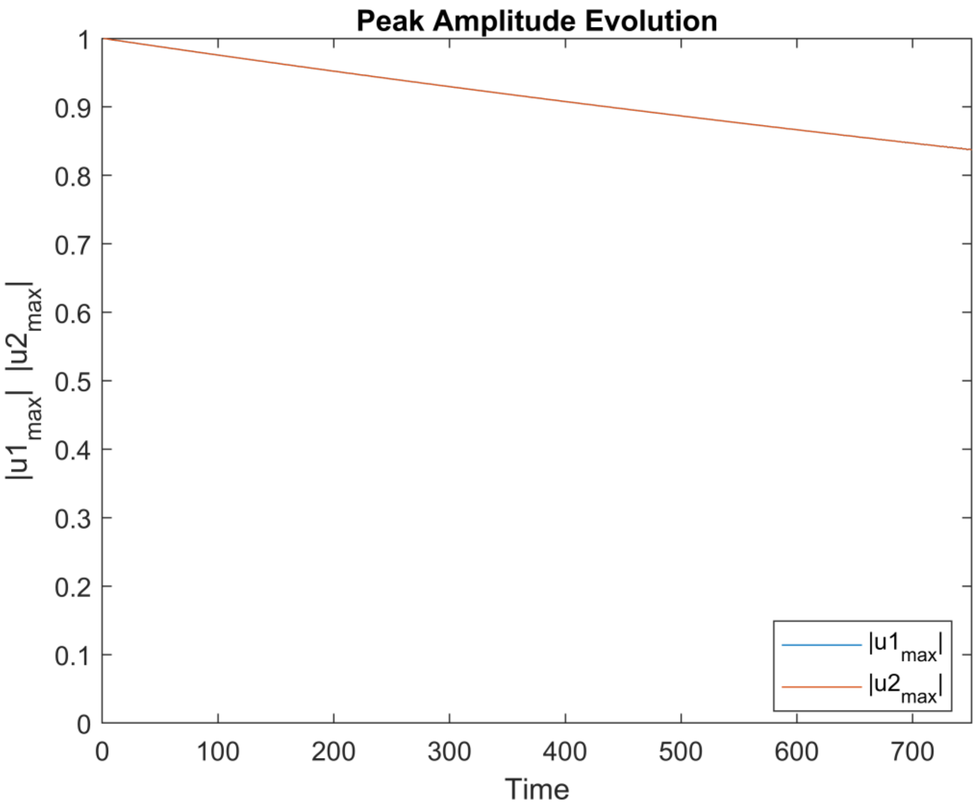

Figure 2.7 Peak amplitude evolution of u_1 and u_2 captures the change in peak amplitude over the duration of the experiment. We only see the u_2 curve because the solutions are symmetric (i.e. u_1 is 'overwritten' by u_2 during the plotting process).

Since it is well known in physics the electromagnetic spectrum may behave as both a wave or a particle depending on the method of observation, we also calculate the centroid of both solutions to observe how the solution behaves as a particle and display the results as the centre of mass evolution such as in Figure 2.8 and centre of mass direction field as in Figure 2.10. The centre of mass is determined from the average value of the solution surface across the spatial domain at each time step. Considering the centre of mass evolution, a stable solution corresponds to a horizontal line across the plot. When a solution becomes narrow and focussed on the heatmap, the centre of mass evolution will decrease (calculating a lower average value near the surface at 0), and as dispersion, noise, or a solution with a wide pulse-width propagates through the field, the value of centre of mass will increase proportionally (the centre of mass increases as there are more peaks in the solution field, thereby raising the average value).

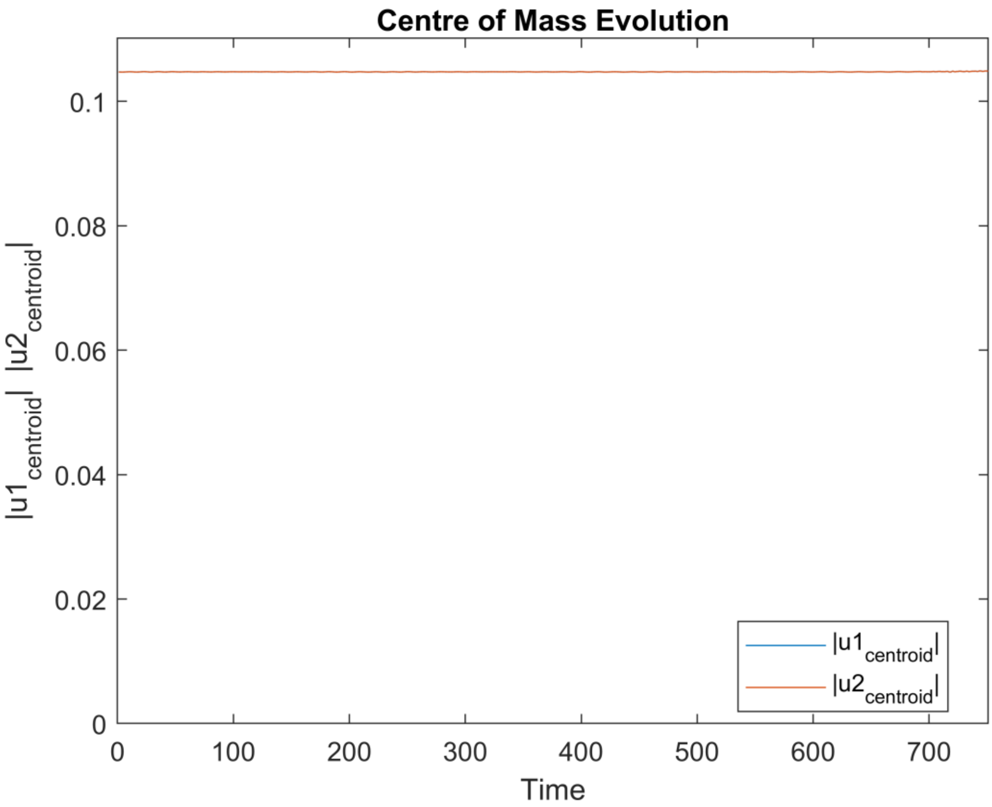

Figure 2.8 Centre of mass evolution corresponding to the peak amplitude evolution in Figure 2.7: a stable, symmetric solution.

To a lesser extent, we may call upon the direction field and phase portrait to help determine stability. Since we use the gradient of the peak amplitude evolution, the plots are not rigorous, true phase portraits or direction fields, rather they provide a qualitative, visual indication of the behaviour of the peak amplitude for each soliton in the pair throughout the experiment.

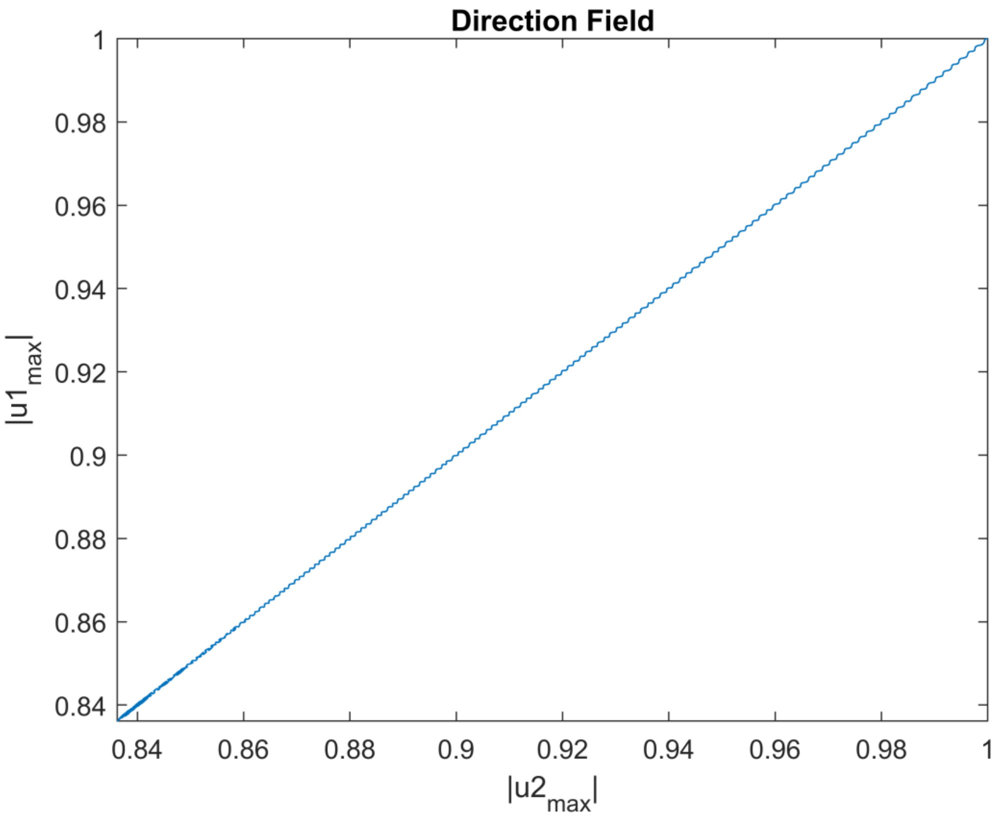

Figure 2.9 The direction field of both u_1 and u_2 from the peak amplitude in Figure 2.7. This plot indicates how well behaved the symmetric solution is and provides information on self-reinforcing properties of the solution.

In Figure 2.9 we see the direction arrows here are densely packed and linear (effectively creating a blue curve), pointing from the value of the peak amplitude, in the direction of the gradient. The reasonably linear and close grouping in the direction field implies the solutions are symmetric, and peak amplitudes slowly increase or decrease over time. In conjunction with Figure 2.11, we observe very tight grouping around the point (0, 0), meaning the derivative of both solutions remain very close to zero, and therefore the peak amplitude has very little change over the experiment, and is well-behaved.

The centre of mass direction field was also available for consideration, where we look for evidence of reasonably 'tight' grouping to support stability. In Figure 2.10 we see the centroids do not wander around the direction field, and they take values that support relatively linear behaviour. The width of the line in the centre of mass direction field provides an indication of dispersion (note the small axis scale), and variance of peak amplitude throughout the experiment. Therefore a 'tight' grouping represents reasonably well-behaved solutions.

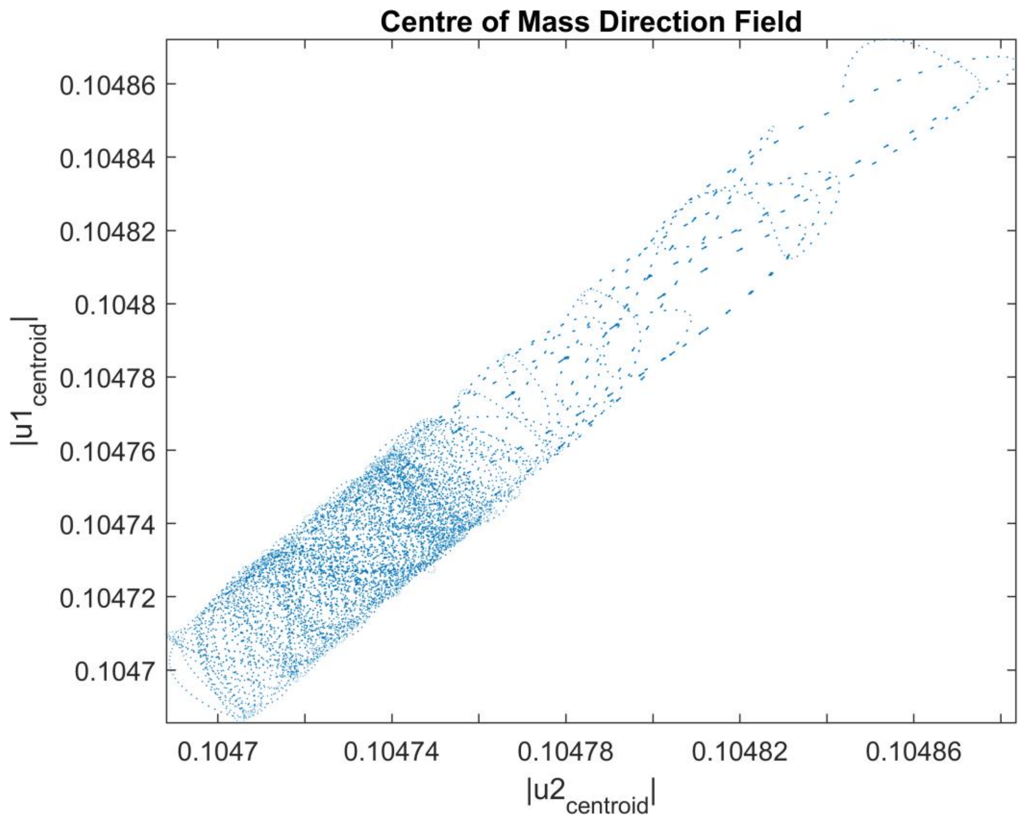

Figure 2.10 Centroid direction field of u_1 and u_2 corresponding to the previous centre of mass evolution plot in figure 2.8.

Considering the phase portrait of peak amplitude and centre of mass: the phase trajectory behaves like an unstable attractor, known as Arnold diffusion, seen in

Hamiltonian systems where phase portraits of oscillating, nonlinear systems have been shown to contain stability points [41, 44, 58-62].

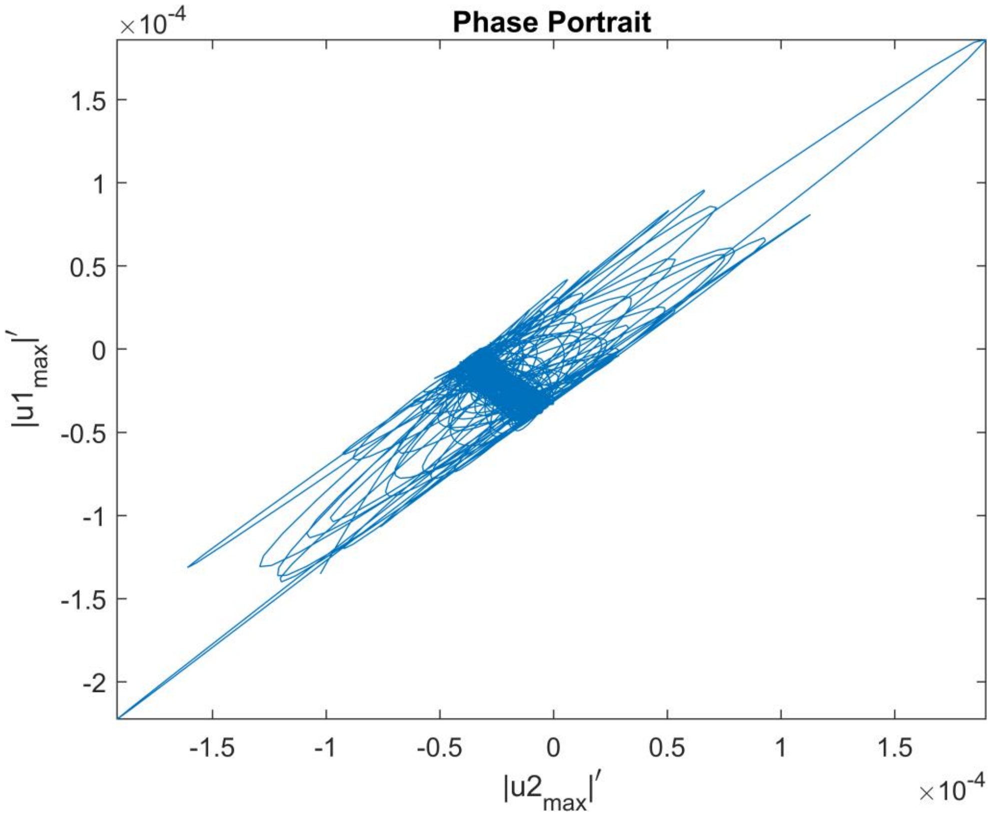

Figure 2.11 The phase portrait of the gradient of peak amplitude of u_1 and u_2 provide information on nodes and stability points. Since the phase portrait is not using the true gradient, we must be careful when relying on this plot (note the small scale of units and close proximity to the point (0, 0) implies stability).

The purpose of the phase portrait in Figure 2.11is to show the behaviour of the peak amplitude gradient throughout the experiment. For the purposes of this research, gradients centred around the zero point may indicate little change or variation in the peak amplitude (depending on the scale) over the course of the experiment, whereas a 'noisy' phase portrait may indicate erratic oscillations in the peak amplitude, as shown in Figure 2.13. Displaying phase portraits in this manner allow the researcher to see detail of changes in the solution which are not easily visible in the waterfall plots or heatmaps. Therefore, calculating and displaying phase portraits and direction fields offer further insight and closer scrutiny into the behaviour and stability of solutions.

Both phase portraits in Figure 2.11 and Figure 2.12 behave as unstable attractors. Therefore, we rely on the scale, as well as the general behaviour of the phase portraits to help determine stability when necessary [58-62].

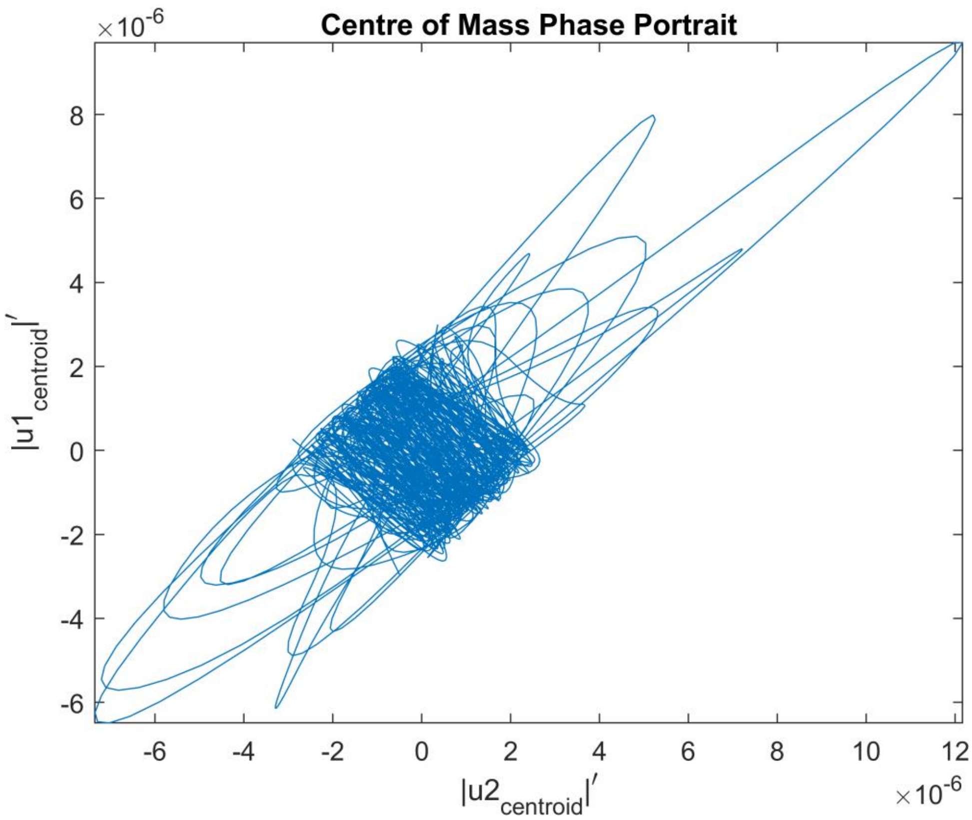

Figure 2.12 Centre of mass phase portrait corresponding to the previous peak amplitude phase portrait.

So far, the figures presented in this chapter display the results of well-behaved soliton solutions (which will be examined in closer detail in Chapter 3). For unstable solutions, we expect to see results such as in Figure 2.13 below.

The first unstable plot in Figure 2.13 begins with an unstable, asymmetric pair. The solutions are asymmetric because of the average difference in peak amplitude throughout the experiment, yet the solutions are unstable due to oscillations. The instability becomes clear when the solutions switch (swap their asymmetries, i.e. u_1 and u_2 reach a critical point in the numerical experiment where they exchange behaviour), then disperse completely, evident as a 'noisy' solution field.

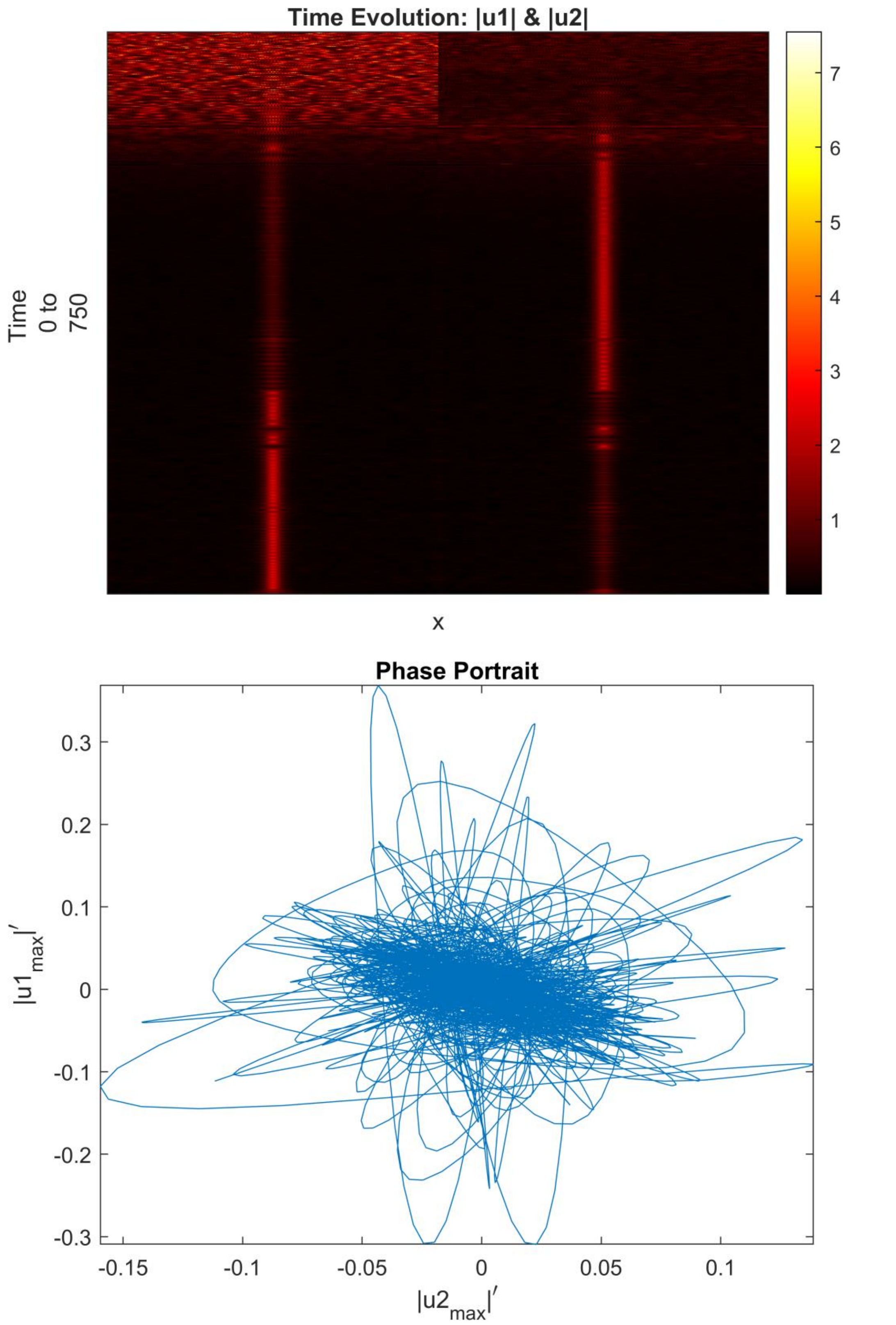

Figure 2.13 Asymmetric, unstable solution heatmap (top) and its corresponding phase portrait (bottom). Note the difference in axis scale magnitude for the phase portrait reflects asymmetry between u_1 and u_2, and note the axis limits as compared to Figure 2.12 illustrate instability.

We see the phase portrait in Figure 2.13, the values for u_1 and u_2 wander around the phase space in a disordered manner. Comparing the phase portrait in Figure 2.13 to the direction field in Figure 2.14 below, we see the peak amplitudes have been widely distributed across the direction field for both u_1 and u_2: we conclude the phase portrait and direction field in Figure 2.14 represent unstable, asymmetric solutions.

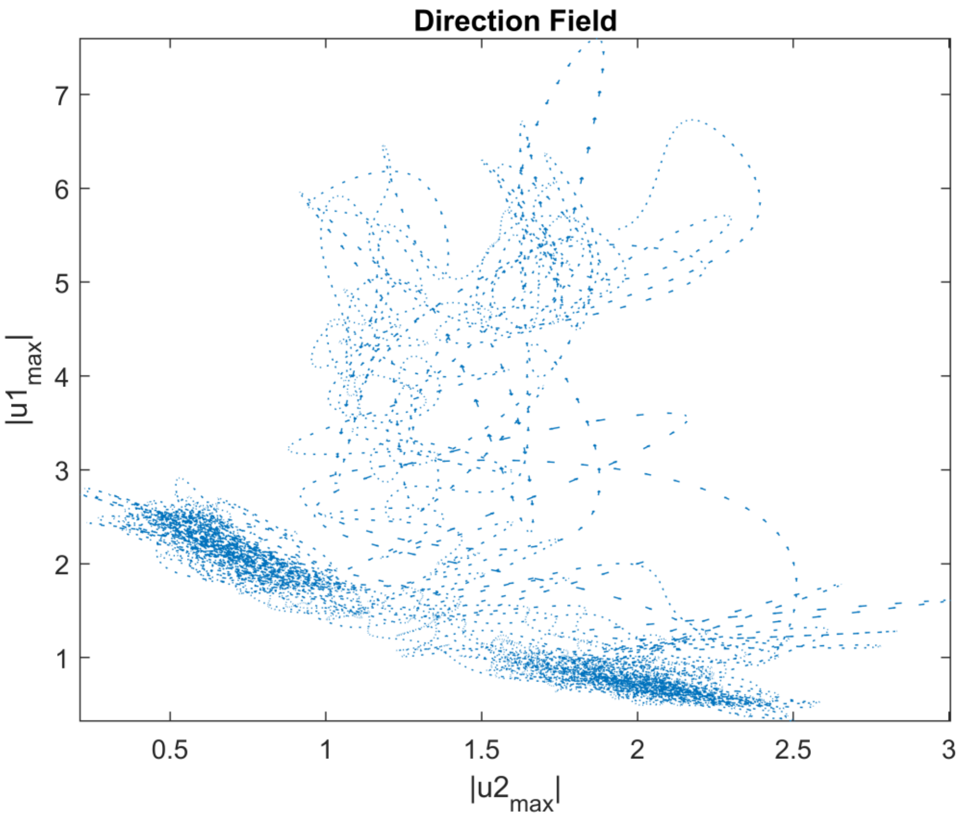

Figure 2.14 Direction field for unstable asymmetric soliton pair shows the distribution of peak amplitude values and the direction of change at each point.

Using axis scale and curve behaviour to determine stability applies to the centre of mass phase portrait and direction field in Figure 2.15. We must pay attention to the general behaviour of the phase and the distribution of direction field as an indication of stability because the phase generally behaves as a chaotic, unstable attractor. Therefore, stability is determined from the axis scale, rather than behaviour.

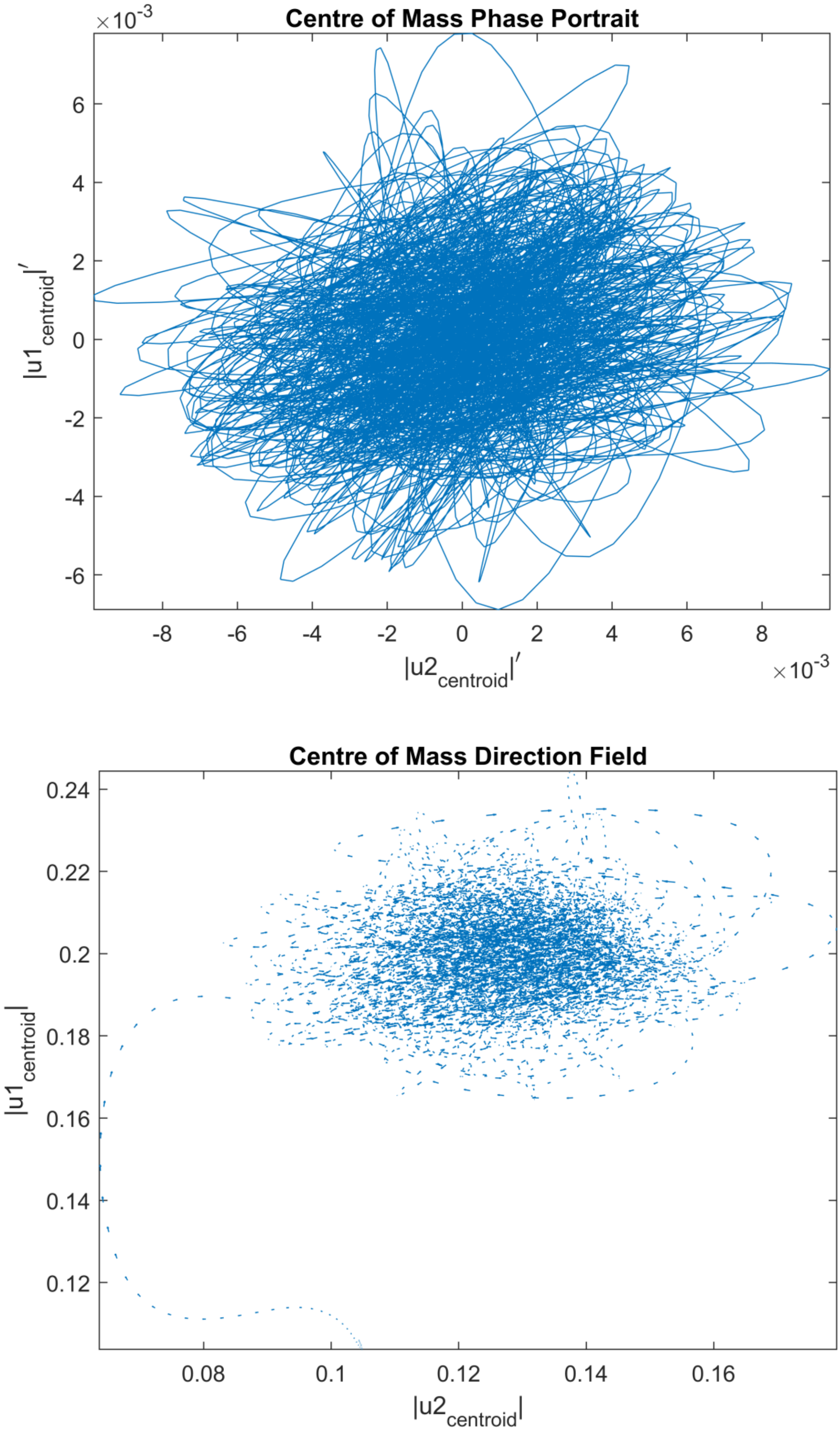

Figure 2.15 Phase portrait and direction field of the centre of mass for unstable, asymmetric solutions from the previous Figure 2.13 and Figure 2.14.

We see in the phase portraits in Figure 2.16 and Figure 2.17 two unstable, chaotic nodes for the asymmetric u_1 solution at approximately 0.8, and 2.2, and there are some oscillations between 3 and 7.5 on the $|u_{1_{max}}|$ axis. Interpreting the phase portrait in Figure 2.16 in conjunction with the heatmap in Figure 2.13, by induction, we see these groups correspond to initial oscillations of the solution between 0 and 300t, swapping asymmetries and oscillations from approximately 300t to 600t, then dispersion from 600t to 750t respectively.

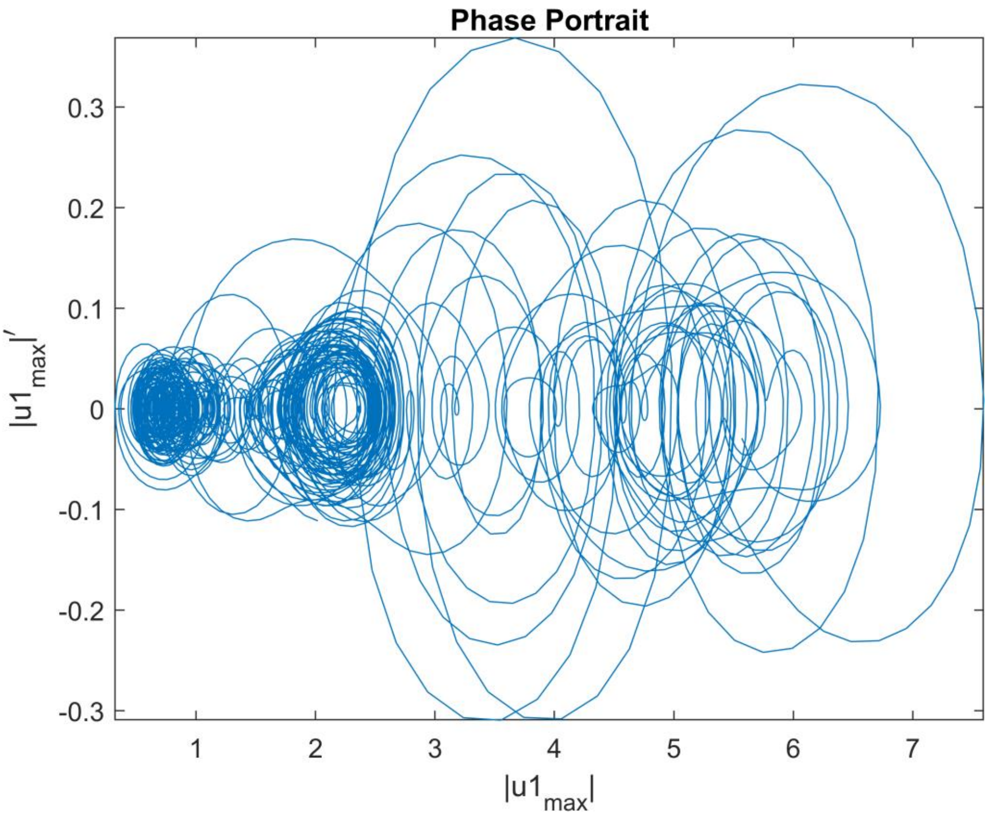

Figure 2.16 Phase portrait for solution u_1. Note there are numerous unstable equilibrium points that correspond to the peak amplitude as it decays from initial conditions (from 7 to 3), begins oscillating (from 3 to 1), then disperses (1 to 0). The density of the phase portrait curve indicates how long the solution has existed at a given amplitude.

When considering the phase portrait and direction field for the centre of mass, we need to pay attention to the value of the centroid on the x-axis and compare this value to its corresponding heatmap. Recall the centre of mass is calculated from the surface value of the solution at each time point, therefore the centre of mass phase portrait may behave as stable, but it reflects the steady state of noise in the solution field, as in Figure 2.17. Without reference to other figures, Figure 2.17 may appear to be a stable solution, when it is in fact, an unstable solution.

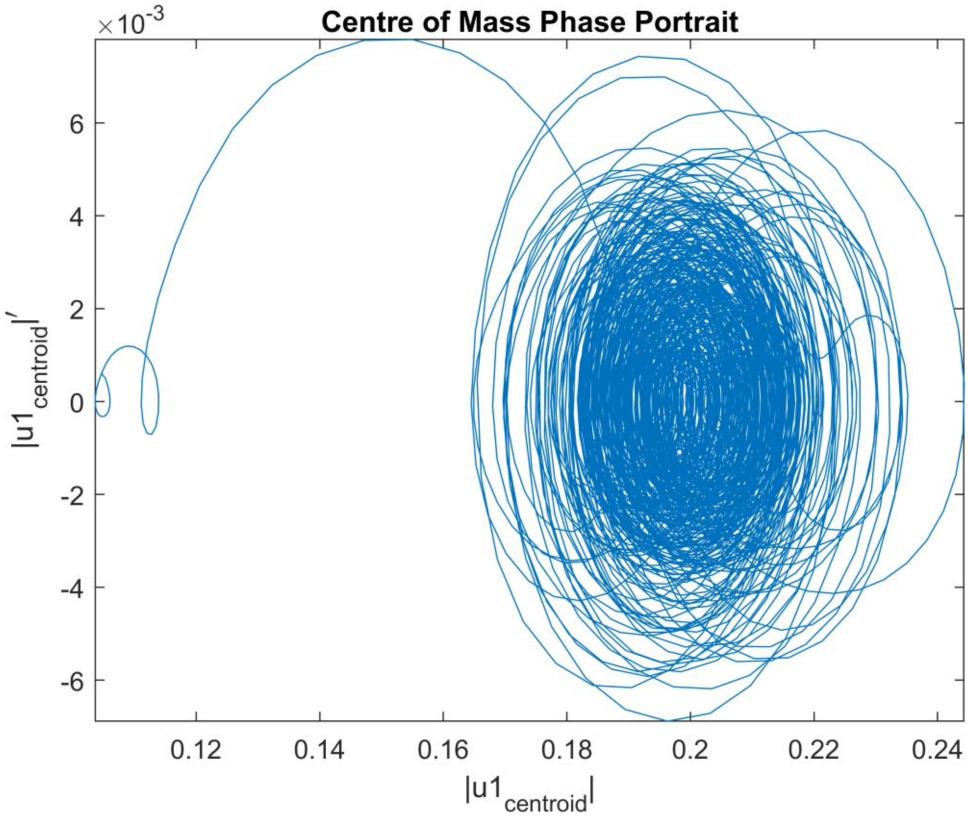

Figure 2.17 Centre of mass phase portrait corresponding to the previous phase portrait in Figure 2.16.

In Figure 2.18 we see examples of waterfall plots, where we easily discern noise in the solution field due to the contrast of the plot and the background for times t < 600t. We see the solutions disperse into noise from approximately 600t until the conclusion of the experiment at 750t.

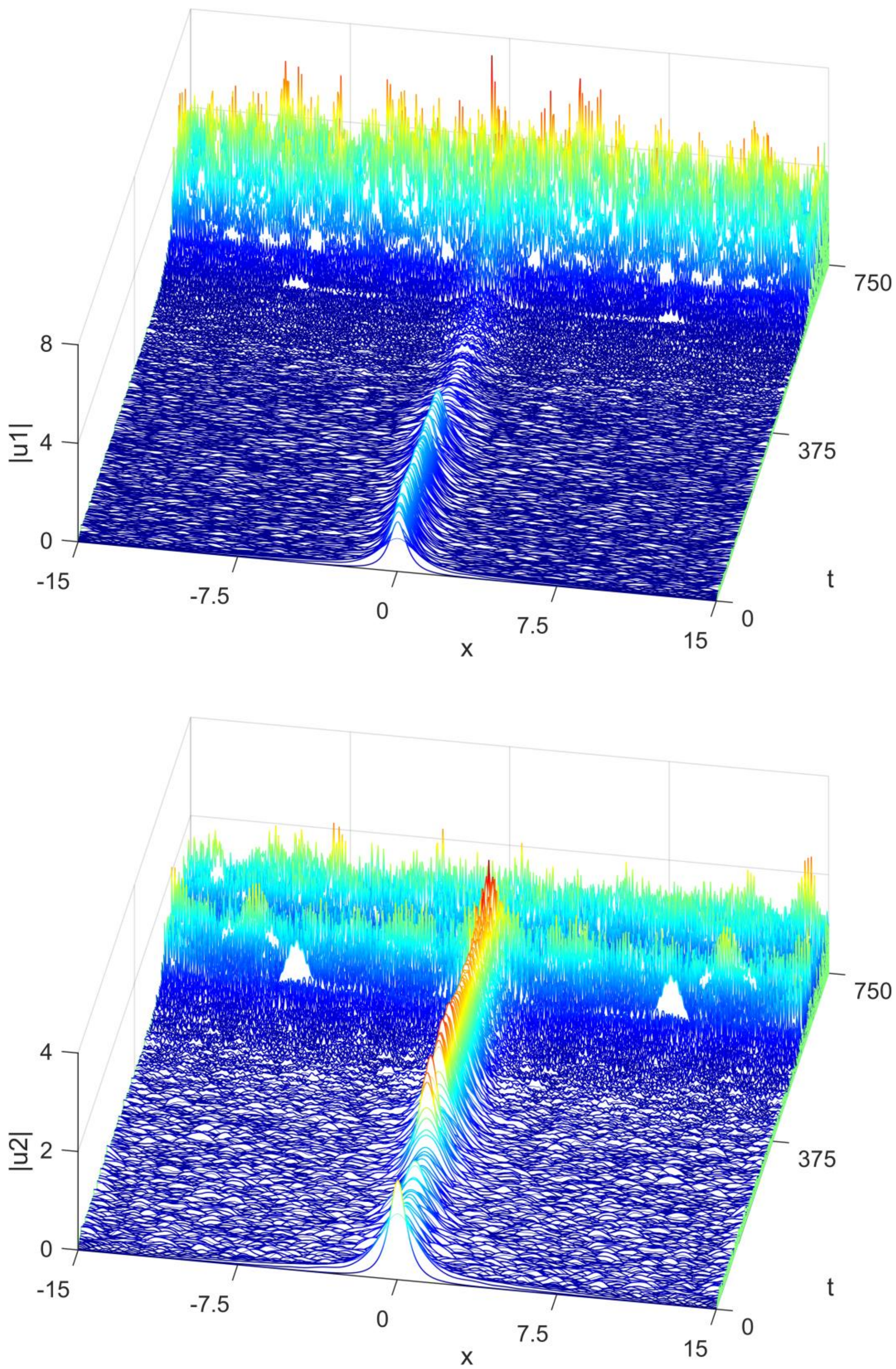

Figure 2.18 Example of unstable waterfall plots. Noise and dispersion in the solution field is easily discernible due to the high contrast of the plot against the neutral background.

Finally, we collected numerical data MATLAB output to table to supplement the plots. MATLAB calculated and collated the data type (including fractional derivative order α, and phase propagation constant μ as 'a' and 'mu' in the nomenclature respectively), its determined stability, maximum amplitude and the power of the initial conditions, the arithmetic mean of the peak amplitudes, the root mean square of the peak amplitude: from there the dispersion was determined [63].

2.2.1 Power and propagation constants

We explore solutions of the form

$$u(x,t) = Ae^{i\mu(kx-\omega t)}. \tag{2.1}$$

The solutions here include constants to ensure the arguments of the functions remain non-dimensional, that is, the wave frequency ω, the wave number k, and additionally the phase propagation constant μ.

The constant μ is defined as the complex number $\mu = \alpha + i\beta$, where α represents the real attenuation, and β is the phase constant [19, 49, 64]. The phase propagation constant μ provides a measure of amplitude attenuation and phase change per wavelength.

The power of the soliton wave is defined as follows:

$$P = \int_{-L}^{L} |u(x,t)|^2 dx \tag{2.2}$$

Where L represents the spatial boundary limit, and $u(x,t)$ is the initial condition of the solution. The physical interpretation of soliton power is the power required for a soliton with a certain pulse width to propagate effectively through a medium [19, 49, 64].

At the end of each different fractional derivative order α, we present a bifurcation diagram using the initial conditions with the power 'P' and maximum peak amplitude at t = x = 0 to calculate the value of the bifurcation parameter μ [3, 5, 7-9, 22, 36, 51, 65]. Information calculated to supplement the plots were output to table, such as Table 2.1, for each dataset.

Table 2.1: Stability data

Data Pair	Stability	Abs. Max. Amp.	Power	u_1 Ar. Mean	u_2 Ar. Mean	u_1 RMS	u_2 RMS	u_1 Disp.	u_2 Disp.
a_2p0_ mu_1p5	Stable	1	4	0.91	0.91	0.91	0.91	0.04	0.04

Five programs of MATLAB code were written to calculate the FFT, collect data and generate figures (available in Appendix B). Close to 10000 files and 6 gigabytes of data were produced from the experiments and considered for the results section.

2.3 Experimental procedure and results

The data sets were processed in terms of fractional derivative order α, phase propagation constant μ, and bifurcation plots are presented in terms of power, P, and phase propagation constant μ [36]. Solutions u_1 and u_2 were grouped in pairs classified simply as 'u', where the fractional derivative value α → a, the phase propagation constant μ → mu, and whether the solutions initial values were symmetric or asymmetric. Therefore, solution pairs followed the nomenclature of 'u_data_a_X_mu_Y_sym' corresponding to a fractional derivative of order 'X', phase propagation constant 'Y' for a symmetric soliton pair 'u' consisting of u_1 and u_2. For an asymmetric soliton pair, the name contains the suffix ‘asym’. The experiments were run from the customary second order derivative $\alpha = 2$, iteratively reducing the order by tenths until $\alpha = 1.1$.

Not all figures will be produced for each soliton pair. Instead, figures used to guide the stability assessment will be displayed in the results section. Given the qualitative nature of identifying stability in solitons, and without strict definitions of solitons or their stability, we collect as much information as possible during the data collection process to support our conclusions and approach a more quantitative analysis.

CHAPTER 3 RESULTS

We display results in groups of fractional derivative order from $\alpha = 2.0$, to $\alpha = 1.1$, where we present stability and other dynamics associated with the same solution pair for different values of α. Not all results from each fractional experiment will be displayed. Instead, the general behaviour of the system will be described between displays of more interesting dynamics produced between various values of α.

3.1 Fractional derivative $\alpha = 2.0$

In this section we present results corresponding to the fractional derivative of order $\alpha = 2.0$.

3.1.1 u_data_a_2_mu_1p5_sym

We see in Figure 3.1 a stable, symmetric soliton pair with a phase propagation constant $\mu = 1.5$.

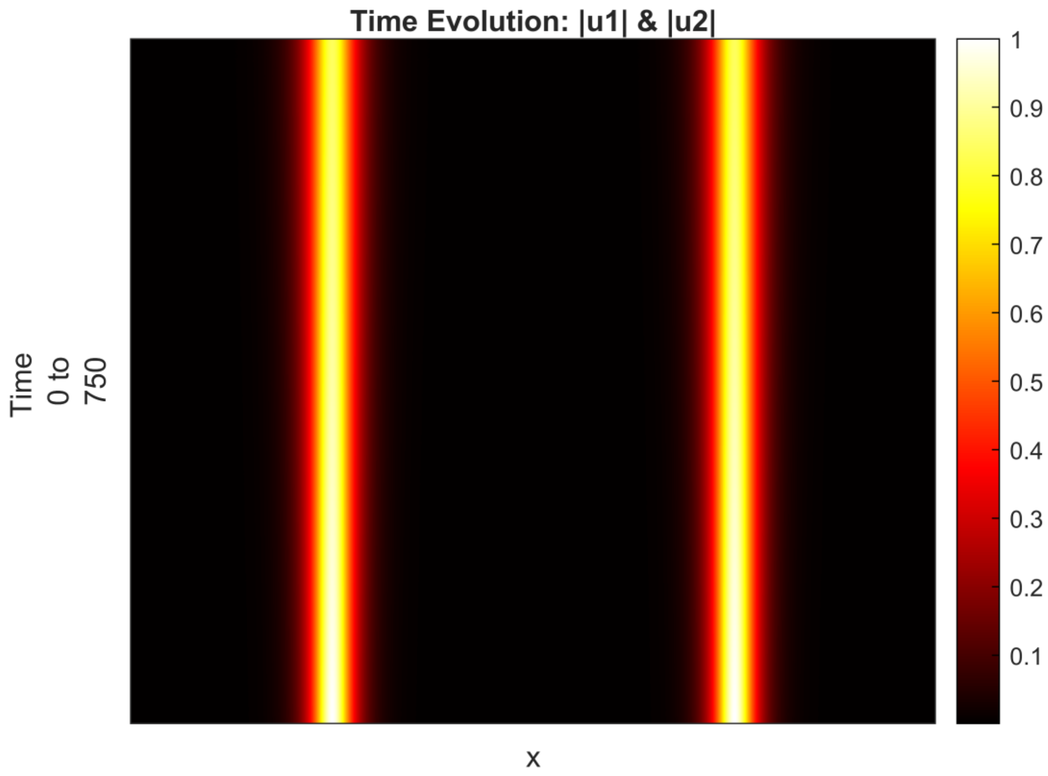

Figure 3.1 Stable, symmetric soliton pair.

From Figure 3.1, we can see there is little decline in peak amplitude over the course of the experiment, and there is no evidence of oscillatory behaviour or dispersion throughout the experiment, so we conclude this solution is a stable, symmetric, soliton pair.

3.1.2 u_data_a_2_mu_1p8_asym

Here we present an asymmetric solution with a phase propagation constant $\mu = 1.8$.

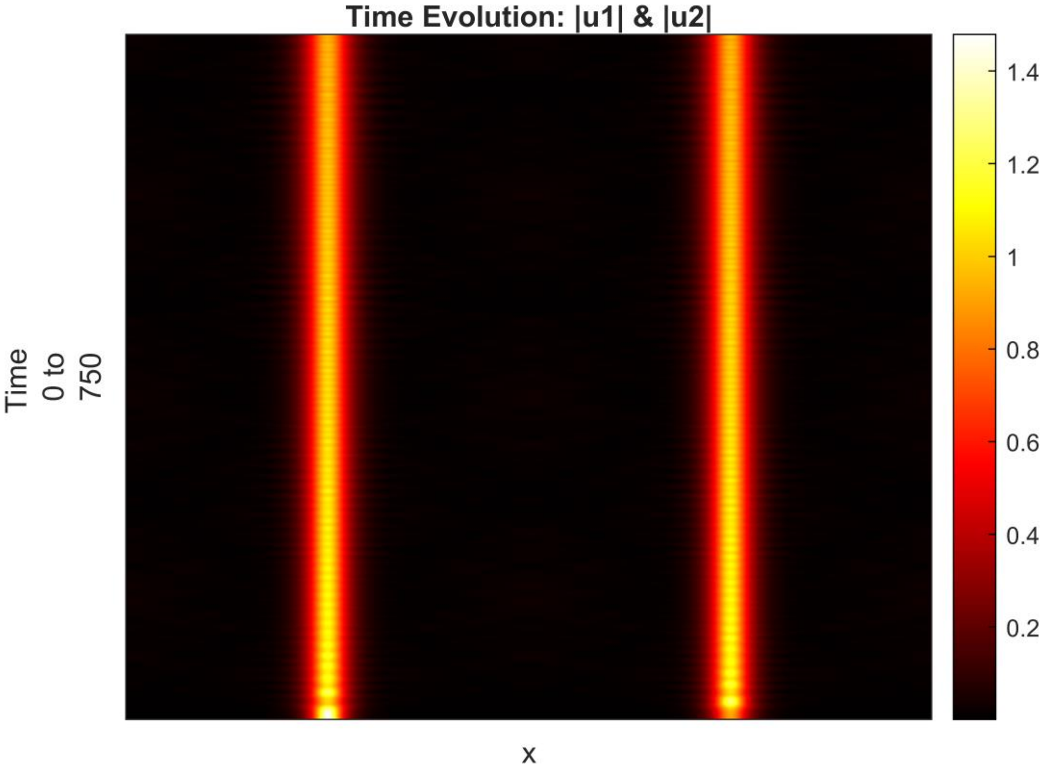

Figure 3.2 Unstable, asymmetric soliton pair.

We see from the heatmap in Figure 3.2 what appears to be unstable, asymmetric solutions. Looking closely in Figure 3.3 we observe dispersion and irregular oscillations throughout the experiment. Therefore, we conclude this solution is an unstable, asymmetric solution pair.

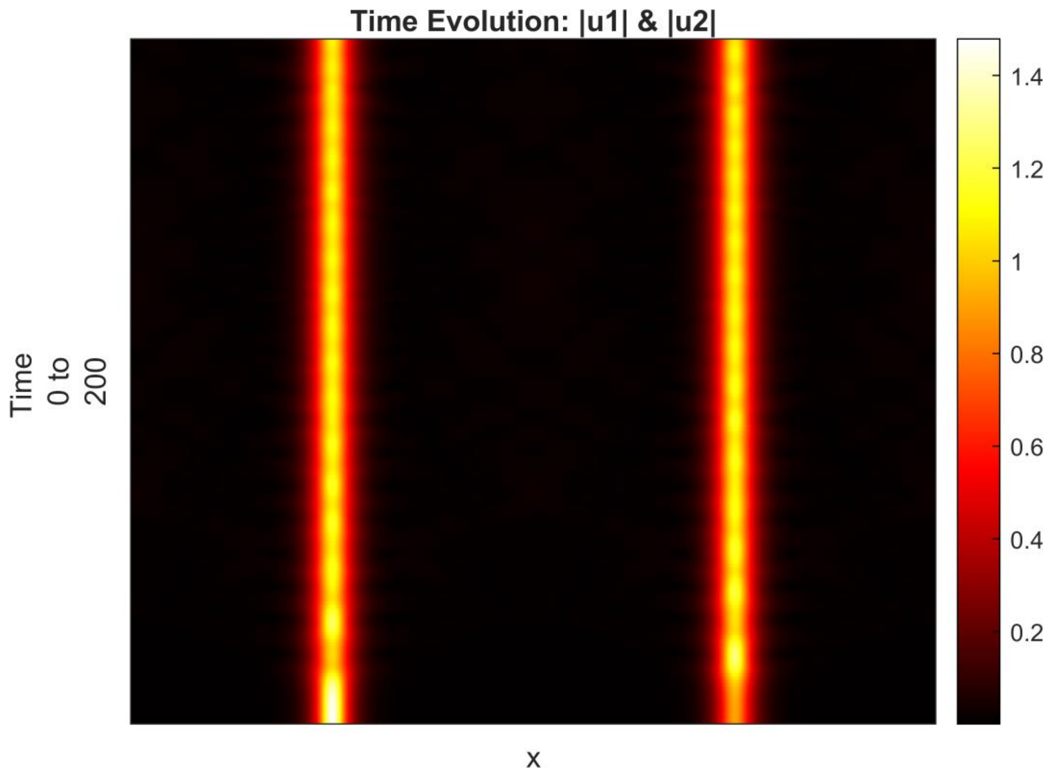

Figure 3.3 A closer inspection at 200t more clearly shows the asymmetry of the soliton pair, and varying oscillation wavelengths throughout the experiment.

We confirm the unstable assessment by looking at the peak amplitude evolution in Figure 3.4 and direction field in Figure 3.5, which both show behaviour consistent with unstable asymmetry for these experiments. We see asymmetry and group velocity oscillations in the peak amplitude evolution, and instability in terms of erratic phase. These erratic oscillations result in the direction field shown in Figure 3.5 with a relatively wide ‘tornado’ or ‘funnel’ pattern, indicating unstable behaviour from the solutions.

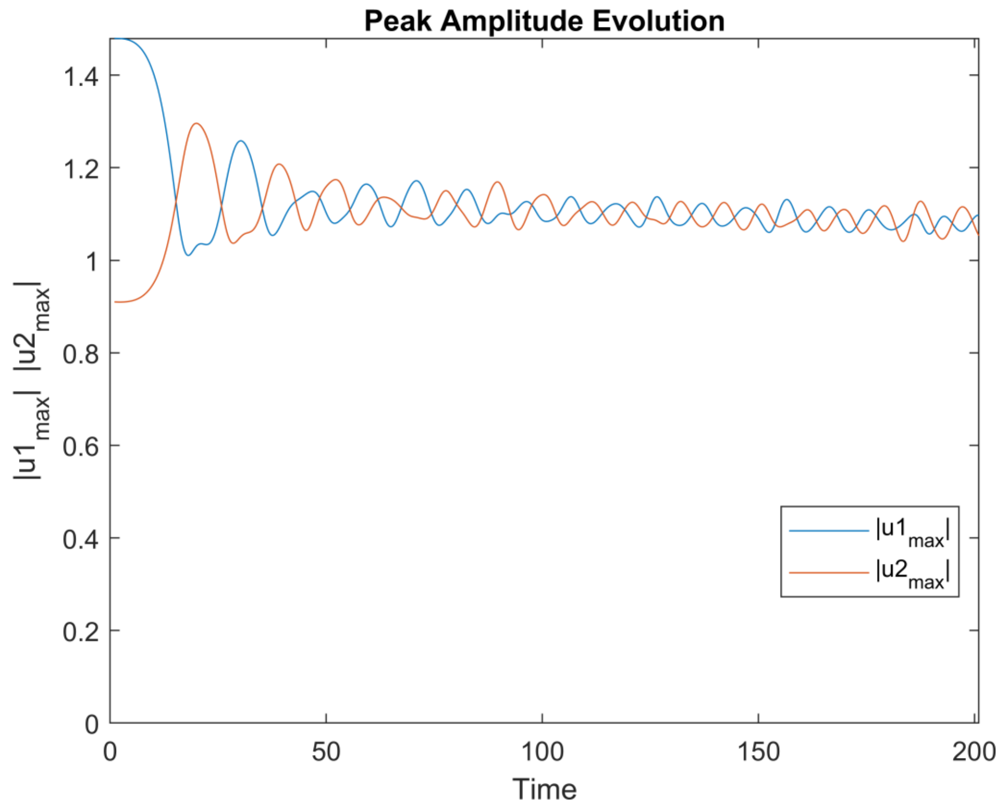

Figure 3.4 The peak amplitude shows asymmetry and erratic oscillations.

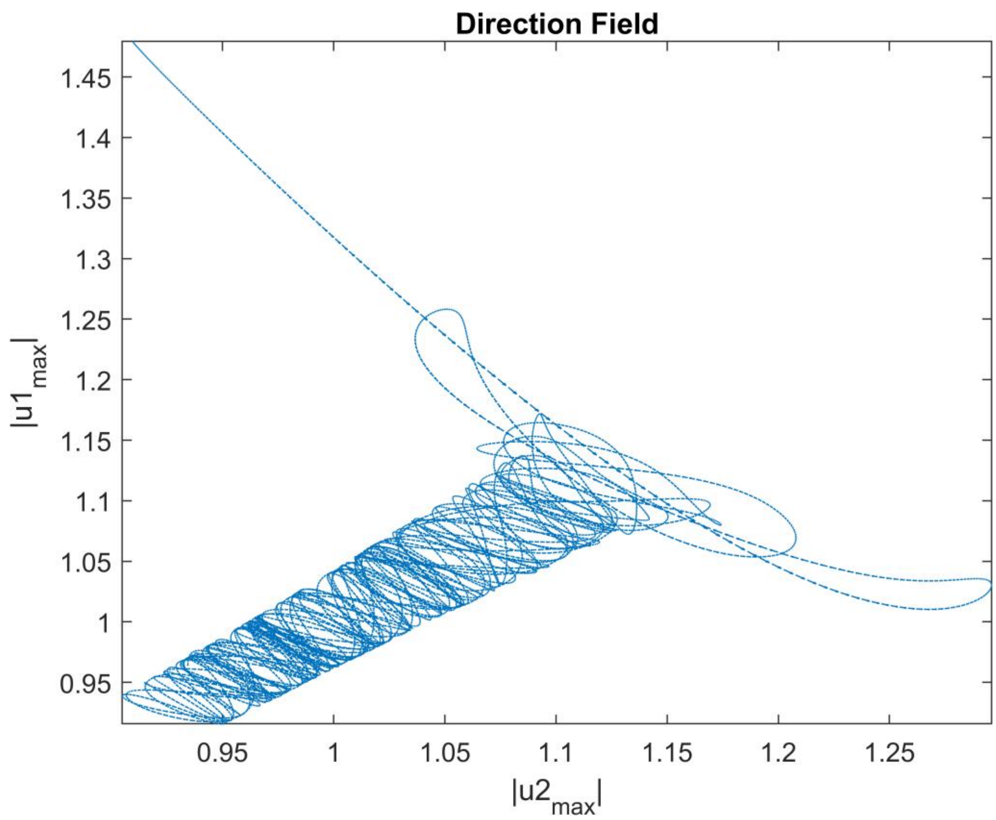

Figure 3.5 Direction field for unstable asymmetric pair.

3.1.3 u_data_a_2_mu_1p8_sym

The following results correspond to symmetric solutions with a phase propagation constant $\mu = 1.8$.

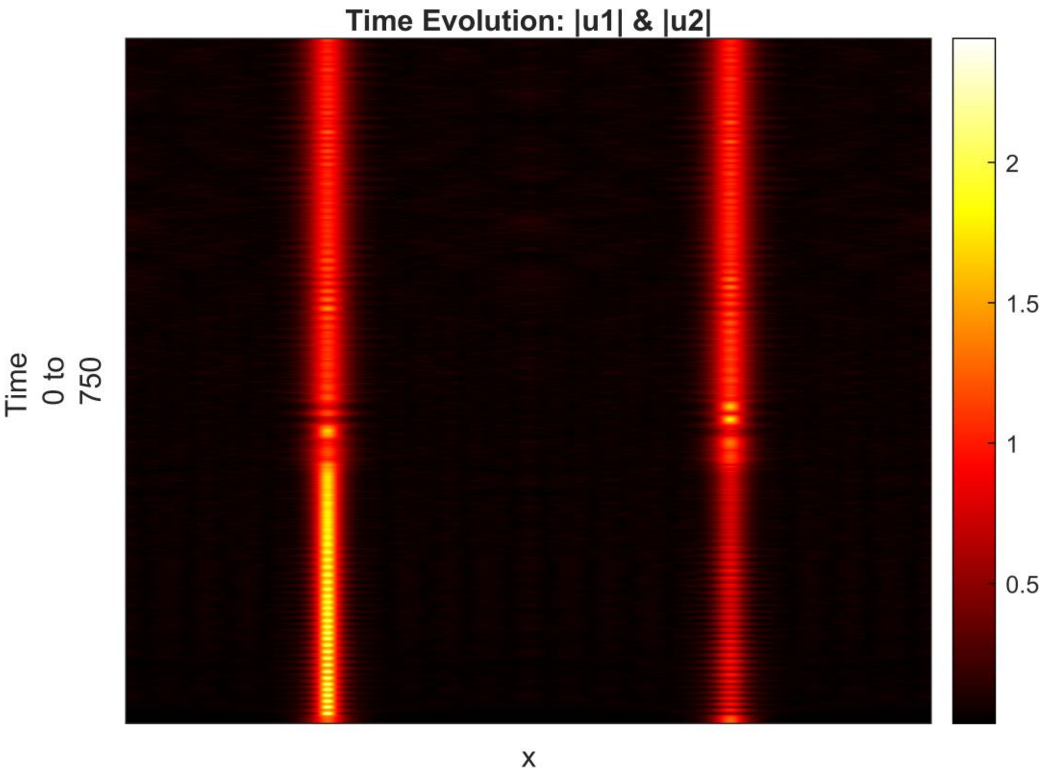

Figure 3.6 Asymmetric, unstable solution pair.

From the heatmap in Figure 3.6, we notice a break in symmetry almost immediately, leading to the solutions converging asymmetrically, followed by bright/dark pulses. The experiment concludes with oscillations and dispersion. Instability is confirmed from inspection of the peak amplitude and centre of mass evolution in Figure 3.7.

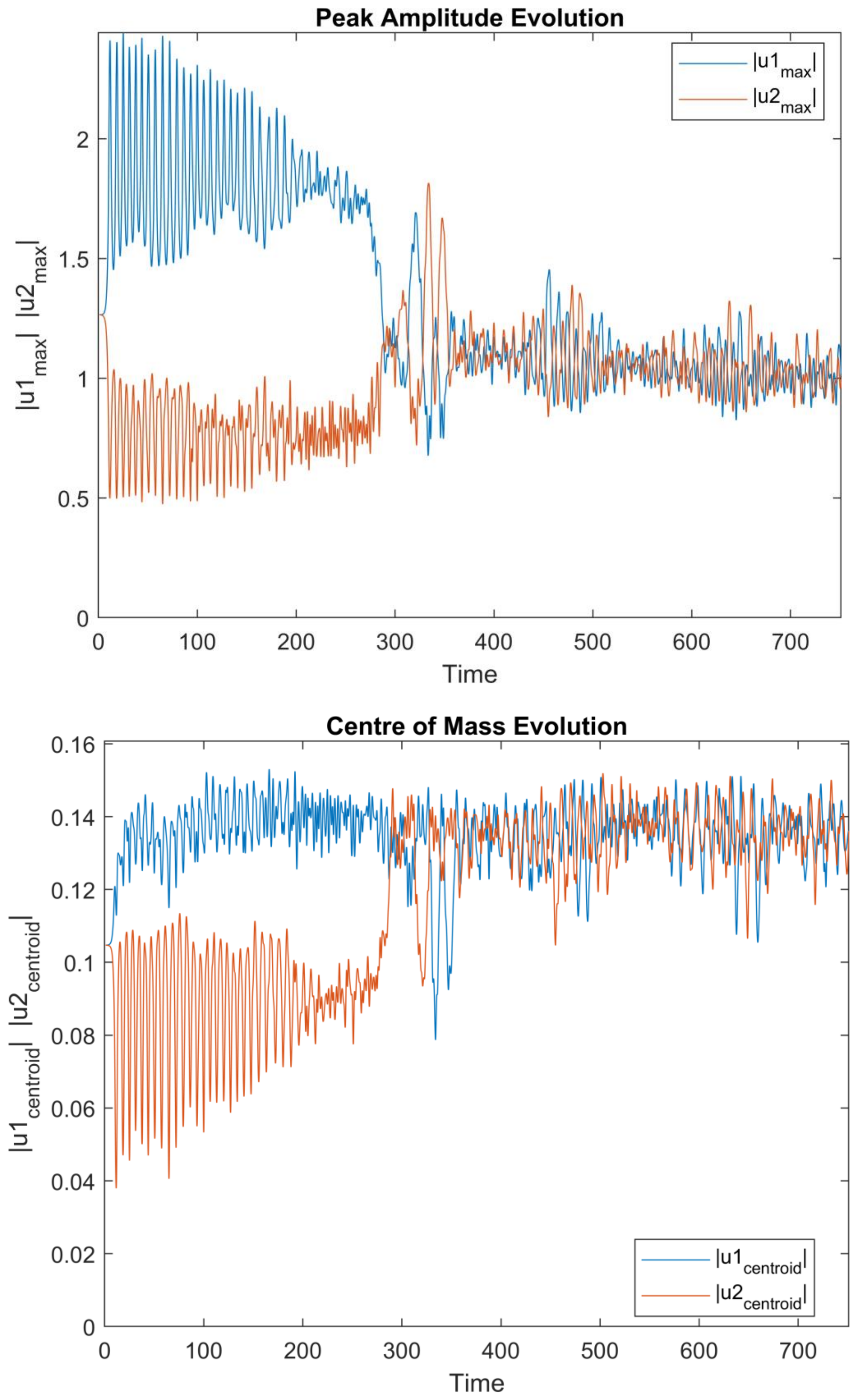

Figure 3.7 The peak amplitude evolution illustrates the instability and convergence of this asymmetric pair (top), and the centre of mass evolution for reference (bottom).

If we inspect the peak amplitude evolution in Figure 3.8, we see symmetry break very early in the experiment.

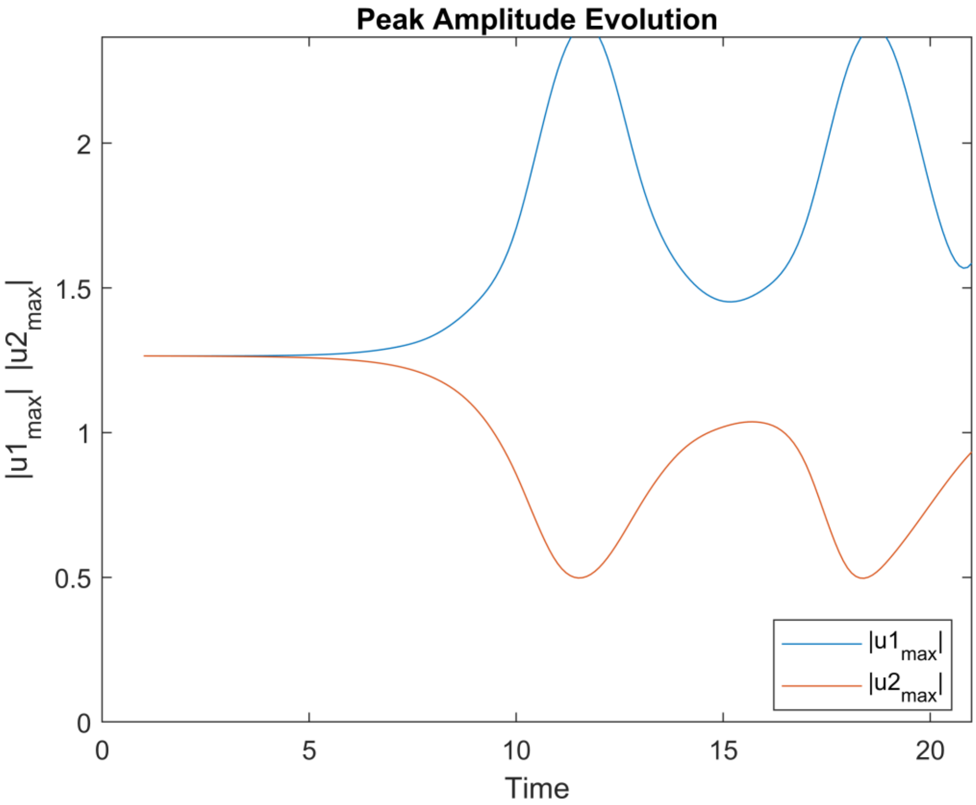

Figure 3.8 Here we see the solutions break symmetry almost immediately, and quickly continue oscillating as an asymmetric solution pair.

3.1.4 u_data_a_2_mu_2_asym

The following results correspond to an asymmetric solution with a phase propagation constant $\mu = 2$.

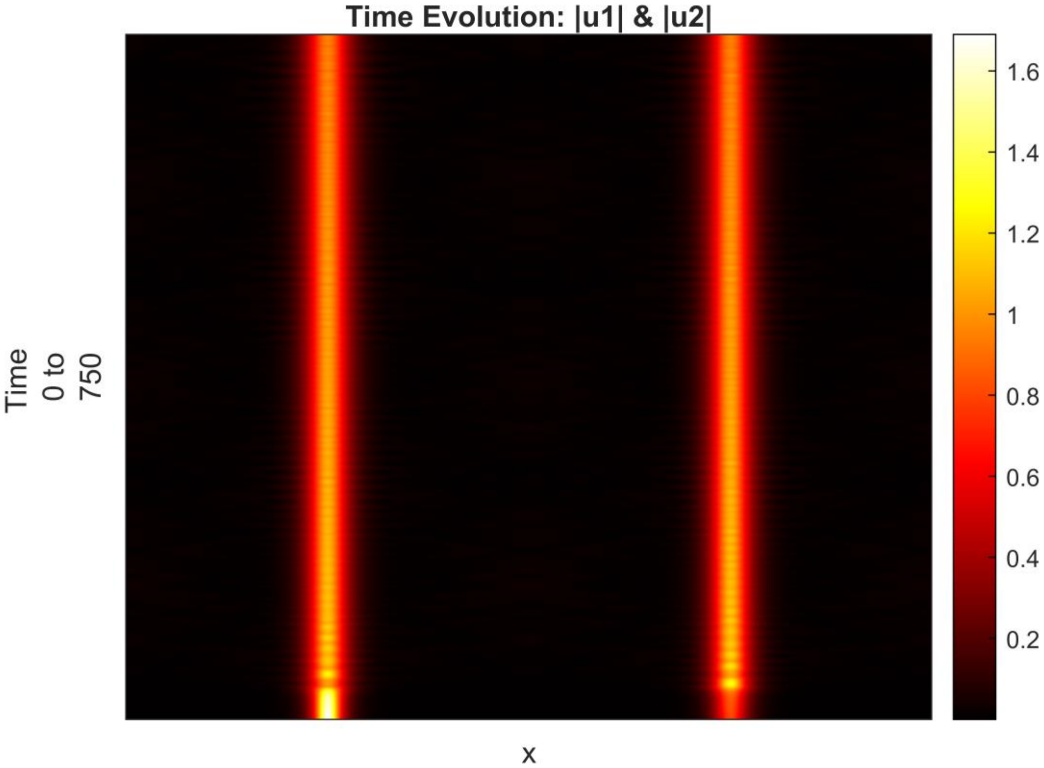

Figure 3.9 Stable, asymmetric solutions when $\alpha = 2$

The heatmap in Figure 3.9 shows the results for a stable, asymmetric solution pair. We see some decay in peak amplitude and a corresponding increase in dispersion throughout the progression of the experiment. Therefore, we refer to the direction fields in Figure 3.10 below which indicate stable, asymmetric solutions with corresponding narrow 'tornado' effects.

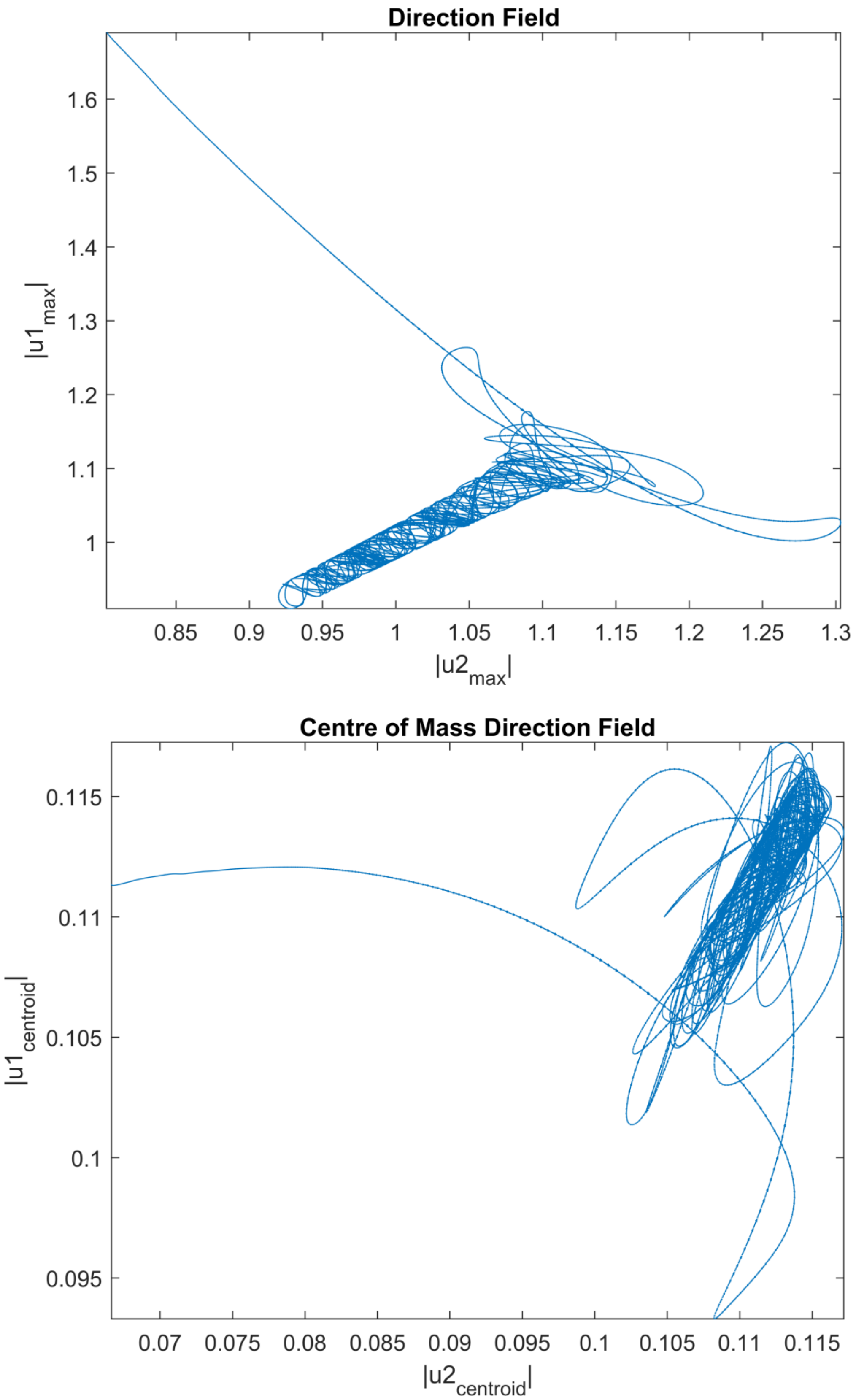

Figure 3.10 Direction field behaviour for stable, asymmetric pair, with peak amplitude (top) and centre of mass (bottom).

We see convergence in the centre of mass as the solutions become more symmetric over the course of the experiment. The peak amplitude evolution in Figure 3.11 shows the solutions become stable after approximately 200t, where oscillations remain consistent until approximately 900t, when the experiment becomes numerically unstable.

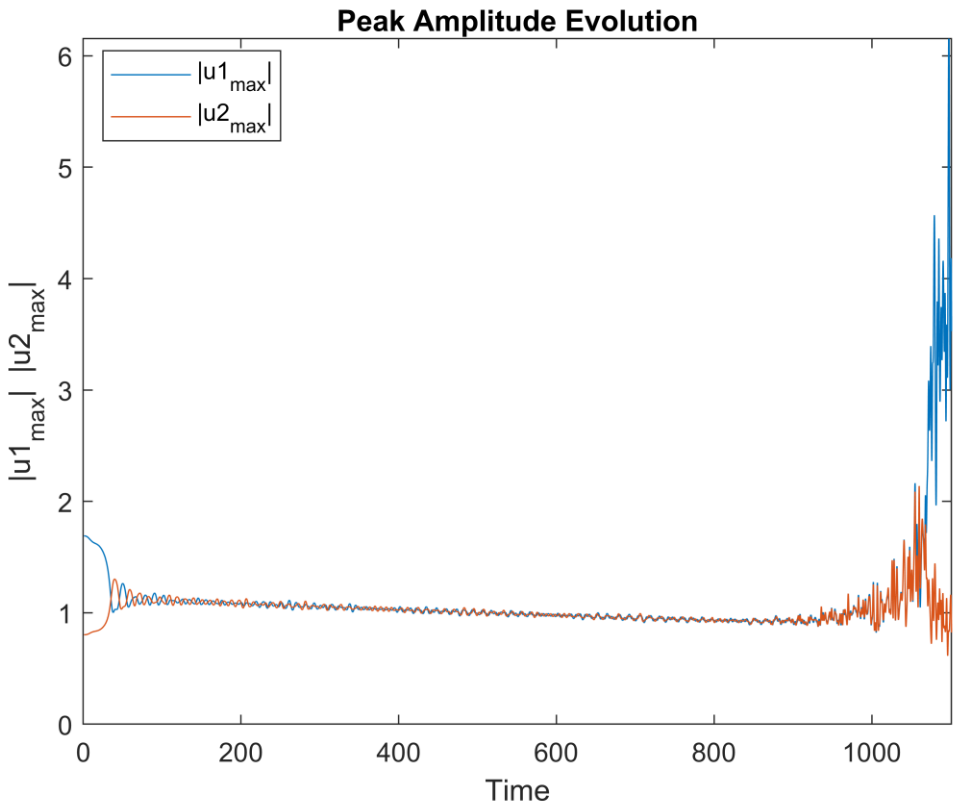

Figure 3.11 The peak amplitude evolution shows the inner wave of the solutions converge and begin propagating symmetrically until approximately 900t.

A close inspection of the peak amplitude evolution appears to show u_1 and u_2 as asymmetric and converging at the beginning of the experiment until approximately 200t, where it appears the solutions converge, matching group velocity. Here we have evidence of symmetry making behaviour.

3.1.5 u_data_a_2p0_mu_2p0_sym

Here we show the results of a symmetric solution with a phase propagation constant $\mu = 2$.

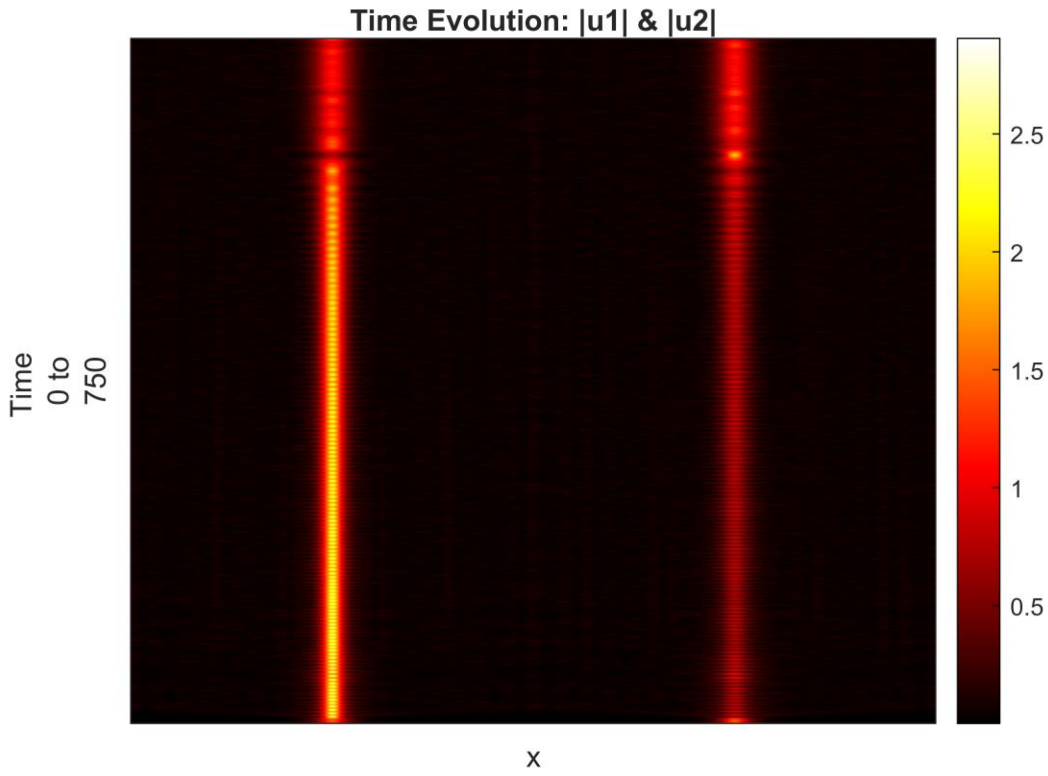

Figure 3.12 Unstable, asymmetric solution pair

The heatmap in Figure 3.12 shows a symmetric solution pair quickly break symmetry and propagate as an unstable asymmetric solution pair. We classify this solution as unstable because it breaks symmetry, and as an asymmetric solution, the peak amplitude oscillations are erratic. From Figure 3.12 and the peak amplitude plot Figure 3.13 we can see u_1 decrease in peak amplitude over time, and a reduction in oscillation frequency over time, switching symmetry before a bright/dark pulse is seen. The experiment concludes with erratic peak amplitude oscillations.

The peak amplitude evolution in Figure 3.13 reveals the extent of instability and shows u_1 and u_2 slowly converging over the course of the experiment.

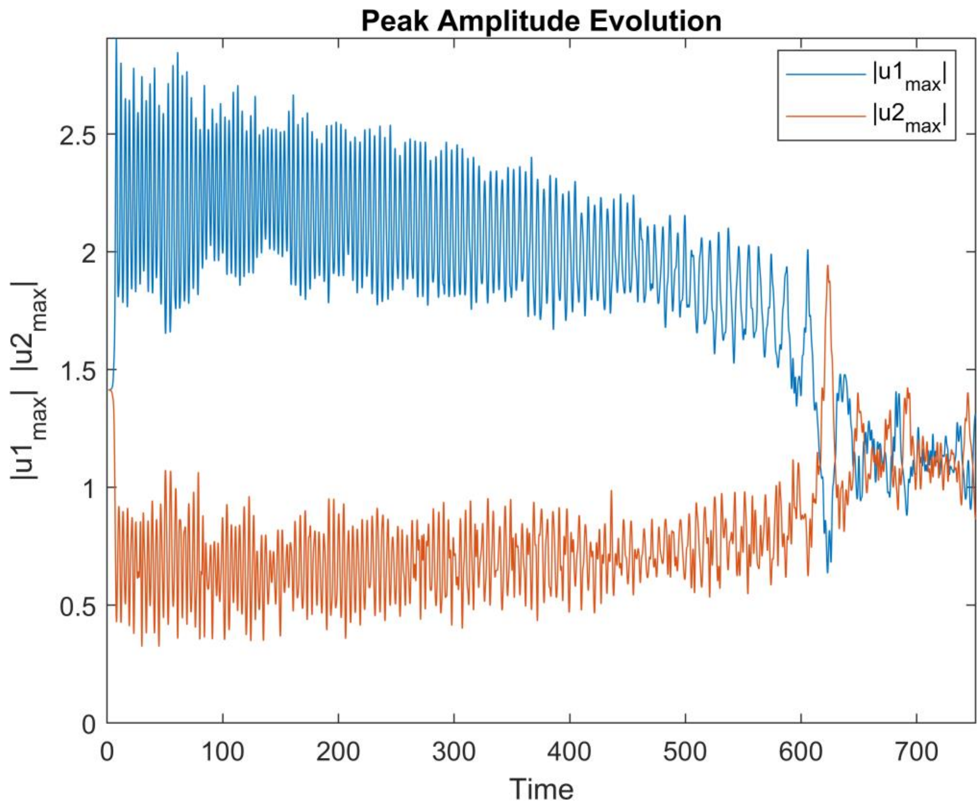

Figure 3.13 The peak amplitude evolution reveals the extent of instability, showing both solutions converging at approximately 610t, switching symmetry, then followed by a bright/dark pulse.

3.1.6 u_data_a_2p0_mu_2p2_asym

Now we present the results of an asymmetric solution with a phase propagation constant $\mu = 2.2$.

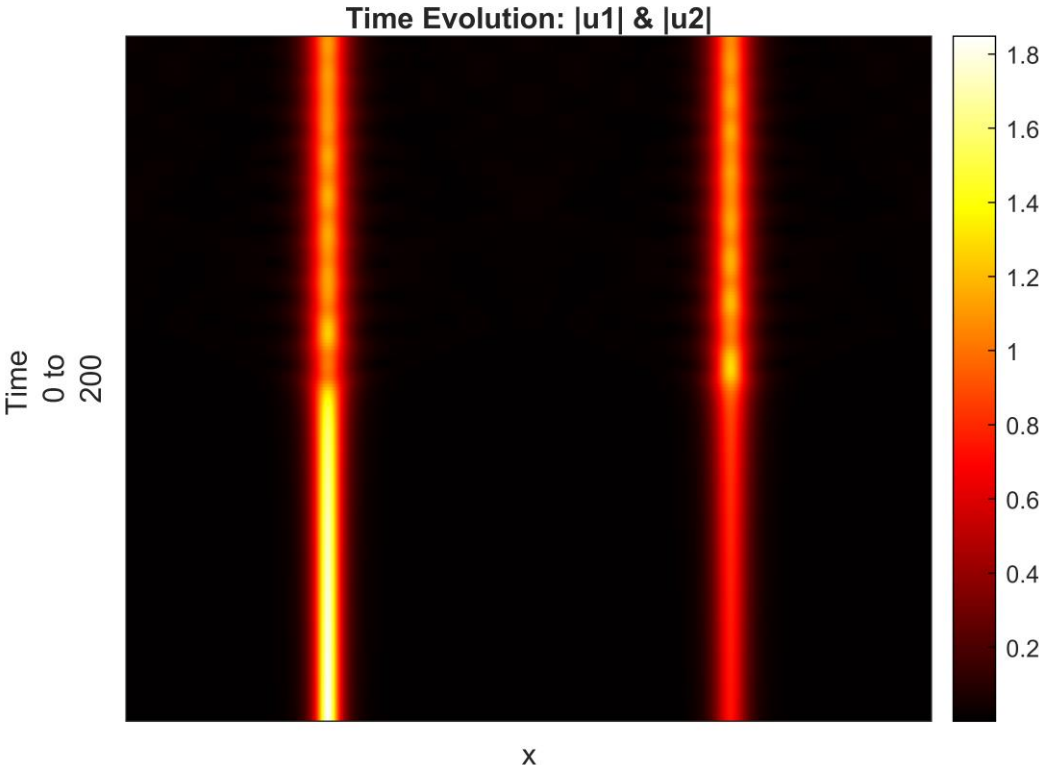

Figure 3.14 Stable, asymmetric pair when $\alpha = 2$.

In Figure 3.14 this experiment shows a stable asymmetric solution pair that begins oscillating after 100t. The peak amplitude evolution in Figure 3.15 confirms the asymmetric solutions converging at approximately 500t.

We determine this solution is stable from Figure 3.15 below. The group velocity is shown to converge in the peak amplitude evolution, consistent with symmetry making behaviour, while stable, symmetric oscillations continue until numerical instability occurs late in the experiment at approximately 900t.

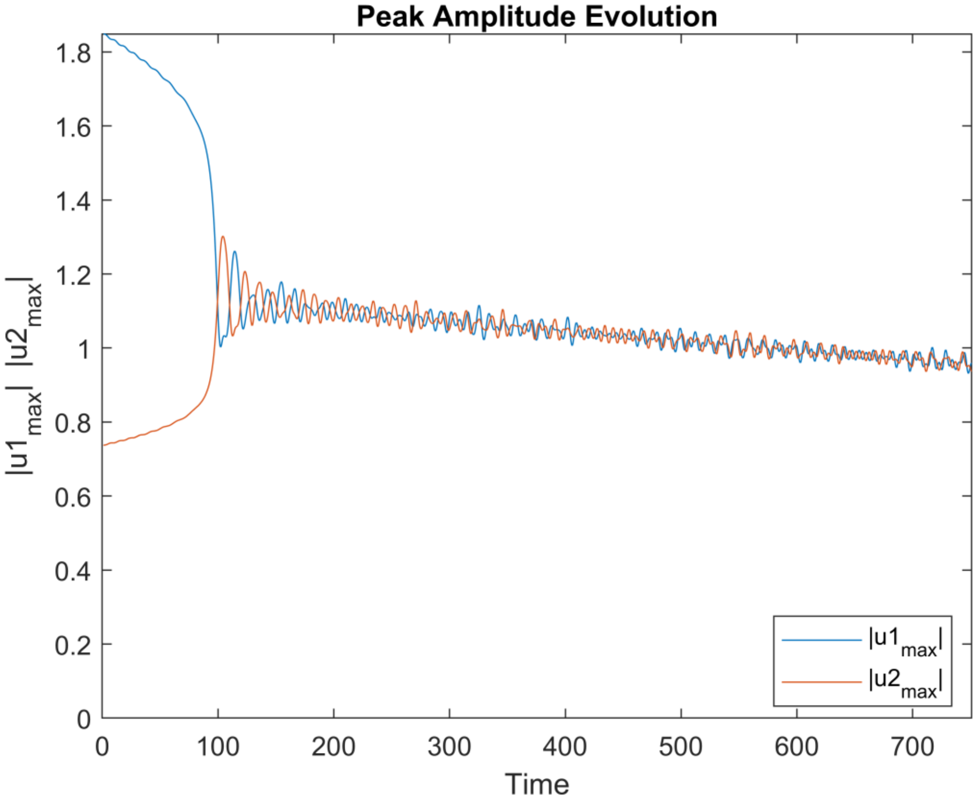

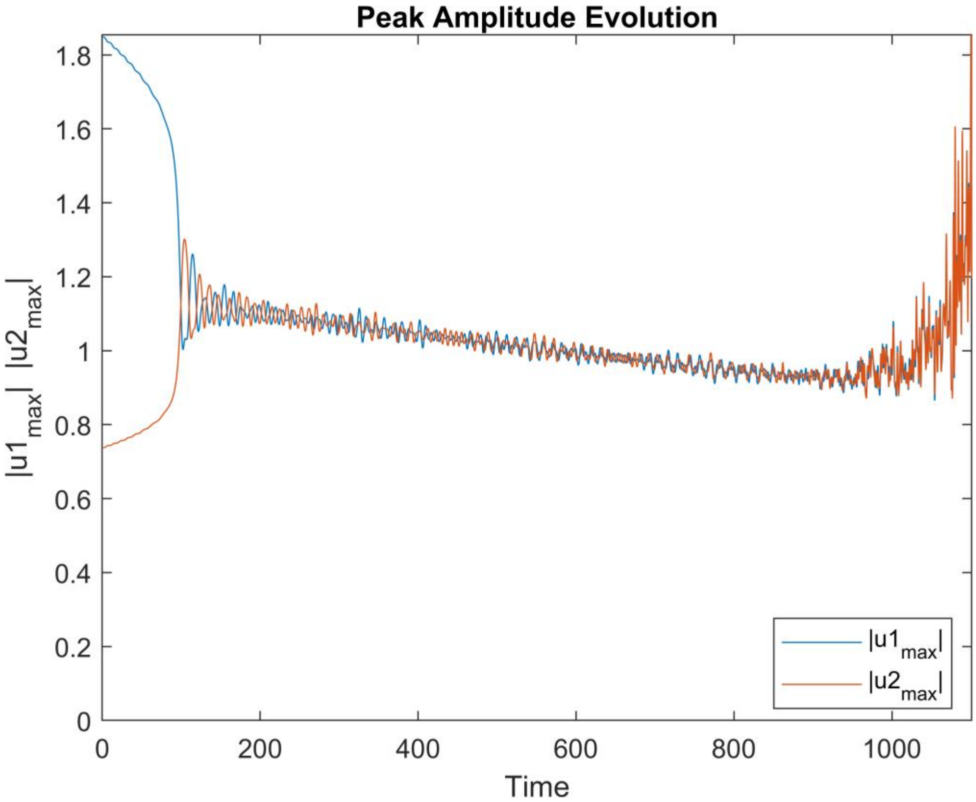

Figure 3.15 Peak amplitude evolution shows converging solutions (top). We see symmetric group velocity propagation from approximately 450t until 800t.

3.1.7 u_data_a_2p0_mu_2p2_sym

The heatmap in Figure 3.16 reveals an unstable, asymmetric solution pair, as the frequency of the oscillations varies from the initial conditions throughout the experiment. Here the solutions have a phase propagation constant $\mu = 2.2$.

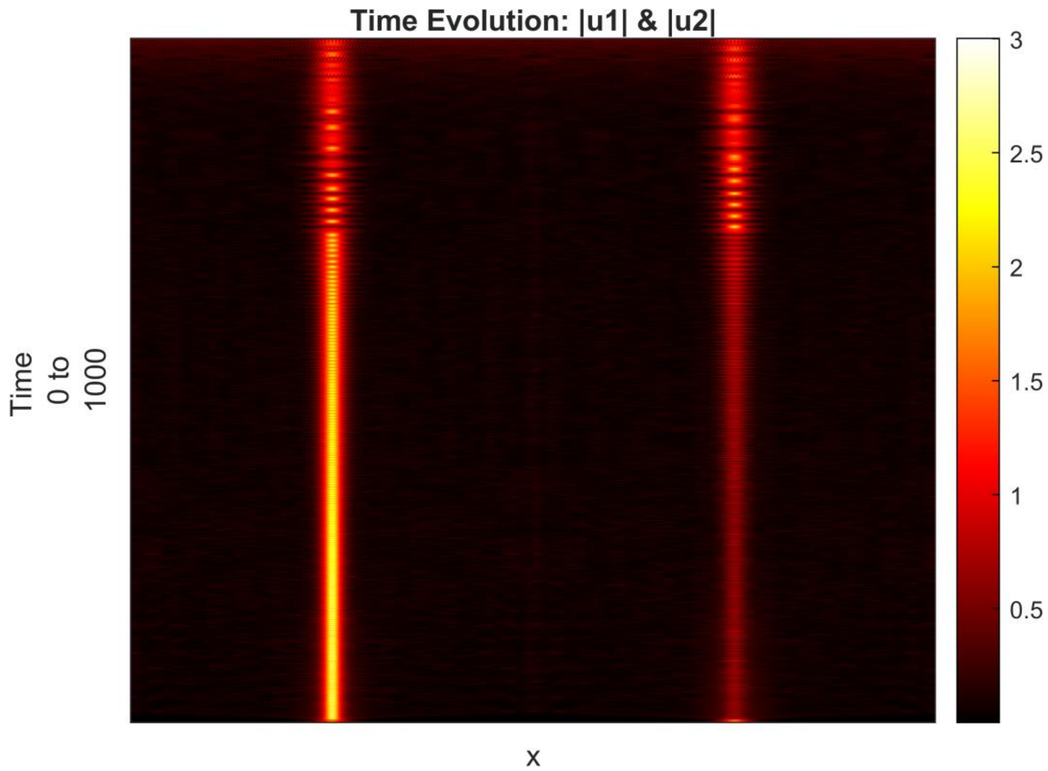

Figure 3.16 The heatmap reveals this unstable solution pair propagates asymmetrically.

Looking at the following peak amplitude plot in Figure 3.17, we see u_1 and u_2 have the same initial amplitude, however the solutions quickly break symmetry, then converge on each other until what appears to be unstable dark/bright pulses at approximately 725t.

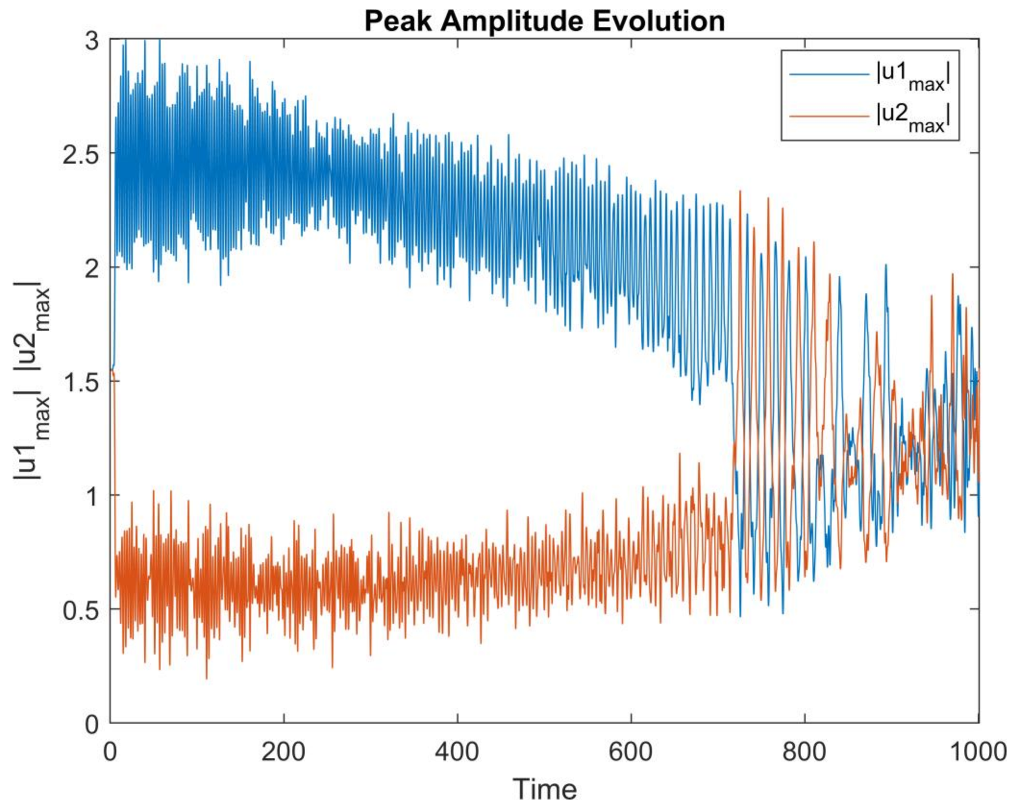

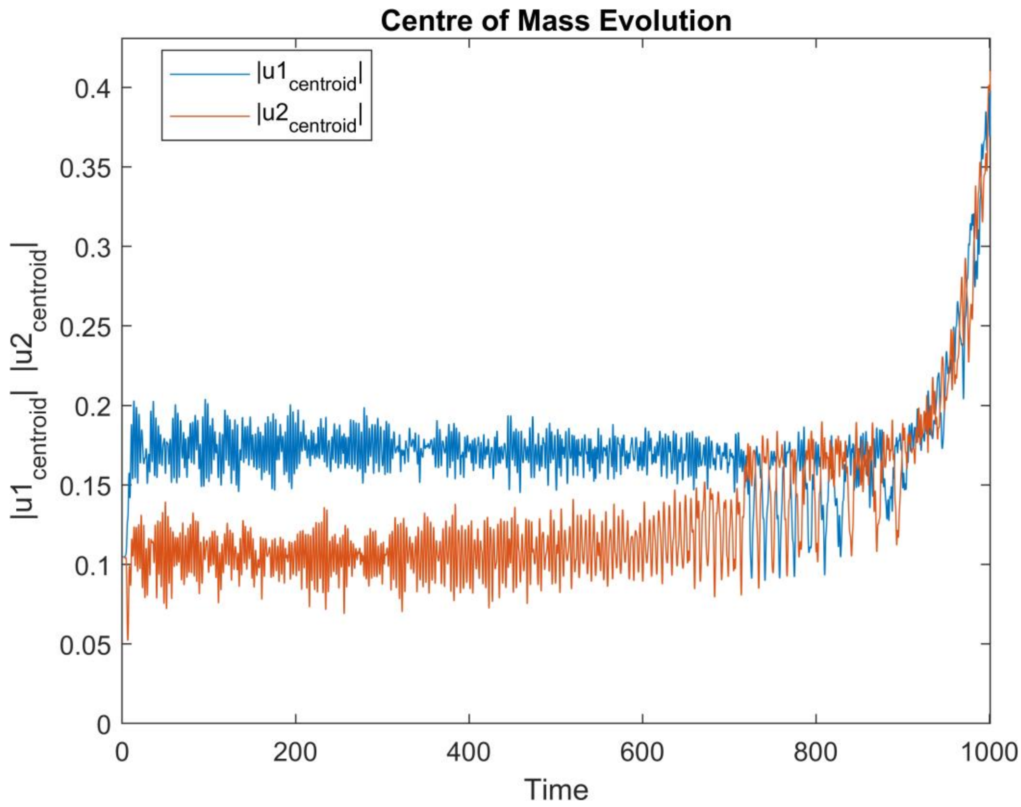

Figure 3.17 The peak amplitude evolution (top) shows convergence and instability for the solution pair. Centre of mass evolution shows increased dispersion as the experiment concludes (bottom).

3.1.8 u_data_a_2p0_mu_2p4_asym

Here we have asymmetric solutions with a phase propagation constant $\mu = 2.4$.

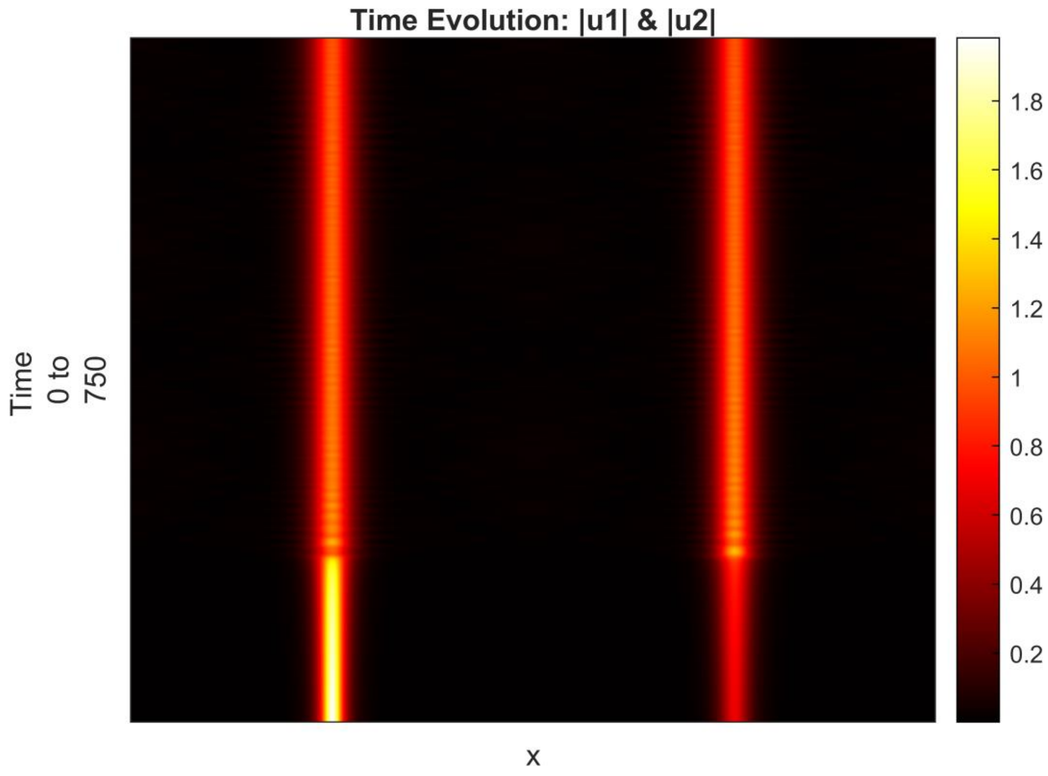

Figure 3.18 Heatmap results of a stable, asymmetric, solution pair.

The heatmap from Figure 3.18 reveals a stable, asymmetric solution pair. There is some evidence of oscillation and dispersion, but after convergence the solutions conserve their behaviour reasonably well throughout the experiment. We see from the peak amplitude plot in Figure 3.19 the true extent of the oscillations, and the convergence of the solution pair ‘u’ over large values of ‘t’.

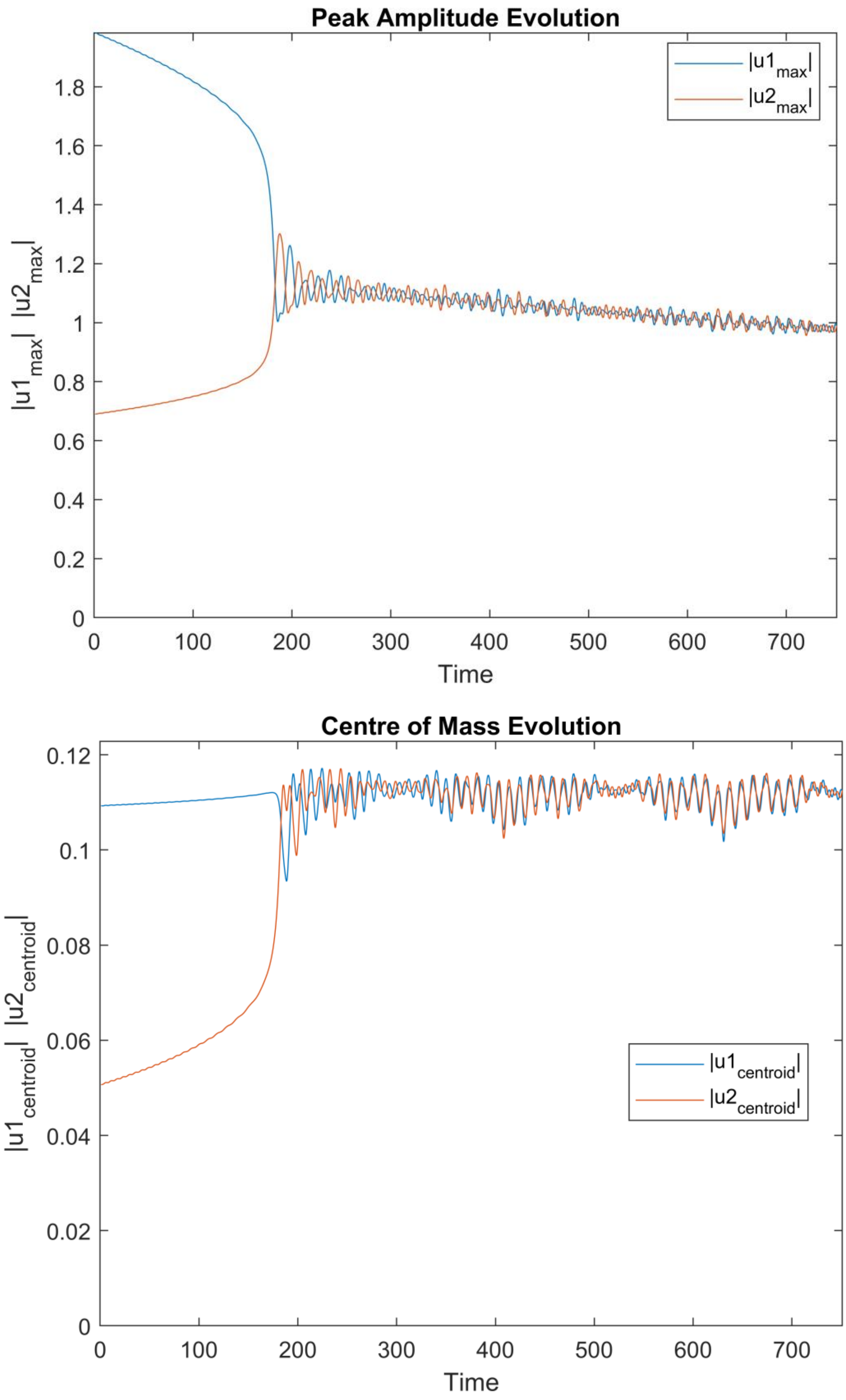

Figure 3.19 Peak amplitude (top) shows u_1 converging on u_2 at approximately 150t. The centre of mass remains reasonably consistent throughout the experiment, indicating minimal dispersion.

The waterfall plots in Figure 3.20 illustrate stability of the solutions.

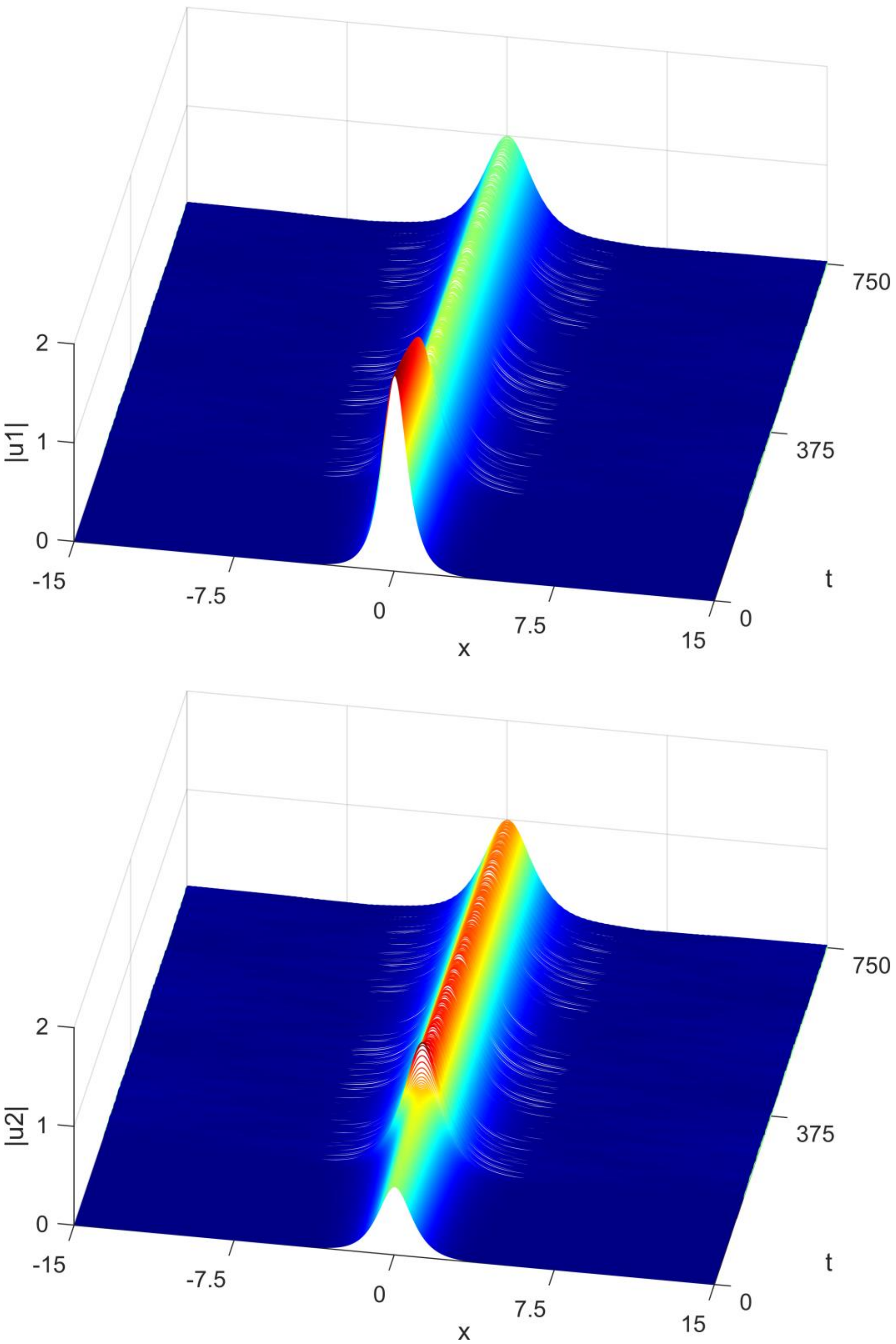

Figure 3.20 Despite the apparent dispersion evident in the heatmap, the waterfall plots show the solutions to be reasonably stable.

3.1.9 u_data_a_2p0_mu_2p4_sym

The Figure 3.21 heatmap from this experiment reveals an unstable, symmetric solution pair with a phase propagation constant $\mu = 2.4$.

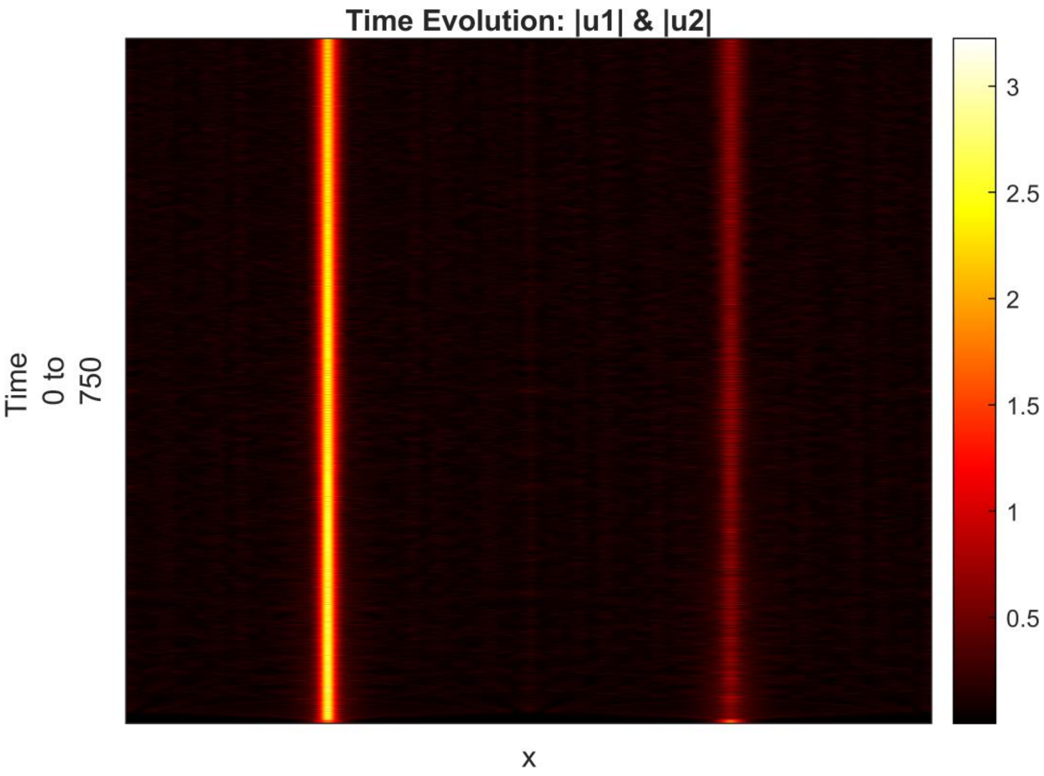

Figure 3.21 Unstable, symmetric solution pair.

If we review the peak amplitude spectrum in Figure 3.22 below, we see evidence of u_1 and u_2 converging as the experiment progresses with erratic oscillations. The centre of mass plot illustrates the oscillatory behaviour of the solutions, however, as the curves maintain a horizontal trend throughout the experiment, we determine there is little evidence of dispersion.

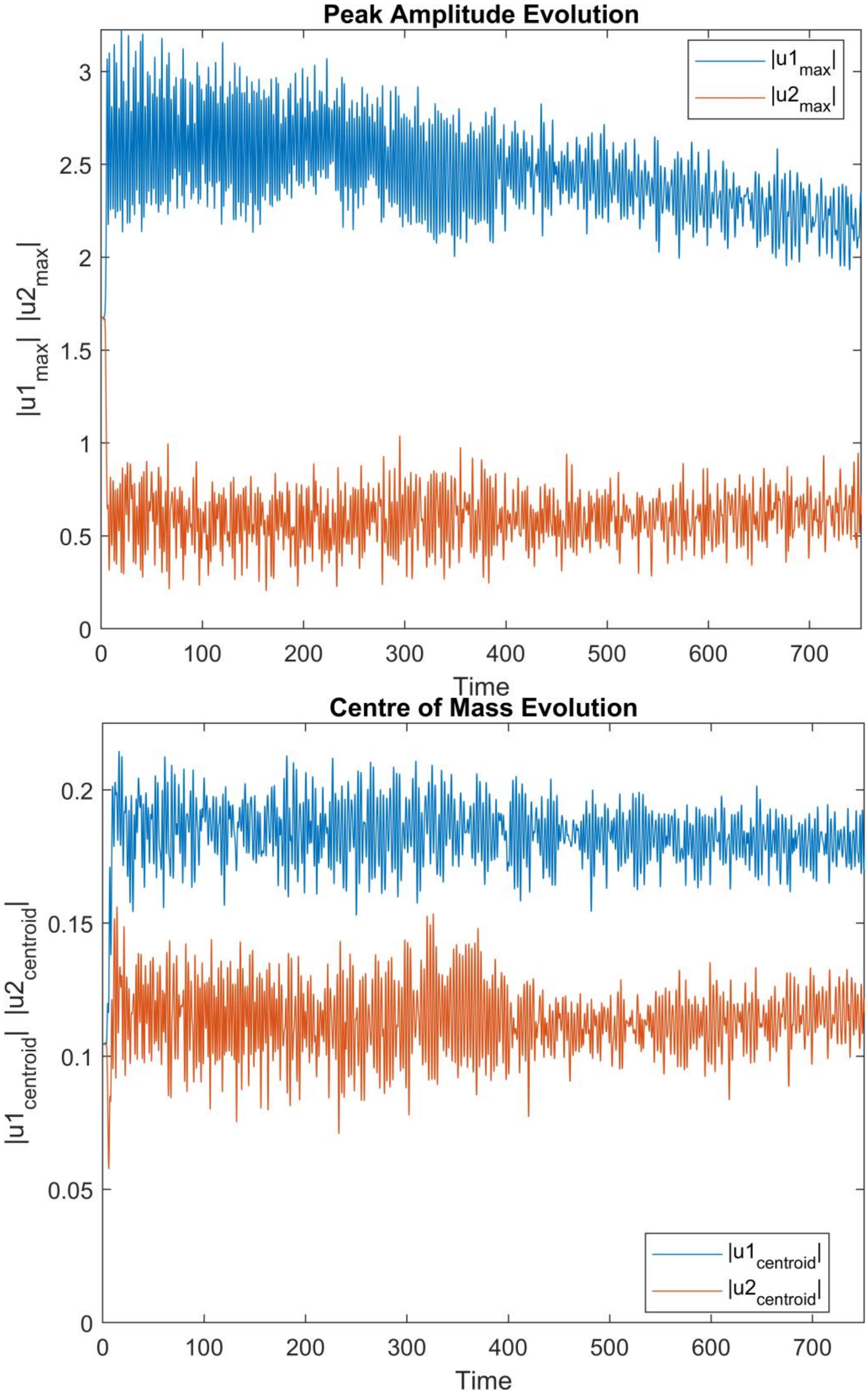

Figure 3.22 Peak amplitude evolution (top) shows u_1 decaying as u_2 increases. The centre of mass evolution (bottom) shows evidence of oscillation, but not dispersion. These plots confirm the asymmetry and instability of the solutions.

3.1.10 u_data_a_2p0_mu_2p8_asym

Experimental results in Figure 3.23 indicate a stable, asymmetric solution pair which begins oscillating approximately halfway through the experiment. The solutions have a corresponding phase propagation constant $\mu = 2.8$.

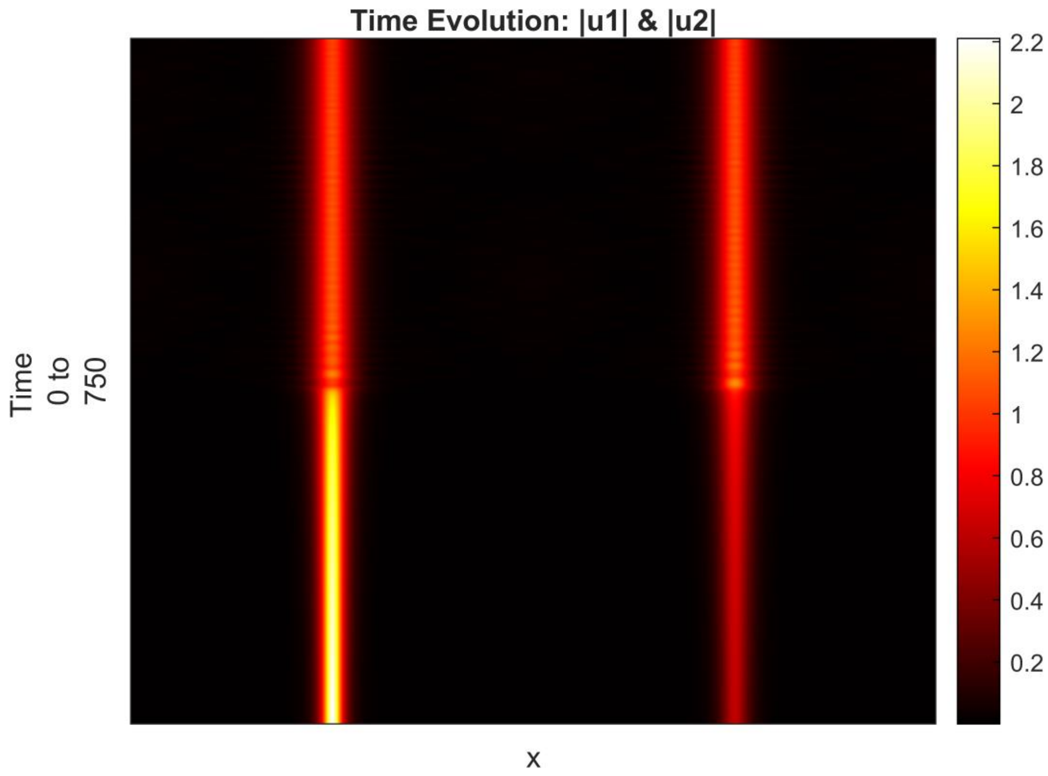

Figure 3.23 Stable, asymmetric solution pair.

Looking at the peak amplitude plot in Figure 3.24, we see u_1 and u_2 converging on each other from the initial conditions until meeting halfway through the experiment at approximately 350t, when the solutions are shown to oscillate asymmetrically.

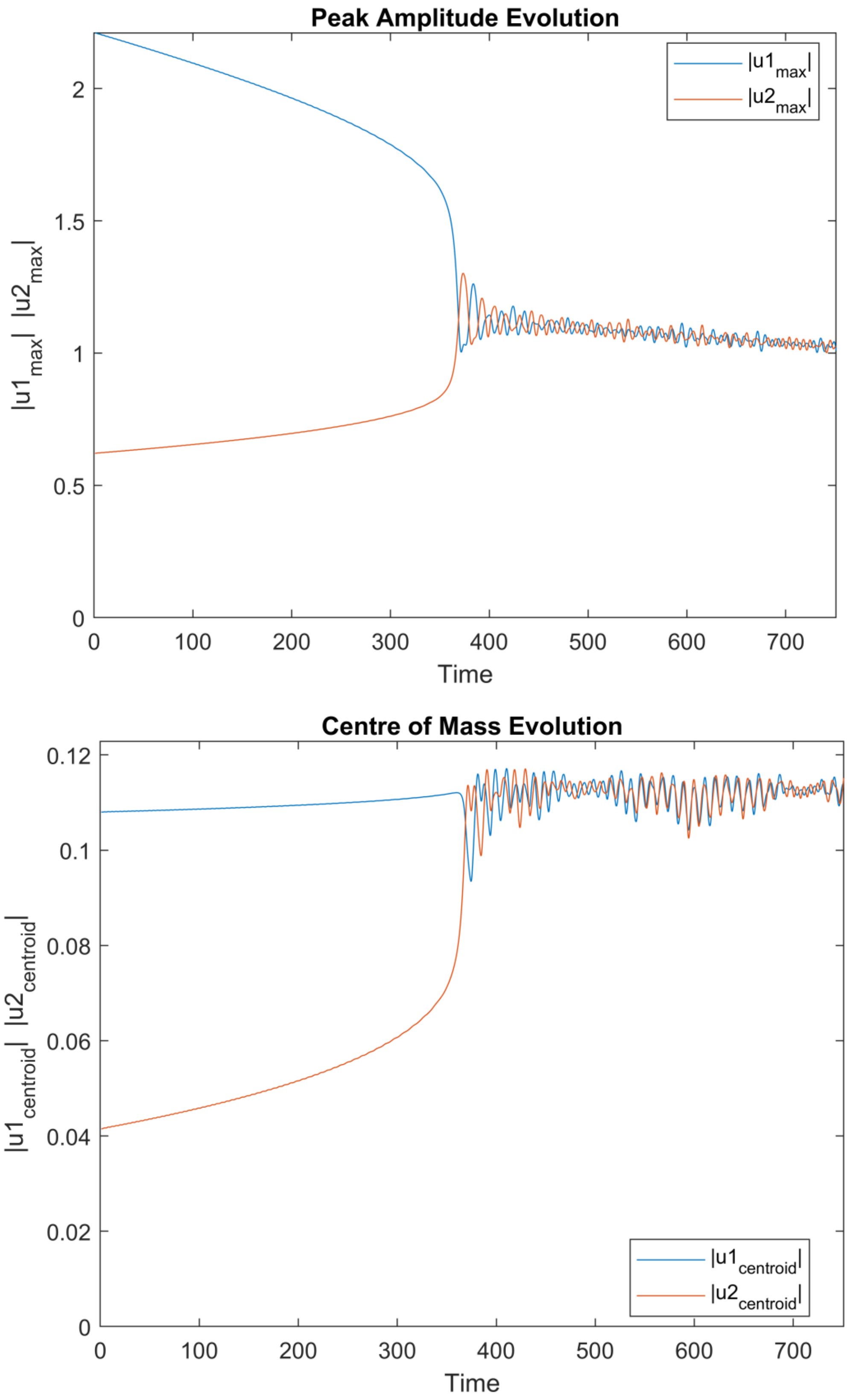

Figure 3.24 The peak amplitude evolution (top) shows asymmetric behaviour for the duration of the experiment. The centre of mass (bottom) for reference indicating oscillations with minimal dispersion.

3.1.11 u_data_a_2p0_mu_2p8_sym

The heatmap in Figure 3.25 shows the results of unstable, focussed, and asymmetric solutions with a phase propagation constant $\mu = 2.8$.

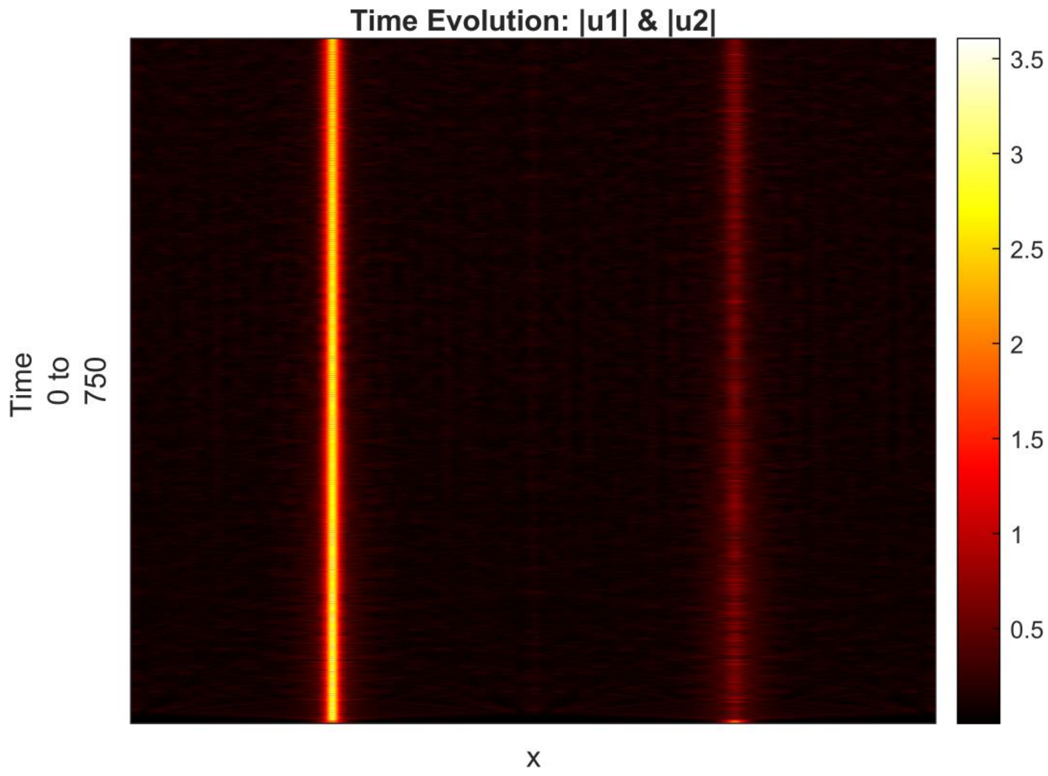

Figure 3.25 Asymmetric, unstable solutions.

We see the peak amplitude plot in Figure 3.26 reveals the full extent of oscillations from the solutions, where we see a difference in group velocity for each solution, and a low peak amplitude from u_2.

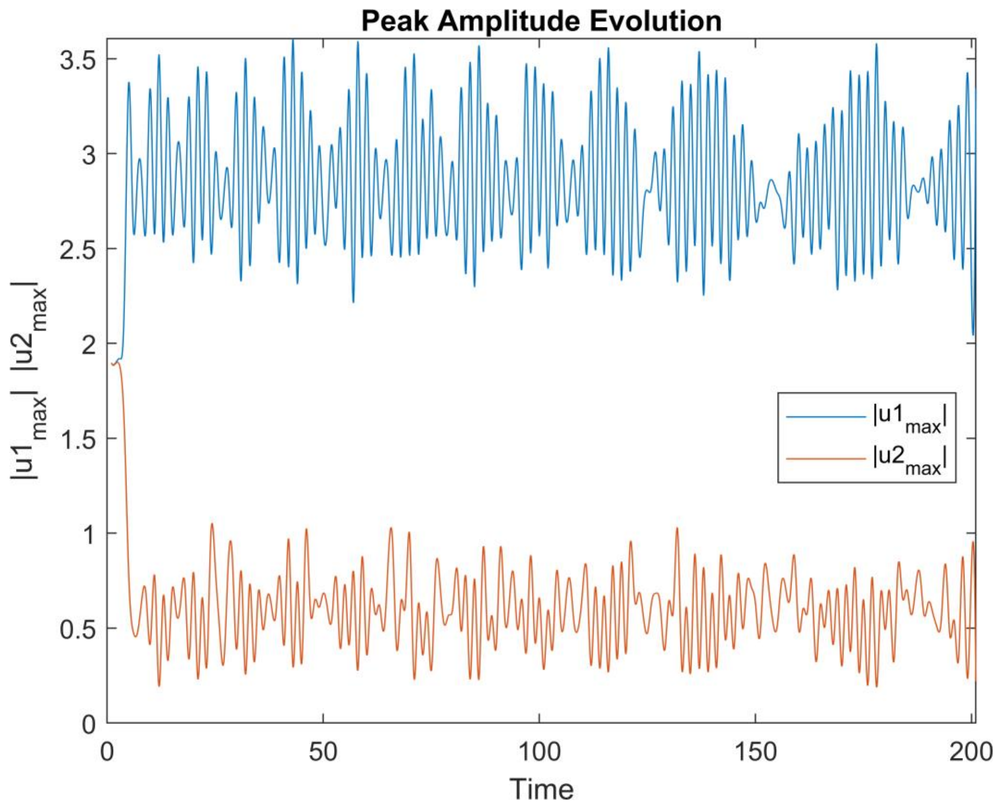

Figure 3.26 The peak amplitudes reveal changing group velocity as each solution evolves.

The instability of the solutions is clear in the peak amplitude evolution plot Figure 3.26, where we see wave envelopes evolving over time for both solutions. If we look closely, we can see the solutions remain symmetric for a very short time period at the beginning of the experiment, before breaking symmetry and evolving asymmetrically.

3.2 Bifurcation diagram: portion α = 2.0

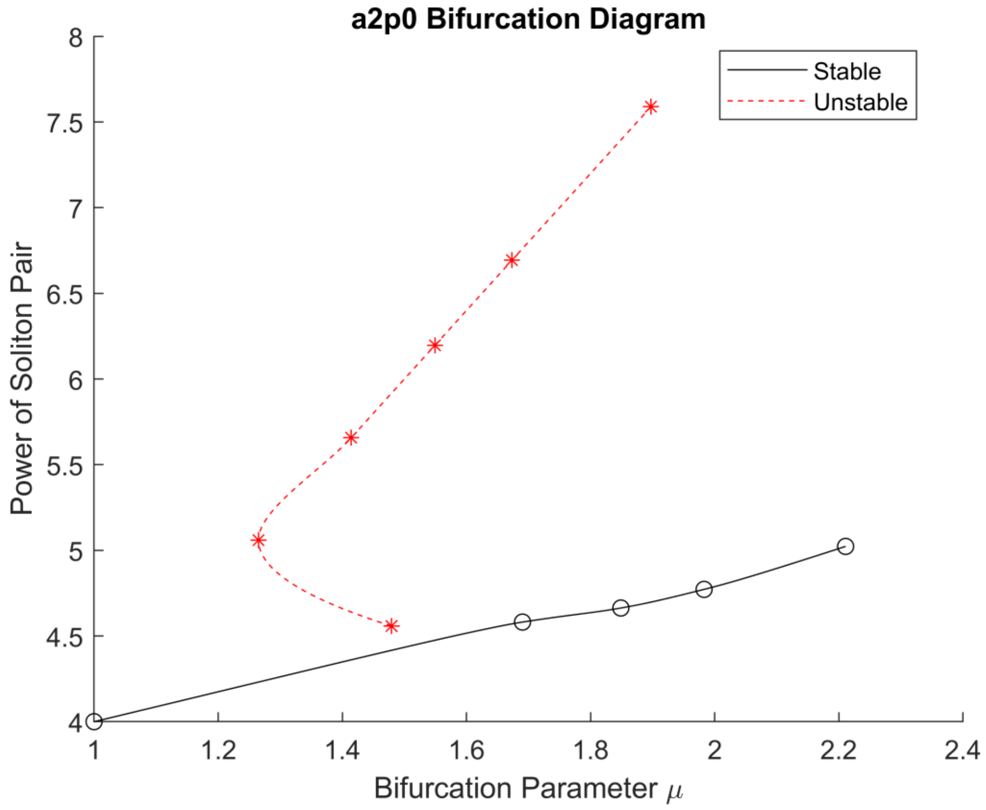

Figure 3.27 Bifurcation diagram for solutions evaluated at fractional derivative value α = 2.

The bifurcation plot for the dataset when the fractional derivative order α = 2 shows instability when the average ratio for power and the bifurcation parameter μ exceeds 3.8, whereas the solutions remain stable when the average ratio of power and μ is less than 3.

If we compare the branches of the bifurcation plot with Table 3.1, we see the unstable branch (in red) corresponds to symmetric solutions, whereas the stable branch (black) corresponds to asymmetric solutions: there exists a correlation between symmetry and stability.

Table 3.1: Fractional derivative group $\alpha = 2$

Data Pair	Stability	Abs. Max. Amplitude	Power
a_2p0_mu_1p5_sym	Stable	1	4
a_2p0_mu_1p8_asym	Unstable	1.4792903	4.558345401
a_2p0_mu_1p8_sym	Unstable	1.2649111	5.059644339
a_2p0_mu_2p0_asym	Stable	1.6902419	4.581384019
a_2p0_mu_2p0_sym	Unstable	1.4142136	5.656854204
a_2p0_mu_2p2_asym	Stable	1.8487053	4.66340266
a_2p0_mu_2p2_sym	Unstable	1.5491933	6.196773221
a_2p0_mu_2p4_asym	Stable	1.9828059	4.772180225
a_2p0_mu_2p4_sym	Unstable	1.6733201	6.693280204
a_2p0_mu_2p8_asym	Stable	2.2107771	5.022978064
a_2p0_mu_2p8_sym	Unstable	1.8973666	7.589466386

3.3 Fractional derivative $\alpha = 1.7$

Generally, from fractional derivative order $\alpha = 2$, to $\alpha = 1.8$ soliton quality degraded, and solutions became less stable as the fractional derivative order α reduced from 2. However, Figure 3.28 is an unusual example for a solution when the fractional value $\alpha = 1.7$ and a phase propagation constant $\mu = 2.8$.

3.3.1 u_data_a_1p7_mu_2p8_asym

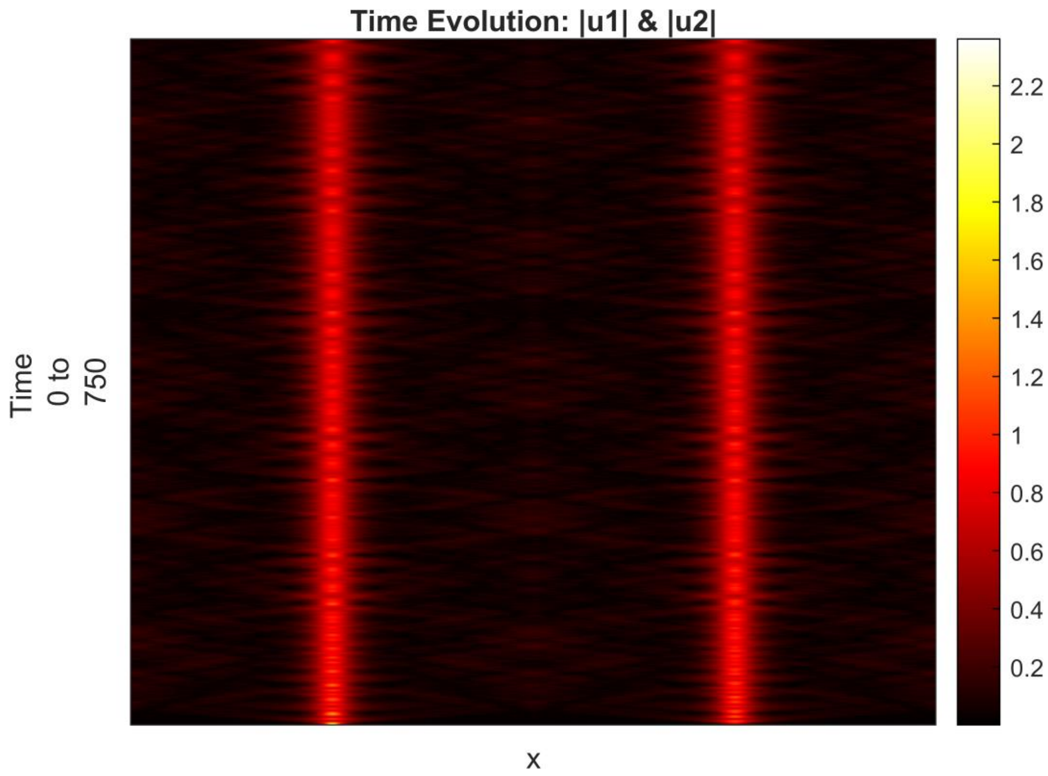

Figure 3.28 The solutions appear be become symmetric when α = 1.7.

Considering the peak amplitude evolution and centre of mass evolution in Figure 3.29, we can see the internal (higher frequency) peak amplitude wave oscillations approach symmetry, with the phase shift resulting in asymmetric surface (wave envelope) oscillations. However, it appears the surface waves also converge as the solution evolves. When α = 1.7, these asymmetric solutions appear to converge and become symmetric: this solution appears to be representative of symmetry making conditions.

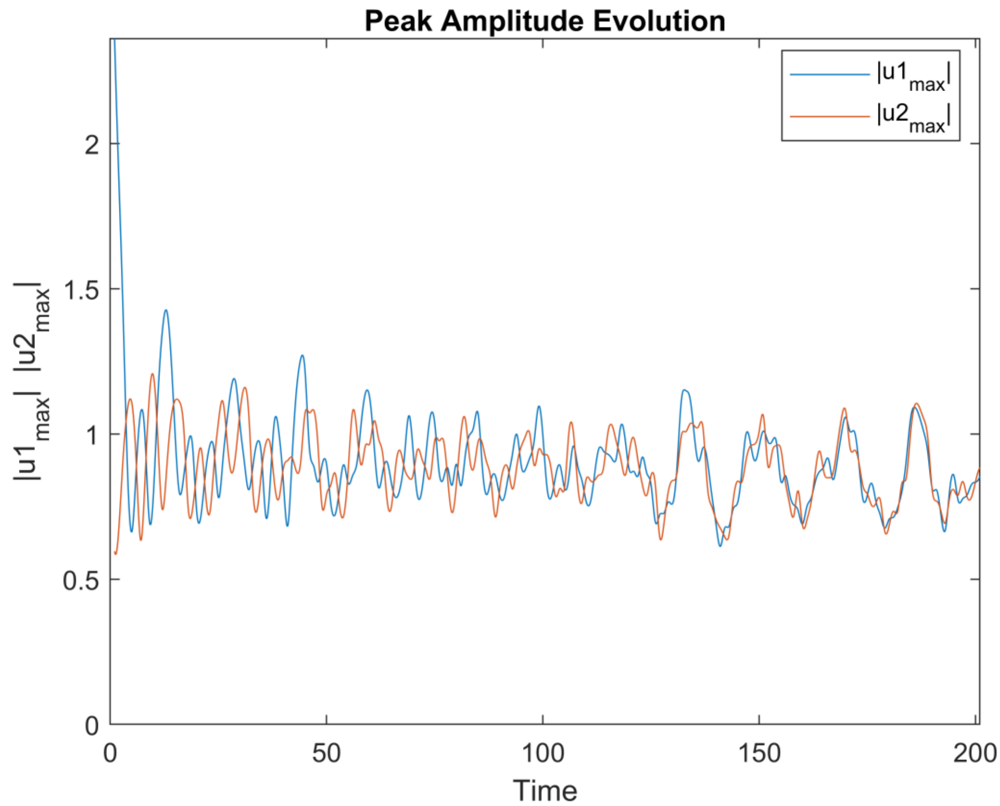

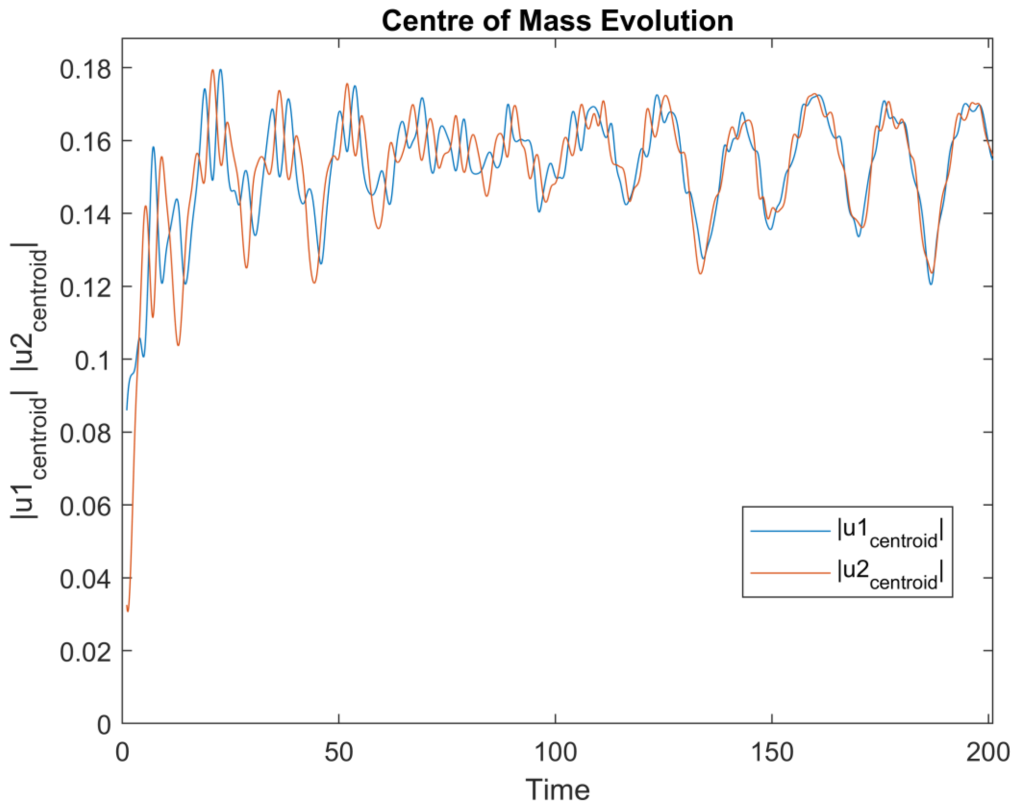

Figure 3.29 We see u_1 and u_2 converge early in the experiment for both inner and surface wave amplitudes. When α = 1.7 the group and phase velocities approach equivalence: i.e., symmetry making.

We confirm our conclusion by observing long-term stability of the solutions, where symmetry improves over time. Thus, we have symmetric behaviour when $\alpha = 1.7$.

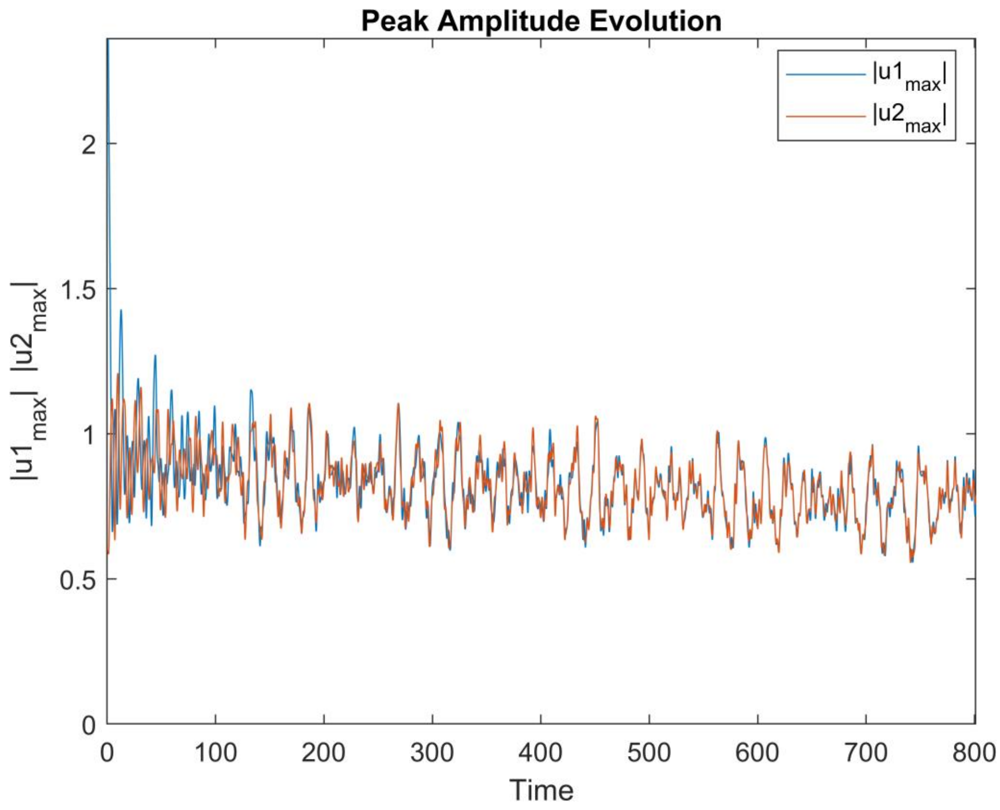

Figure 3.30 The solutions match group and phase velocity as the experiment evolves. This system becomes numerically unstable for $t > 800$.

3.4 Fractional derivative α = 1.6

Within this dataset where we evaluate fractional derivative values of order α = 1.6, we note solutions are highly dispersive from α = 2, until α = 1.6, when the dispersive effects and oscillation frequencies are minimised.

3.4.1 u_data_a_1p6_mu_1p2_sym

The fractional derivative value with order α = 1.6 and phase propagation constant μ = 1.2 data begins with a very stable and distinct solution pair seen in Figure 3.31.

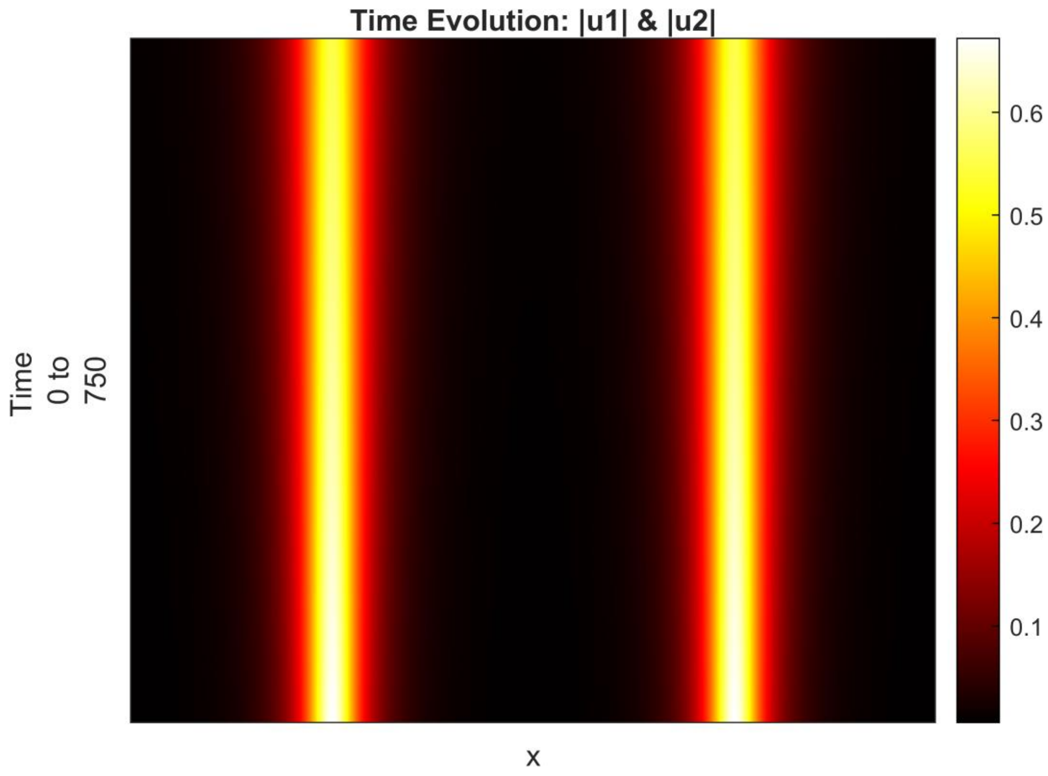

Figure 3.31 This is an example of a well-behaved symmetric pair of solitons.

We notice subtle dispersion, and ‘wide’, unfocussed solution pairs. If we look at the waterfall ED in Figure 3.32, we observe some evidence of instability in the solution, as dispersion and oscillatory effects become more obvious, but are still minimal. The peak amplitude plot in Figure 3.33 confirms symmetry and stability over the length of the experiment, with minimal oscillations and slight decay in peak amplitude over the course of the experiment.

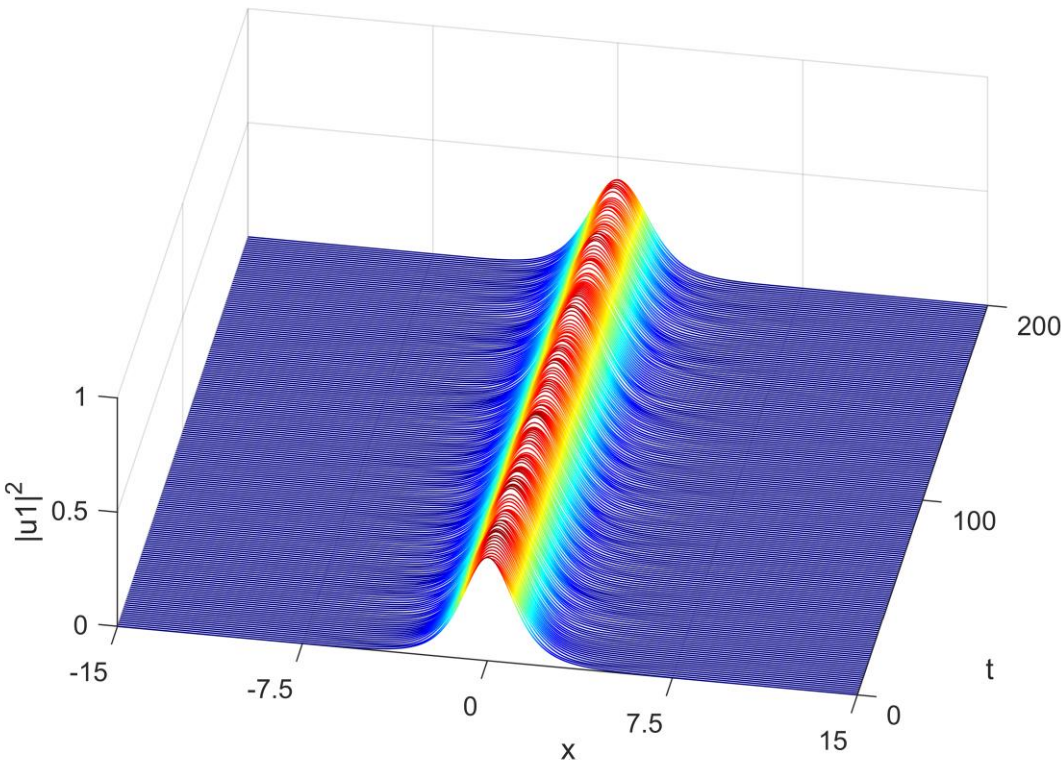

Figure 3.32 The ED for u_1 shows oscillatory behaviour and dispersion throughout the experiment.

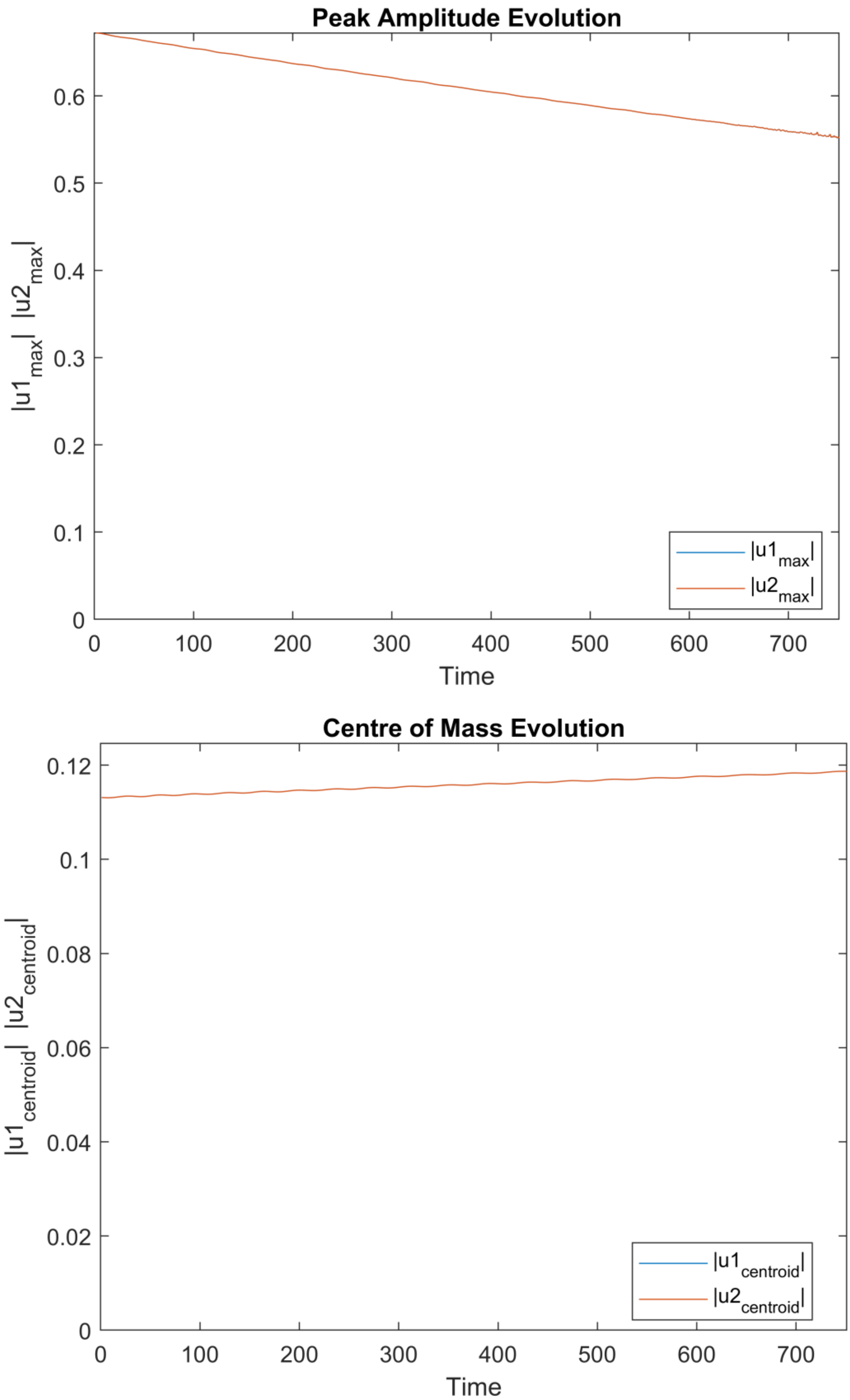

Figure 3.33 The peak amplitude evolution (top) confirms the soliton pair are symmetrical throughout the experiment, while exhibiting minimal oscillations. The centre of mass (bottom) correlates with increased dispersion seen in the waterfall ED in Figure 3.32.

3.4.2 u_data_a_1p6_mu_1p4_sym

From fractional derivative order α = 2, until α = 1.6, there is a steady, consistent reduction in dispersion and oscillation frequency, until the solutions are optimised, becoming stable at α = 1.6 with a phase propagation constant μ = 1.4. The results are available in the Figure 3.34.

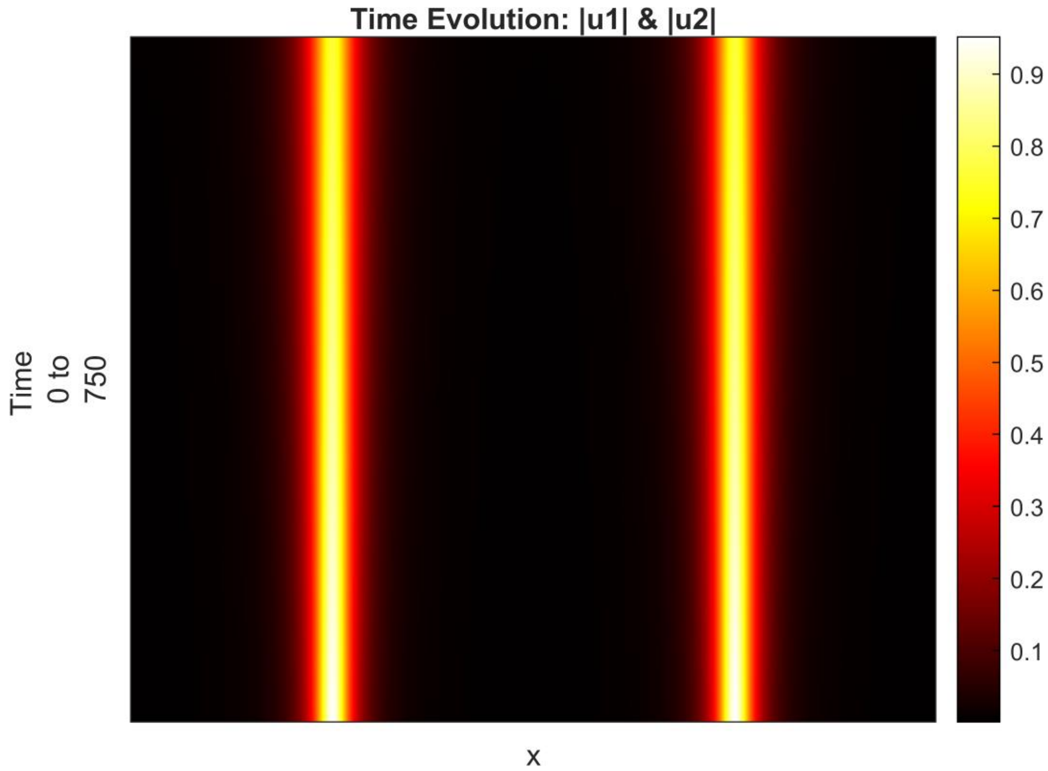

Figure 3.34 The heatmap shows optimised stability when the fractional derivative α = 1.6.

The following peak amplitude plot and waterfall ED illustrate the stability of the solutions when α = 1.6. We do not see evidence of oscillations in either the peak amplitude evolution in Figure 3.35, or the waterfall ED plot in Figure 3.36, indicating a stable soliton solution.

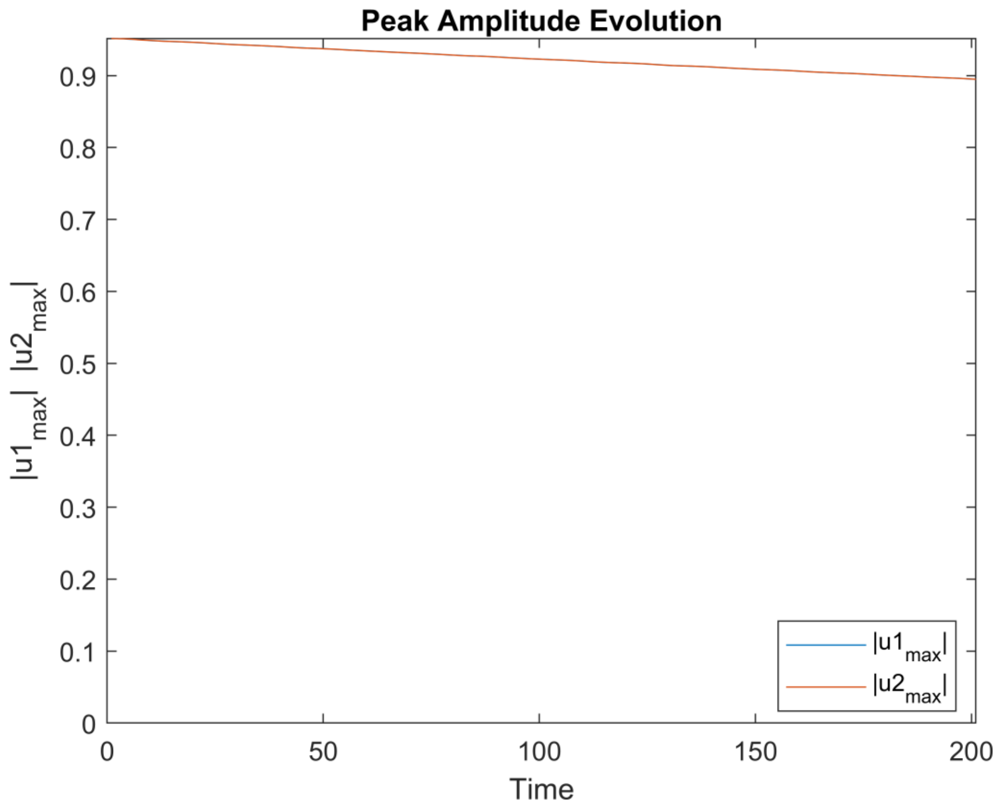

Figure 3.35 The peak amplitude evolution shows little evidence of oscillations.

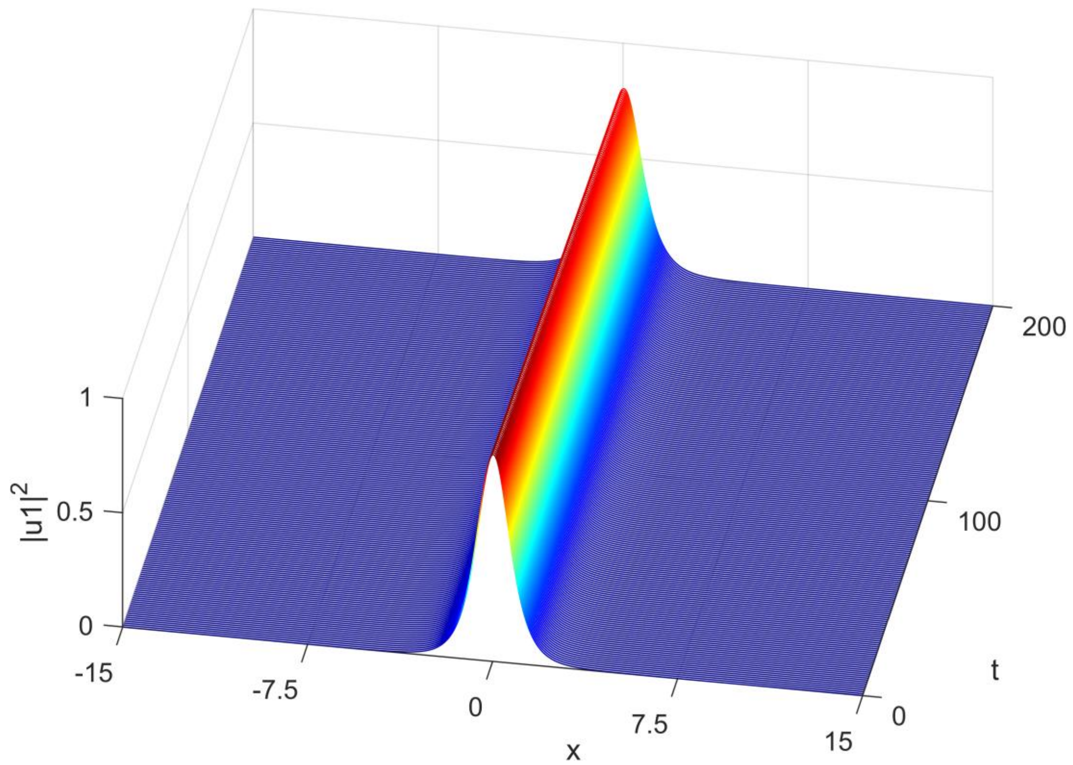

Figure 3.36 The waterfall ED with optimised solution stability when the fractional derivative $\alpha = 1.6$.

3.4.3 u_data_a_1p6_mu_1p5_sym

Decrementing the fractional derivative order α resulted in increased dispersion and decay rate until $\alpha = 1.6$. As the fractional derivative value decreased and approached 1.6 with a phase propagation constant $\mu = 1.5$, so too did the soliton stability decrease, until an abrupt change occurred: displayed in Figure 3.37.

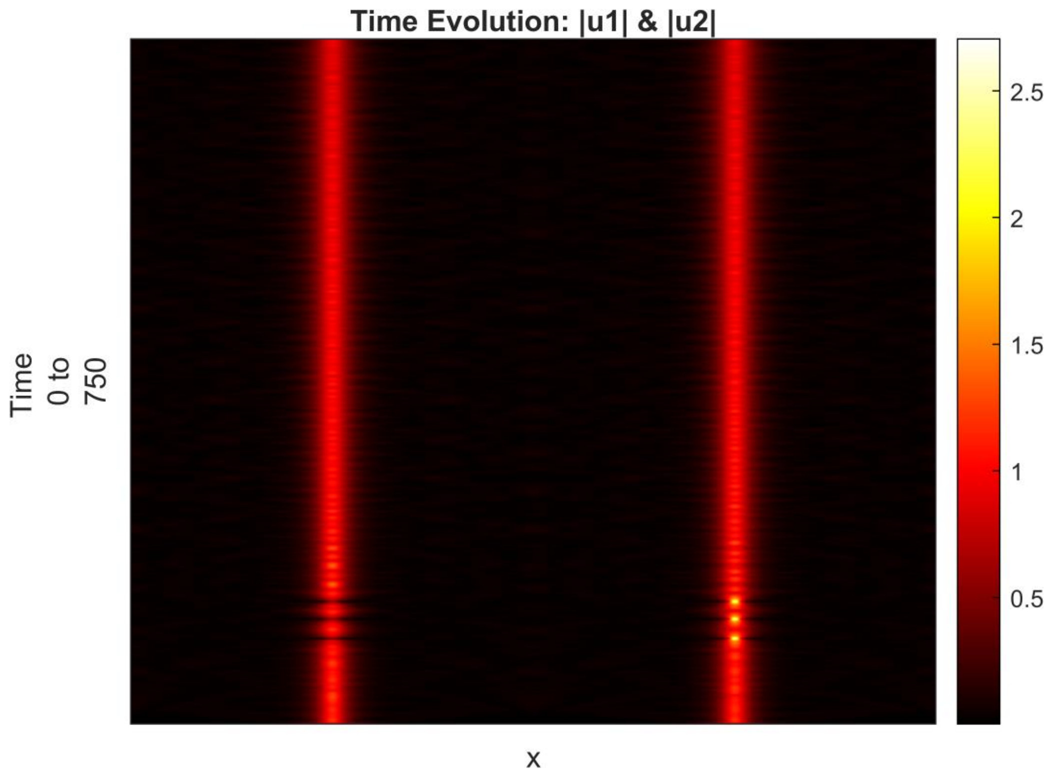

Figure 3.37 Broken symmetry and bright/dark soliton pulses when $\alpha = 1.6$.

From the heatmap in Figure 3.37, we see what appears to be an unstable symmetric solution pair, except for brief symmetry switching resulting in three bright/dark soliton pulses at approximately 100t. We see from Figure 3.37 evidence of both continuous oscillations and dispersion throughout the experiment. We examine the solutions in more detail by examining the peak amplitude evolution for 200t in Figure 3.38.

In Figure 3.38, we see the solutions behave symmetrically until approximately 25t, when a break in symmetry occurs and unstable, asymmetric oscillations propagate. The solutions switch symmetry, and three bright/dark soliton pulses are created at approximately 100t, after which the solutions continue with asymmetric oscillations.

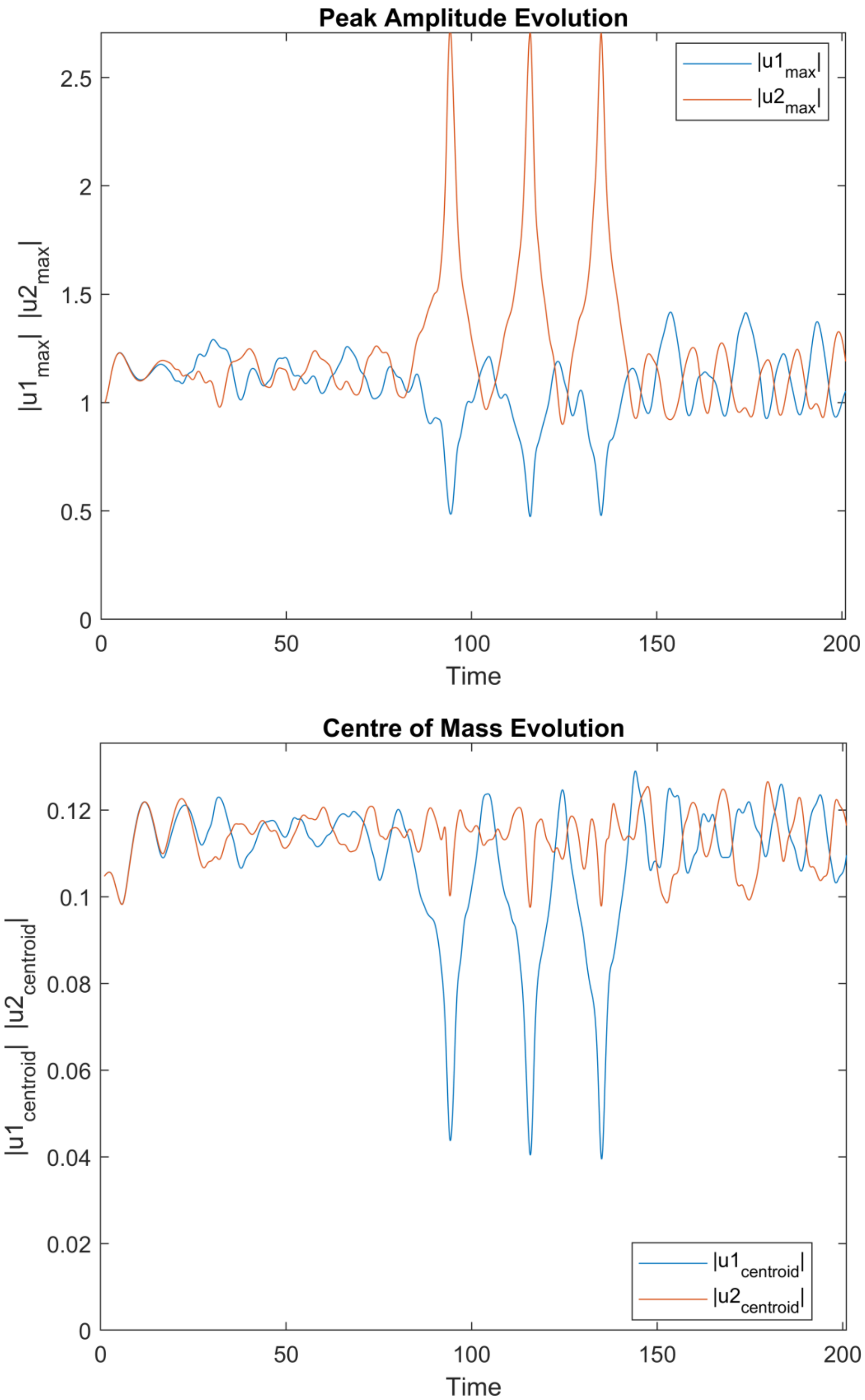

Figure 3.38 Amplitude evolution of α = 1.6, shows unstable, oscillating, asymmetric solutions, with bright/dark solitons (top). Corresponding centre of mass evolution (bottom).

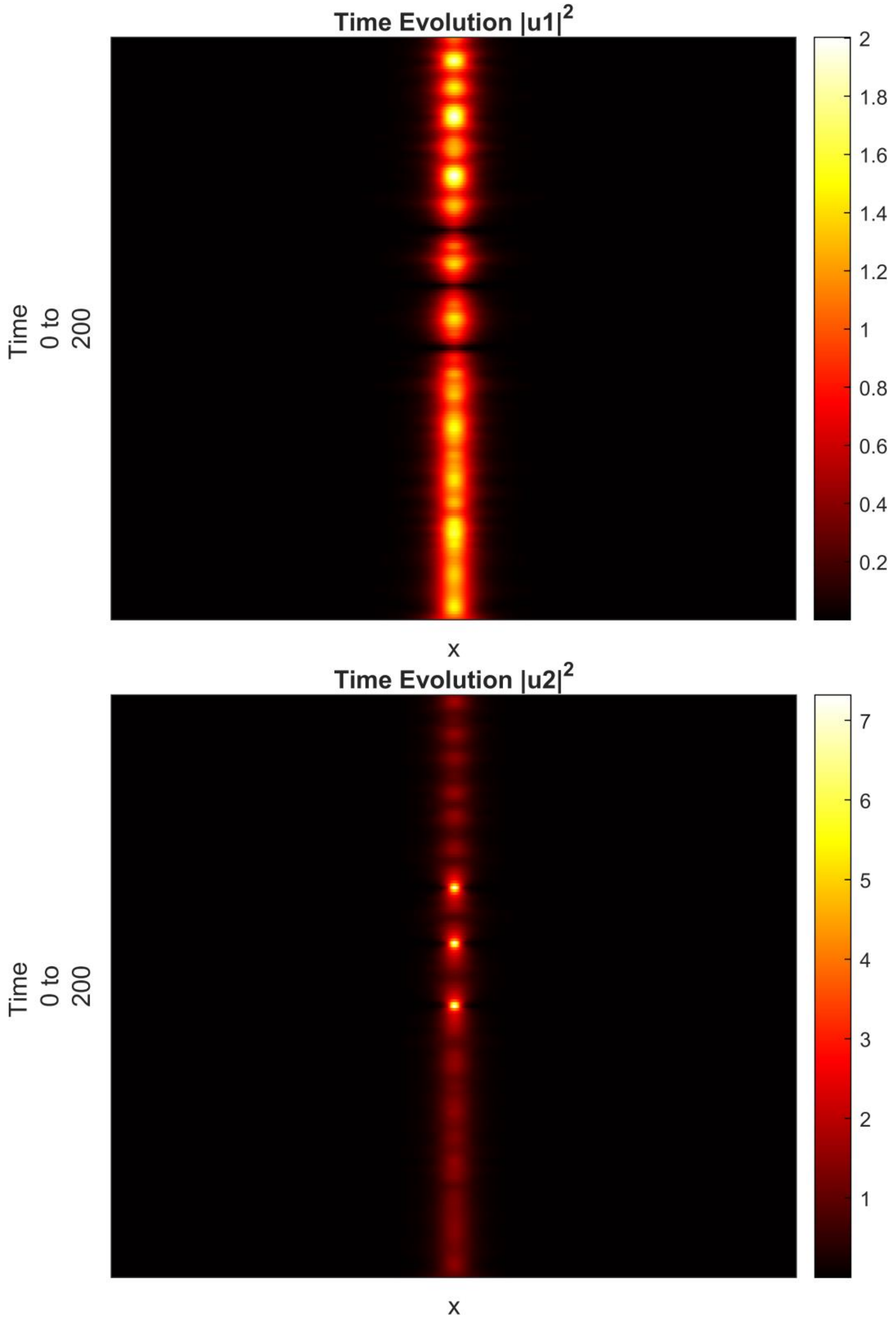

Figure 3.39 Heatmap showing switching and bright/dark soliton pulses when the fractional derivative α = 1.6, from a previously stable, symmetric pair.

Figure 3.39 above shows the evolution of the bright/dark pulses in terms of the heatmap. The peak amplitude direction field in Figure 3.40 provides an indication of self-correcting behaviour around (1.1, 1.1), after which we see a ‘tornado’ effect typical of asymmetric solution pairs in our experiments.

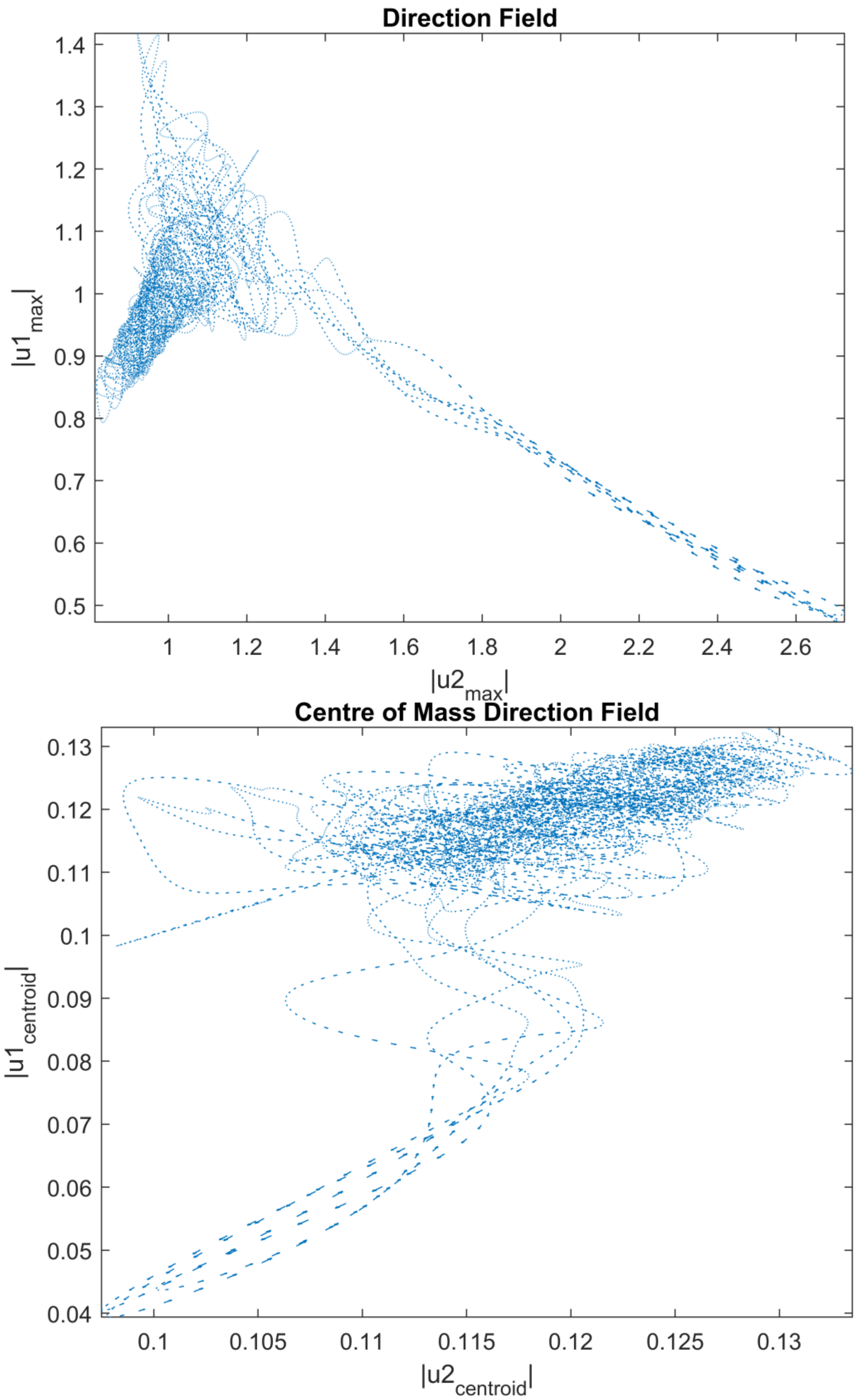

Figure 3.40 Direction fields of unstable asymmetric solutions for reference. Peak amplitude direction field (top). The centre of mass direction field (bottom) provides an indication of the instability of the solutions evident as a dynamic centre of mass.

3.4.4 u_data_a_1p6_mu_1p8_asym

Here we display the results for an asymmetric solution with a phase propagation constant $\mu = 1.8$.

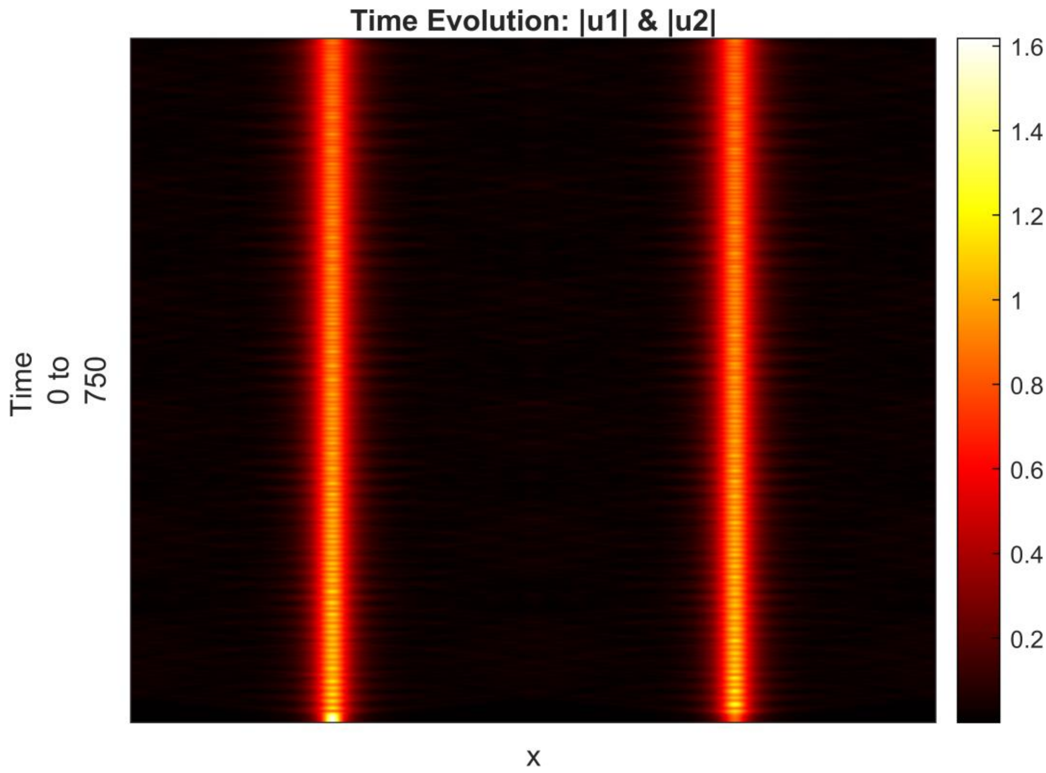

Figure 3.41 Asymmetric, unstable solution pair.

The heatmap in Figure 3.41 shows asymmetric, unstable solutions with a high degree of dispersion throughout the experiment. If we review the peak amplitude evolution in Figure 3.42, we see erratic, high-frequency oscillations contributing to the instability of the solutions.

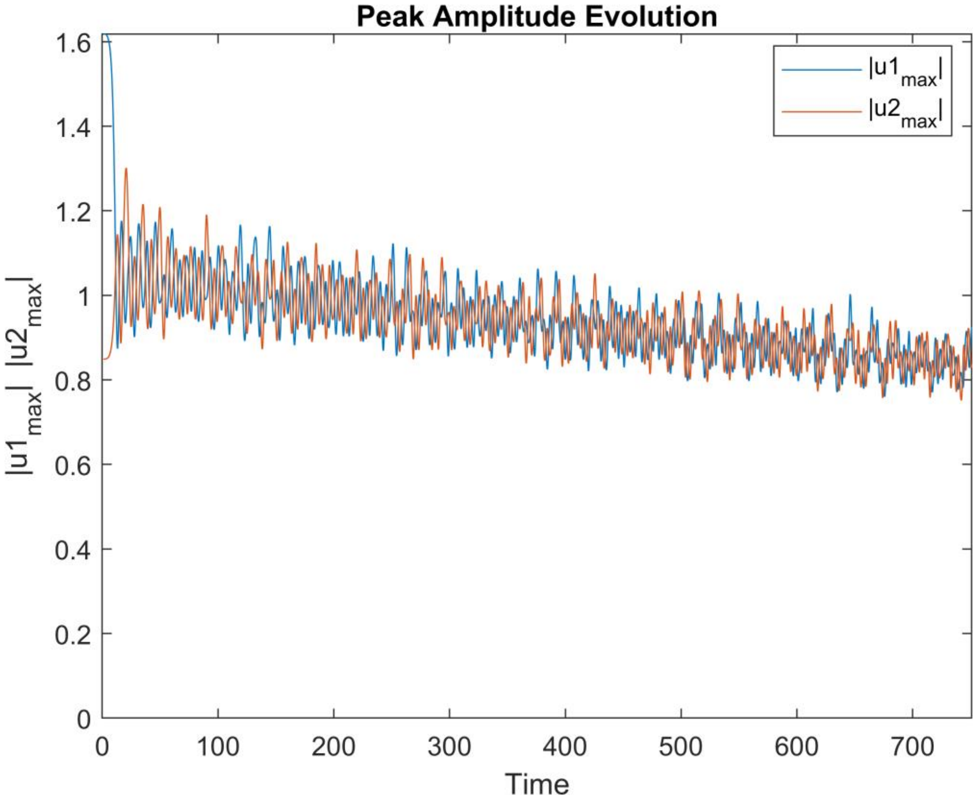

Figure 3.42 Erratic oscillations indicate instability.

Later in the experiment we observe the group velocity of the solutions converging, but the solutions continue to propagate out of phase. The peak amplitude evolution Figure 3.42 indicates the solutions converging symmetries as the experiment progresses.

3.4.5 u_data_a_1p6_mu_1p8_sym

From fractional derivative α = 2, until α = 1.6, the solutions are symmetric and unstable, however once the fractional derivative order α = 1.6 with a phase propagation constant μ = 1.8, we get the following asymmetric results in Figure 3.43.

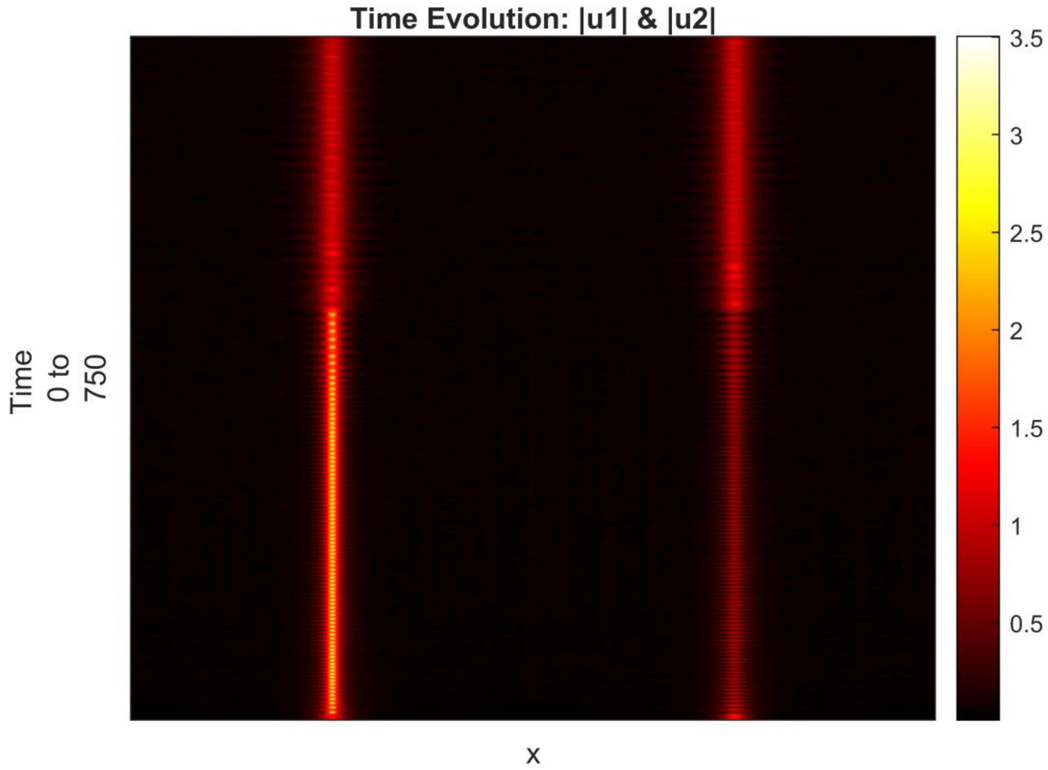

Figure 3.43 Asymmetric solution pair converging.

We see the solutions break symmetry early in the experiment and display high-frequency oscillations for approximately 400t before converging on each other. After the solutions converge, they remain asymmetric and continue to oscillate out of phase.

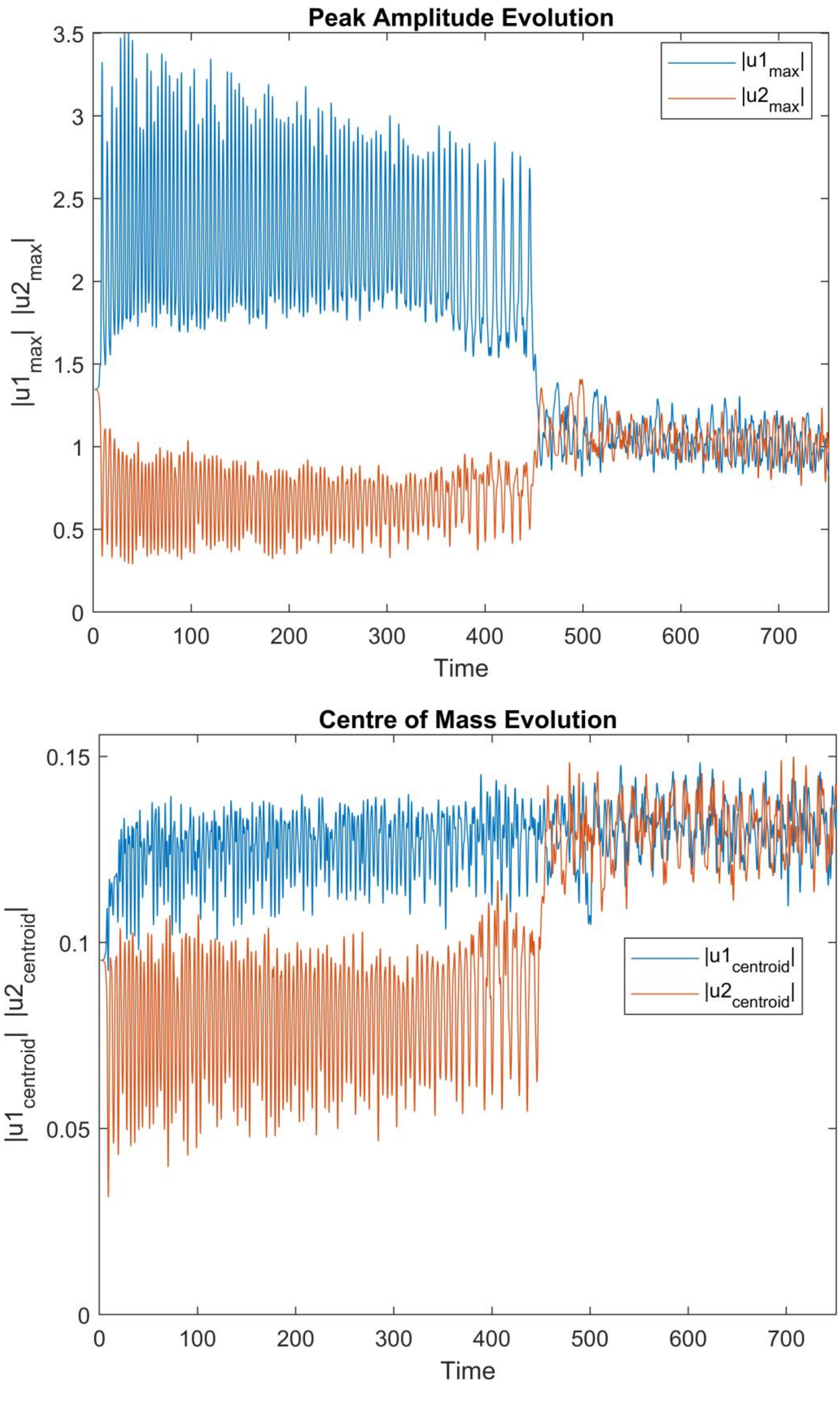

Figure 3.44 Peak amplitude (top) and the centre of mass (bottom) show the solutions breaking symmetry, then converging at approximately 450t.

From the peak amplitude evolution in Figure 3.44, we see the extent of the instability of the solutions due to high-frequency oscillations. Furthermore, after the solutions converge on each other, we see despite the oscillations, the solutions do not decay overall, but seem to conserve their average peak amplitude while continuing to evolve out of phase.

When reviewing the centre of mass evolution in Figure 3.44, we see after the solutions converge, the centre of mass approaches symmetry while continuing to oscillate. While the asymmetric solutions are oscillating, which affects the value produced in the centre of mass plot, the overall trend is horizontal, indicating reduced dispersion.

3.4.6 u_data_a_1p6_mu_2p4_asym

Looking at the heatmap in Figure 3.45, we see solutions with a phase propagation constant $\mu = 2.4$ start the experiment as asymmetric with minimal oscillations. However, the solutions converge early in the experiment followed by oscillations and dispersion. Despite the oscillations and dispersion after convergence, it appears the solutions conserve their shape throughout the experiment.

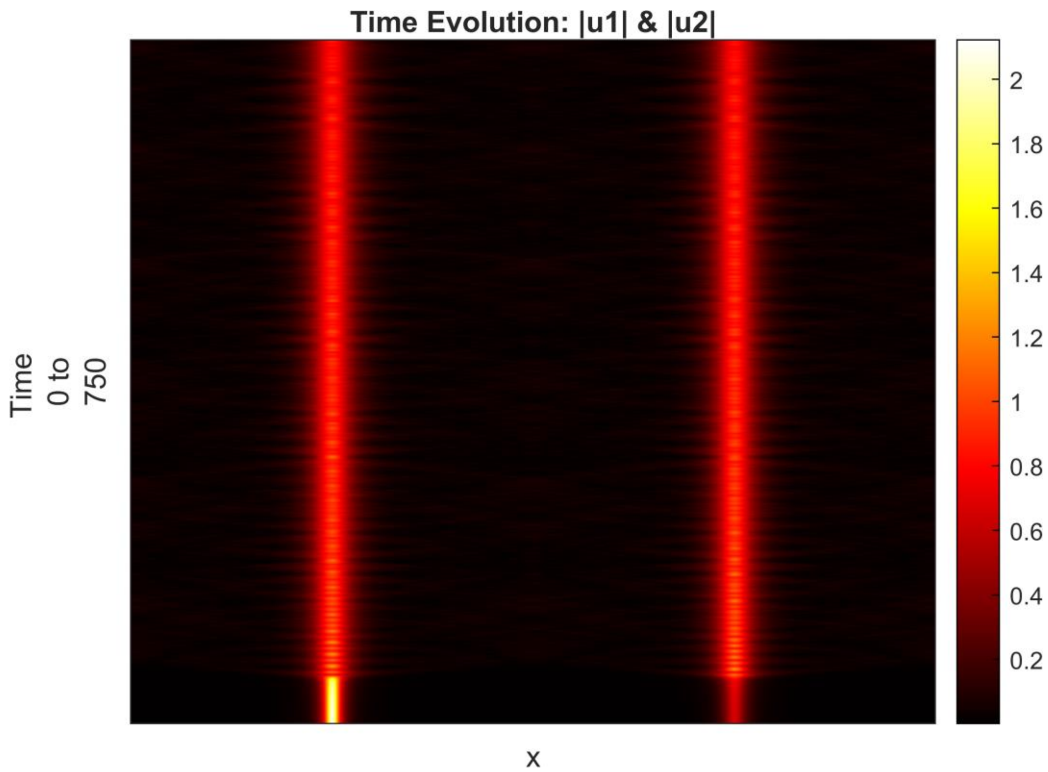

Figure 3.45 Asymmetric, stable solution pair.

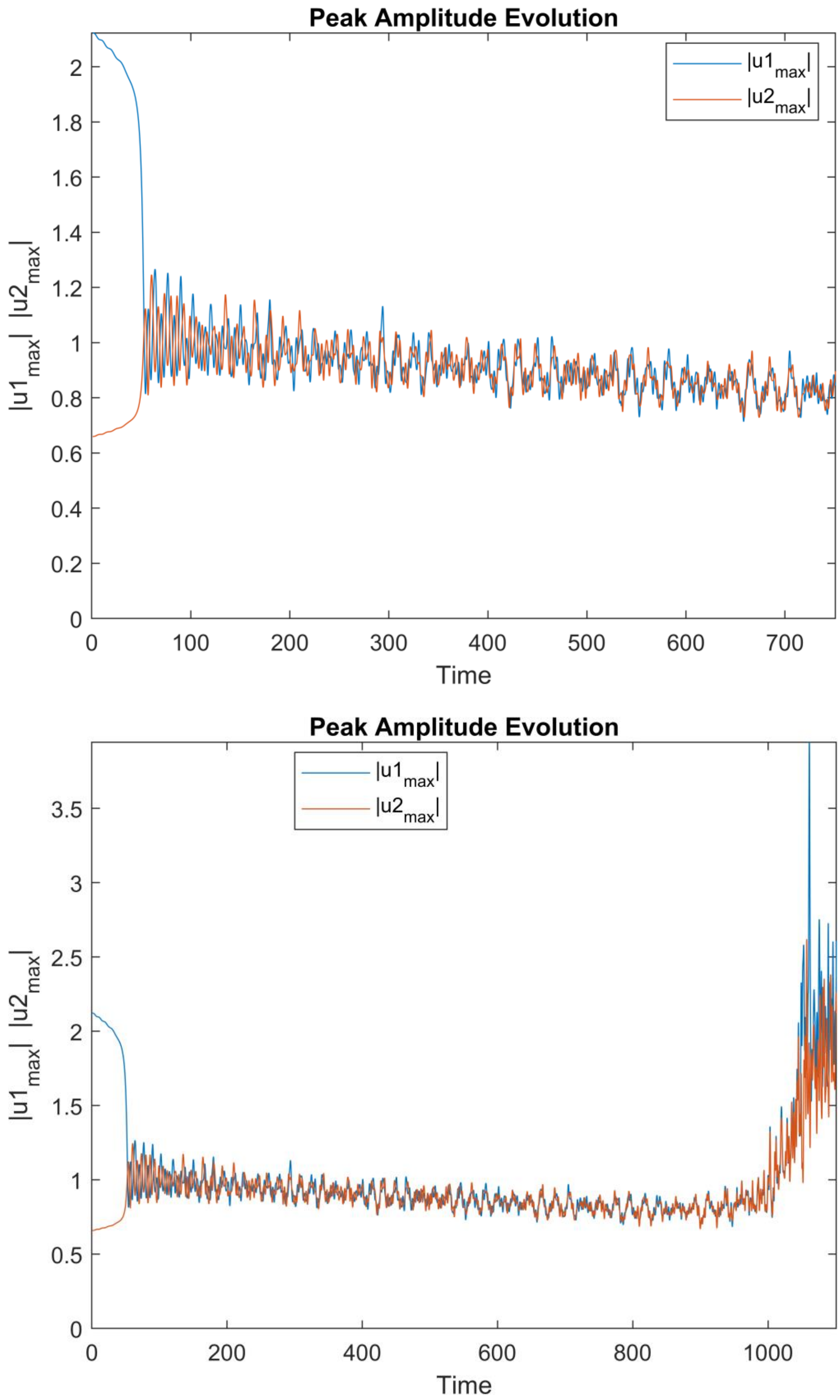

Figure 3.46 Peak amplitude evolution up to 250t indicates oscillating, asymmetric solutions (top), whereas the peak amplitude evolution (bottom) shows the asymmetric pair converge: the inner wave oscillates symmetrically until numerical instability occurs at 950t.

Figure 3.46 shows the solutions converge early in the experiment, then oscillate asymmetrically out of phase. At approximately 250t surface waves of the peak amplitude appear to oscillate out of phase. However, the internal peak amplitude wave begins oscillating symmetrically: the group velocity of both solutions propagate symmetrically. In Figure 3.47 we observe the centre of mass is largely unchanged, as we see a horizontal trend throughout the experiment. Therefore, we consider this solution stable, as it conserves its behaviour, and does not appear to undergo dispersive losses until numerical instability occurs when the experiment time exceeds 900t.

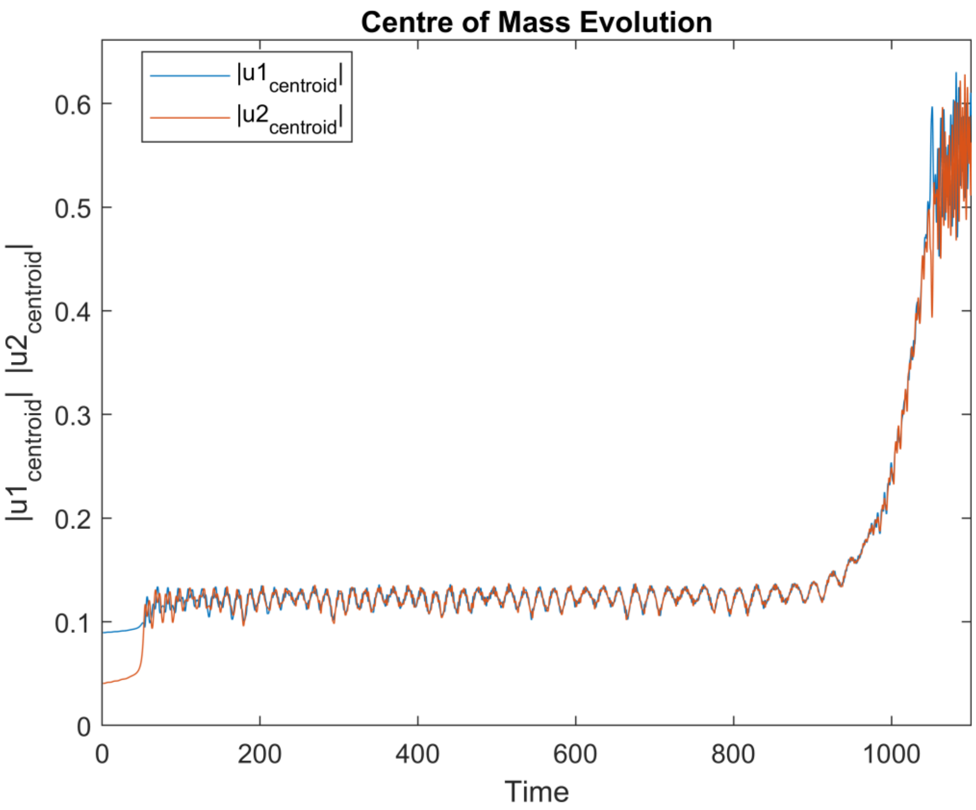

Figure 3.47 The centre of mass evolution shows signs of oscillations, but little evidence of dispersion until numerical stability occurs after 900t.

3.4.7 u_data_a_1p6_mu_2p4_sym

In Figure 3.48 , we see what appears to be a symmetric solution pair with a phase propagation constant $\mu = 2.4$ at the beginning of the experiment become unstable: breaking symmetry and showing signs of oscillations and dispersion throughout the experiment.

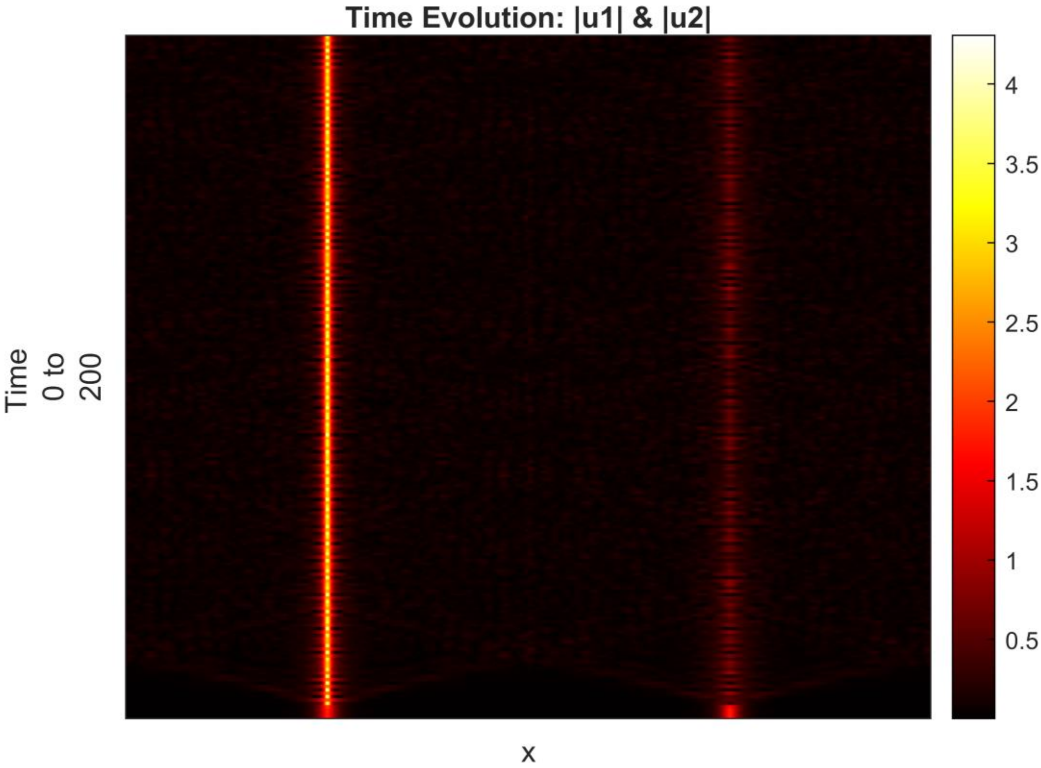

Figure 3.48 The heatmap shows u_1 and u_2 appear to symmetric initially, but ultimately destabilise and break symmetry.

Taking a closer look at the peak amplitude evolution in Figure 3.49 (top), we see the solutions immediately break symmetry and oscillate asymmetrically throughout the experiment. Considering the centre of mass evolution in Figure 3.49 (bottom), we can see the effects of dispersion, as the distribution of mass in the solution field increases throughout the experiment, so too do both centroids increase in value. Comparing the centre of mass to the peak amplitude plot in Figure 3.49, it is interesting to note the centroids start the experiment symmetrically, whereas the peak amplitude propagates asymmetrically for experiment time $t < 5$. This solution is classified as unstable due to erratic peak amplitude oscillations.

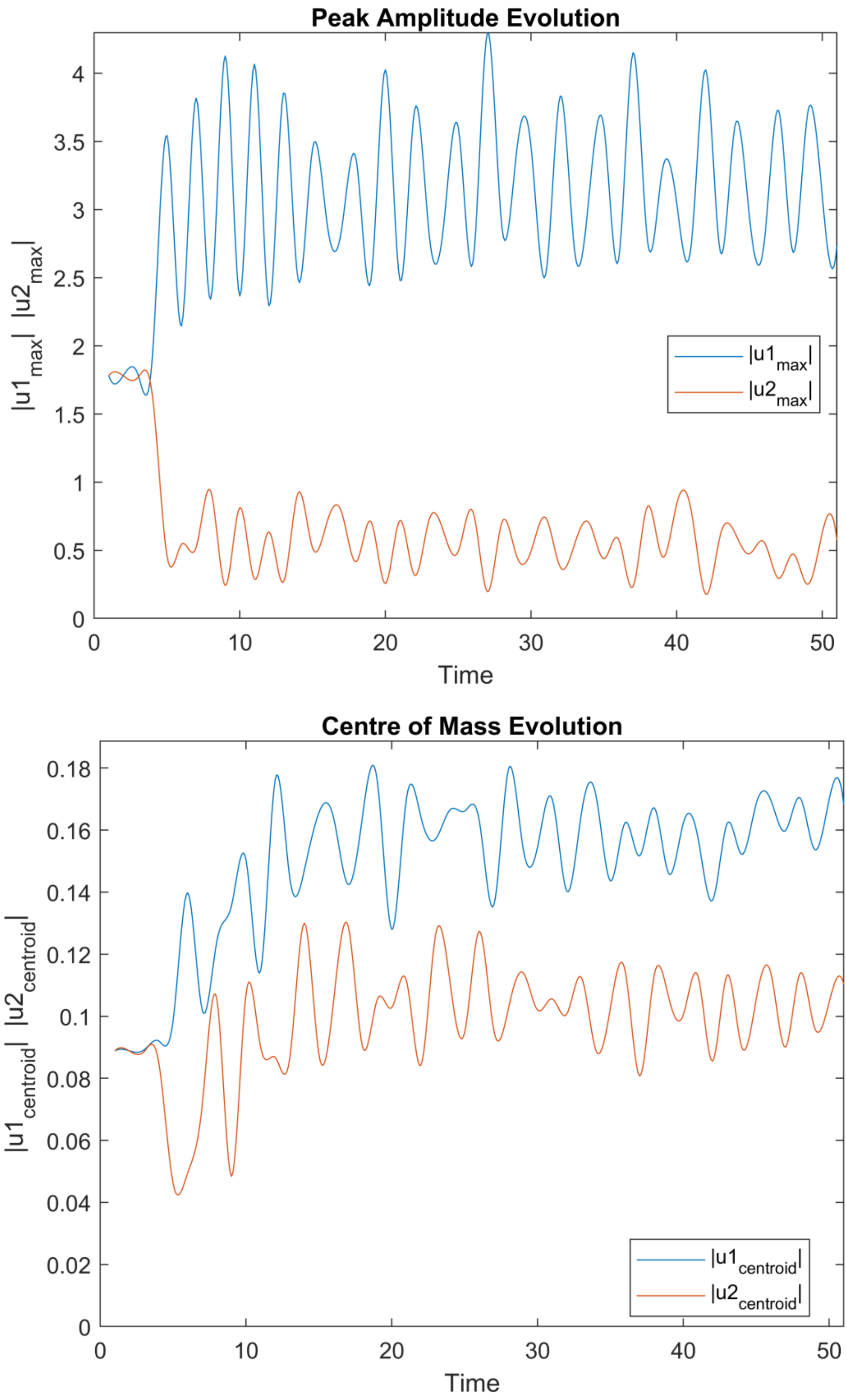

Figure 3.49 Peak amplitude evolution (top) shows the solutions are asymmetric very early in the experiment ($t < 5$), then u_2 quickly disperses. The centre of mass evolution (bottom) shows the solutions to be symmetric before dispersion.

3.4.8 u_data_a_1p6_mu_2p8_asym

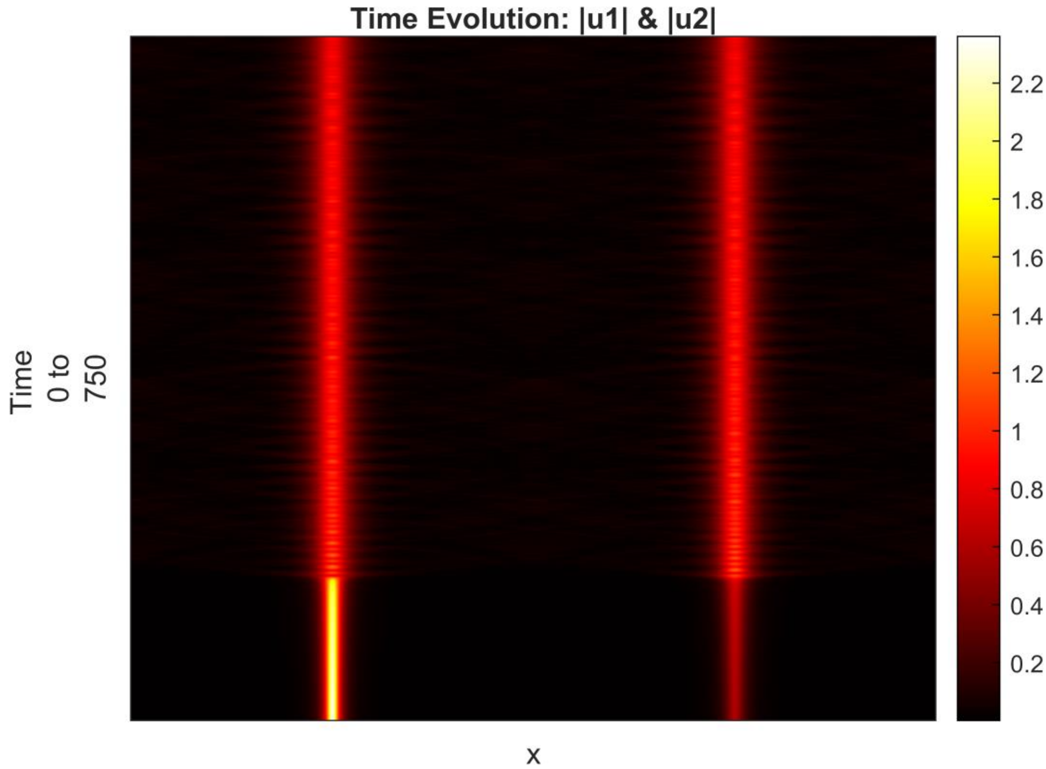

Figure 3.50 Asymmetric, stable solution pair.

Figure 3.50 shows asymmetric solutions with a phase propagation constant $\mu = 2.8$ appear stable until approximately 150t, when the solutions converge and begin dispersion and oscillations. Considering the peak amplitude plot in Figure 3.51 below, we see the solutions behave similarly to the previous section 3.4.6 u_data_a_1p6_mu_2p4_asym, where the internal peak amplitude wave oscillates symmetrically, while asymmetric 'surface' oscillations occur due to a difference in phase. Since the trend in Figure 3.51 remains horizontal, indicating dispersion is minimal, we conclude the solutions are self-supporting and stable.

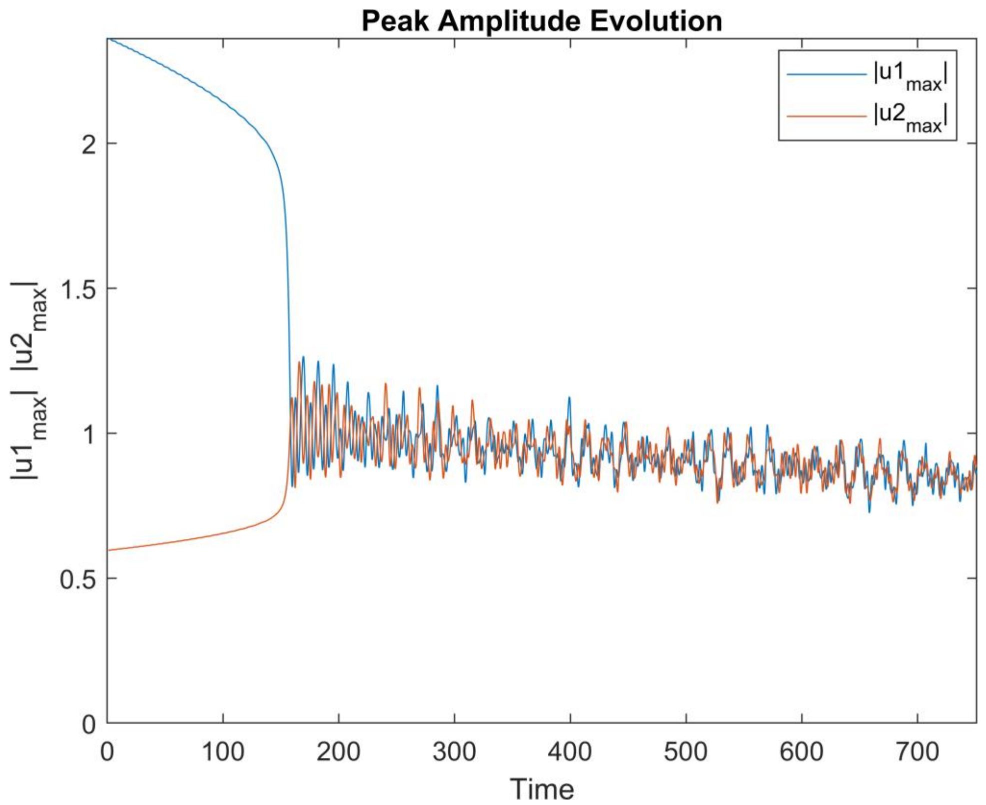

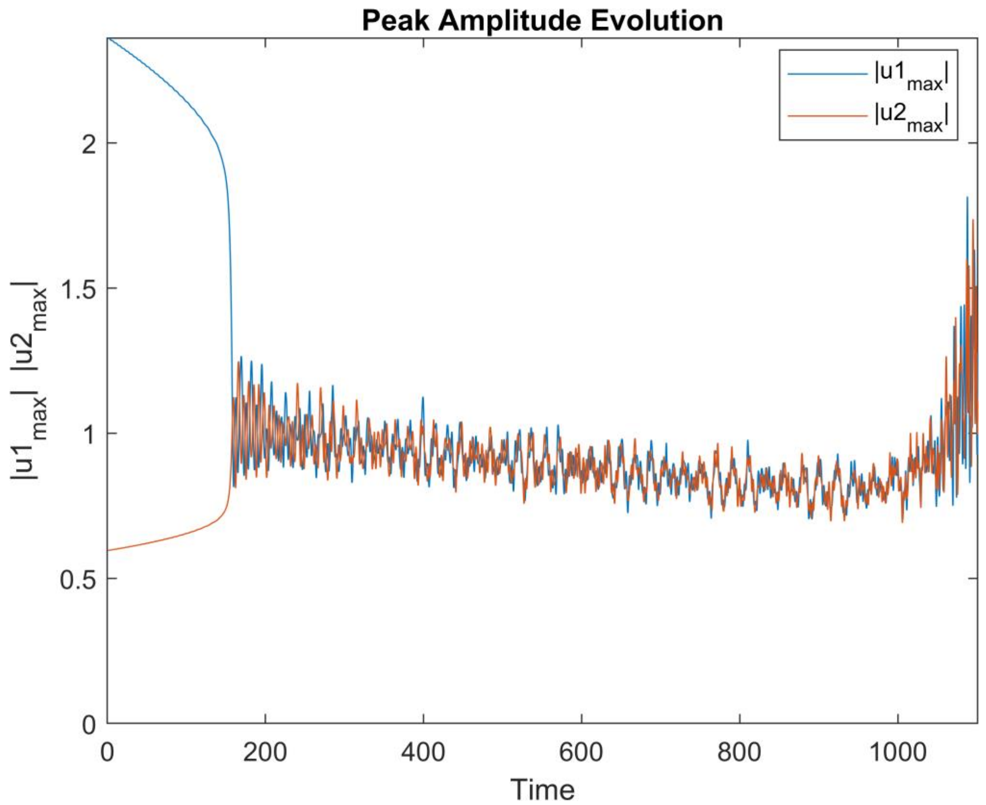

Figure 3.51 Peak amplitude evolution shows asymmetry until 250t (top), whereas the peak amplitude evolution (bottom) indicates symmetric oscillations of the inner wave until 1000t, when the system becomes numerically unstable.

3.4.9 u_data_a_1p6_mu_2p8_sym

Figure 3.52 displays the results of symmetric solutions with a phase propagation constant $\mu = 2.8$.

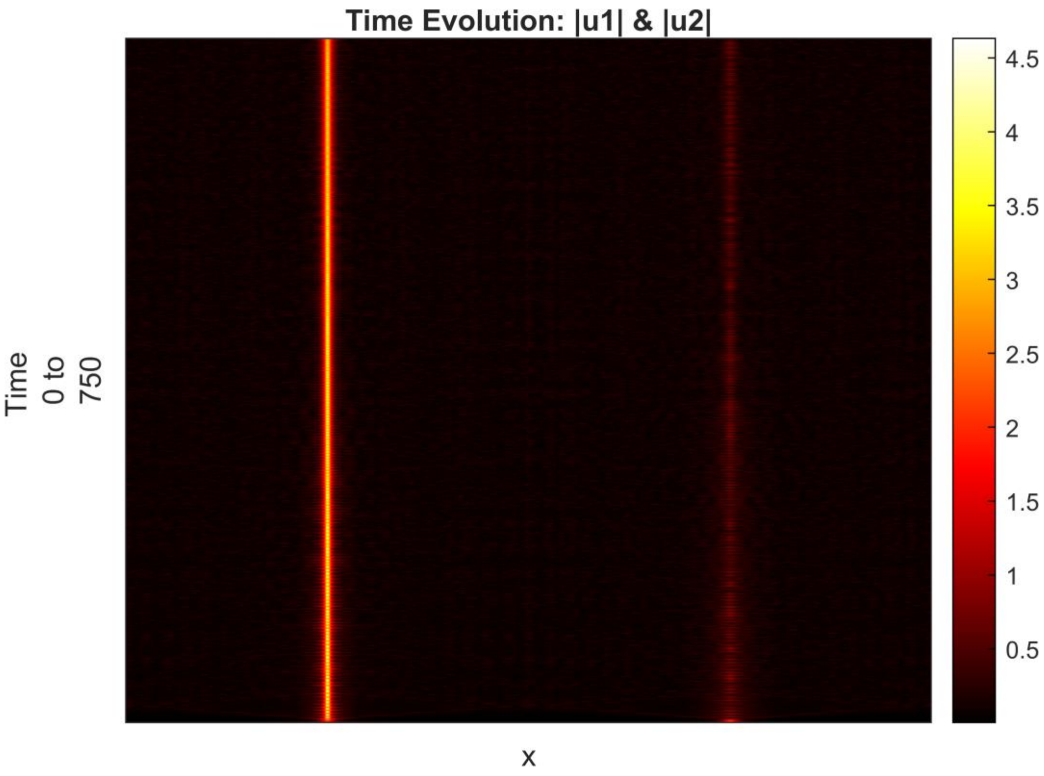

Figure 3.52 Asymmetric, unstable solutions.

While the data begins with identical peak amplitudes, we see the solutions evolve asymmetrically. Observing the peak amplitude and centre of mass evolution plots in Figure 3.53, we see solutions are unstable as both solutions show high frequency peak amplitude oscillations. In Figure 3.53 we note as u_2 decays almost completely after the initial conditions, u_1 slowly converges on u_2 throughout the experiment.

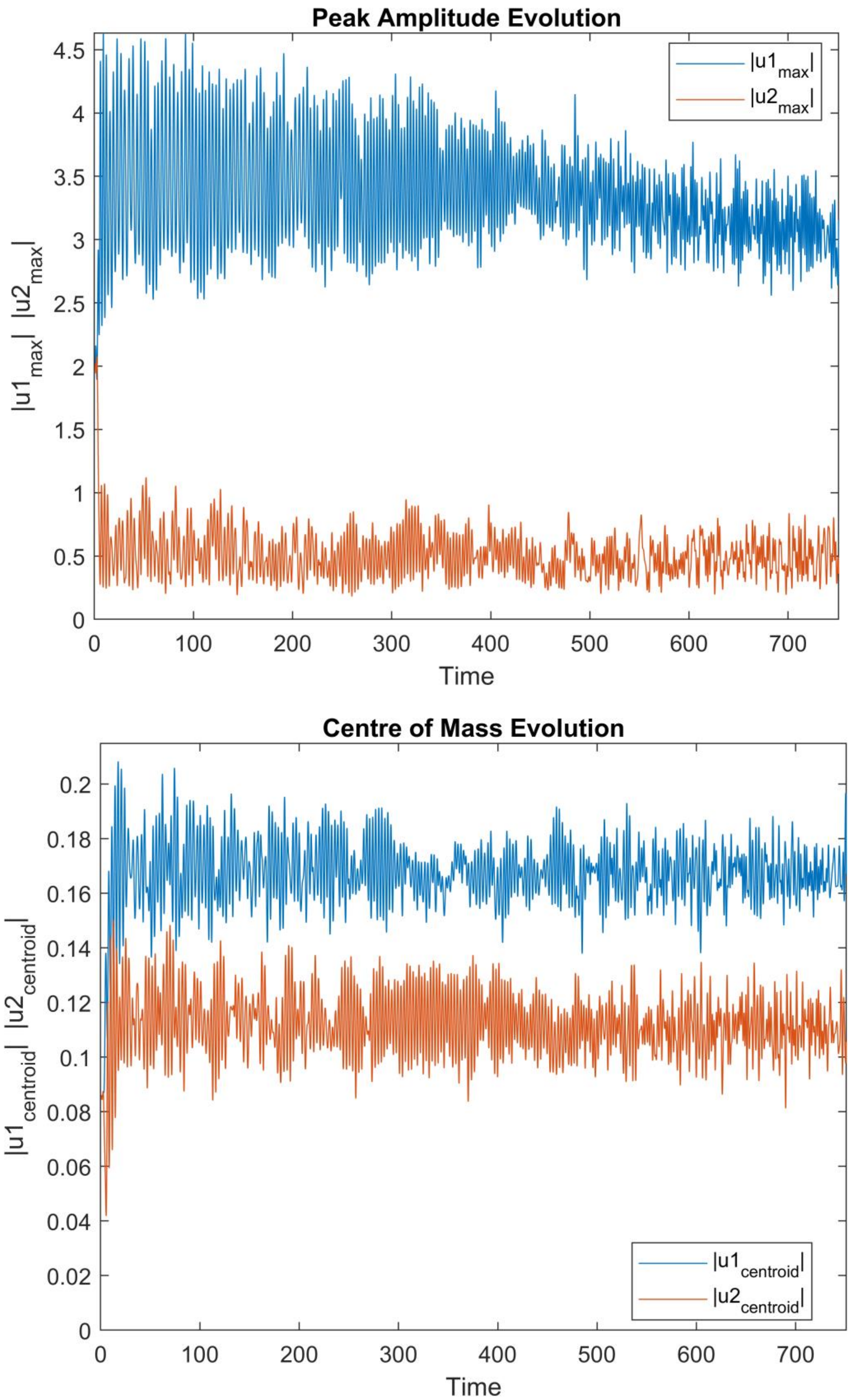

Figure 3.53 The peak amplitude evolution (top) and centre of mass (bottom) indicate asymmetric, highly oscillatory, unstable solutions.

3.5 Bifurcation diagram: portion α = 1.6

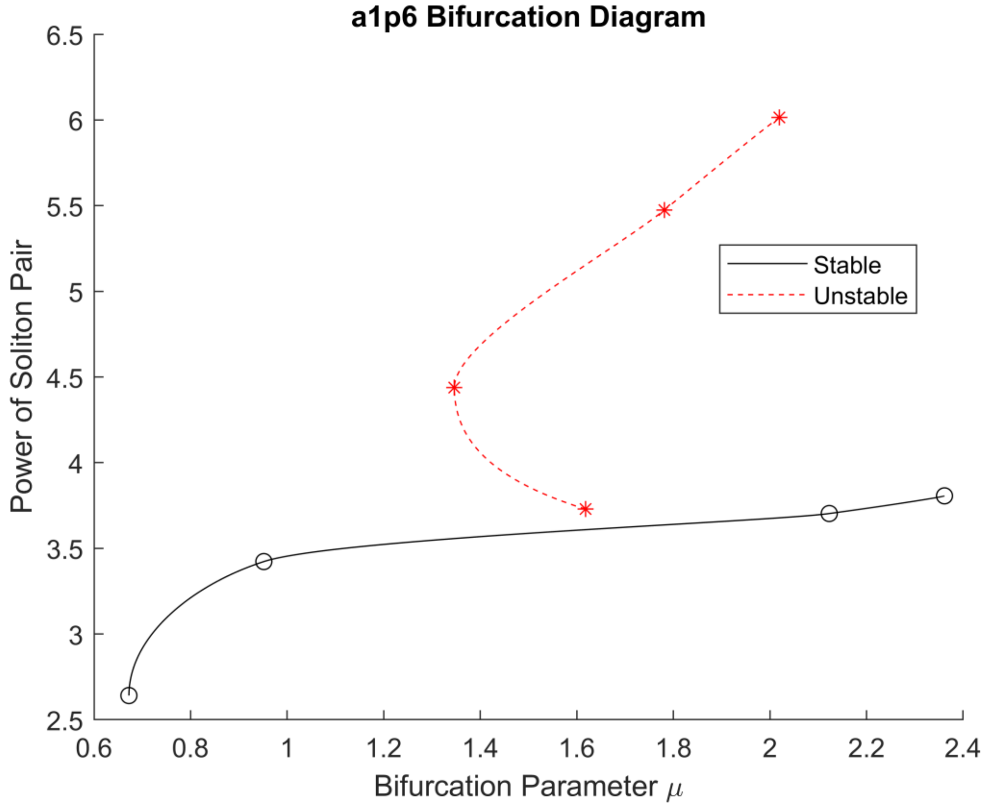

Figure 3.54 Bifurcation diagram for data with α = 1.6.

Taking the average slope of each bifurcation, we determine a stable branch corresponds to the average ratio of power to peak amplitude less than approximately 2.75, and an unstable branch corresponds to a ratio exceeding approximately 2.9.

When reviewing Table 3.2, we note for phase propagation constant $\mu \geq 2.4$ we see an unstable branch (in red) corresponds to symmetric solutions, whereas the stable branch (black) corresponds to asymmetric solutions. This trend does not hold for a phase propagation constant $\mu < 2.4$.

Table 3.2: Fractional value group $\alpha = 1.6$

Data Pair	Stability	Abs. Max. Amplitude	Power
a_1p6_mu_1p2_sym	Stable	0.67217559	2.64103256
a_1p6_mu_1p4_sym	Stable	0.95164944	3.422833531
a_1p6_mu_1p8_asym	Unstable	1.6183659	3.728858558
a_1p6_mu_1p8_sym	Unstable	1.3462826	4.438167627
a_1p6_mu_2p4_asym	Stable	2.1228634	3.703225888
a_1p6_mu_2p4_sym	Unstable	1.7811287	5.474263998
a_1p6_mu_2p8_asym	Stable	2.3615327	3.806348531
a_1p6_mu_2p8_sym	Unstable	2.0196517	6.01521567

3.6 Fractional derivative $\alpha = 1.5$

Here we present various dynamics for fractional derivatives of order $\alpha = 1.5$.

3.6.1 u_data_a_1p5_mu_2p4_sym

Decrementing the fractional derivative order, the solution quality deteriorates with increased oscillations and dispersion until $\alpha = 1.5$ and the phase propagation constant $\mu = 2.4$, when we observe non-stationary behaviour where the solution propagates to the left of the solution field in Figure 3.55.

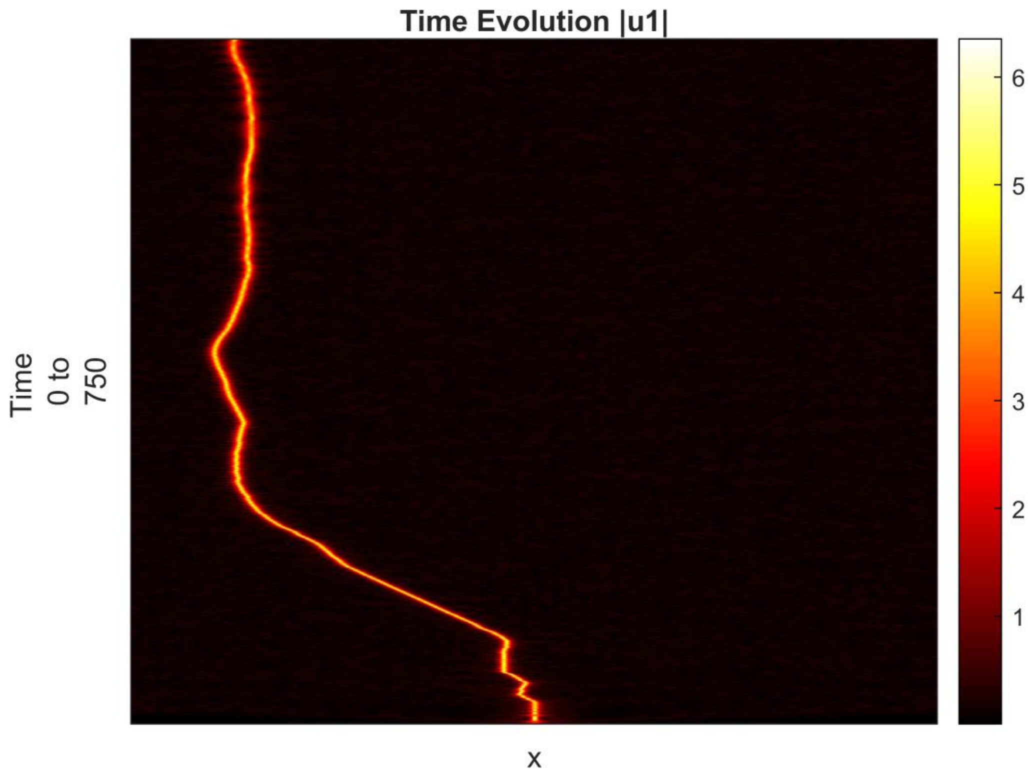

Figure 3.55 Non-stationary, asymmetric solution propagating to the left.

The waterfall plots of the ED in Figure 3.56 show u_1 as a highly focussed, decaying solution. From the u_1 ED, we see gradual decay of peak amplitude over time, with unstable oscillations, which may correspond to the dispersion evident for latter time periods in the heatmap in Figure 3.55. We confirm some dispersion in the centre of mass evolution plot in Figure 3.56 below.

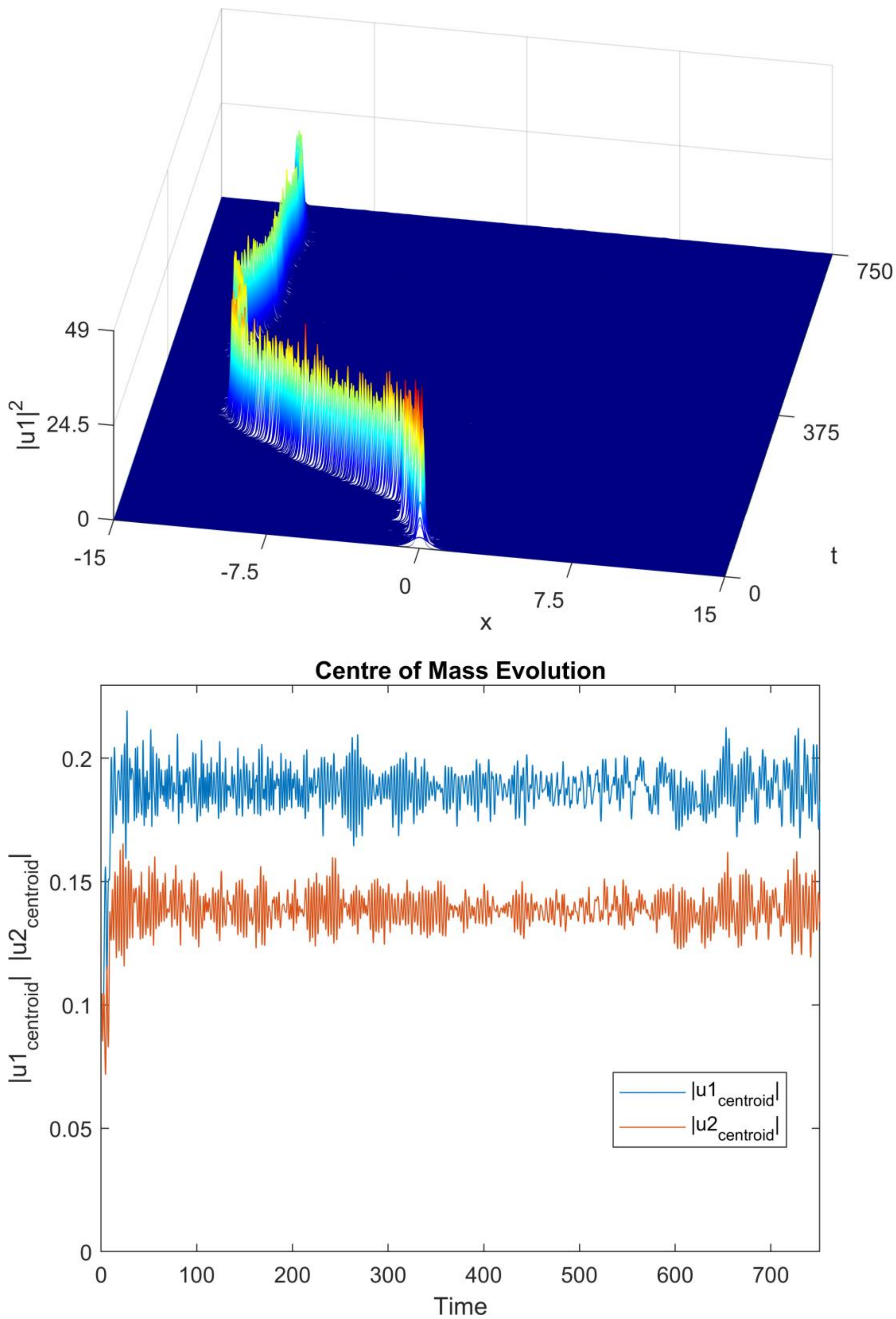

Figure 3.56 ED of u_1 and shows how focussed u_1 is (top), and the corresponding increase in dispersion late in the experiment (bottom).

3.6.2 u_data_a_1p5_mu_2p8_sym

From fractional derivative order $\alpha = 2.0$, to $\alpha = 1.5$, the solution oscillation frequency and dispersion increases, and solutions generally become more unstable until $\alpha = 1.5$, when u_1 becomes highly focussed, non-stationary, and u_2 disperses almost completely.

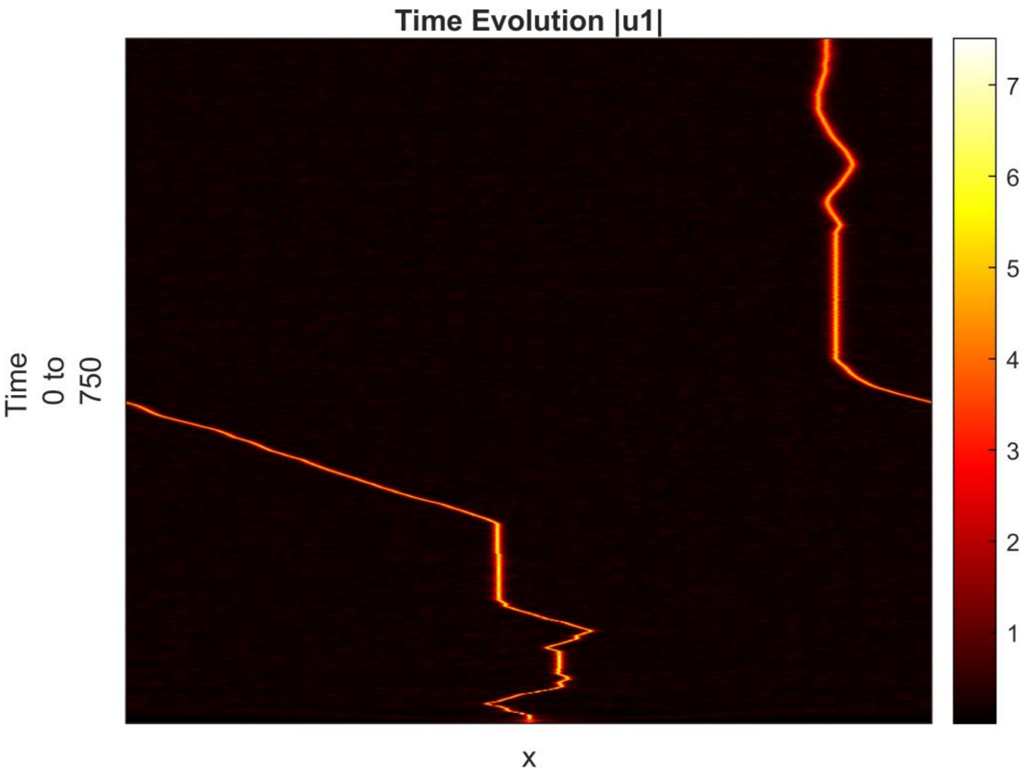

Figure 3.57 Heatmap of non-stationary solution u_1 when $\alpha = 1.5$. u_2 is not shown because it decays immediately.

In the heatmap in Figure 3.57 above, we observe u_1 deviate left, then right, and left again, leaving the boundary and ‘wrapping’, returning to the right of the heatmap consistent with periodic boundary conditions. Figure 3.58 shows disparity in the peak amplitude evolutions of u_1 and u_2, whereas the centre of mass evolution shows the solutions u_1 and u_2 dispersing throughout the experiment.

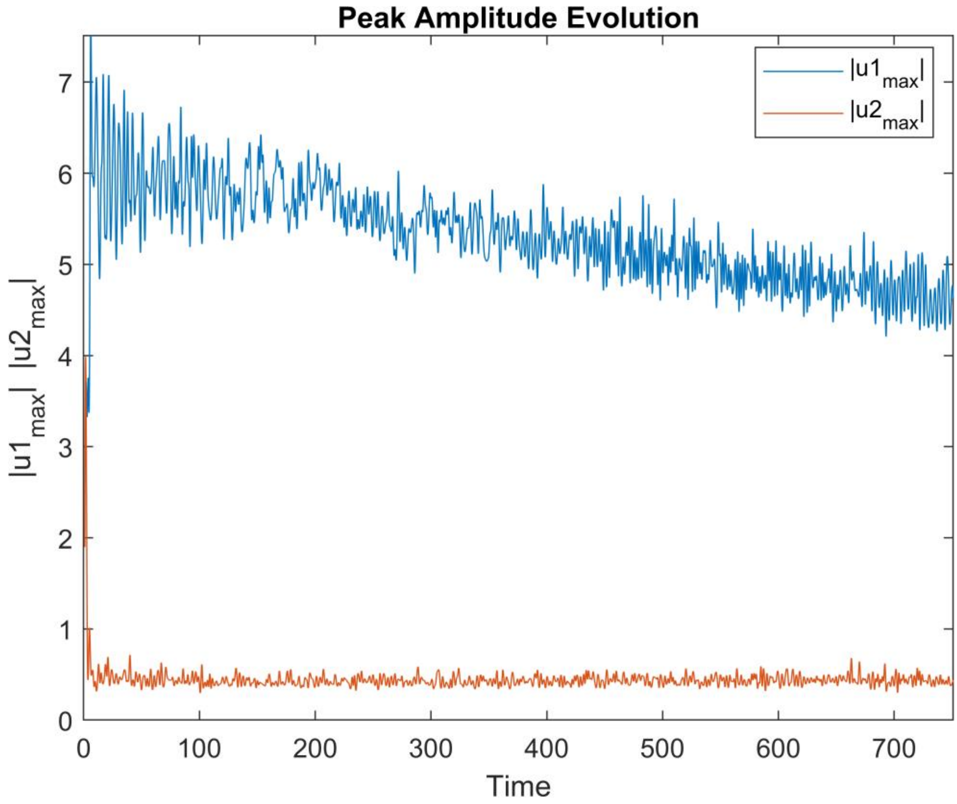

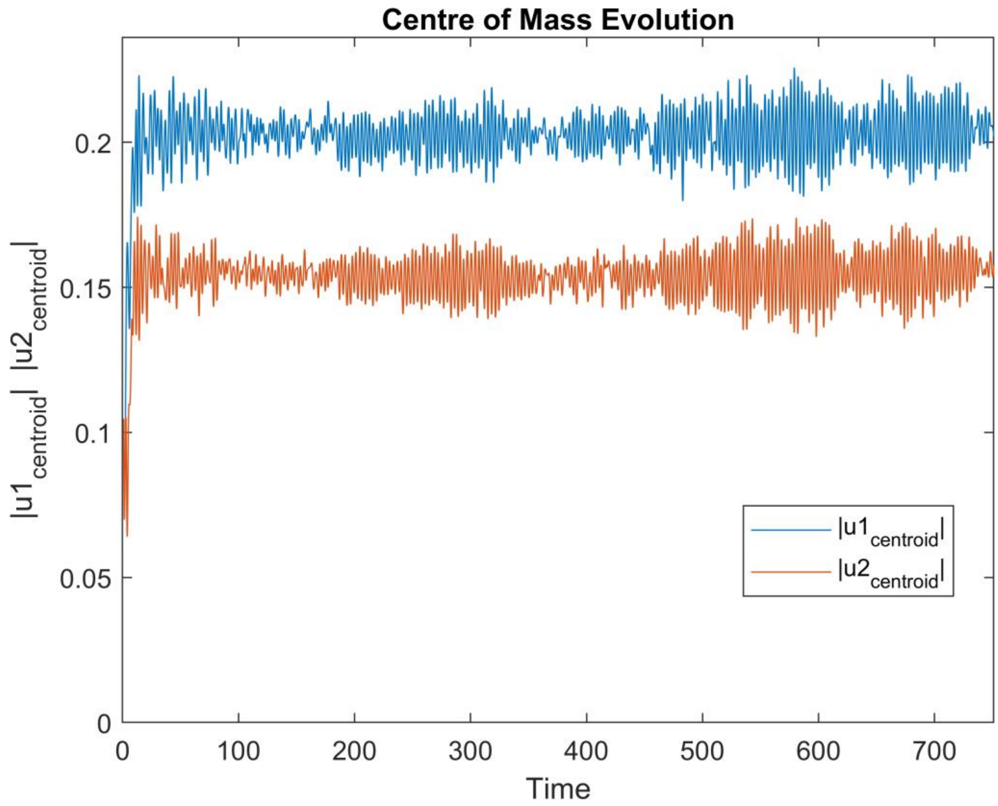

Figure 3.58 Peak amplitude evolution (top) shows gradual decay and high-frequency oscillations of u_1 over time. The centre of mass evolution increases over time, proportional to increased dispersion.

3.7 Fractional derivative α = 1.4

Here we present various dynamics for fractional derivative order $\alpha = 1.4$.

3.7.1 u_data_a_1p4_mu_1p8_asym

From fractional derivative order $\alpha = 2$, until $\alpha = 1.4$, the solution pair increases oscillation frequency and dispersion effects until we see aberrant, non-stationary, asymmetric behaviour with a phase propagation constant $\mu = 1.8$. We also note u_1 maintains a higher peak amplitude than u_2, which propagates in the solution field with a peak amplitude slightly higher than background noise in Figure 3.59.

In Figure 3.59 we observe the solution pair commence the experiment with amplitudes of approximately 5 and 0.9 for u_1 and u_2 respectively, after which the solutions quickly become non-stationary. If we look closely in Figure 3.59, we see the background radiation in u_2 largely propagates to the right.

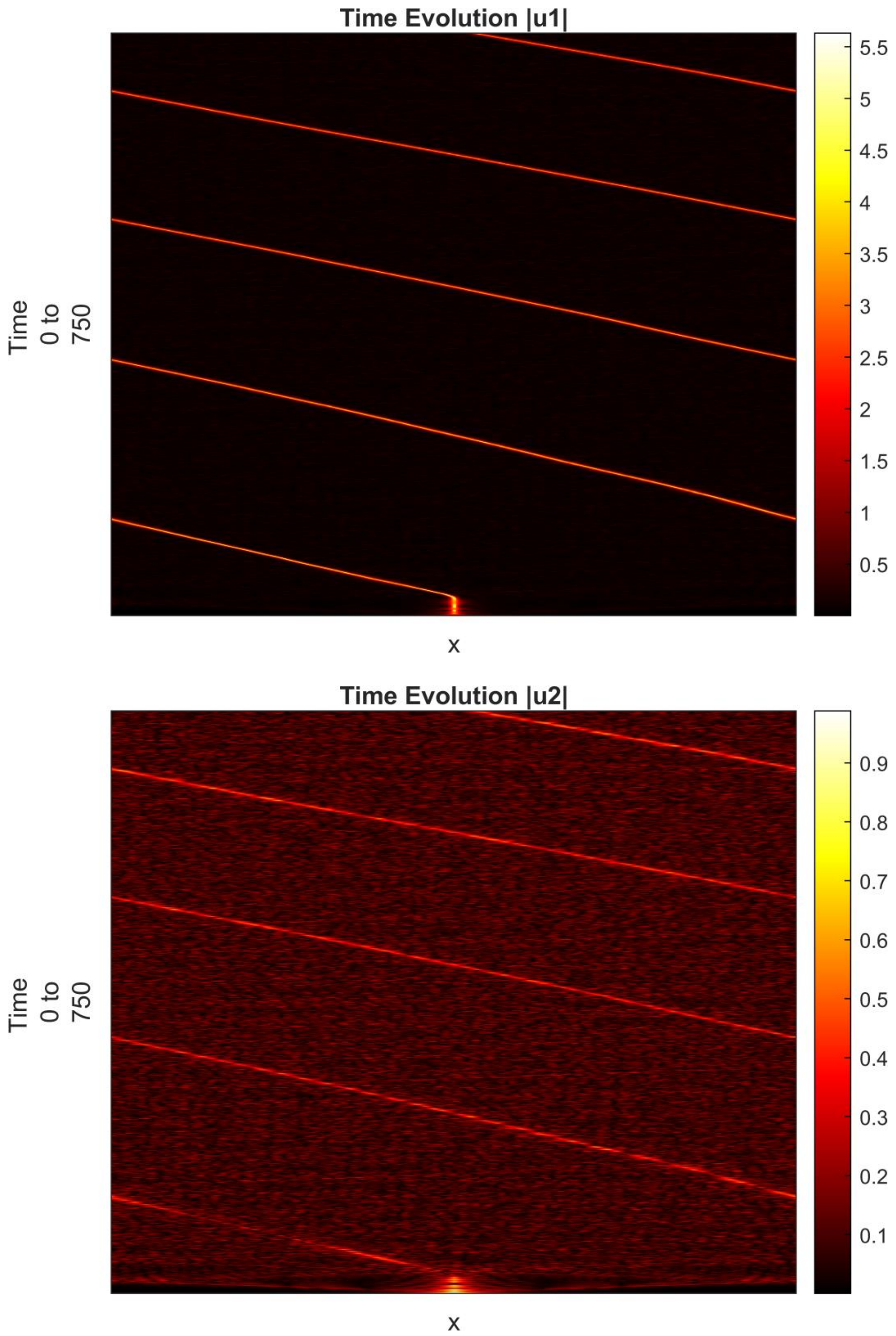

Figure 3.59 Non-stationary asymmetry when the fractional derivative $\alpha = 1.4$. The solution u_2 mainly radiates to the right (bottom).

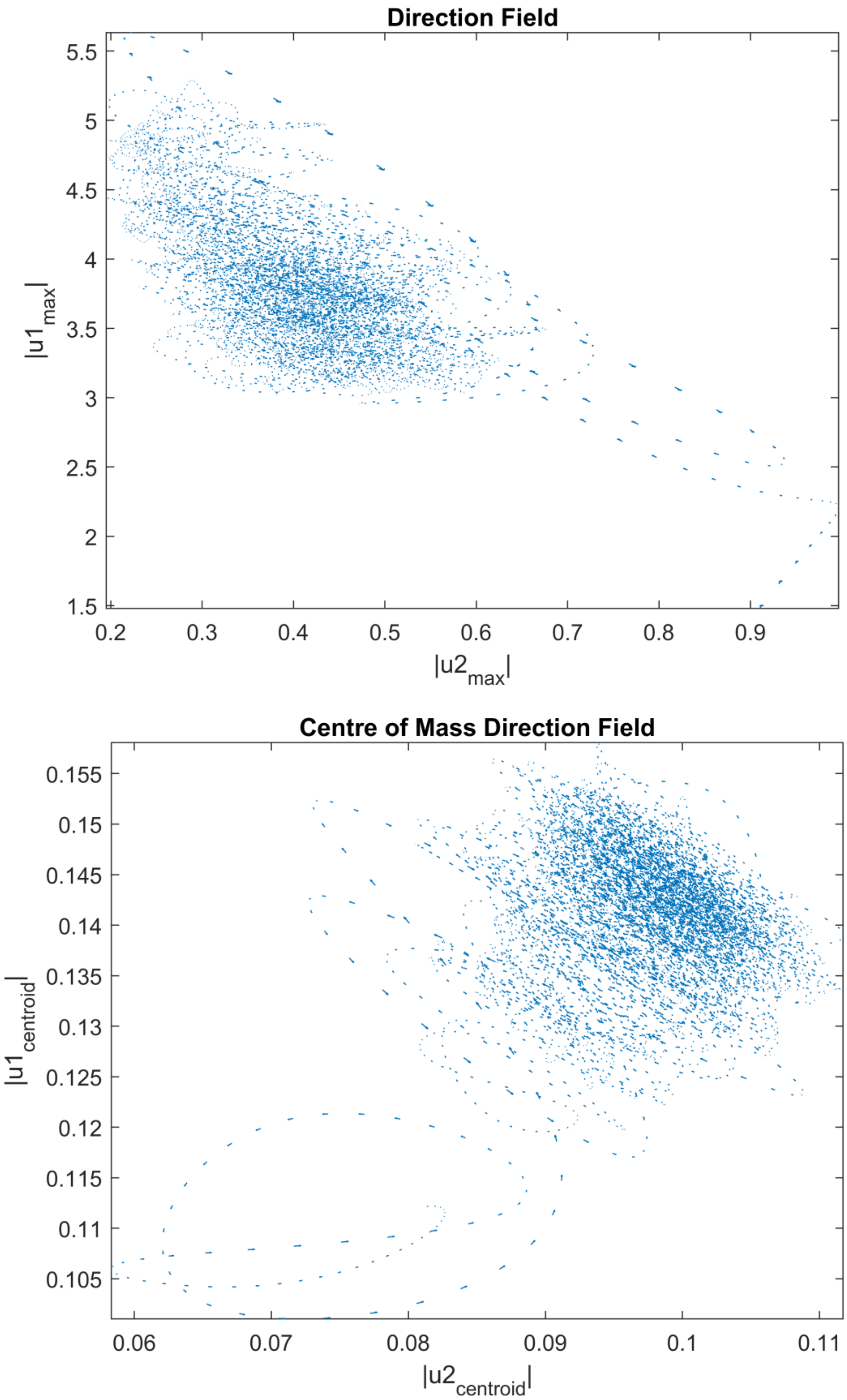

Figure 3.60 The direction fields of unstable non-stationary solutions. Peak amplitude direction field (top), and centre of mass direction field (bottom) for reference.

The direction field in Figure 3.60 above shows u_1 to be unstable, as there is substantial variance in the peak amplitude and centre of mass data from both u_1 and u_2 in both direction fields. The relatively wide distribution of direction points for u_1 and u_2 supports our conclusion this solution is unstable.

We see the following waterfall plots in Figure 3.61 have more dispersion detail than the heatmap in Figure 3.59, where the waterfall plot shows the extent of oscillations and decay from u_1. The u_2 solution disperses almost completely from initial conditions, yet still appears to be self-supporting. In Figure 3.61 we notice u_1 is highly focussed, narrow and appears to disperse continually throughout the experiment. Dispersion is evidenced by continuous decay in peak amplitude and consistent radiation throughout the solution field. From a closer inspection of Figure 3.61 it is possible the self-supporting behaviour evident in u_2, and the noise evident in the solution field u_1 may be the result of coupling between the solutions.

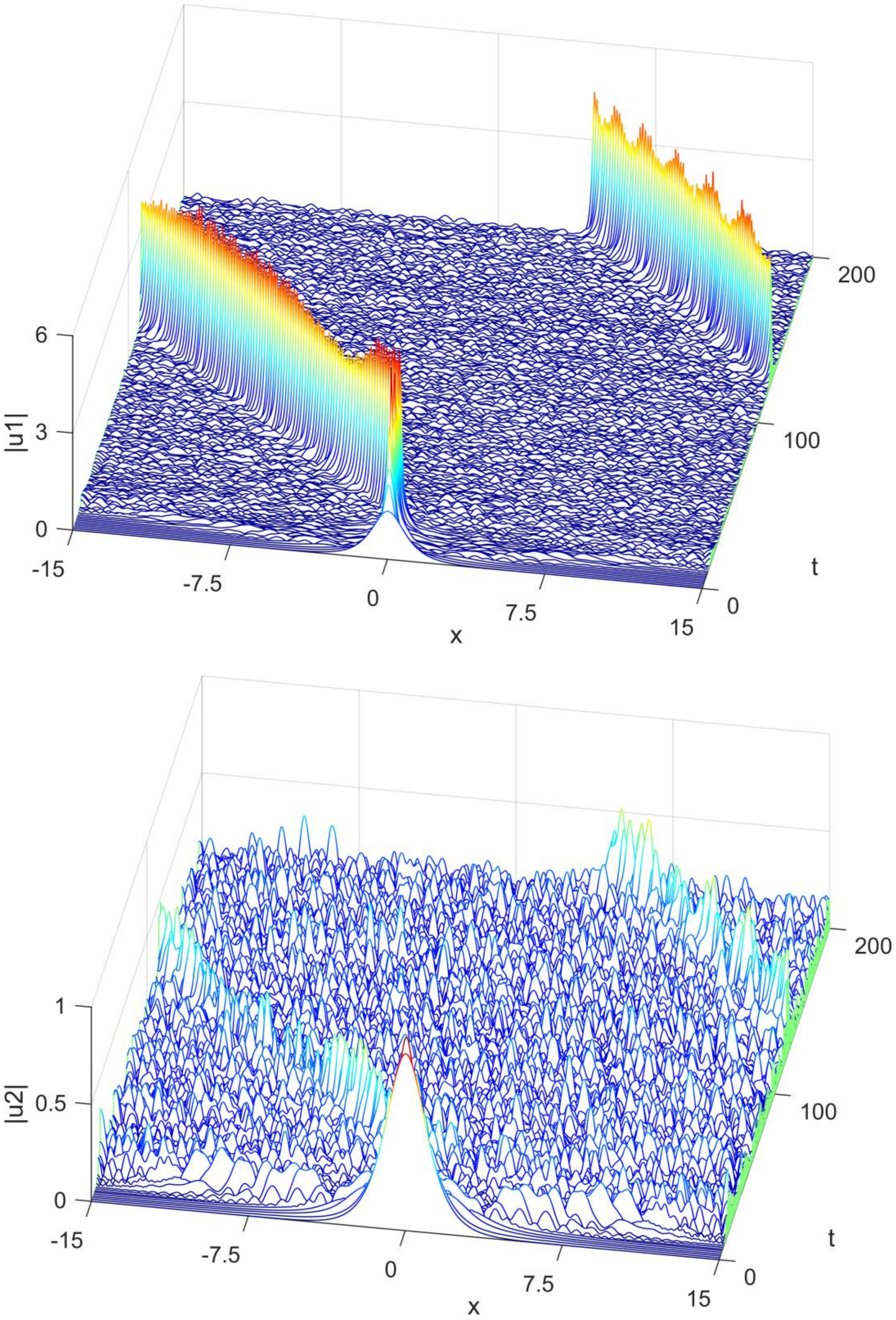

Figure 3.61 A closer inspection of the non-stationary solutions show u_1 is highly focussed, while u_2 is barely distinguishable from background radiation.

3.7.2 u_data_a_1p4_mu_1p8_sym

The solution quality continues to decay asymmetrically from fractional derivative order $\alpha = 2$, until $\alpha = 1.4$ with a phase propagation constant $\mu = 1.8$. The solutions display behaviour consistent with increasing oscillations and dispersion until we observe the following unstable, non-stationary behaviour in Figure 3.62. We see from the heatmap in Figure 3.62 a high degree of asymmetry, and a more focussed solution in the form of u_1, consistent with previous non-stationary solutions.

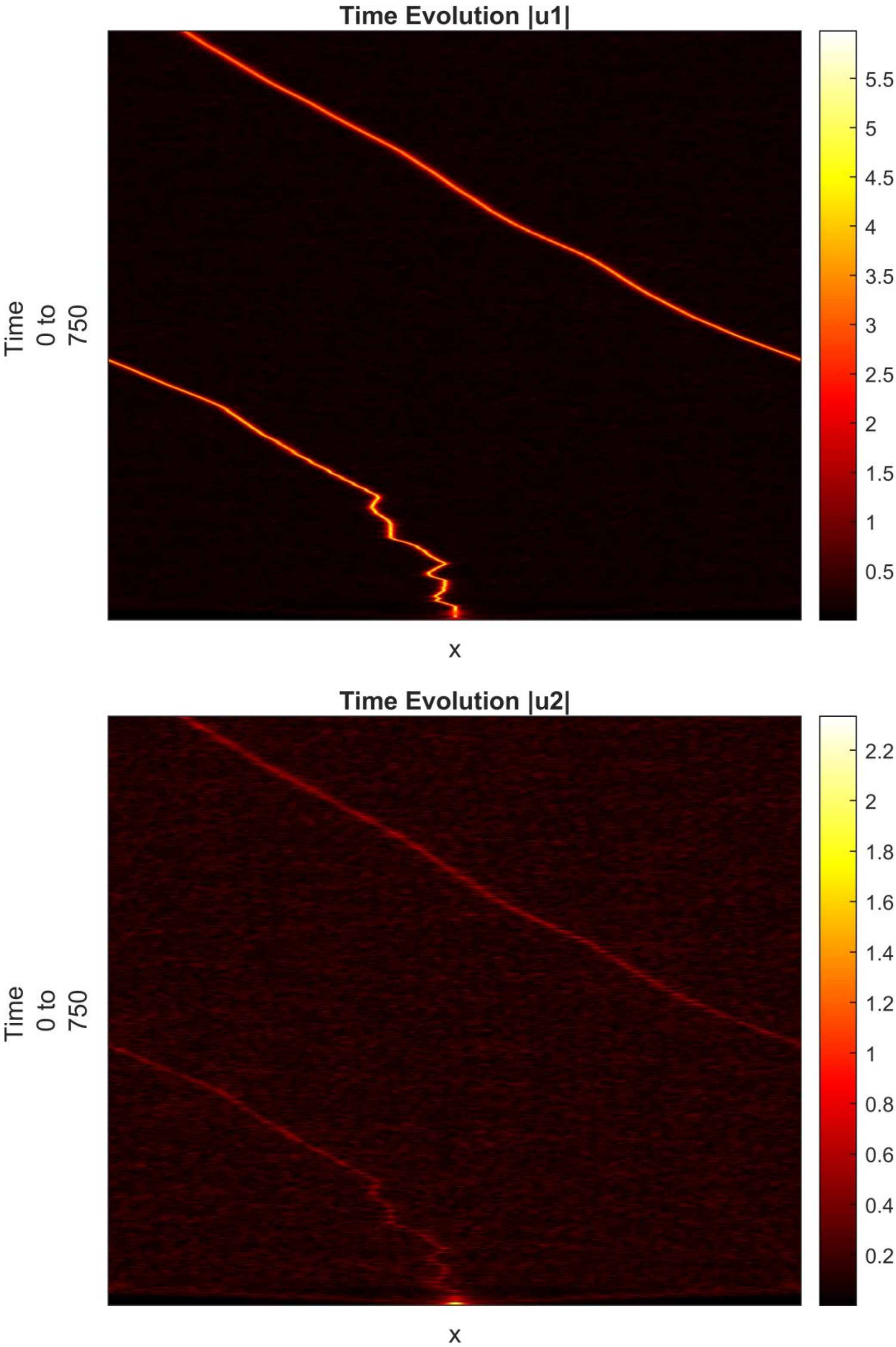

Figure 3.62 Highly asymmetric, non-stationary solutions propagating left when the fractional derivative $\alpha = 1.4$.

If we look at the following peak amplitude evolution in Figure 3.63, we see u_1 and u_2 appear to be converging throughout the experiment.

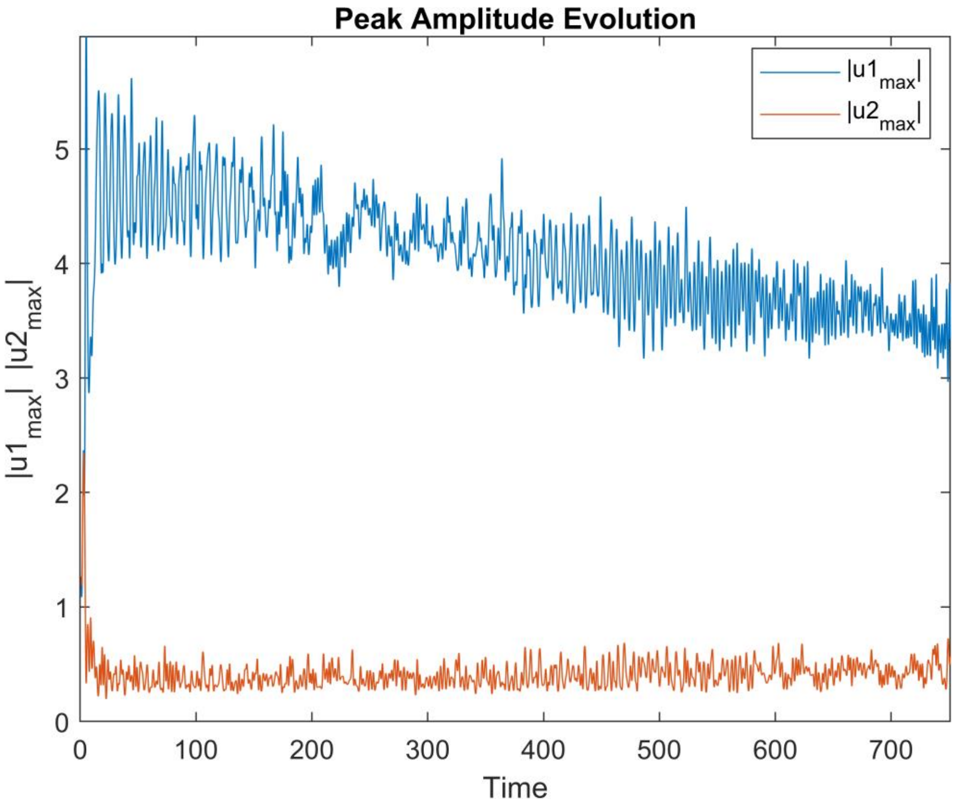

Figure 3.63 The peak amplitude plot and phase portrait shows u_1 decaying over time, whereas u_2 peak amplitude slowly increases.

3.7.3 u_data_a_1p4_mu_2_asym

From fractional derivative order $\alpha = 2$, until $\alpha = 1.4$ with a phase propagation constant $\mu = 2$, the asymmetric solution quality decreases, with a corresponding increase in oscillations and dispersion until we see the following solution in the heatmap in Figure 3.64.

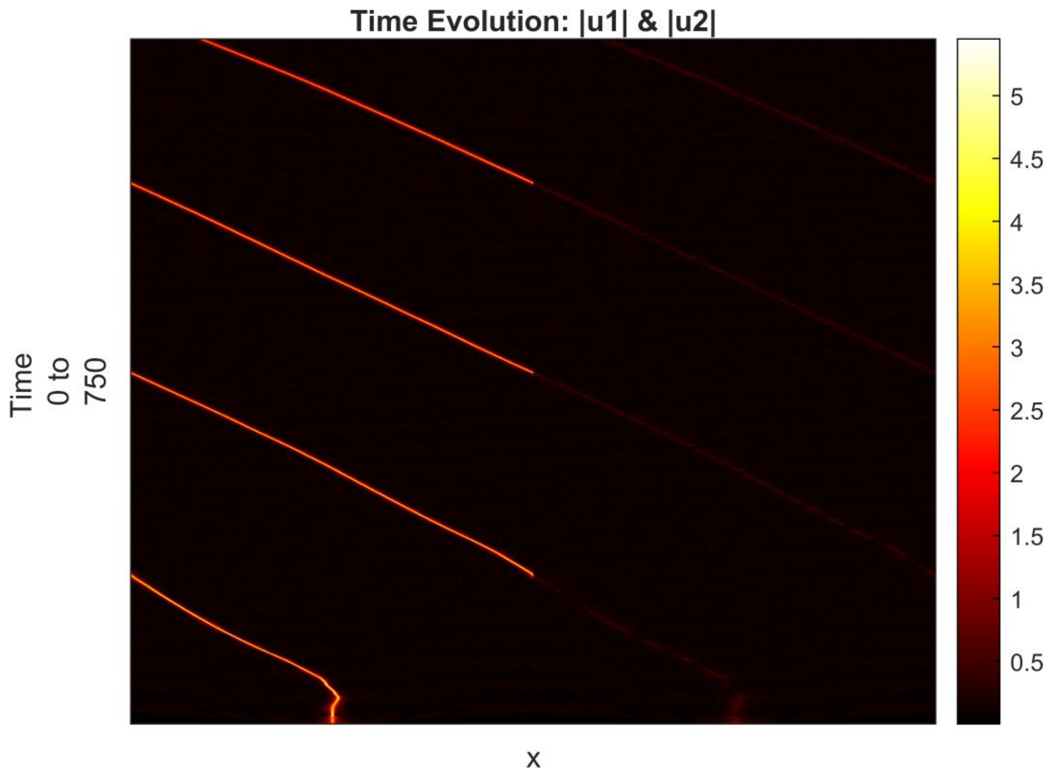

Figure 3.64 Aberrant, non-stationary, asymmetric behaviour when the fractional derivative $\alpha = 1.4$.

When the fractional derivative order $\alpha = 1.4$, we see in Figure 3.64 u_1 becomes highly focussed, and u_2 disperses, barely distinguishable from noise. The waterfall plot in Figure 3.65 for 200t showing the ED of u_1 and u_2 illustrates a substantial decay in u_2, radiating both to the right and left of the solution. Conversely, u_1 becomes focussed and maintains erratic oscillations in peak amplitude over time. We note the asymmetric solutions travel briefly to the right, then continuously to the left.

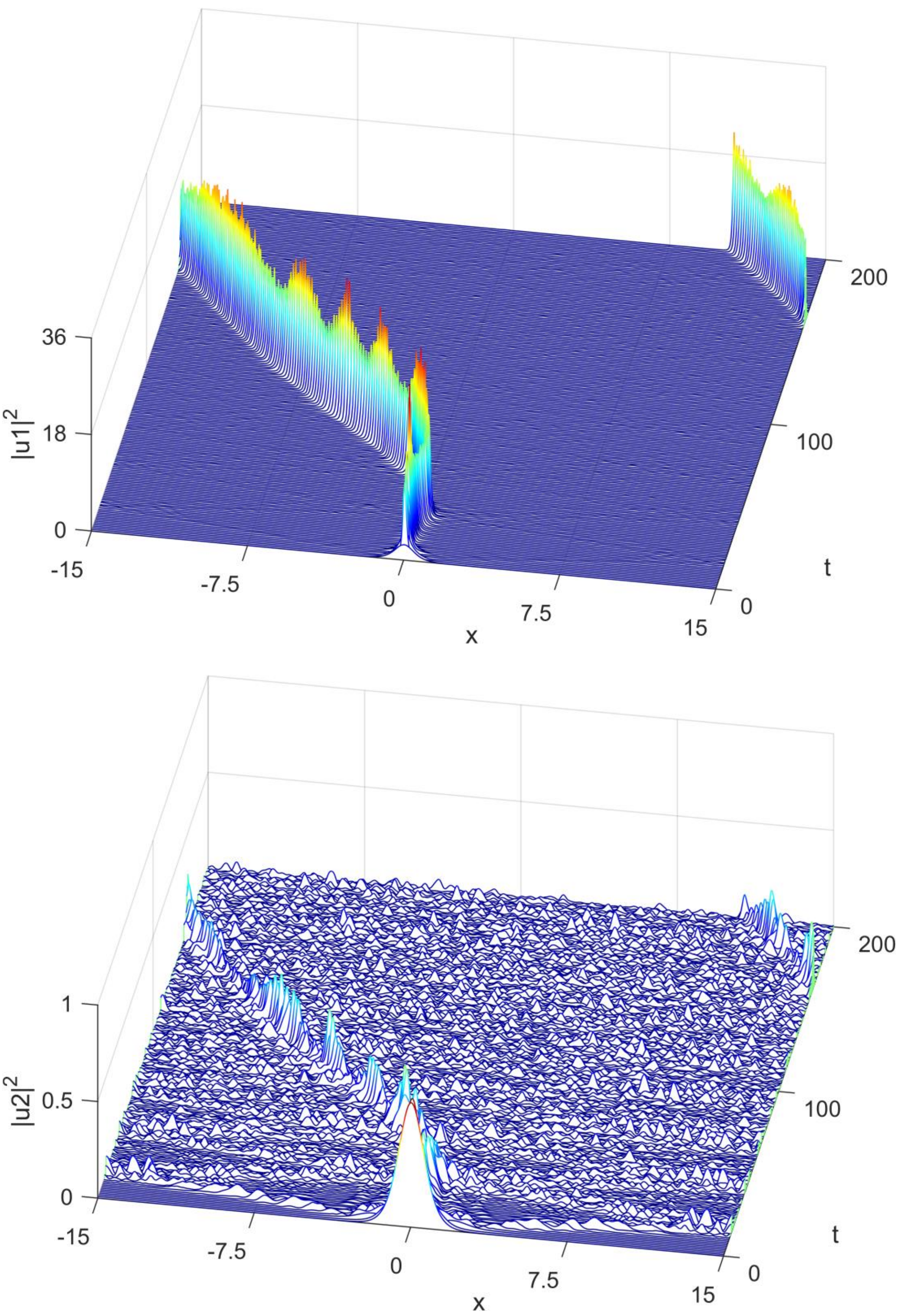

Figure 3.65 ED of u_1 and u_2 reveal u_1 is highly focussed, while u_2 has decayed substantially.

3.7.4 u_data_a_1p4_mu_2p0_sym

The symmetric solution pair continues to deteriorate until the fractional derivative α = 1.4 and the phase propagation constant μ = 2, when we see the following non-stationary behaviour in Figure 3.66. For the symmetric solutions, note as the phase propagation constant μ increases, the solutions become more asymmetric, and the non-stationary solution becomes more erratic, deviating right, then left, then right again.

The centre of mass evolution and centre of mass phase portrait for u_1 in Figure 3.67 shows that despite the non-stationary behaviour, u_1 maintains relatively stable behaviour with minimal dispersion from the centre of mass evolution, and conservation of mass with an unstable sink at approximately 0.18.

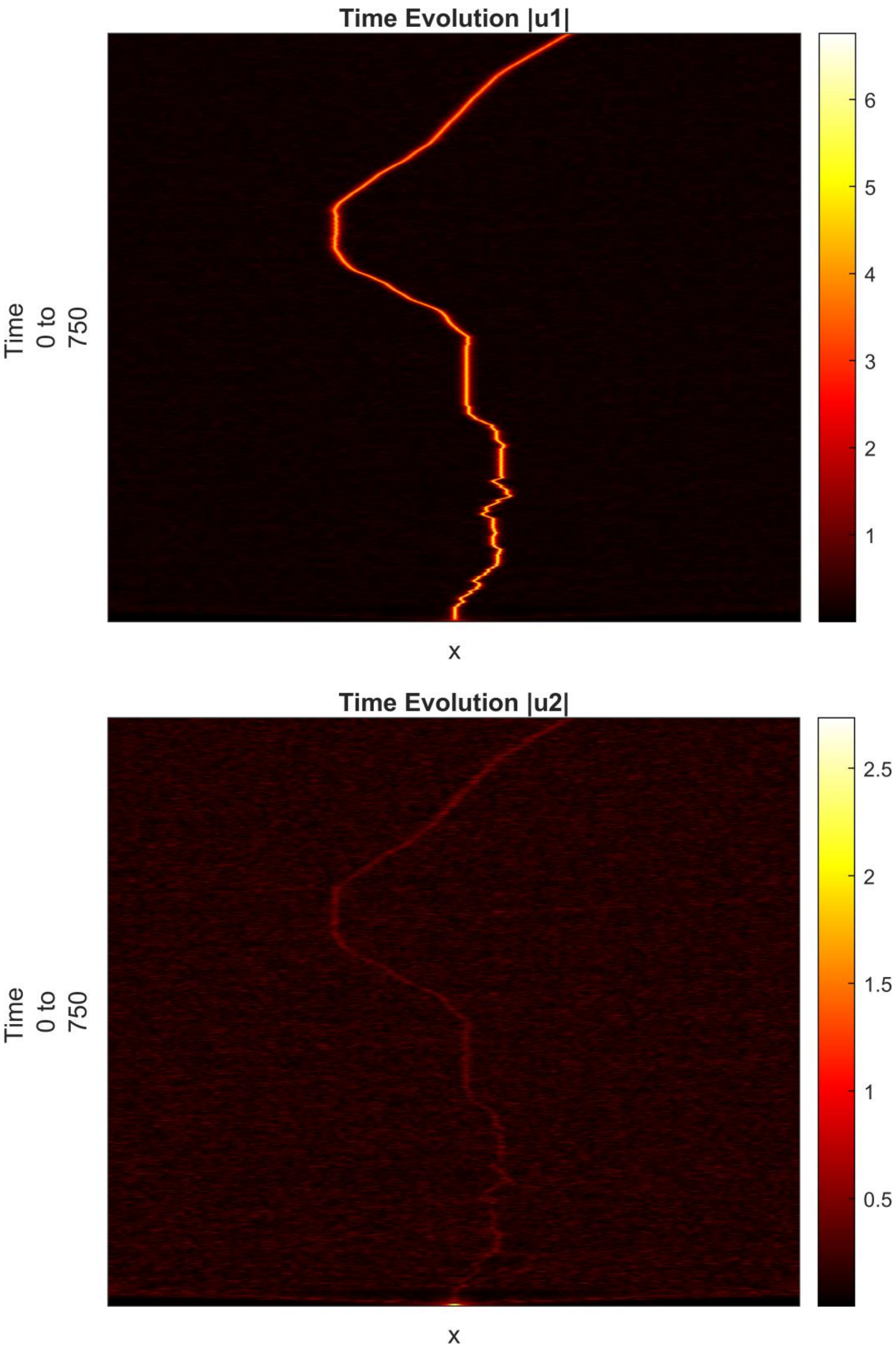

Figure 3.66 Heatmap reveals aberrant path of u_1 and u_2, while remaining highly asymmetric and focussed.

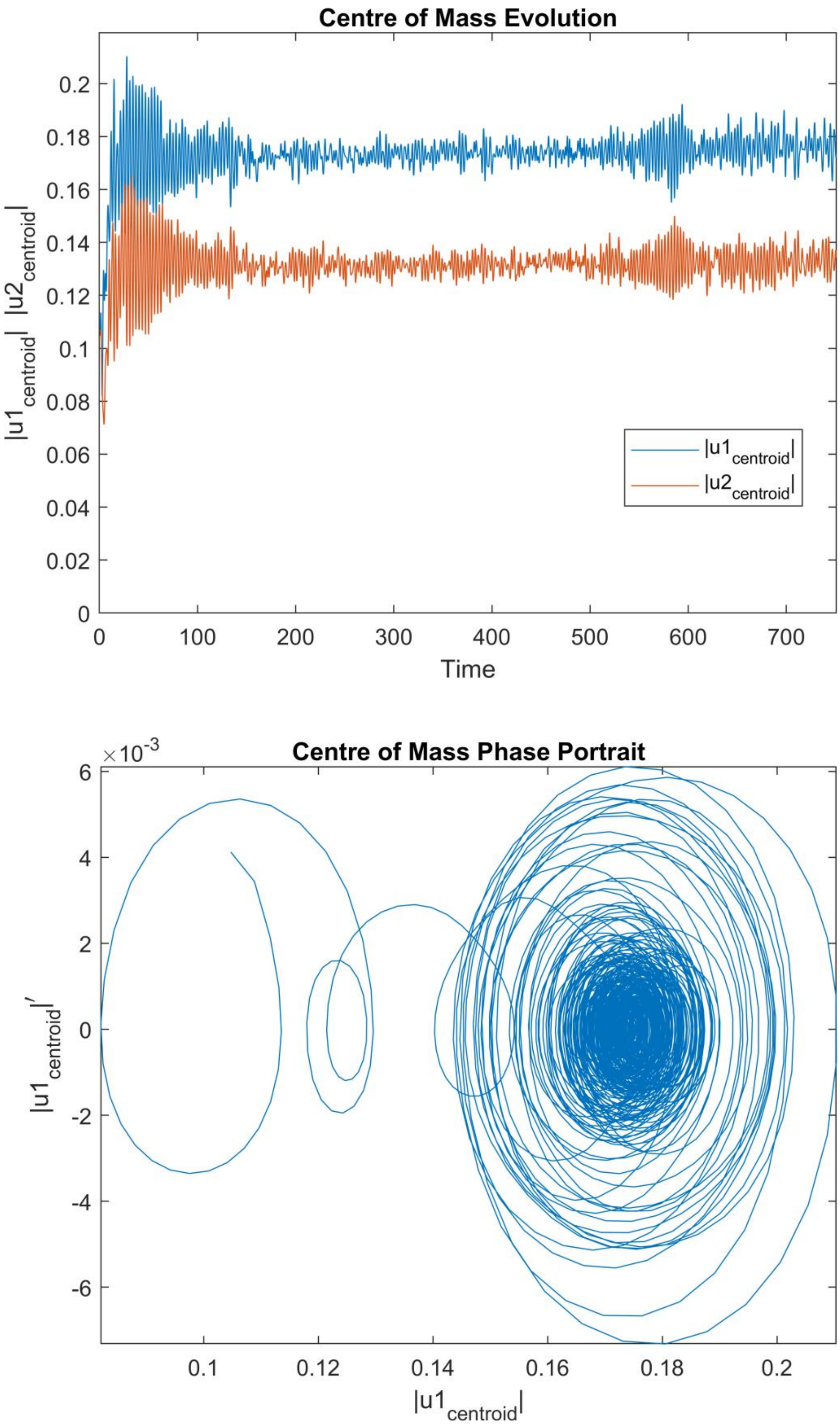

Figure 3.67 Centre of mass evolution (top) and phase portrait (bottom) would appear to indicate stable, asymmetric solutions. However, since we know the solution is non-stationary, it is classified as unstable.

3.7.5 u_data_a_1p4_mu_2p2_asym

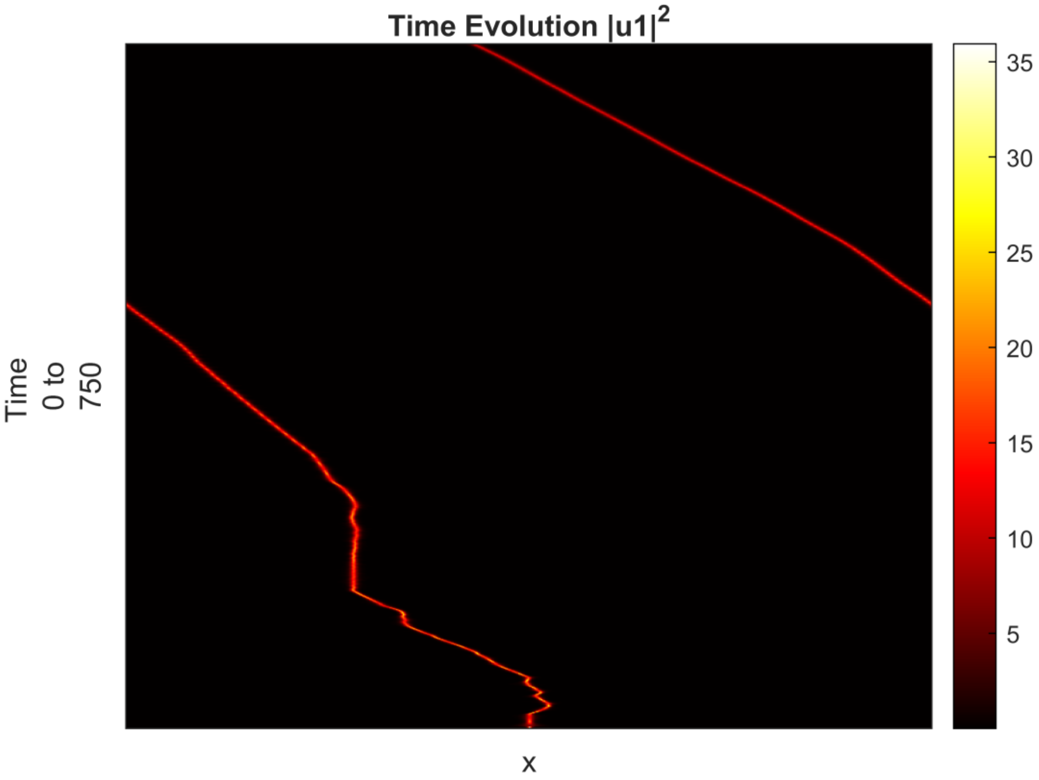

Figure 3.68 Heatmap ED of a highly asymmetric, non-stationary solution.

As the fractional derivative order α approaches 1.4 and the phase propagation constant μ = 2.2, the unstable, asymmetric, and oscillatory behaviour increases until aberrant, non-stationary behaviour occurs, as seen in Figure 3.68. We can see more detail from the following waterfall plots in Figure 3.69, where we notice oscillations in peak amplitude of u_1 decreasing in size during a gradual decay of the solution. Continuing our observation of Figure 3.69, we note u_1 is focussed, and while substantially smaller than u_1, u_2 remains distinguishable from background dispersion.

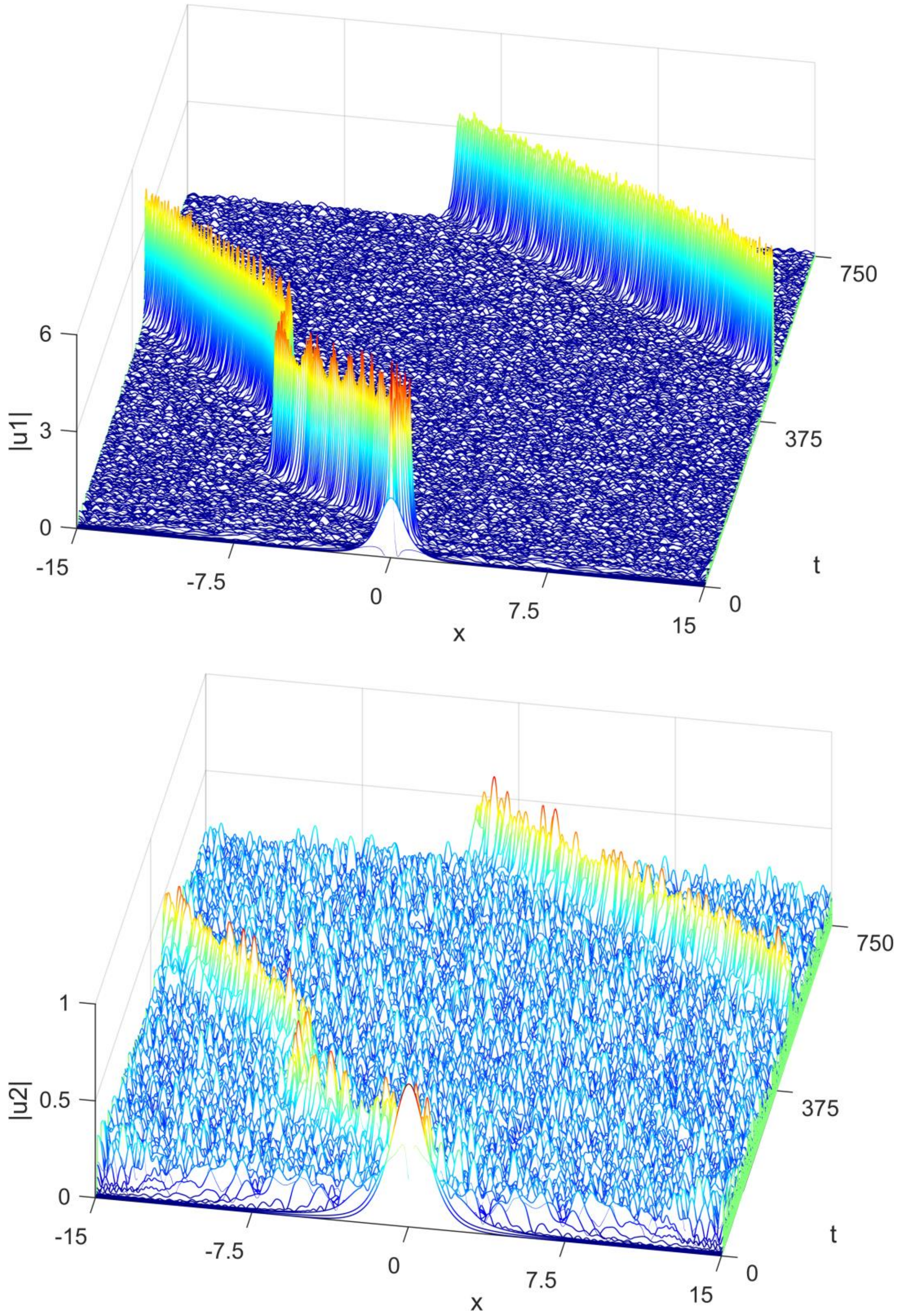

Figure 3.69 Waterfall plots reveal u_1 is highly focussed, while u_2 propagates through a highly dispersed solution field.

The peak amplitude evolution in Figure 3.70 shows the decay of u_1 throughout the experiment as the solution evolves into an oscillating wave envelope while u_2 disperses, where the amplitude approaches background noise levels.

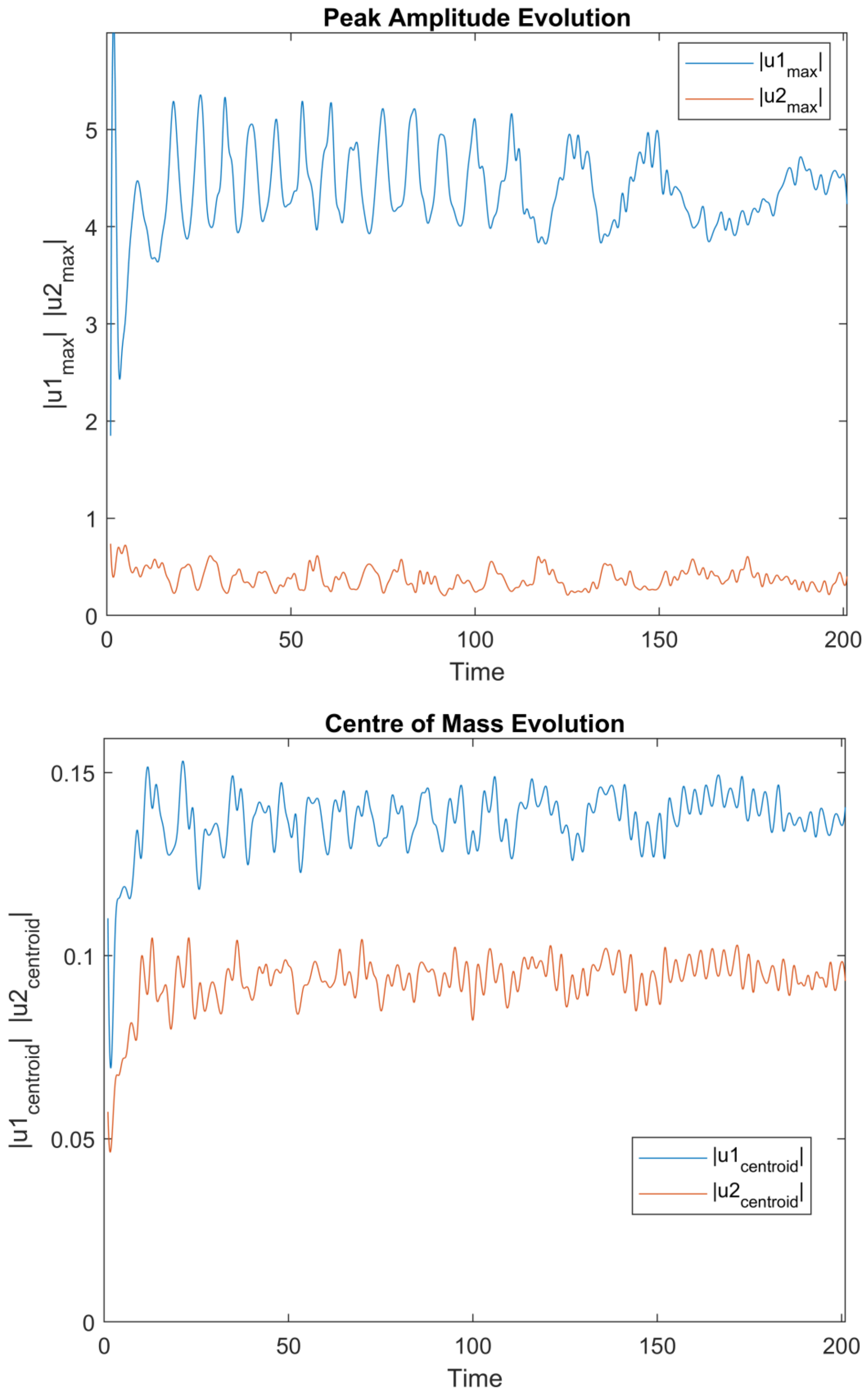

Figure 3.70 The peak amplitude evolution for 200t (top) reveals the gradual increase in dispersion in u_1 as the oscillation frequency increases. Centre of mass evolution (bottom) for reference.

3.7.6 u_data_a_1p4_mu_2p2_sym

As the fractional derivative order decreases from $\alpha = 2$, the solution stability decreases, and dispersion increases until the fractional derivative $\alpha = 1.4$and the phase propagation constant $\mu = 2.2$. In Figure 3.71 we see non-stationary, highly asymmetric behaviour from u_1 and u_2. Figure 3.71 shows u_1 deviate right, before moving to the left at an increasing rate over time. The solution u_2 appears to decay instantly, and leaves behind a noisy solution field.

Observing the phase portrait in Figure 3.72, we see the peak amplitude of u_1 appear relatively stable throughout the experiment with an amplitude value ranging from 5 to 6, despite the non-stationary behaviour of the solution. The relative stability of the peak amplitude is reflected in the centre of mass portrait in Figure 3.72, which appears to behave as an unstable attractor at approximately 0.18.

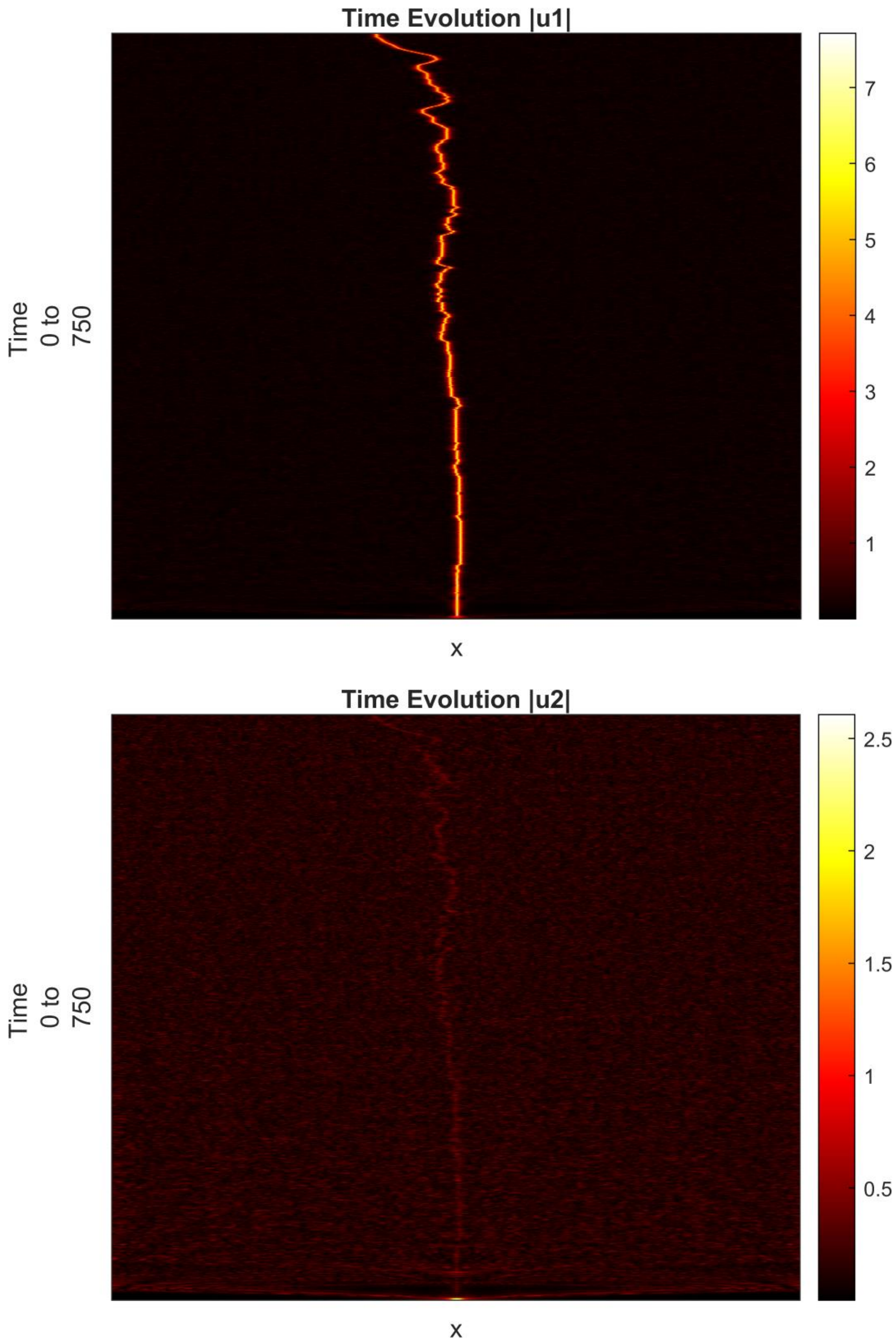

Figure 3.71 The heatmaps show the asymmetry and non-stationary behaviour of the solution pair.

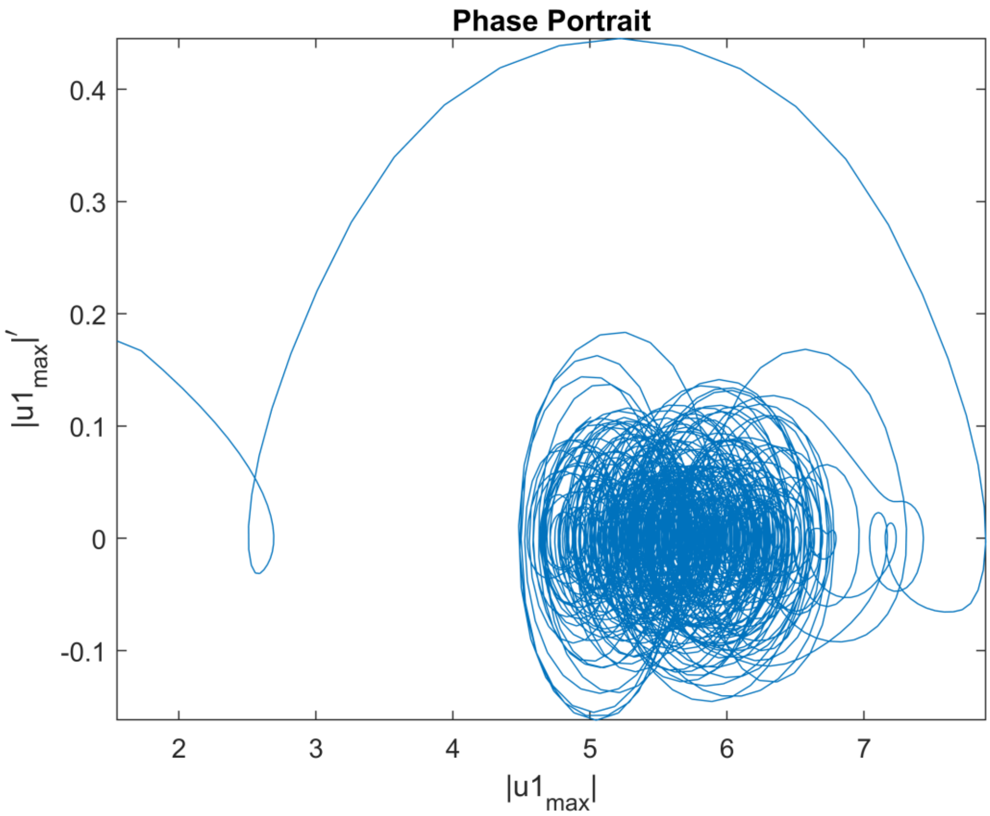

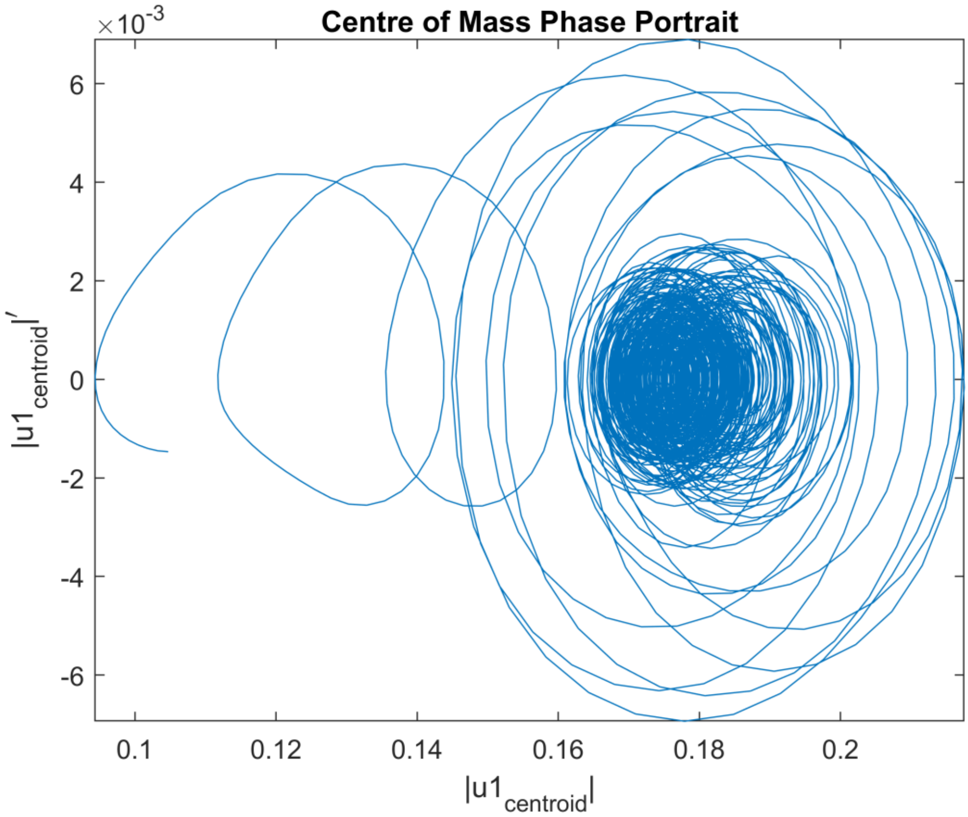

Figure 3.72 The phase portrait for peak amplitude (top) and centre of mass (bottom) reveals an unstable equilibrium point.

3.7.7 u_data_a_1p4_mu_2p4_sym

As the fractional derivative order decreases from α =2, the symmetric solutions continue propagating asymmetrically until becoming non-stationary and propagating to the left of the solution field when $\alpha = 1.4$ and the phase propagation constant $\mu = 2.4$: evident in the heatmap below in Figure 3.73.

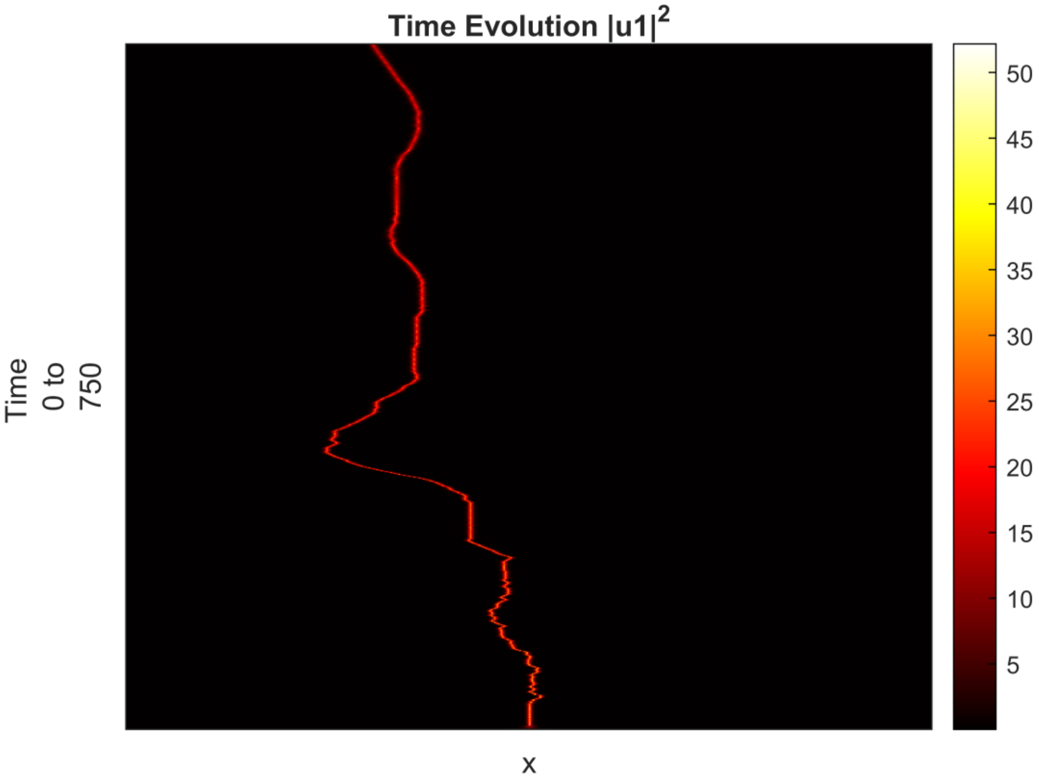

Figure 3.73 ED heatmap shows non-stationary behaviour from u_1. The coupled solution, u_2 is virtually reduced to noise.

The waterfall ED plot Figure 3.74 below, indicates the instability and decay of the solution throughout the experiment. In the peak amplitude evolution in Figure 3.75, we see u_2 immediately disperses into noise, while the solutions converge throughout the experiment.

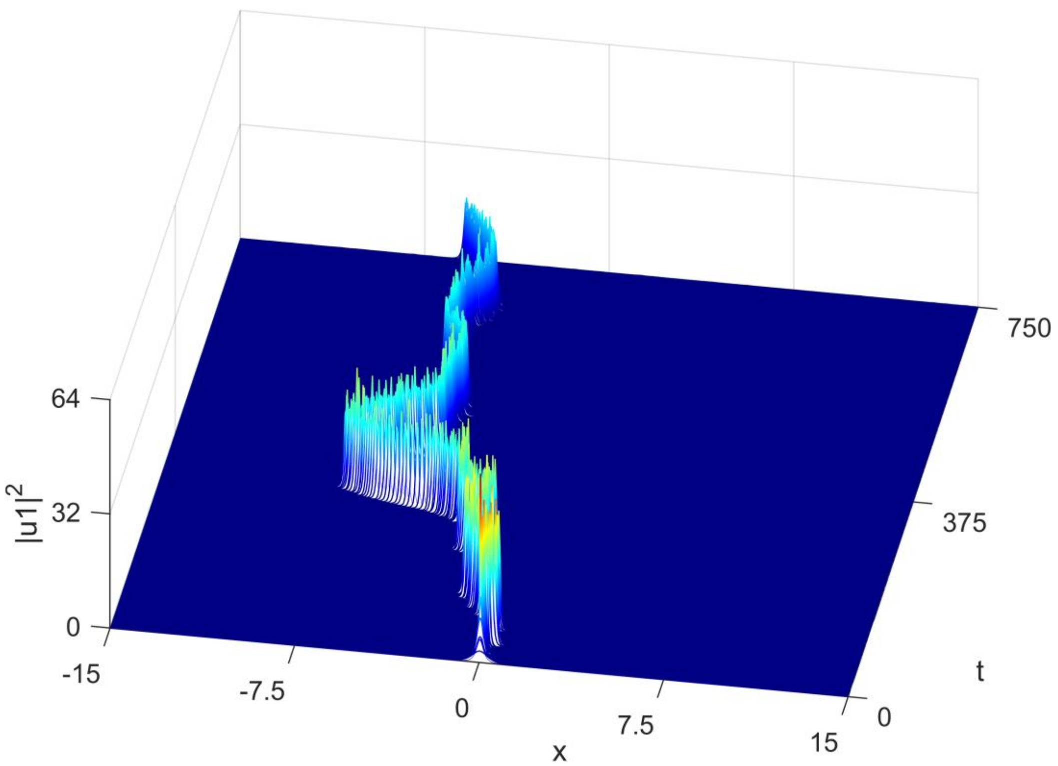

Figure 3.74 Waterfall ED plot shows u_1 to be highly focussed and unstable.

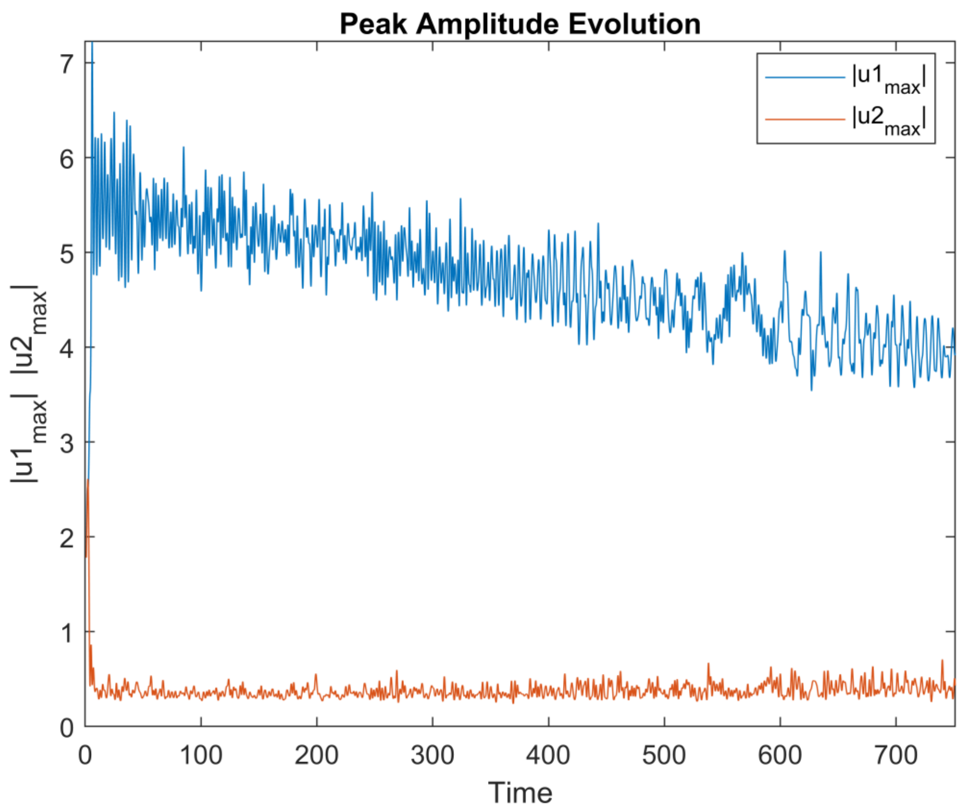

Figure 3.75 The peak amplitude evolution shows converging solutions: u_1 decreases over time, while u_2 increases over time.

3.7.8 u_data_a_1p4_mu_2p4_asym

From fractional derivative order α = 2, until α = 1.4, with the phase propagation constant μ = 2.4, we see a gradual increase in both asymmetry and focus, before non-stationary behaviour occurs, evident in Figure 3.76.

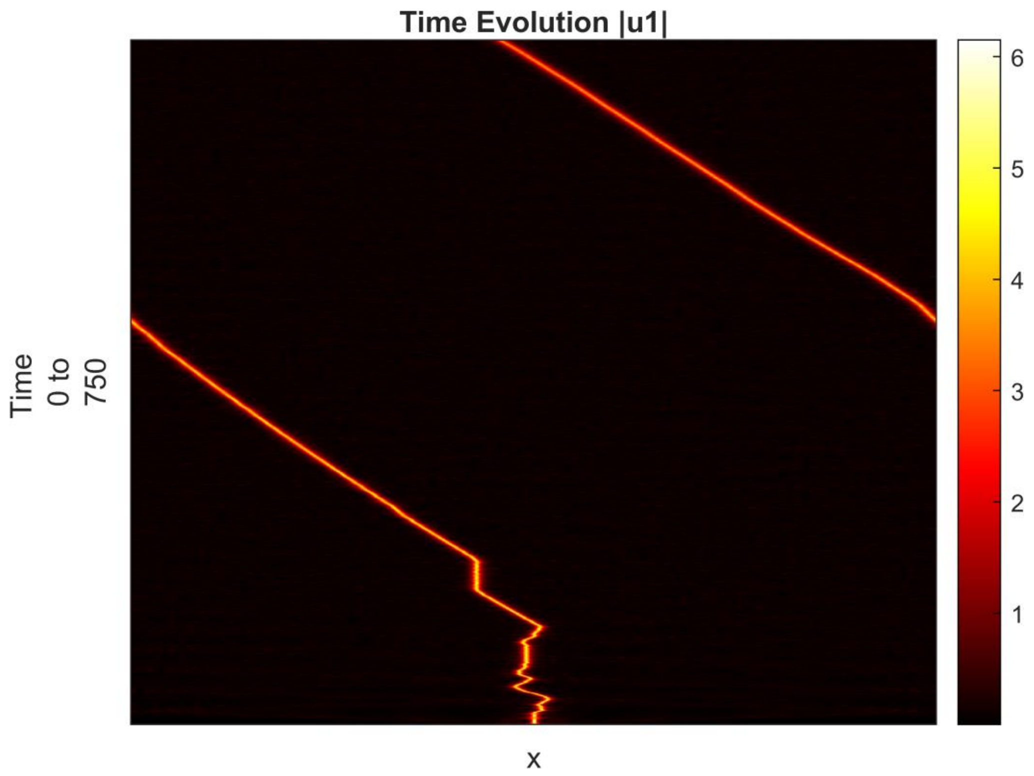

Figure 3.76 Non-stationary behaviour, where the solution propagates left.

The following waterfall plots in Figure 3.77 shows the ED oscillations, instability and the degree of focus of the u_1 solution. It is still possible to see the solution u_2 in the waterfall ED within Figure 3.77.

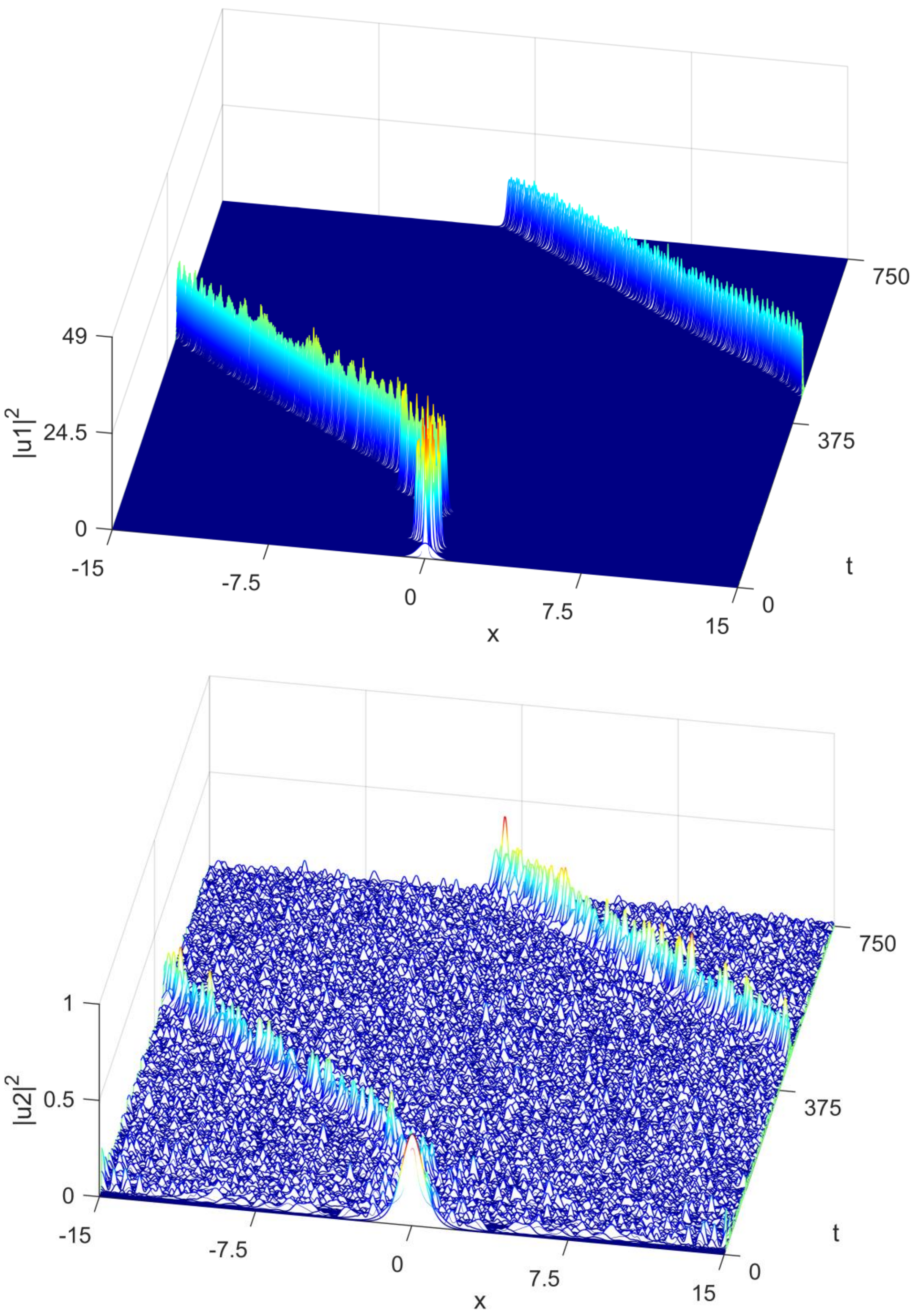

Figure 3.77 Waterfall plots of the ED reveal how focussed u_1 becomes when the fractional derivative $\alpha = 1.4$ and demonstrate the convergence of the peak amplitudes throughout the experiment.

3.7.9 u_data_a_1p4_mu_2p4_sym

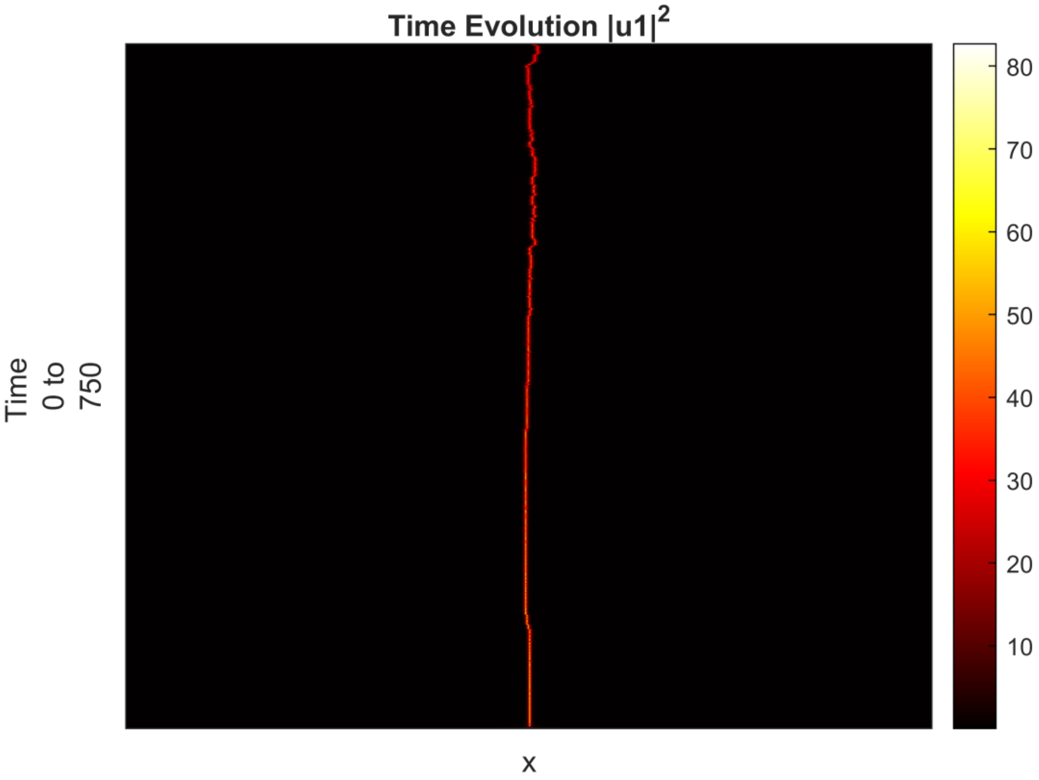

Figure 3.78 Heatmap ED illustrating non-stationary behaviour of u_1.

When the fractional derivative $\alpha = 1.4$ and the phase propagation constant $\mu = 2.4$, u_1 becomes more focussed, and u_2 continues to decay. Figure 3.78 shows the non-stationary behaviour of u_1 ED throughout the experiment. We see on the waterfall plot in Figure 3.79 the maximum peak amplitude for both u_1 and u_2 is greater than the previous results from $\alpha = 1.5$: the ED peak amplitude has effectively doubled from derivative order $\alpha = 1.5$ to $\alpha = 1.4$.

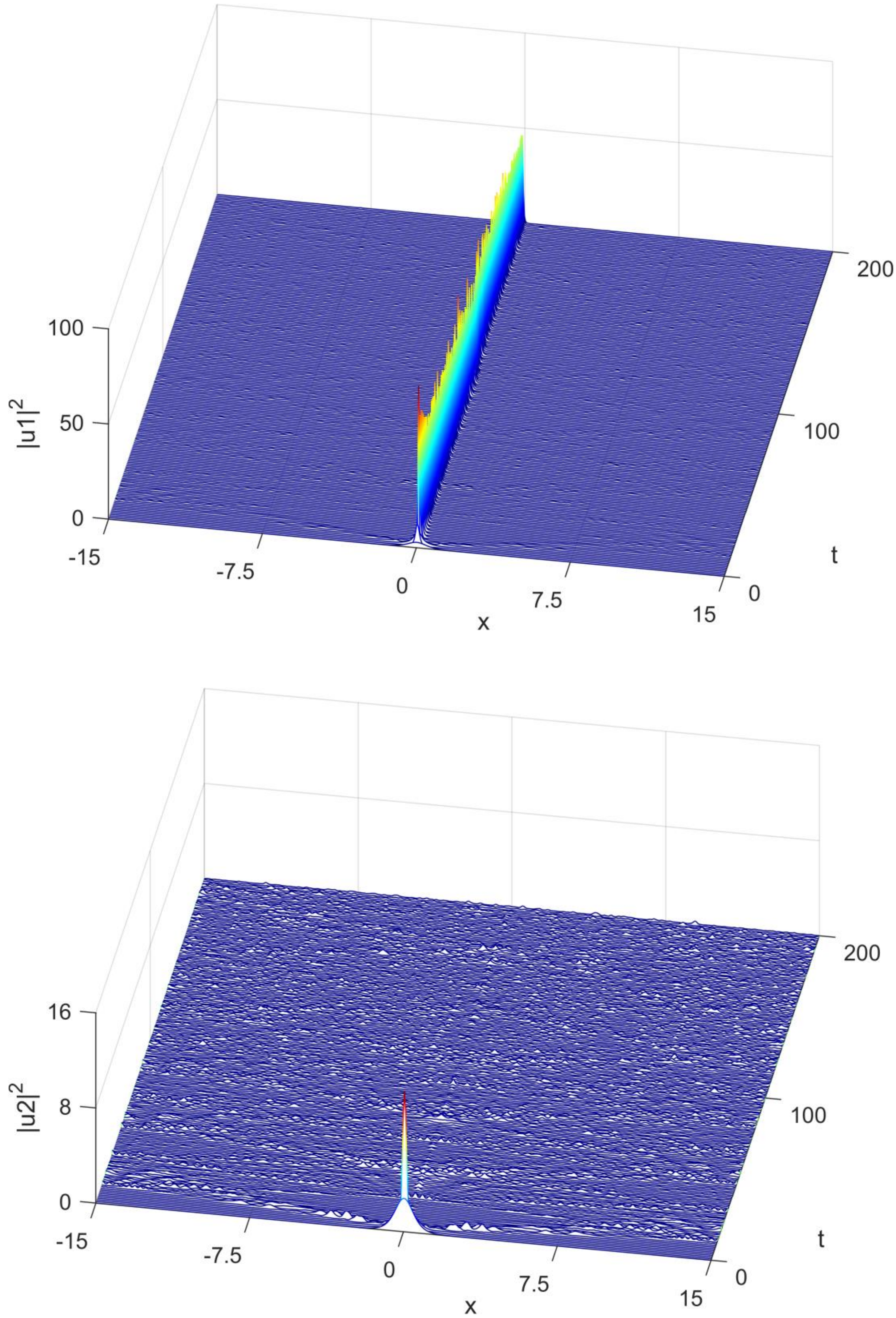

Figure 3.79 Waterfall plot ED for u_1 and u_2 for 200t show dispersive noise evident in both solution fields.

3.7.10 u_data_a_1p4_mu_2p8_asym

As the fractional derivative order α approaches 1.4 and the phase propagation constant $\mu = 2.8$, the solutions undergo increased dispersion until u_1 becomes focussed, and u_2 radiates to background noise, evident in Figure 3.80. If we consider the peak amplitude plot in Figure 3.81, we see u_1 and u_2 converging throughout the experiment. In Figure 3.81 we see the centre of mass evolution of both solutions u_1 and u_2 increase over time, consistent with increased dispersion for both solutions as the experiment evolves, or perhaps the centre of mass increases proportional to the angle of propagation through the solution field.

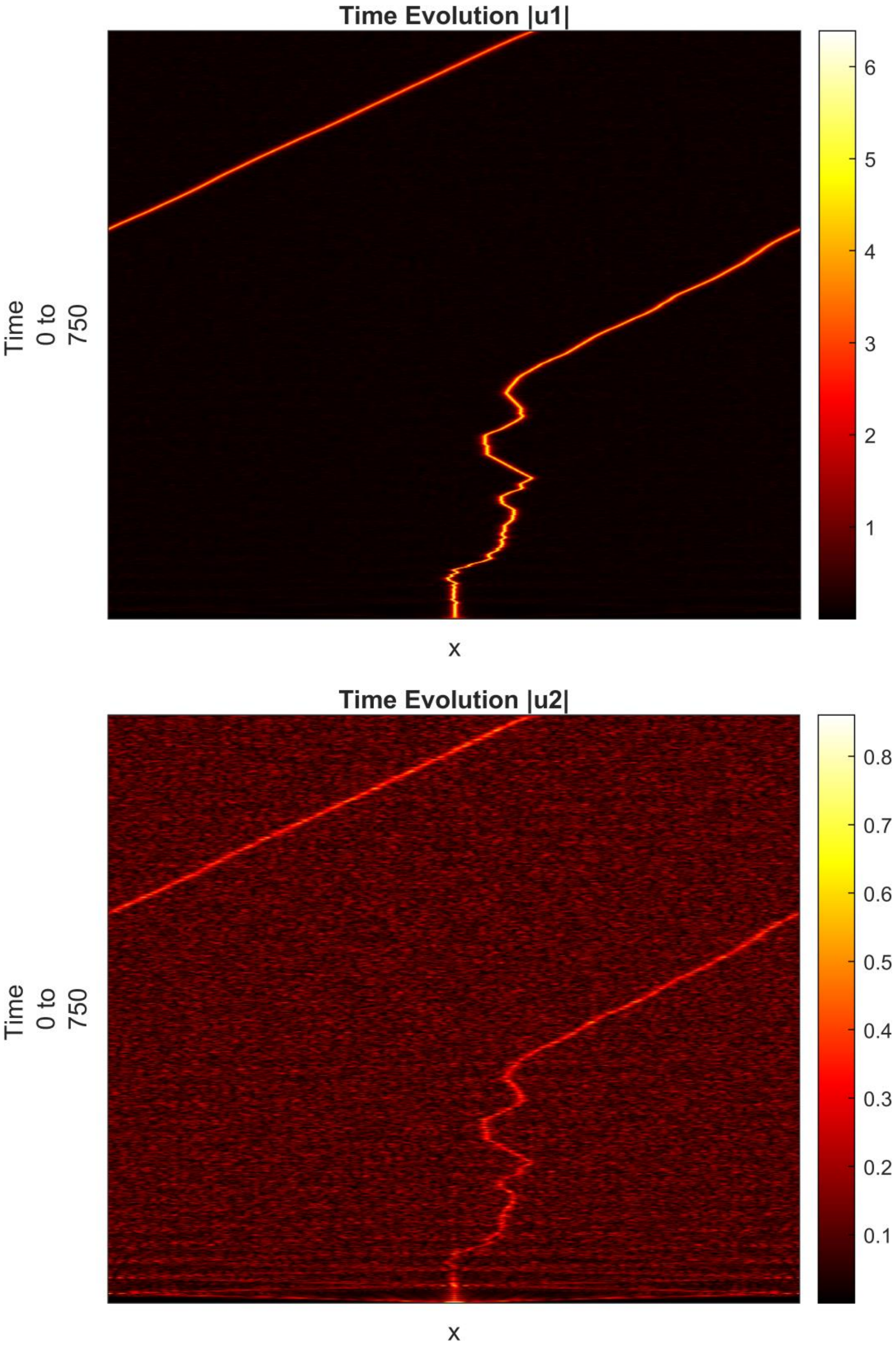

Figure 3.80 Asymmetry increases before non-stationary propagation takes place.

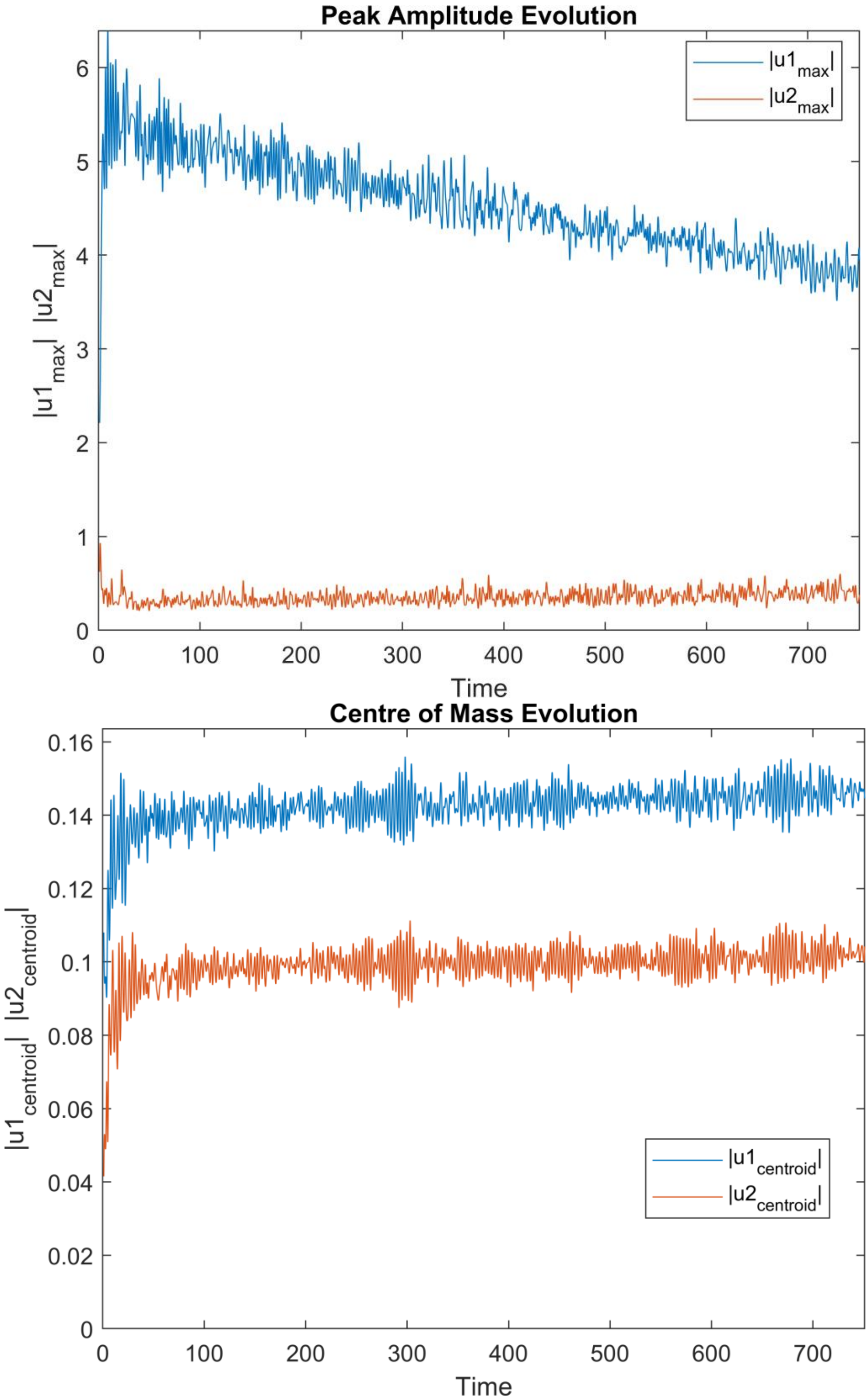

Figure 3.81 The peak amplitude of u_1 decays and the peak amplitude of u_2 increases over time (top). The centre of mass evolution increases throughout the experiment, indicating increased dispersion over time.

3.7.11 u_data_a_1p4_mu_2p8_sym

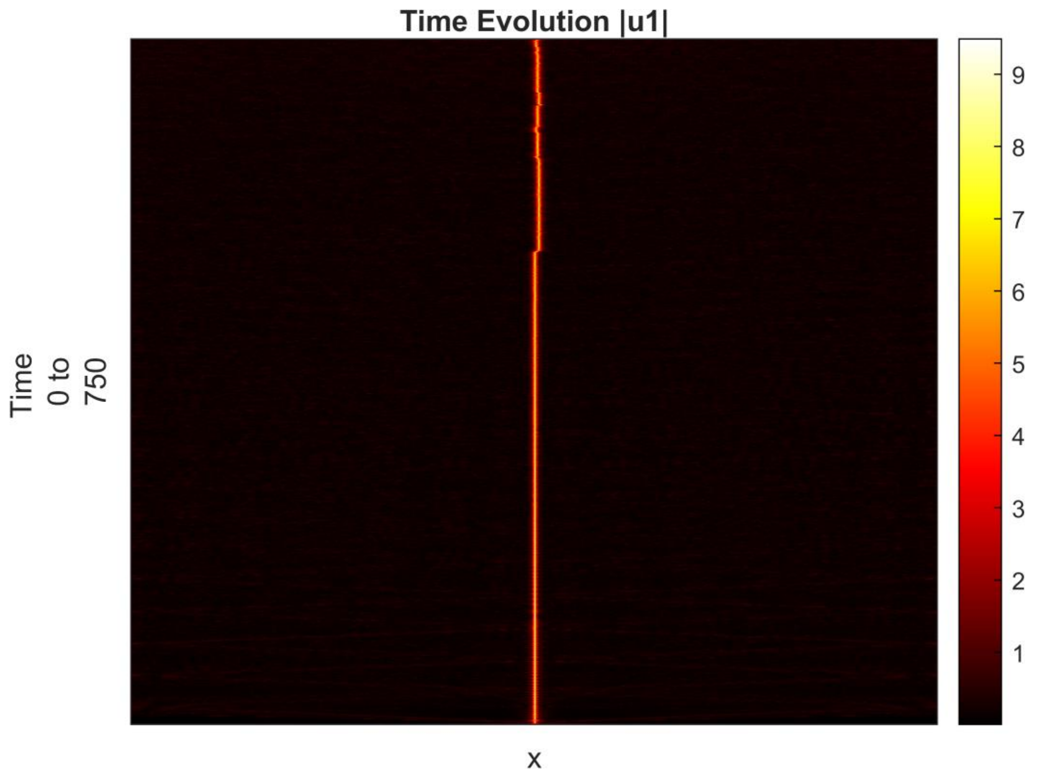

Figure 3.82 Heatmap where u_1 diverges to the right when the fractional derivative order $\alpha = 1.4$.

Comparing Figure 3.57 with Figure 3.82 above, we see when the fractional derivative order $\alpha = 1.4$, u_1 appears to become more focussed than the previous experiment in section 3.6.2 u_data_a_1p5_mu_2p8_sym with the fractional derivative of order $\alpha = 1.5$ while keeping the phase propagation constant with $\mu = 2.8$. While the solution appears stable, we see u_1 deviates from normal approximately halfway through the experiment.

The peak amplitude plot in Figure 3.83 shows the two solutions appear to converge over the course of the experiment, as u_2 slowly increases in peak amplitude while u_1 decays over time while maintaining unstable, oscillatory behaviour. The increase in centre of mass evolution from approximately 600t indicates an increase in dispersion for both solutions over time.

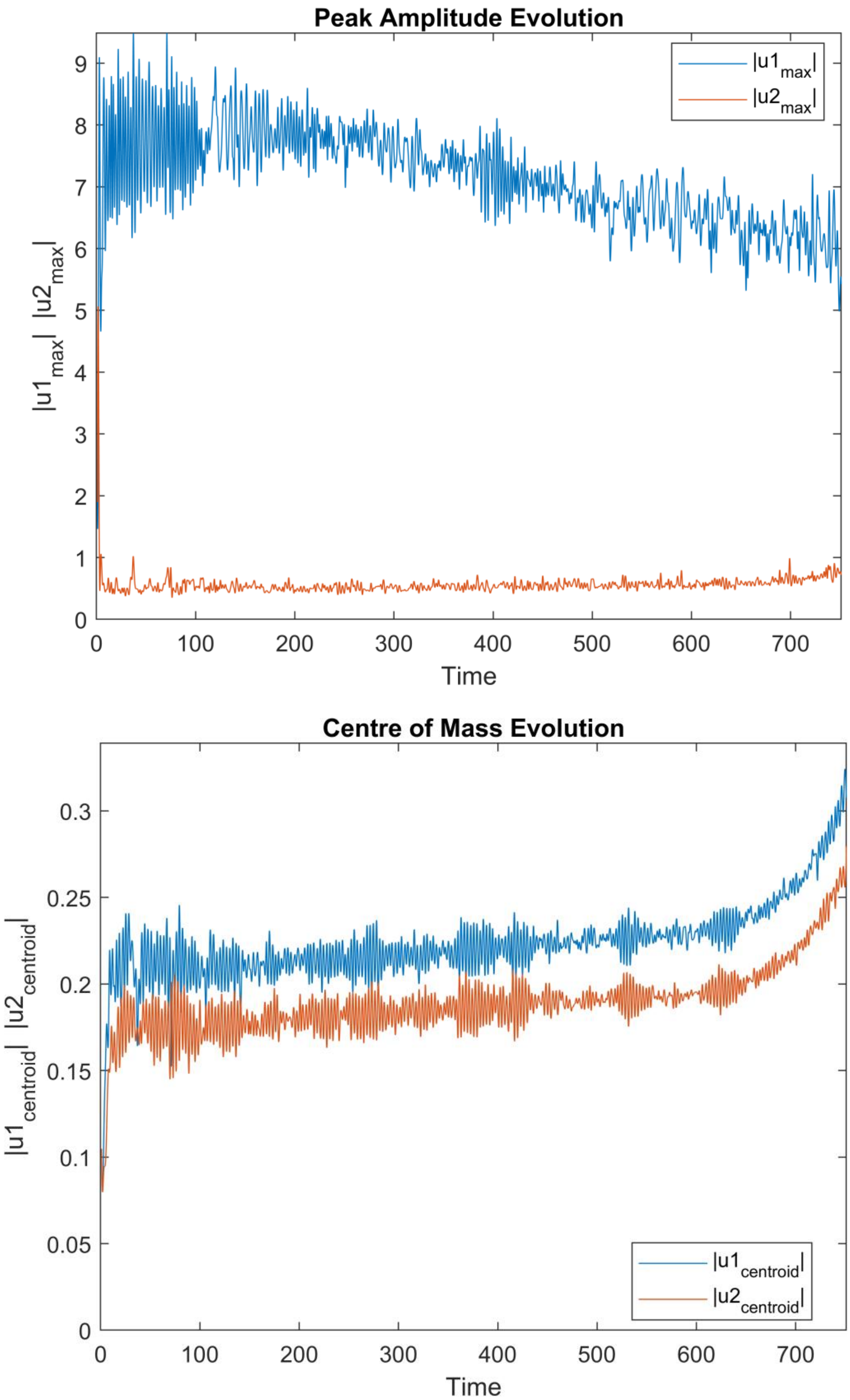

Figure 3.83 Peak amplitude plot (top) shows u_1 with high-frequency oscillations and decay, while u_2 peak amplitude gradually increases around 600t. The centre of mass evolution increases over time (bottom), consistent with increased dispersion.

3.7.12 u_data_a_1p4_mu_2p8_sym

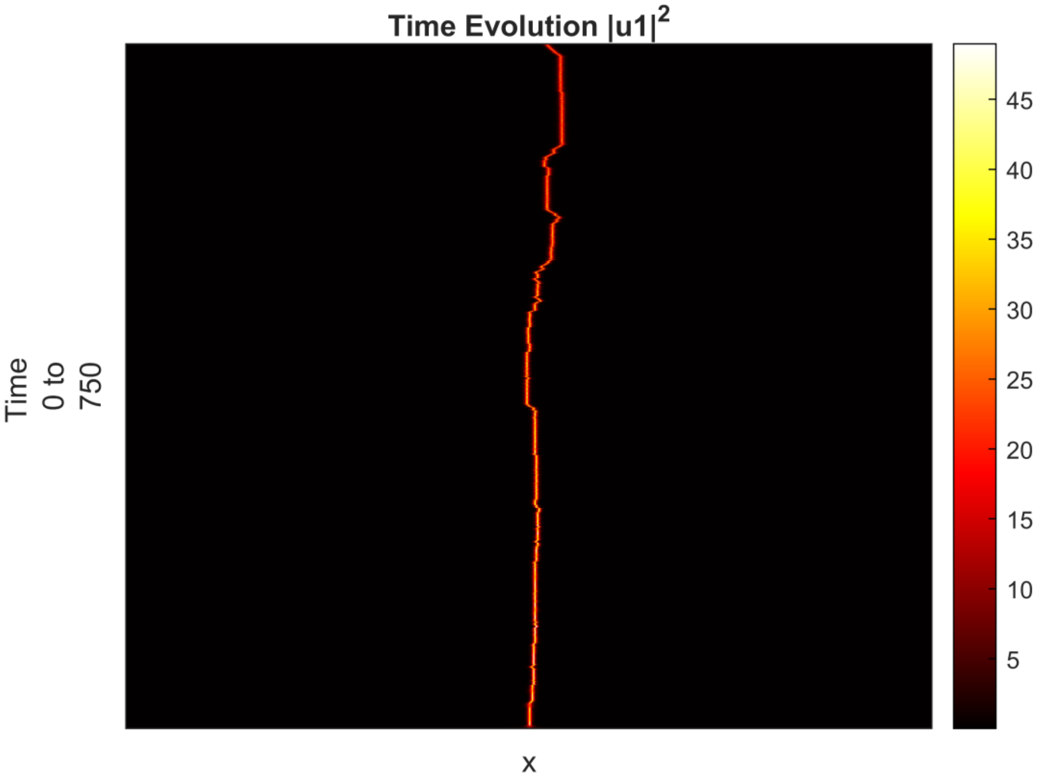

Figure 3.84 The ED heatmap of u_1 shows non-stationary propagation to the right of the solution field.

When the fractional derivative order $\alpha = 1.4$ and the phase propagation constant $\mu = 2.8$, we see non-stationary behaviour propagating to the right of the solution field in Figure 3.84, corresponding to a high degree of focus from the solution u_1. We see further instability in u_1 after examining the peak amplitude evolution plot in Figure 3.85, where we see erratic oscillations and decay throughout the experiment, while u_2 has dispersed to noise.

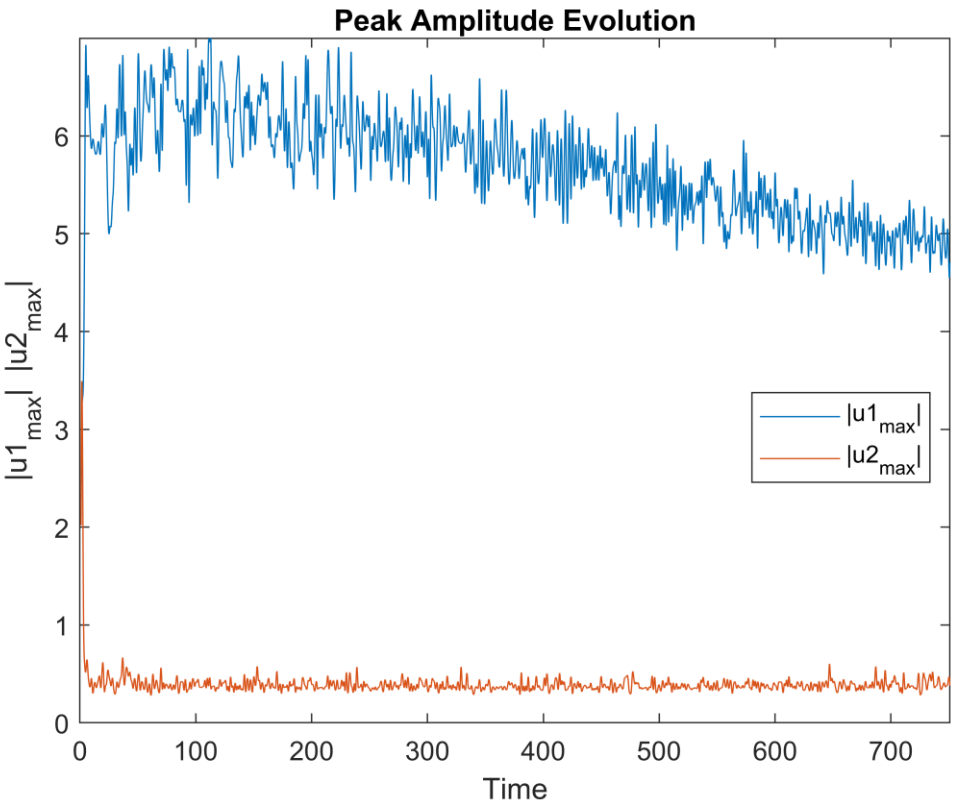

Figure 3.85 The amplitude spectrum reveals the extent of instability of u_1 over the course of the experiment, evident as high frequency oscillations.

3.8 Fractional derivative α = 1.3

Here we present various non-stationary dynamics for fractional derivative of order $\alpha = 1.3$.

3.8.1 u_data_a_1p3_mu_1p4_sym

Decreasing the fractional derivative order from $\alpha = 1.6$ and keeping the phase propagation constant $\mu = 1.4$ the solutions increase oscillations and dispersion while maintaining symmetry, until $\alpha = 1.3$ when we observe non-stationary dynamics in Figure 3.86.

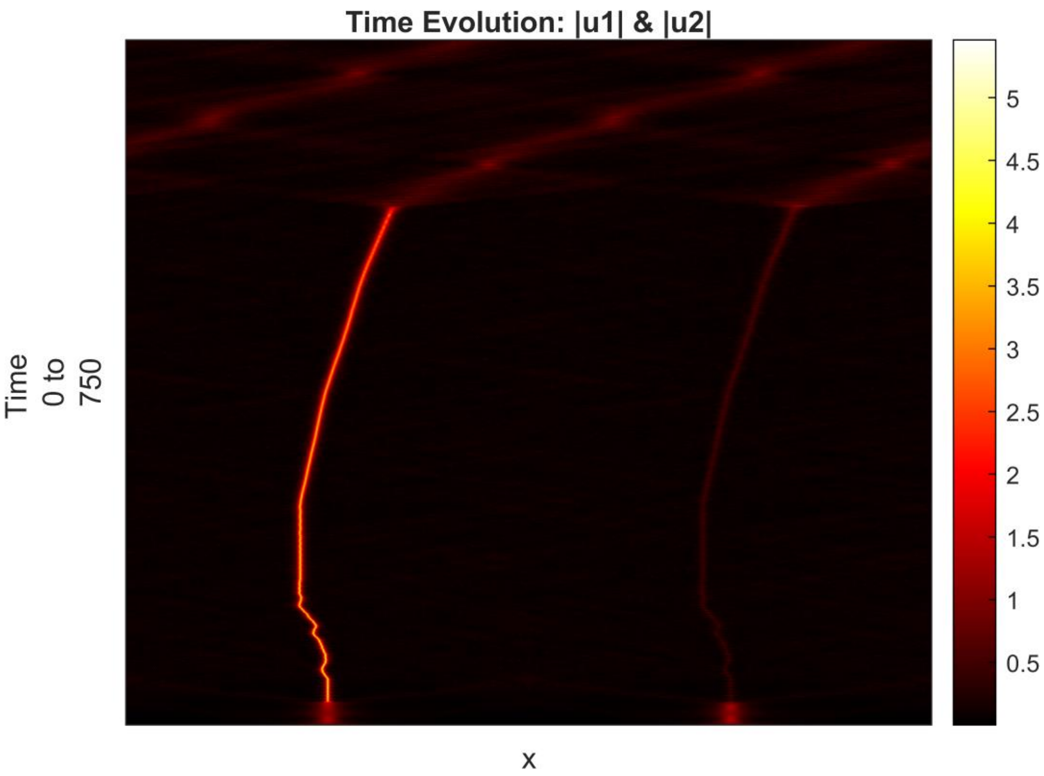

Figure 3.86 When α = 1.3 symmetry breaks, with non-stationary behaviour.

From the heatmap in Figure 3.86, we see the solutions begin the experiment propagating as a symmetric pair, but symmetry is quickly broken when we see asymmetric, highly focussed solutions with non-stationary behaviour. In Figure 3.86 we first see the solution deviate to the left, then continue to radiate to the right. Eventually the solution loses focus (increases wavelength), disperses and widens as it continues to propagate to the right.

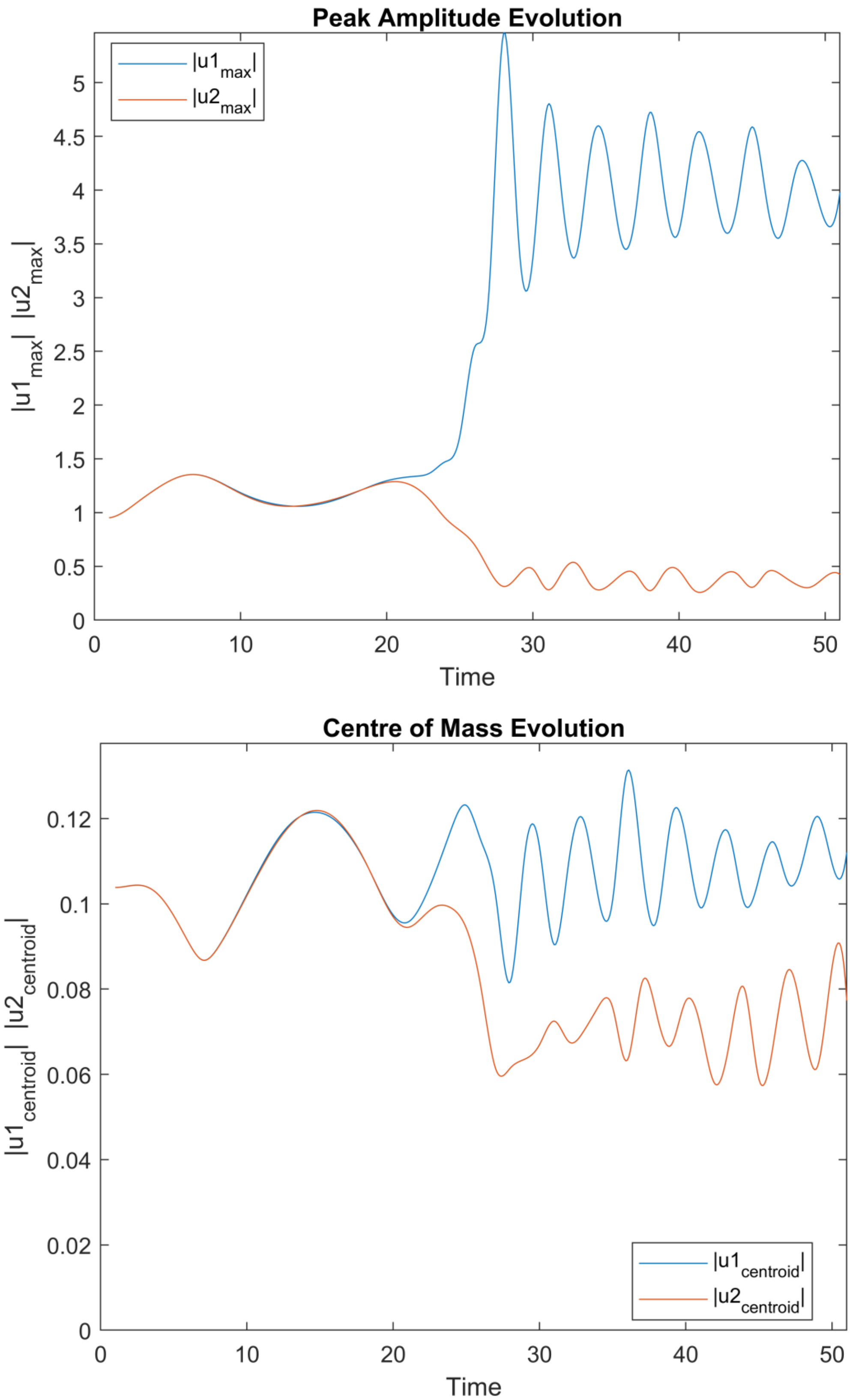

Figure 3.87 Here we can see the solution pair are symmetric until approximately 10t when the solutions shift phase before breaking symmetry.

The peak amplitude plot in Figure 3.87 captures the moment symmetry is broken at approximately 20t. We see the solutions are stable and oscillating symmetrically from the initial conditions until approximately 10t. Then the solutions appear to shift phase before an abrupt break in symmetry occurs. After the break in symmetry the solutions become focussed and non-stationary, evident in Figure 3.86.

The waterfall ED plots in Figure 3.88 show the behaviour of both solutions up to 200t. We see stable oscillations (accounting for the difference in axis scale) at the beginning of the experiment, until the solutions disperse, become highly focussed, and depart from normal propagation. Furthermore, we see u_2 disperses almost entirely after breaking symmetry.

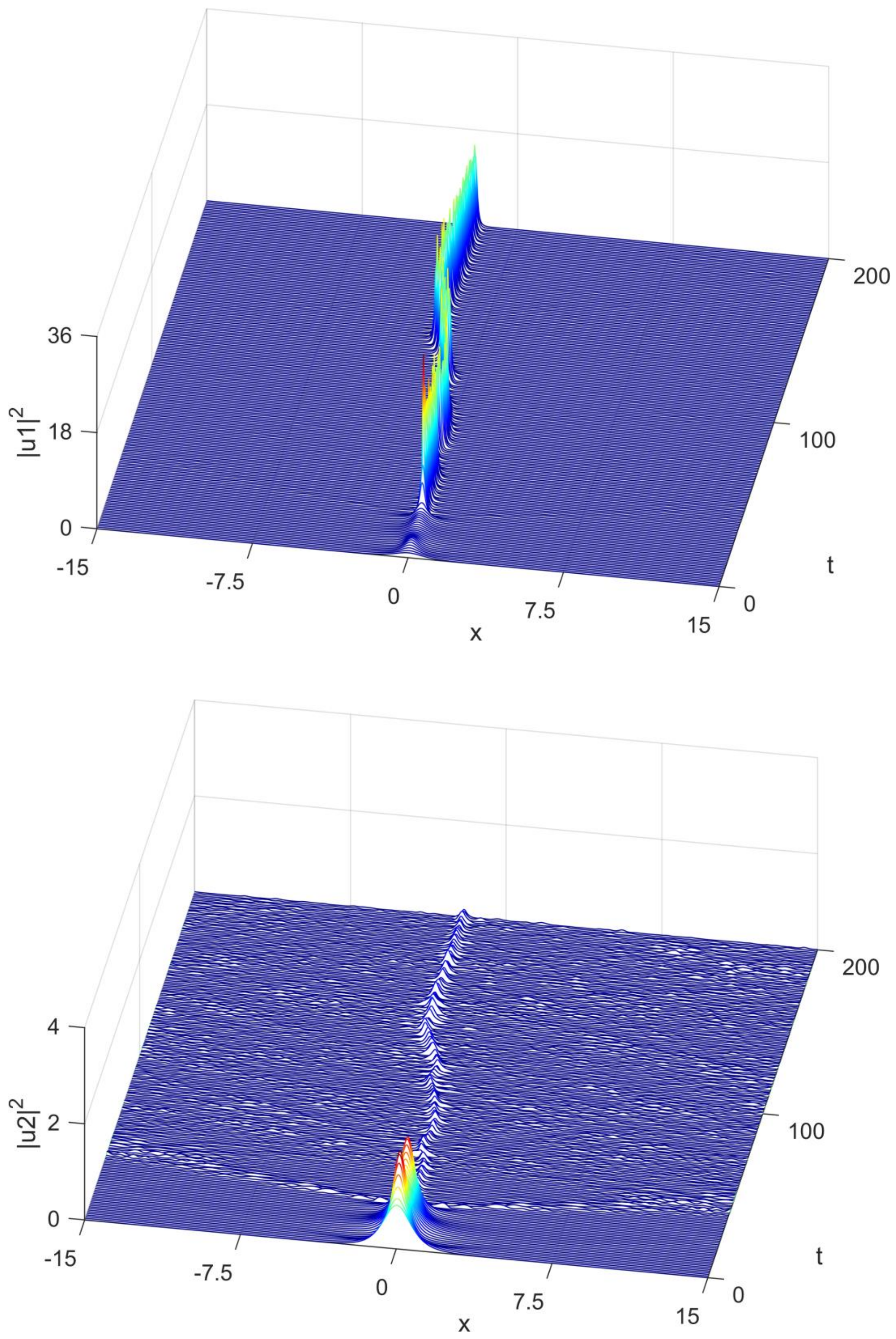

Figure 3.88 The waterfall ED for u_1 and u_2 illustrate the degree of asymmetry between this previously stable and symmetric pair of solitons.

3.8.2 u_data_a_1p3_mu_1p5_sym

From fractional derivative order α = 1.6 to α = 1.3 with a phase propagation constant μ = 1.5, a decay in soliton quality and stability ensued, corresponding with continued asymmetry until the solution became non-stationary and unstable in Figure 3.89.

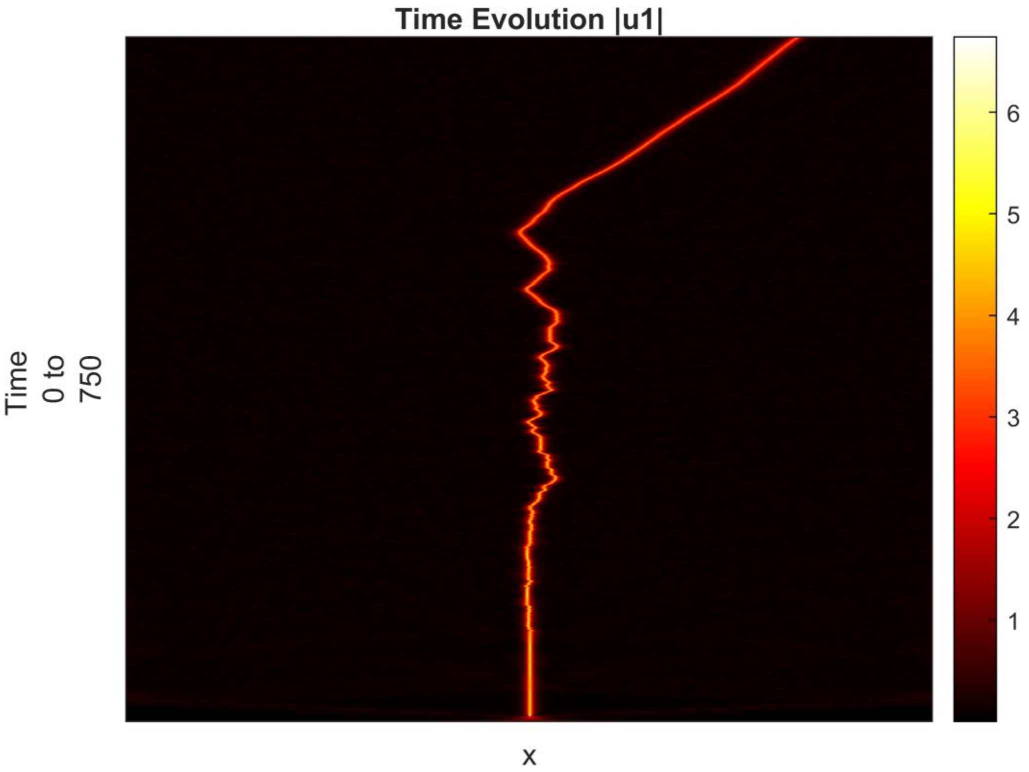

Figure 3.89 Asymmetric, non-stationary behaviour to the right when α = 1.3.

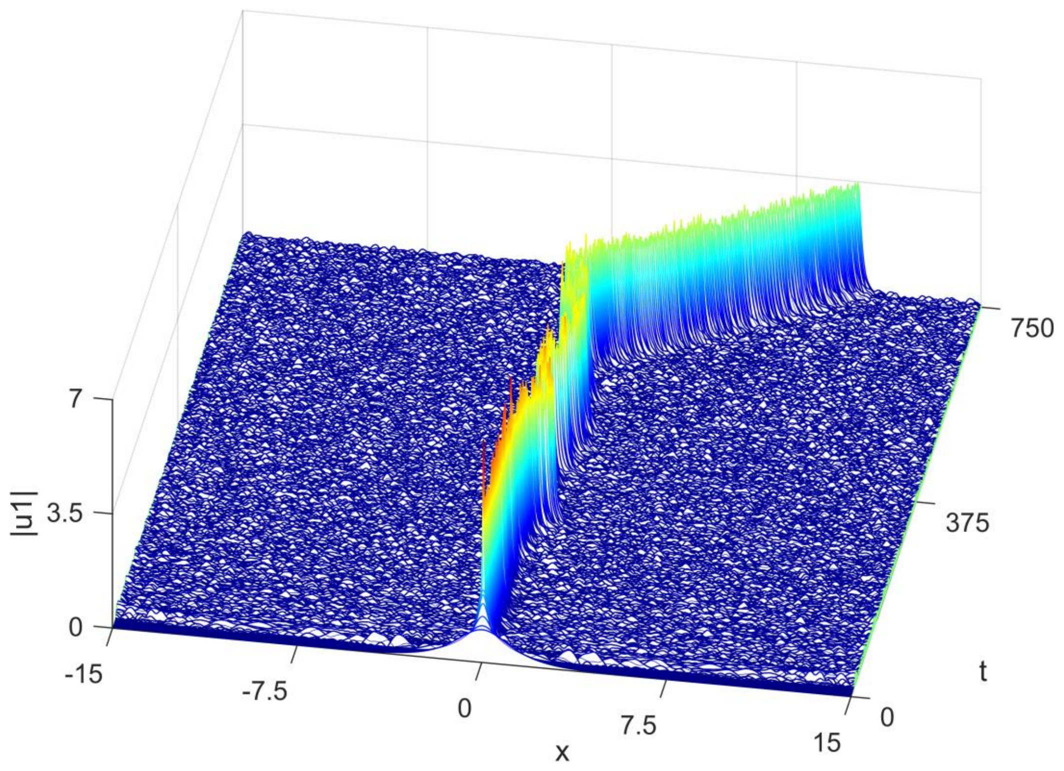

Figure 3.90 Waterfall plot shows u_1 is narrow and highly focussed.

The waterfall plot in Figure 3.90 shows dispersion in the solution field which is not clear in the heatmap. The dispersion is evident as noise, or ripples in the solution field propagating with the highly focussed, narrow soliton. Furthermore, we see a decay in peak amplitude over the course of the experiment corresponding with continued dispersion.

3.8.3 u_data_a_1p3_mu_1p8_asym

The solutions increase oscillation frequency and dispersion until the fractional derivative order $\alpha = 1.3$ and the phase propagation constant $\mu = 1.8$. We see in Figure 3.91 u_1 becomes highly focussed and non-stationary.

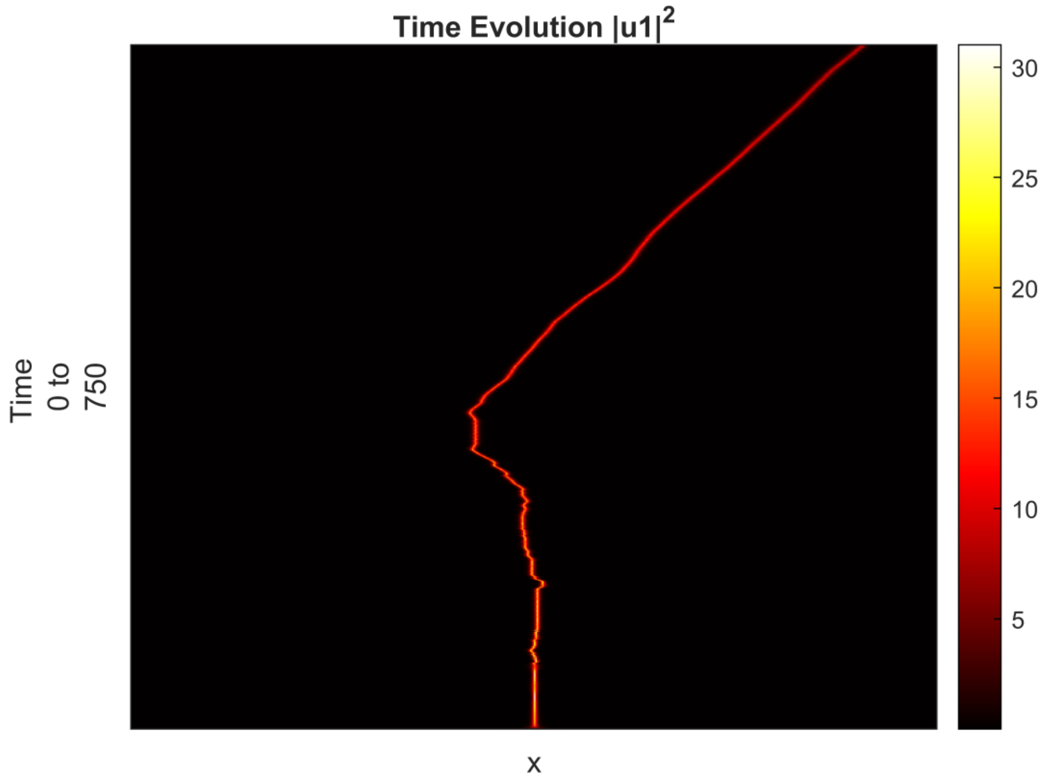

Figure 3.91 The ED heatmap shows the degree of focus and the non-stationary propagation of u_1.

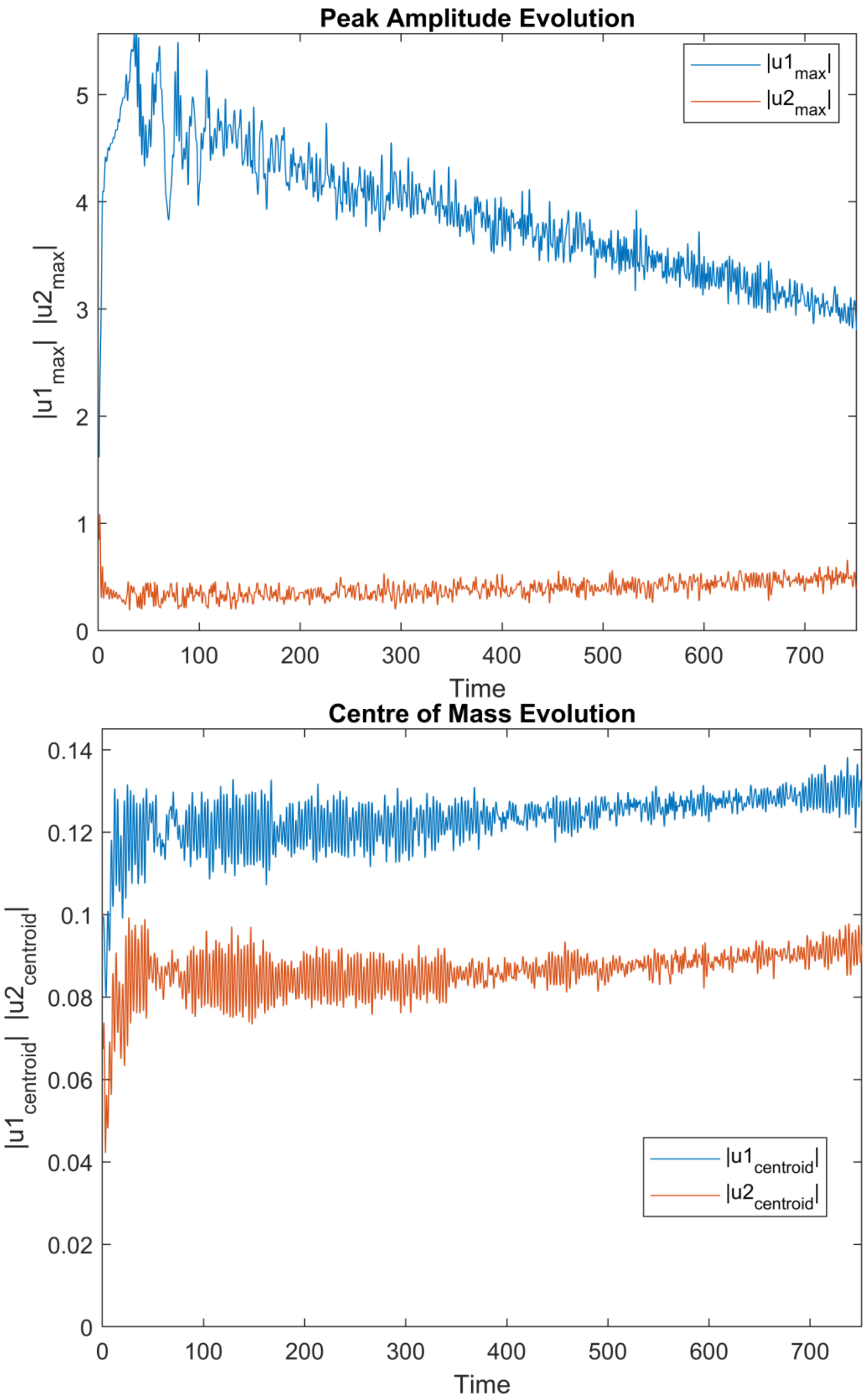

Figure 3.92 The peak amplitude evolution (top) shows u_1 converging on u_2. The centre of mass evolution (bottom) increasing over time corresponds to dispersion in the solution.

The peak amplitude evolution in Figure 3.92 shows the two solutions converge on each other throughout the experiment. Convergence is easier to see in Figure 3.93, where the ED waterfall plots show the solutions deviate to the right of the solution field. We also see evidence of dispersion from the solutions, correlating with the increase in the centre of mass evolution plot in Figure 3.92.

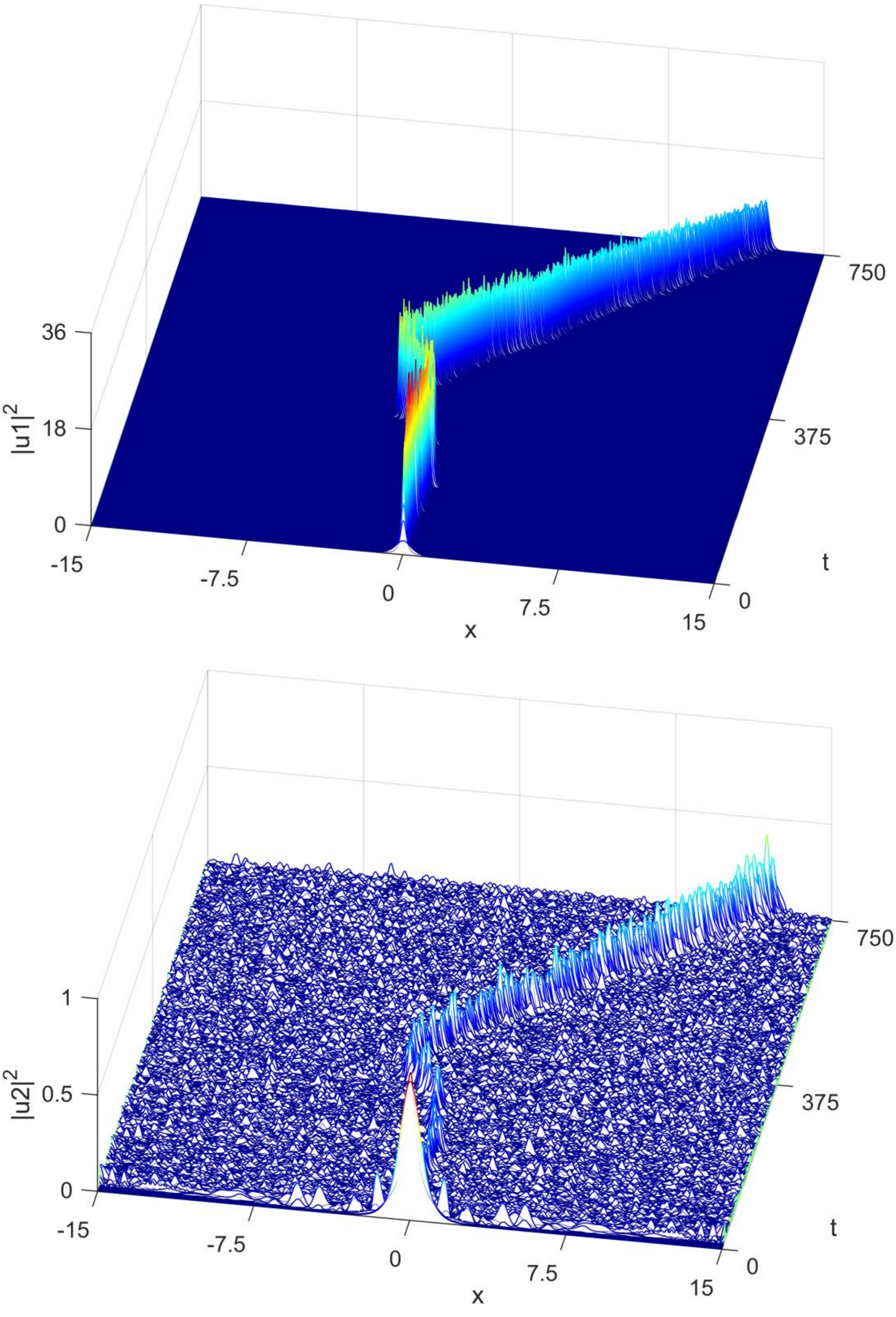

Figure 3.93 The waterfall plots of the ED show the highly focussed and asymmetric solutions converging throughout the experiment.

3.8.4 u_data_a_1p3_mu_1p8_sym

When the fractional derivative order $\alpha = 1.3$ and the phase propagation constant $\mu = 1.8$, we see the solutions hold symmetry for a short period of time before breaking symmetry and becoming non-stationary, deviating to the left of the solution field in Figure 3.94.

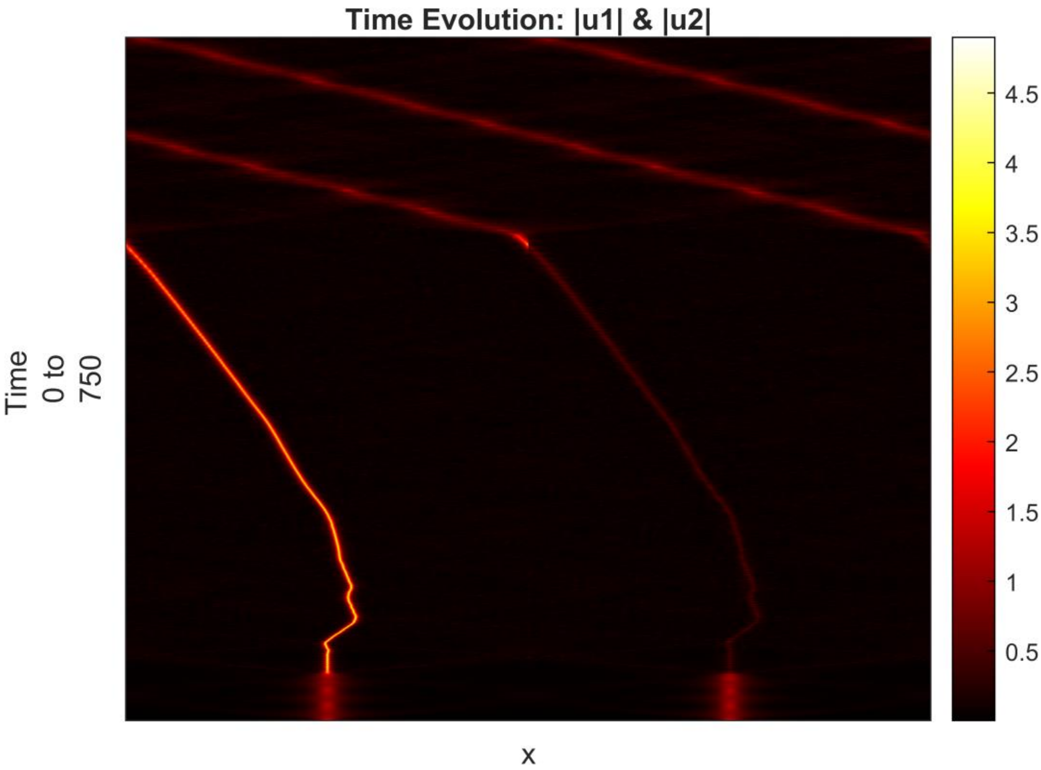

Figure 3.94 Non-stationary solutions when the fractional derivative order $\alpha = 1.3$.

Taking a closer look at the peak amplitude and centre of mass evolution in Figure 3.95, we see the solution maintain symmetry for approximately 20t. After a phase shift occurs: the inner peak amplitude wave becomes asymmetric, and the two solutions break symmetry completely and commence high-frequency oscillations. When the solutions become asymmetric at 50t, u_2 disperses and u_1 propagates as a focussed, decaying solution. As the experiment progresses, both solutions converge before reconvening at approximately 550t, remaining non-stationary, deviating left for the remainder of the experiment. After 550t, we see in Figure 3.95 the inner peak amplitude wave is symmetric, while the surface waves continue propagating asymmetrically.

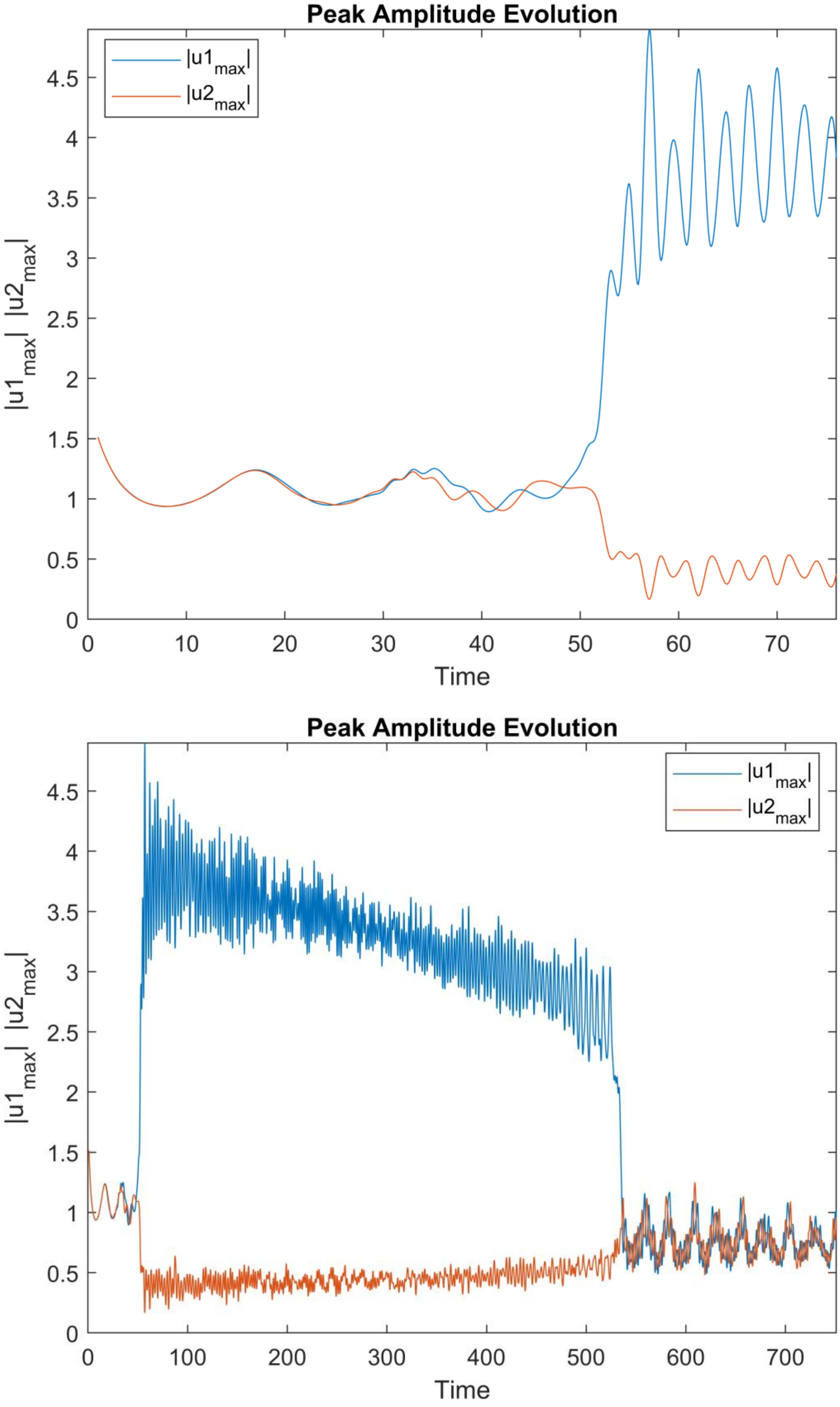

Figure 3.95 The peak amplitude evolution shows the solutions break symmetry at approximately 30t, then converge again at approximately 550t.

3.8.5 u_data_a_1p3_mu_1p8_asym

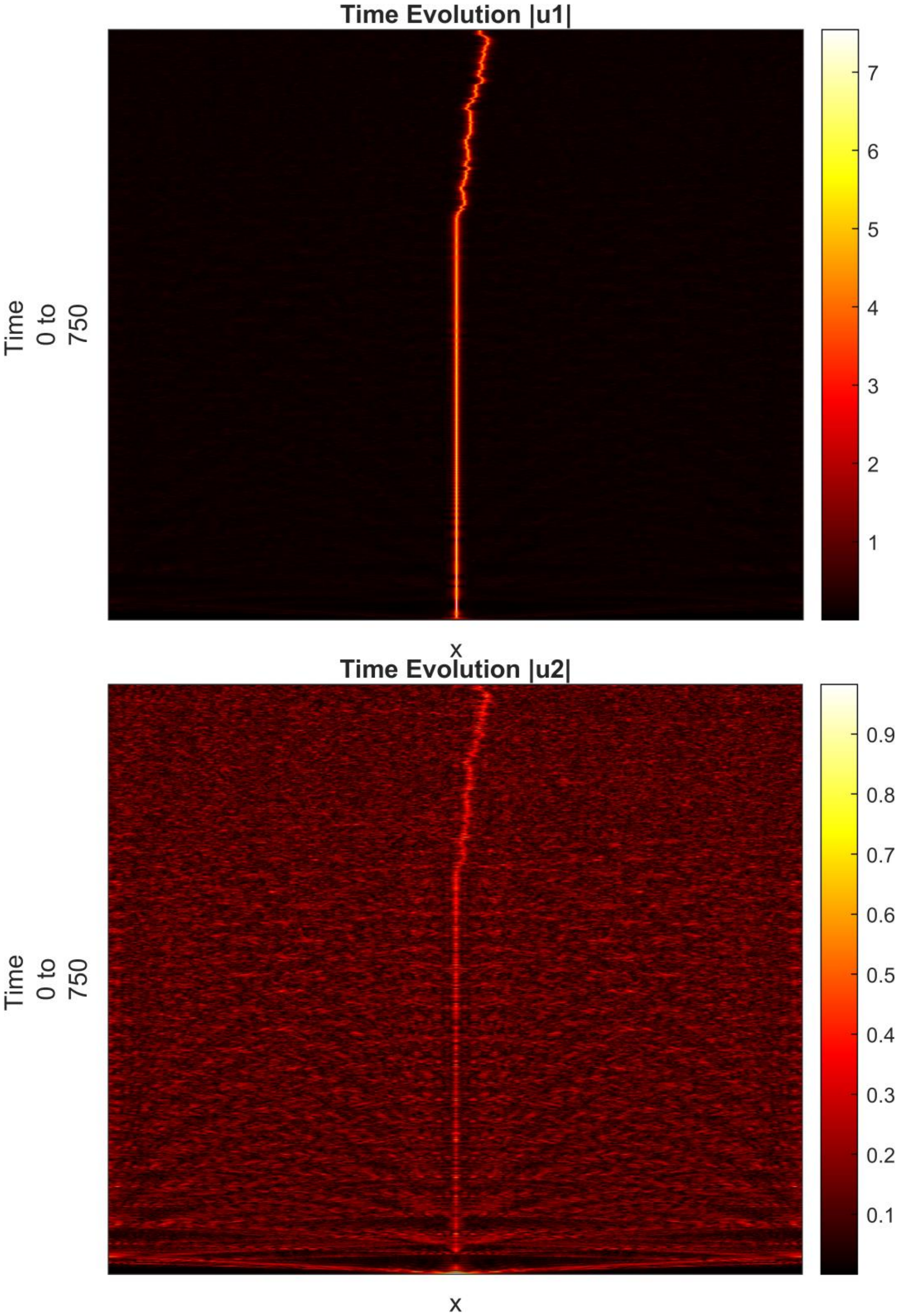

Figure 3.96 When the fractional derivative order $\alpha = 1.3$ we see asymmetric solutions until approximately 400t when the solution becomes non-stationary.

When the fractional derivative order $\alpha = 1.3$ and the phase propagation constant $\mu = 1.8$, we see in Figure 3.96 highly asymmetric solutions which become non-stationary at approximately 450t, travelling to the right of the solution field. As the solutions become non-stationary, u_2 predominantly radiates to the right of the solution field, alongside the primary, non-stationary solution which tends to the right of the solution field.

We display the phase portraits in Figure 3.97, where we see the gradient of the peak amplitude, $|u_{1_{max}}|' \cong 0$, take a range of amplitude values indicating instability in the solution. If we observe the centre of mass phase portrait, we see what appears to be a much more stable solution, but this is a misleading result due to unequal axis scaling.

These phase portraits confirm decay over time, as u_1 does not become stable around a fixed amplitude value, and instead takes a range values between 7 to 4. The peak amplitude spectrum in Figure 3.98 shows oscillations and instability with variation in the peak amplitude of u_1, while u_2 appears to be indistinguishable from noise.

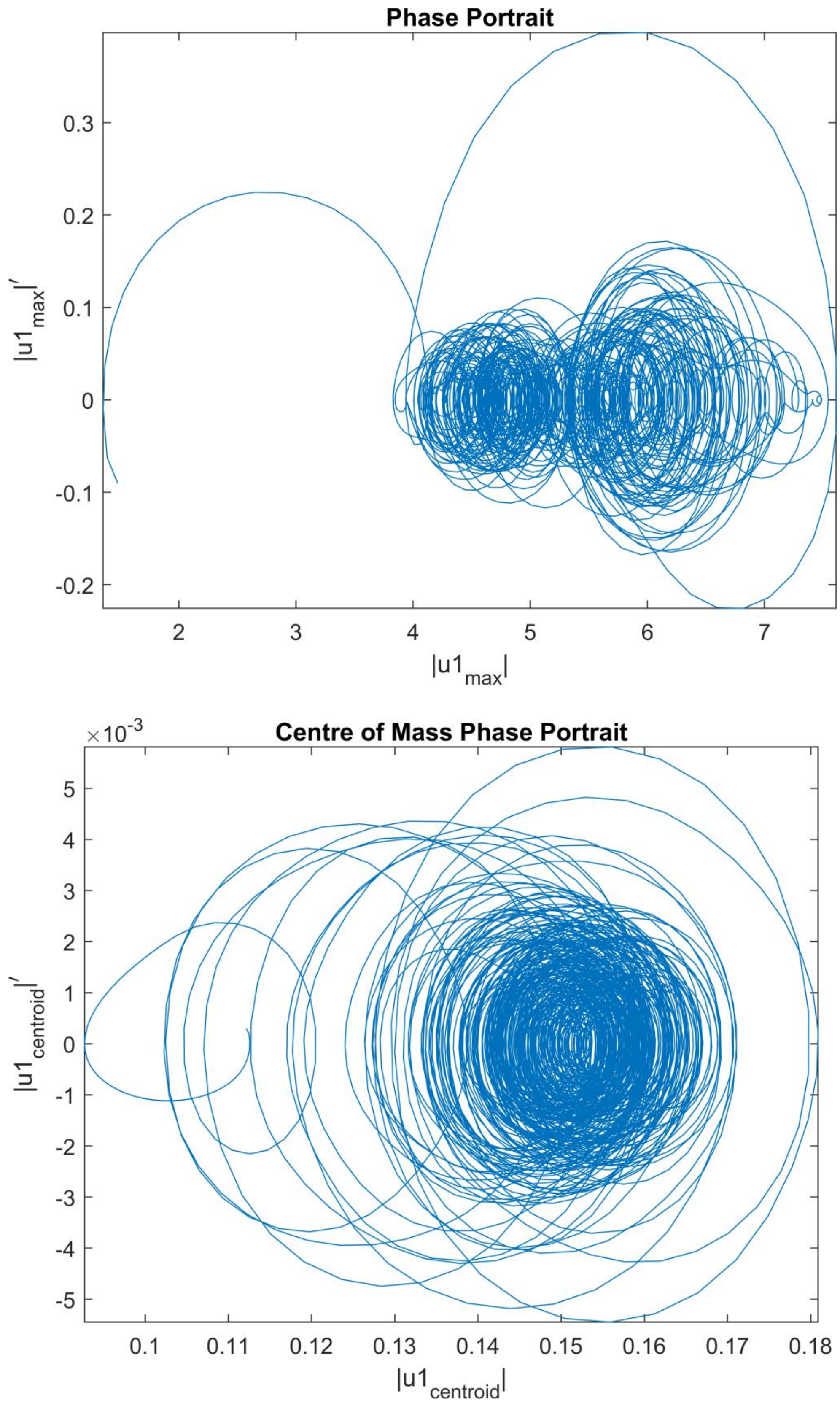

Figure 3.97 The peak amplitude phase portrait (top) shows u_1 to decay, whereas the centre of mass is misleading: appearing to be stable (bottom).

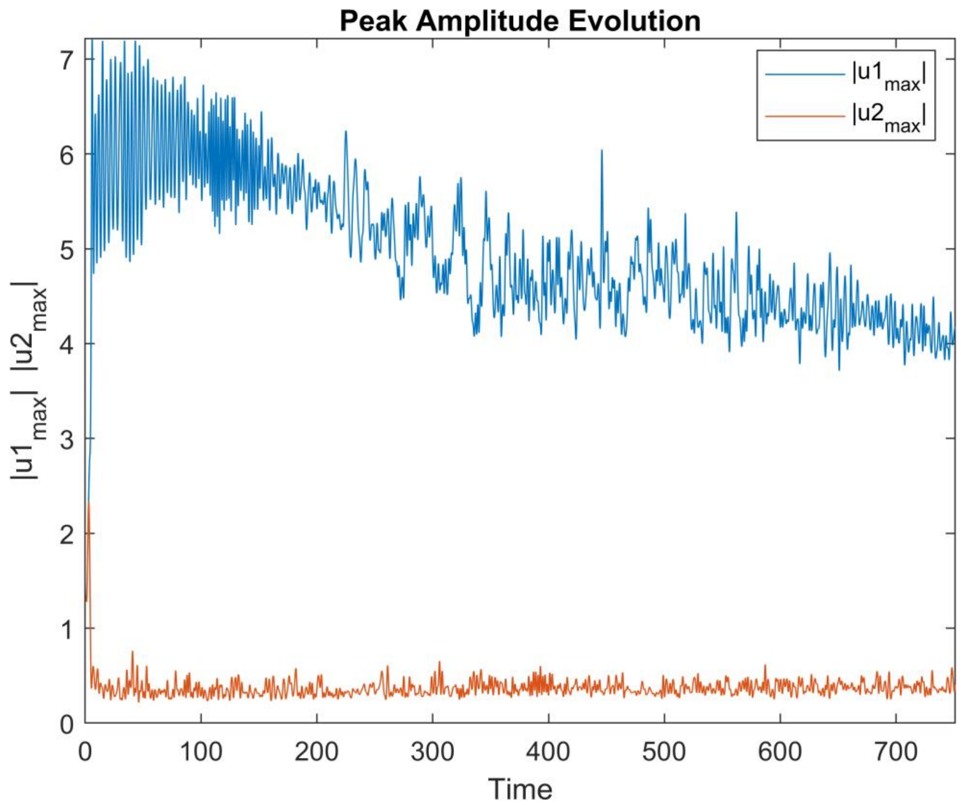

Figure 3.98 The peak amplitude evolution shows unstable, asymmetric solutions, where u_1 converges on u_2, and u_2 is barely indistinguishable from noise.

In Figure 3.98 the peak amplitude plot shows u_1 to be unstable, with high frequency oscillations, converging on u_2 throughout the course of the experiment, whereas u_2 is barely distinguishable from background noise after initial conditions.

3.8.6 u_data_a_1p3_mu_1p8_sym

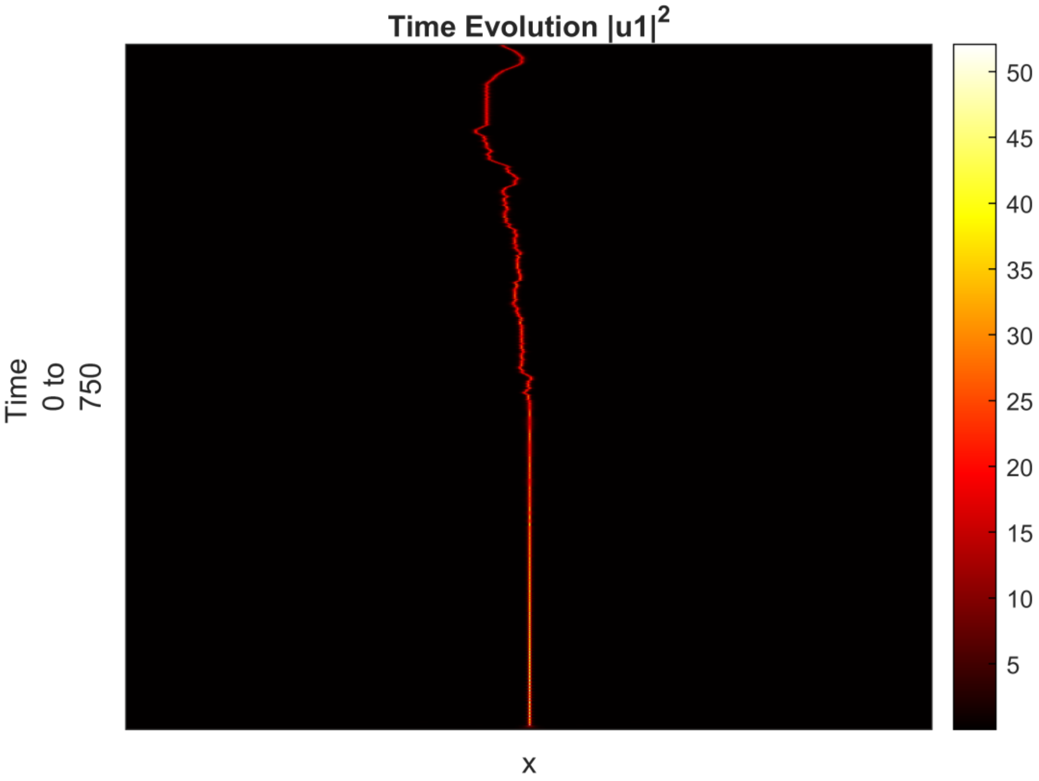

Figure 3.99 When the fractional derivative order α = 1.3, u_1 diverges to the left approximately halfway through the experiment. The coupled solution u_2 decays immediately from initial conditions.

When the fractional derivative order α = 1.3 and the phase propagation constant μ = 1.8, Figure 3.99 shows our unstable solutions (which are symmetric from initial conditions) remain highly focussed and asymmetric with non-stationary behaviour to the left of the solution field. The coupled solution u_2 decays immediately and is not shown here.

3.8.7 u_data_a_1p3_mu_2_asym

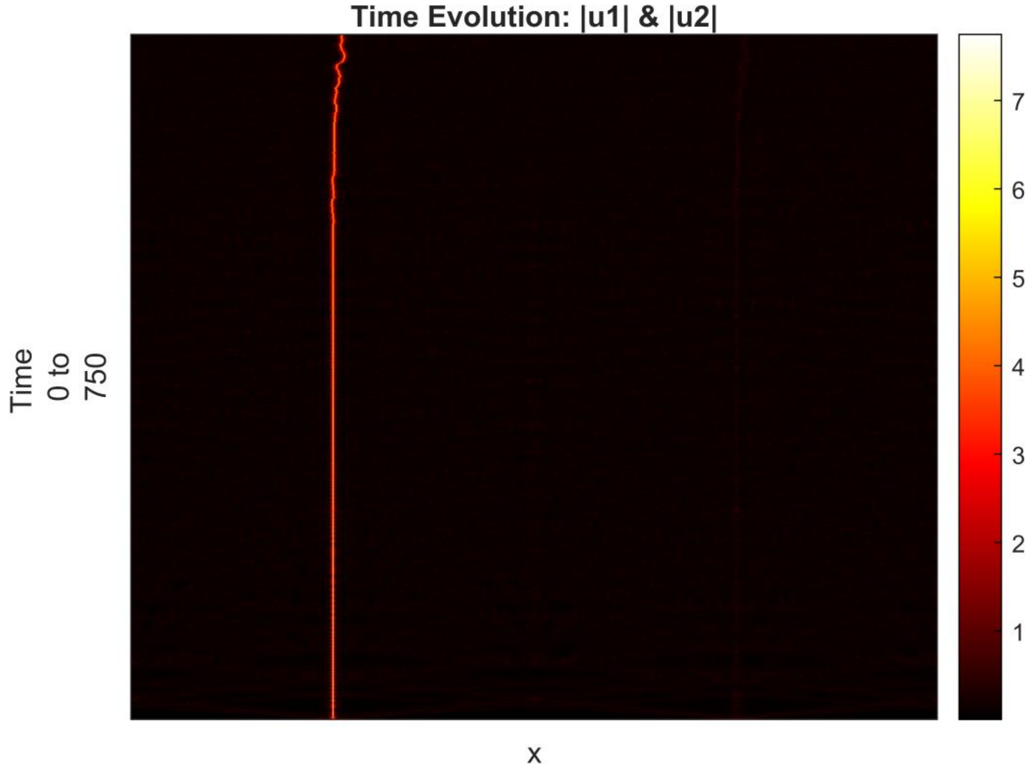

Figure 3.100 The asymmetric pair show non-stationary behaviour for large t when the fractional derivative α = 1.3.

When the fractional derivative order α = 1.3 and with a phase propagation constant μ = 2, we see in Figure 3.100 u_1 continues to maintain a high degree of focus and asymmetry, until approximately 400t, when the solution becomes non-stationary and propagates to the right. The ED waterfall plot in Figure 3.101 reveals details of the instability of the solutions before non-stationary behaviour begins, evident as high frequency oscillations in u_1, and a high level of dispersion from u_2.

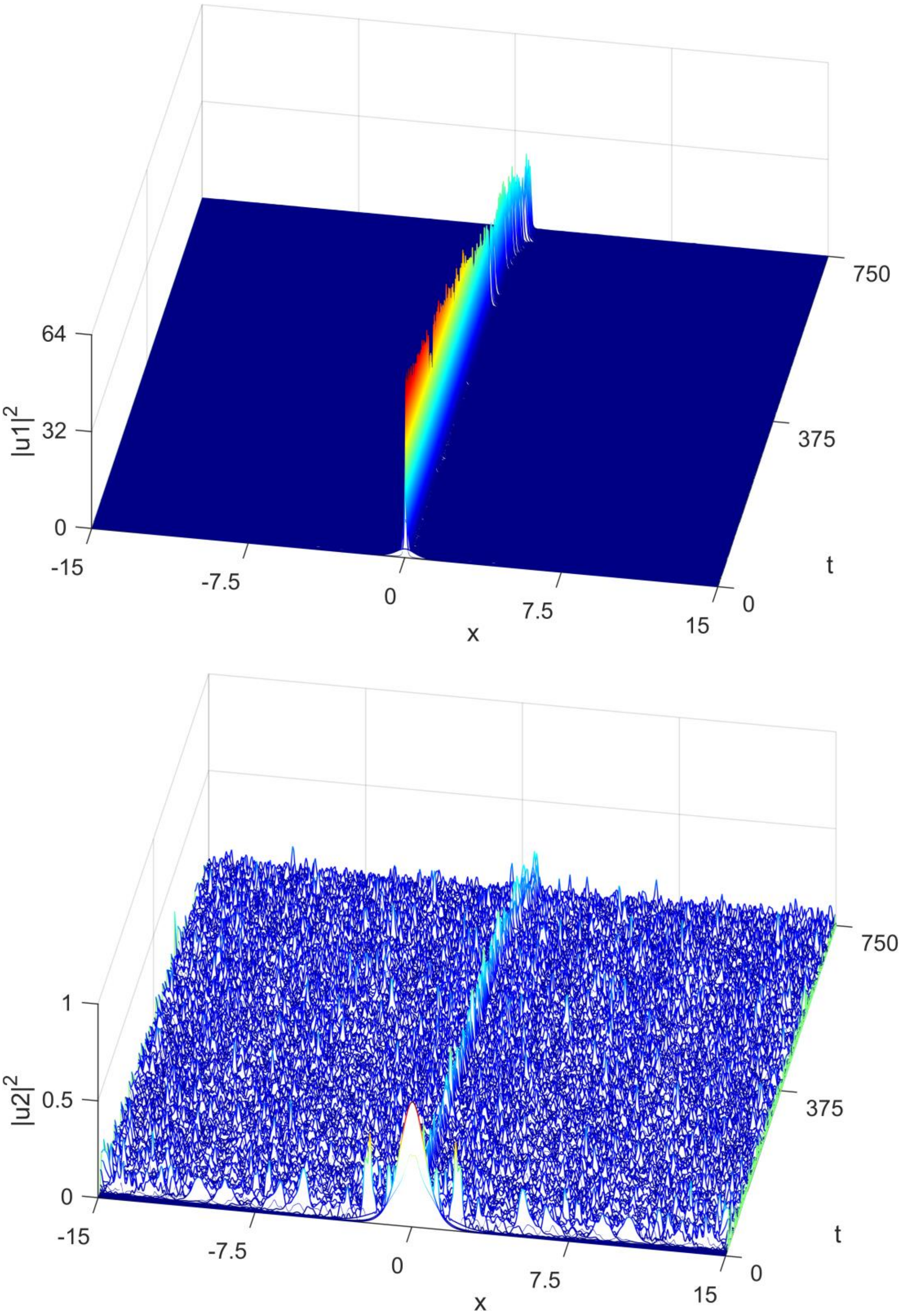

Figure 3.101 Waterfall plots of the ED for u_1 and u_2 show how highly focussed u_1 is, while u_2 remains close to noise. The solution u_1 decays prior to non-stationary propagation.

3.8.8 u_data_a_1p3_mu_2p2_asym

When the fractional derivative order $\alpha = 1.3$ and when the phase propagation constant $\mu = 2.2$, we see in Figure 3.102 the solutions retain stability until late into the experiment. At approximately 650t non-stationary behaviour is observed, and the solution deviates left, then right. We see familiar asymmetry where u_1 becomes highly focussed while u_2 disperses almost immediately, barely distinguishable from background noise.

When reviewing the centre of mass evolution in Figure 3.103, we note the centre of mass for both solutions increases throughout the experiment. This reflects noise in the solution field increasing the value of the mean centre of mass at each time step.

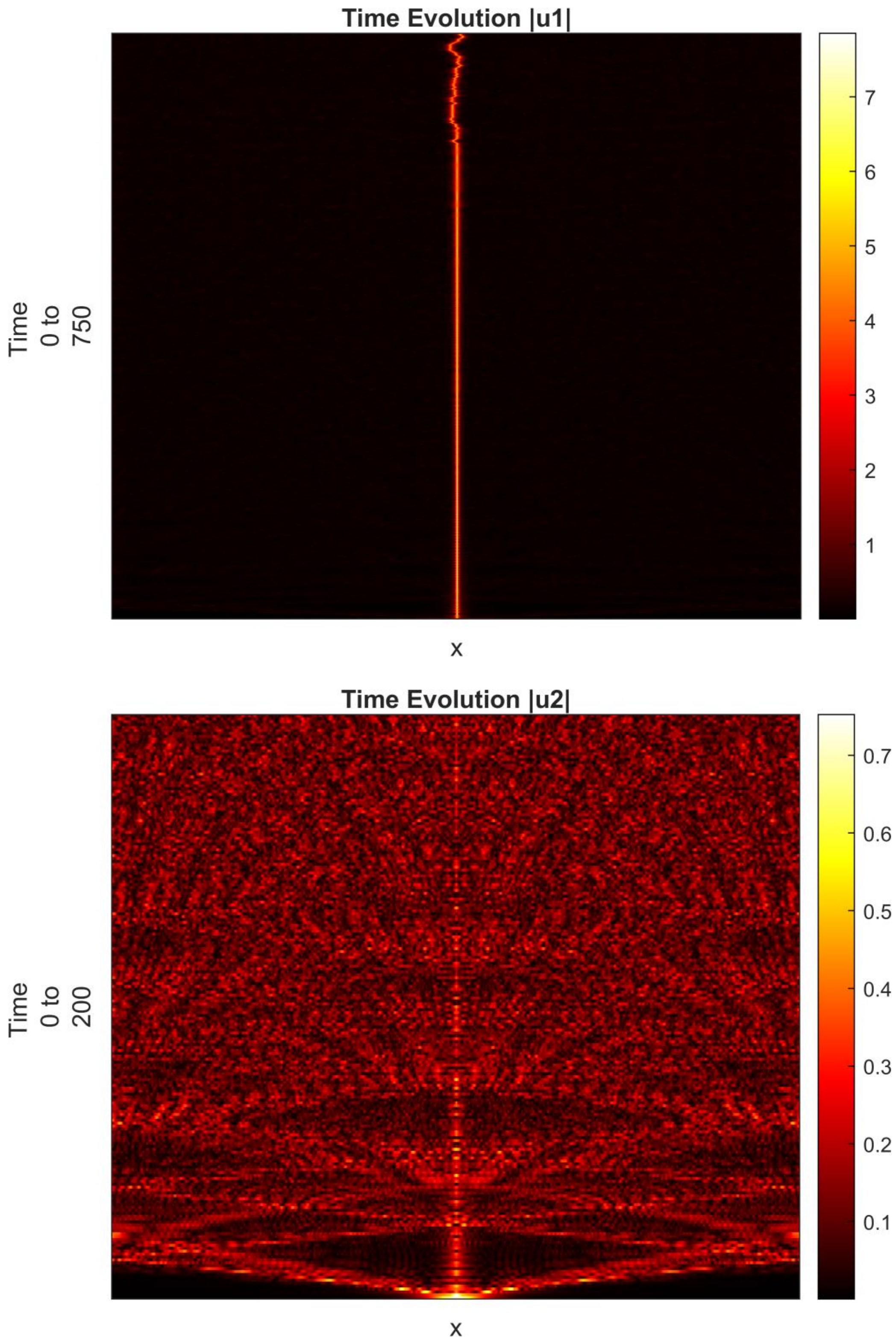

Figure 3.102 Heatmaps reveal asymmetry between u_1 and u_2, capturing non-stationary behaviour for large t values when the fractional derivative order $\alpha = 1.3$.

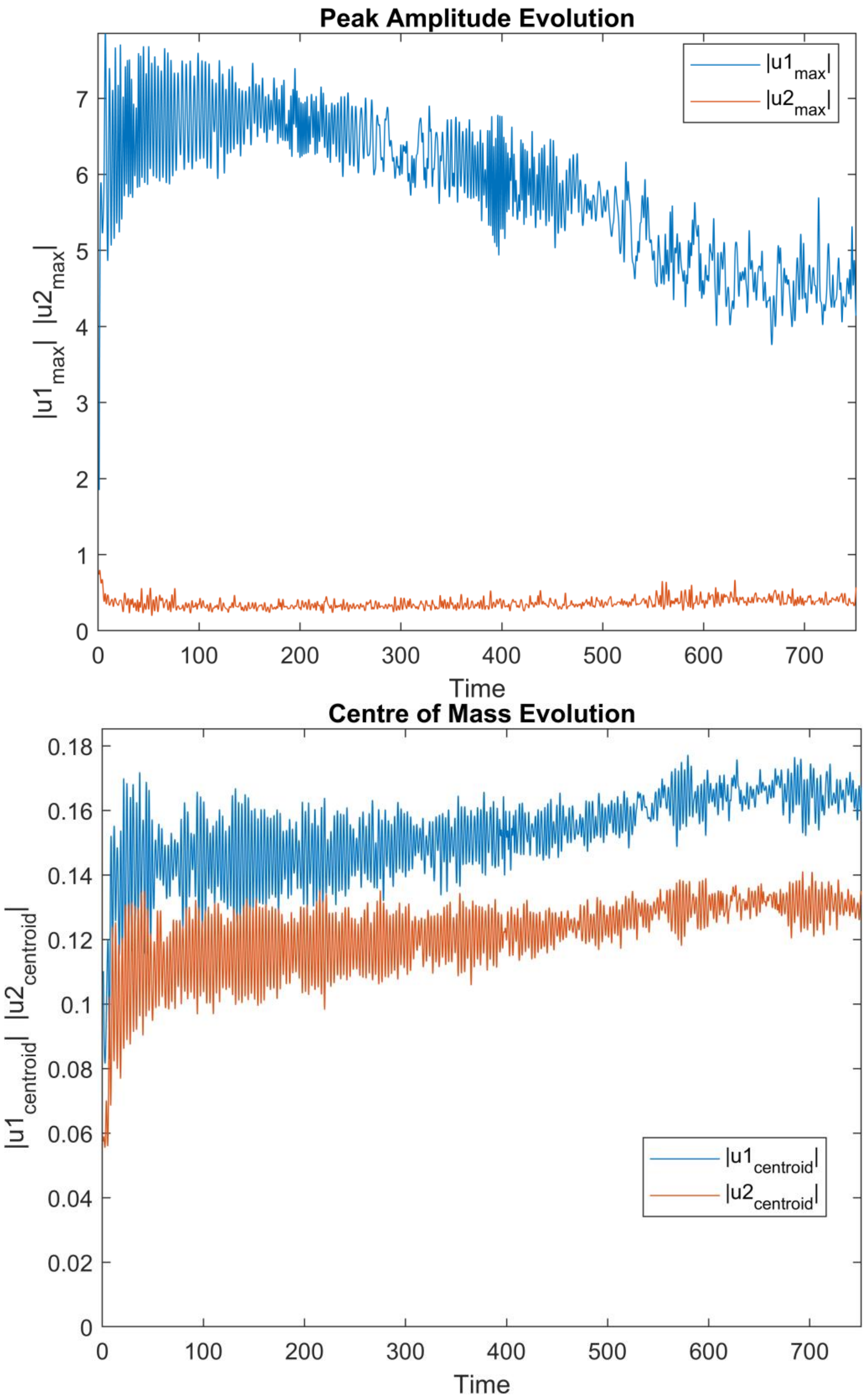

Figure 3.103 Peak amplitude evolution (top) and centre of mass evolution (bottom) shows instability of solution pair.

3.8.9 u_data_a_1p3_mu_2p2_sym

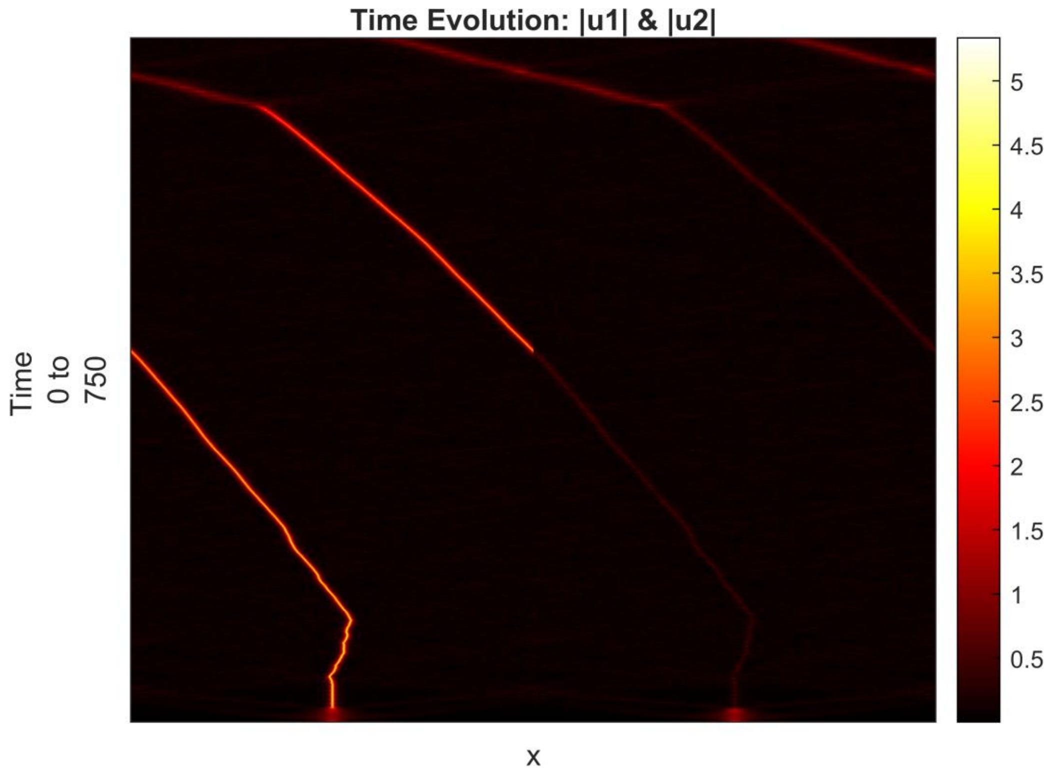

Figure 3.104 Solutions become asymmetric and non-stationary.

When the fractional derivative order $\alpha = 1.3$, and the phase propagation constant $\mu = 2.2$ we see the heatmap in Figure 3.104 and the peak amplitude plot in Figure 3.105 the solutions break symmetry at approximately 10t. In Figure 3.105 the solutions evolve asymmetrically but continue to converge until approximately 680t: the inner wave propagates symmetrically, but the surface waves propagate asymmetrically. We refer to the following peak amplitude and centre of mass plots in Figure 3.105 below to see the solutions break symmetry at approximately 13t, and to see the group velocities approach each other at 680t.

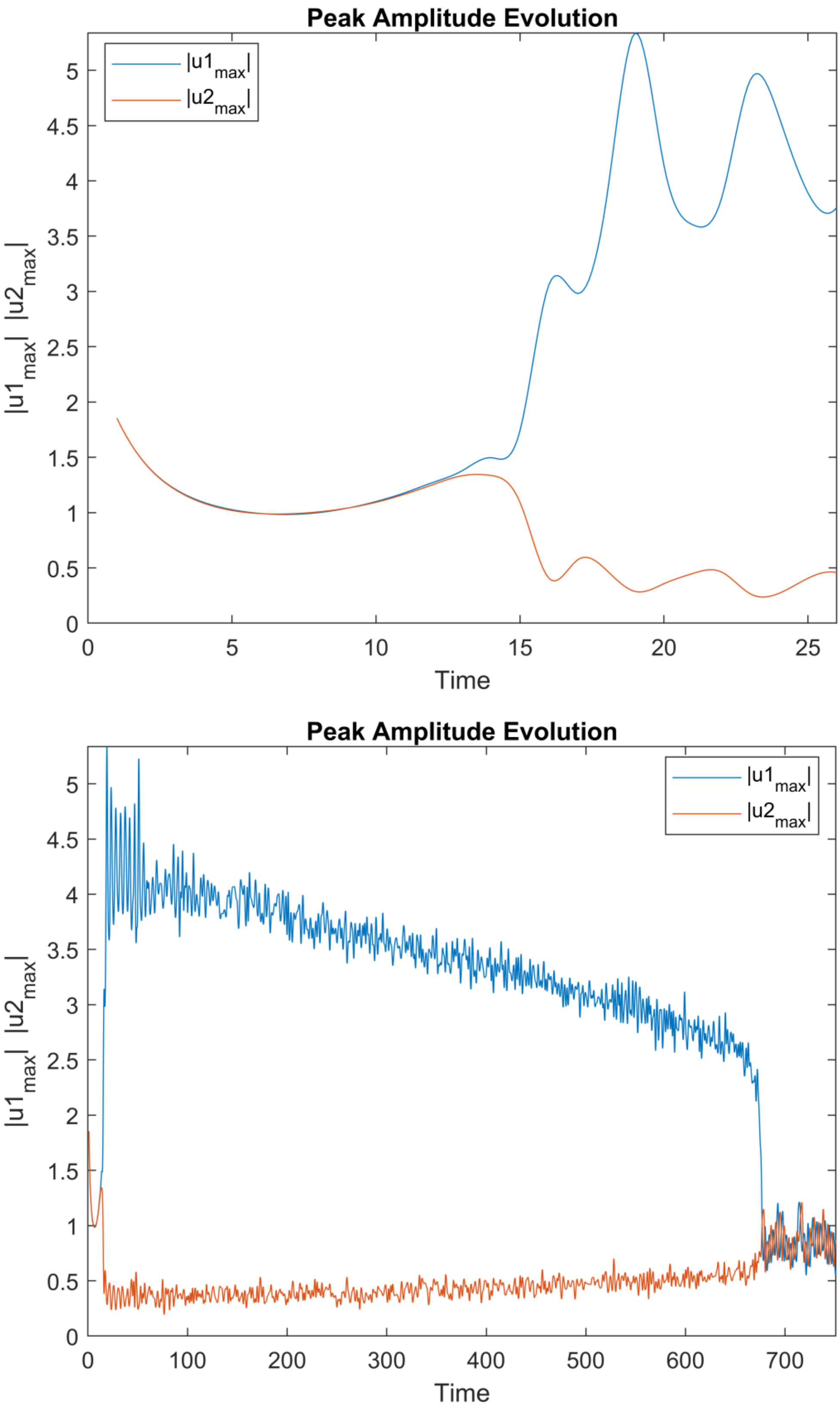

Figure 3.105 Closer inspection of the break in symmetry from the peak amplitude plot (top), and convergence at approximately 680t, continuing as an unstable, asymmetric solution (bottom).

3.8.10 u_data_a_1p3_mu_2p4_asym

As the fractional derivative order α = 1.3, and the phase propagation constant μ = 2.4, the solution quality deteriorates, and continues to evolve asymmetrically until becoming non-stationary as we see in the heatmap in Figure 3.106 below.

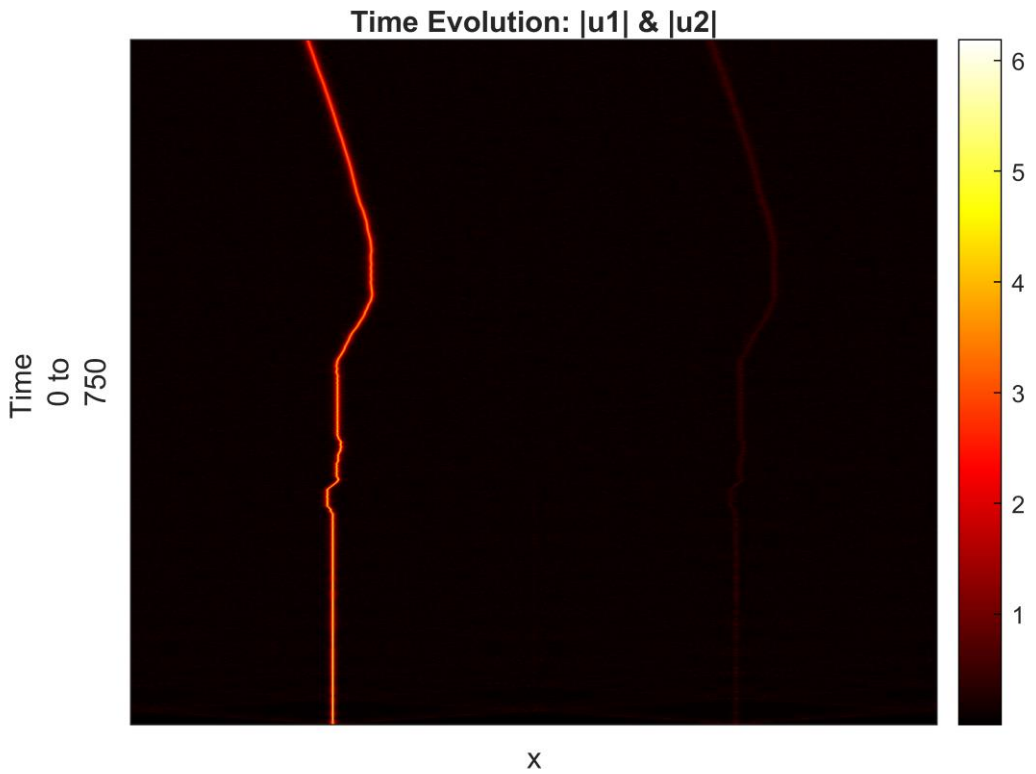

Figure 3.106 The heatmap shows solutions are asymmetric and non-stationary. u_1 is significantly more focussed and prominent than u_2.

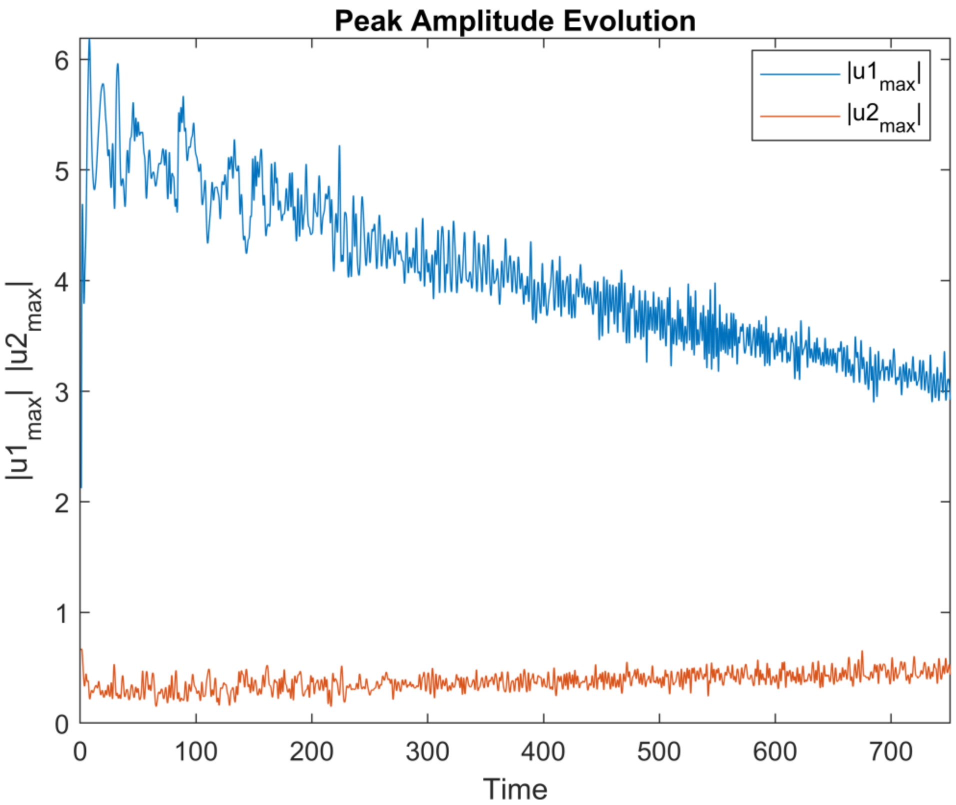

Figure 3.107 The peak amplitude evolution shows u_1 converging on u_2 throughout the experiment.

In the peak amplitude plot in Figure 3.107, we see u_1 and u_2 converging throughout the experiment. We also observe erratic oscillations in peak amplitude from both solutions.

In the waterfall ED plots in Figure 3.108 we see the convergence between the solutions, and we see the dispersion in the solution field of u_2.

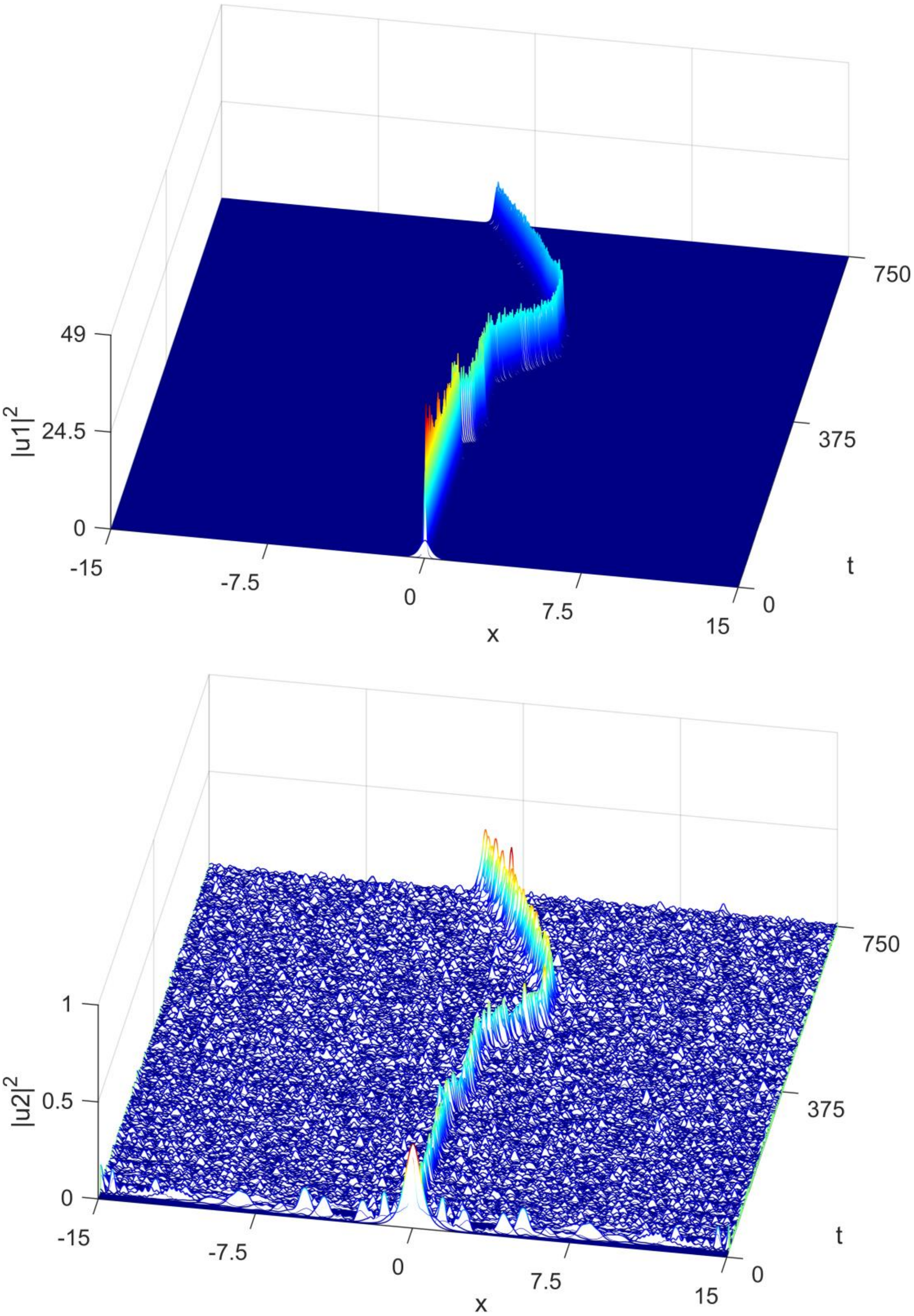

Figure 3.108 The waterfall plot of the ED shows the convergence between u_1 and u_2 as the solutions evolve throughout the experiment (note the difference in amplitude scale).

3.8.11 u_data_a_1p3_mu_2p4_asym

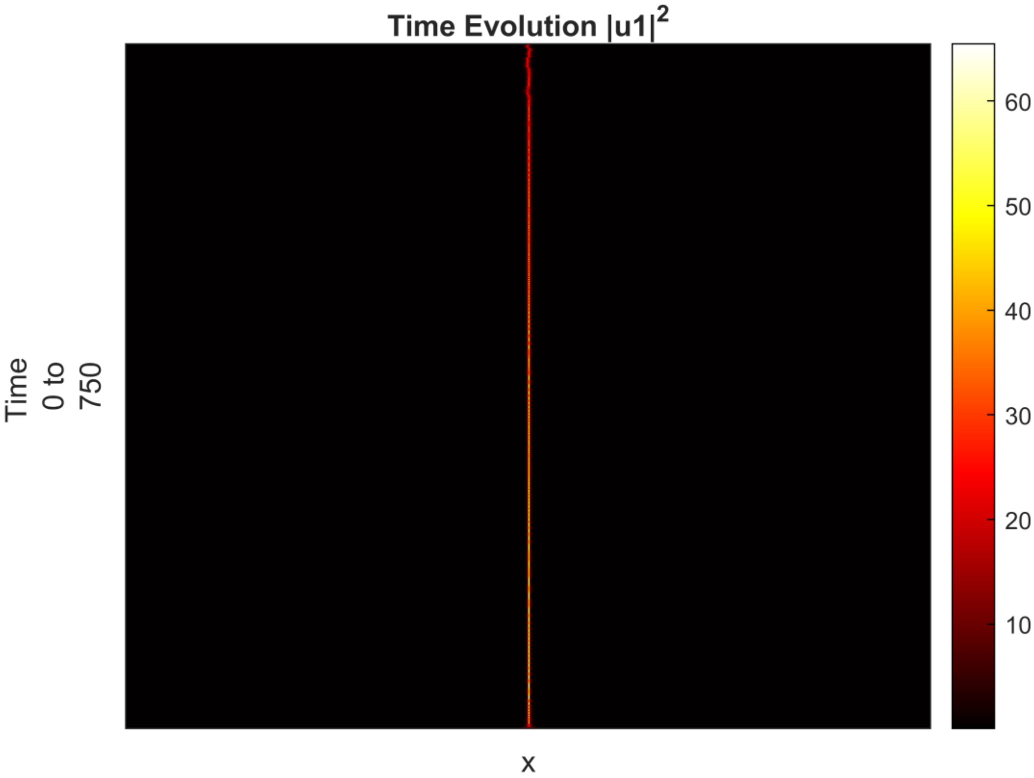

Figure 3.109 The heatmap shows non-stationary behaviour when the fractional derivative order α = 1.3 late in the experiment. u_2 is not shown as it quickly radiates into noise.

When the fractional derivative order α = 1.3 and the phase propagation constant μ = 2.4, u_2 disperses completely, whereas u_1 remains highly focussed but decays over time, visible in Figure 3.109. The waterfall ED in Figure 3.110 and the peak amplitude in Figure 3.111 illustrate the instability of u_1 where we observe erratic oscillations and consistent decay of peak amplitude over the experiment.

The waterfall ED shows a noticeable amount of decay from u_1, and the peak amplitude figure shows u_1 converging on a significantly smaller u_2 throughout the experiment.

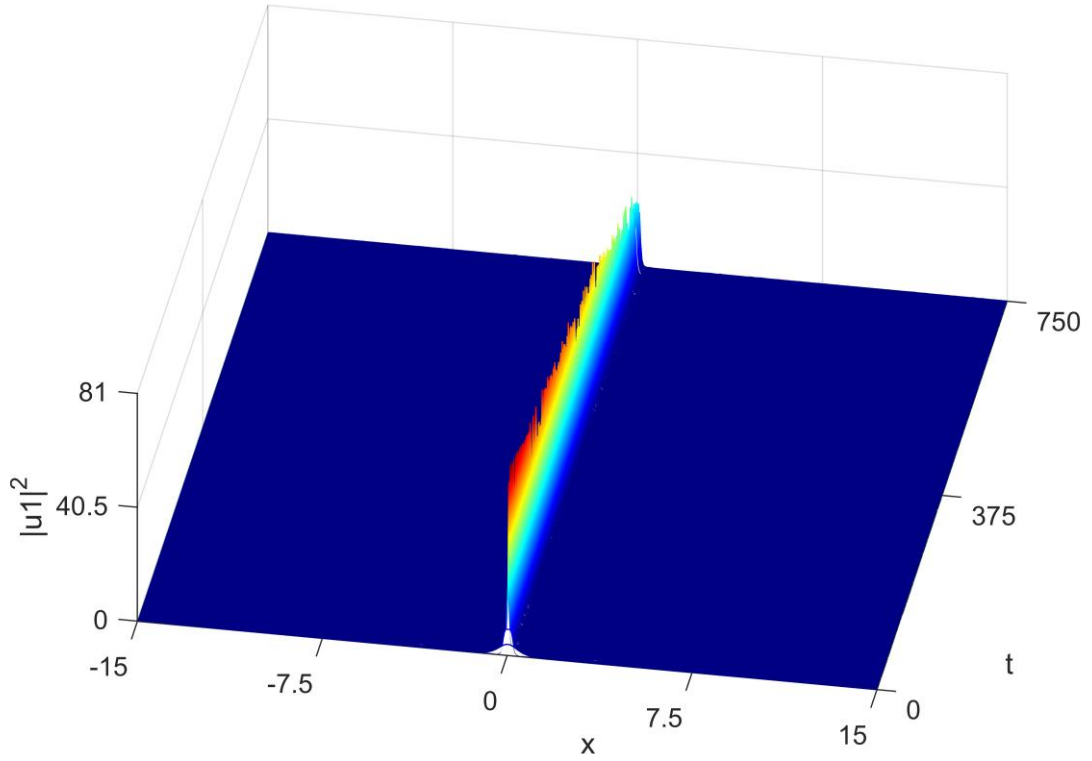

Figure 3.110 A view of the highly focussed u_1 ED.

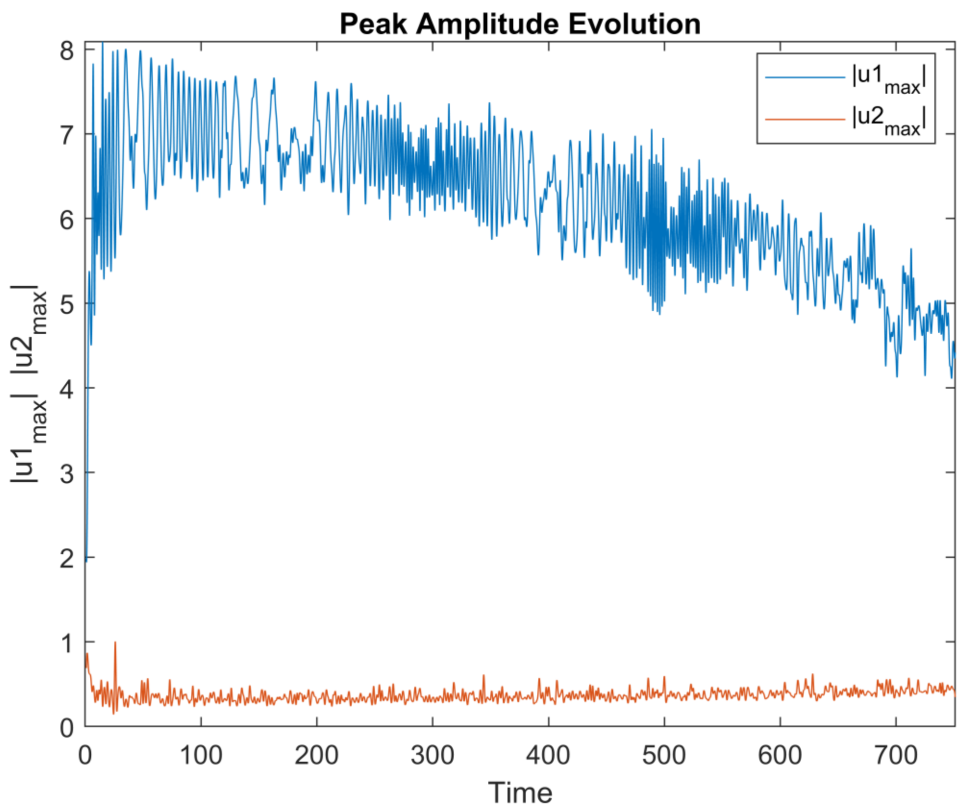

Figure 3.111 Peak amplitude evolution shows u_1 decaying over the course of the experiment. Whereas u_2 decays into background noise.

3.8.12 u_data_a_1p3_mu_2p6_sym

When the fractional derivative order $\alpha = 1.3$ and the phase propagation constant $\mu = 2.6$, Figure 3.112 shows the solutions break symmetry early in the experiment. The solution u_1 becomes highly focussed, and u_2 appears to disperse almost completely. After approximately 150t we observe u_1 becomes non-stationary, deviating predominantly to the left of the solution field.

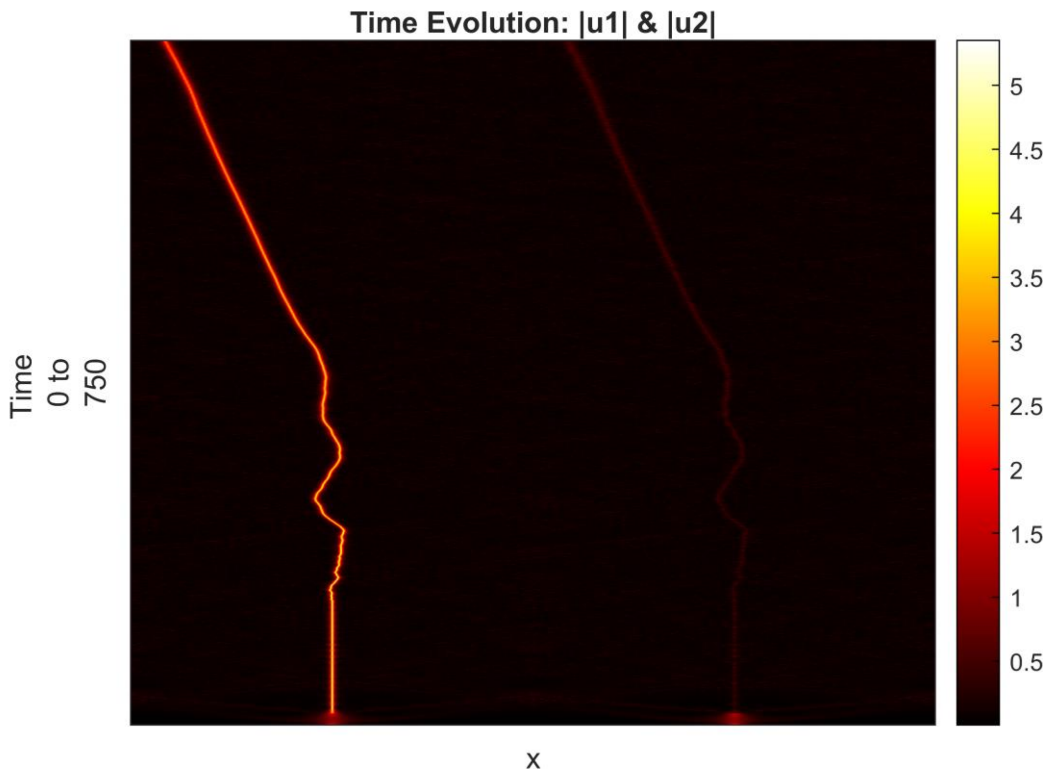

Figure 3.112 The solution becomes asymmetric and non-stationary when $\alpha = 1.3$.

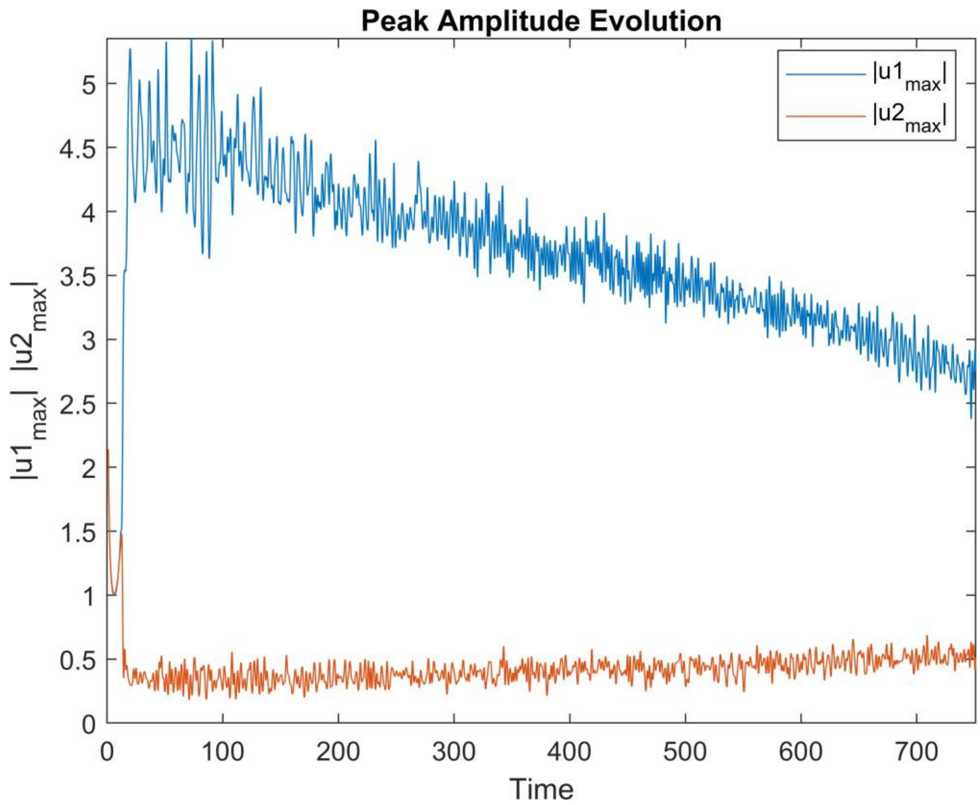

Figure 3.113 We see the solutions break symmetry at approximately 25t, then continue to converge throughout the rest of the experiment.

Looking at the peak amplitude evolution in Figure 3.113, we can see u_1 and u_2 are unstable due to high frequency oscillations. We also observe the solutions converging on each other throughout the experiment, displaying similar behaviour to other results in this section where the fractional derivative order $\alpha \to 1$.

3.8.13 u_data_a_1p3_mu_2p8_asym

From fractional derivative order $\alpha = 1.6$ until 1.3, with the phase propagation constant $\mu = 2.8$, the solutions become more focussed and asymmetric until non-stationary behaviour occurs, evident in the following ED heatmap in Figure 3.114 below. We notice in Figure 3.114 the solution is stationary until approximately halfway through the experiment, when it diverges to the left, then right of the solution field. The peak amplitude evolution in Figure 3.115 shows u_1 and u_2 converging throughout the experiment, with erratic oscillations and clear instability from both solutions.

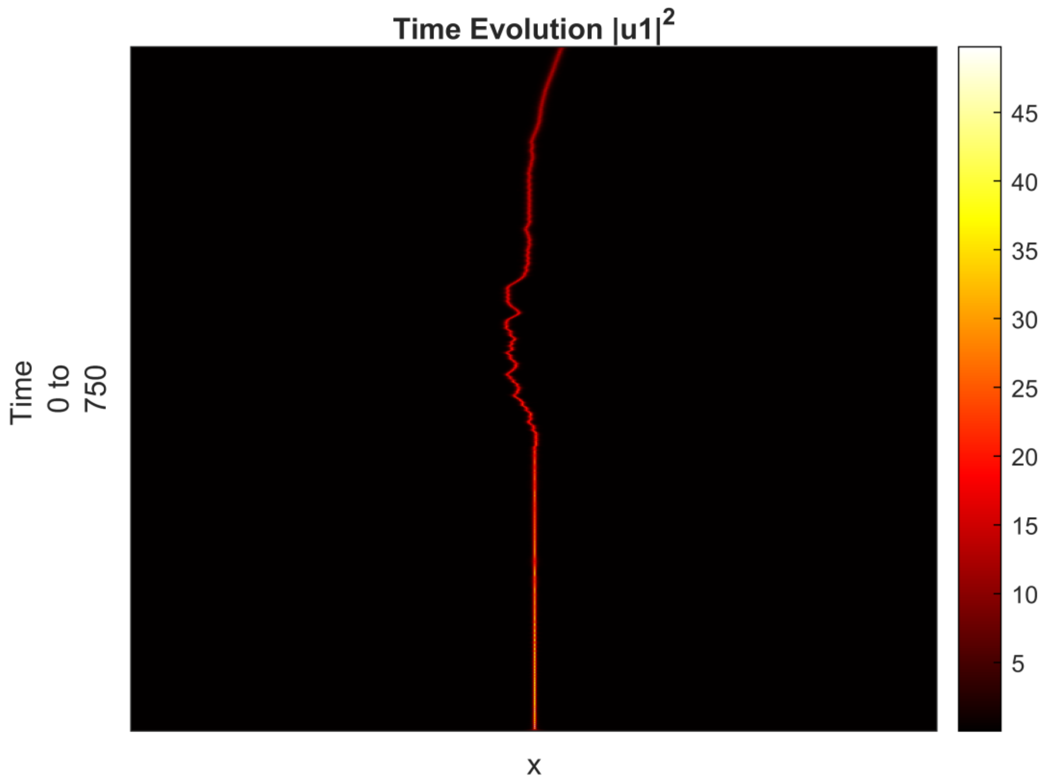

Figure 3.114 The ED heatmap shows non-stationary behaviour from u_1.

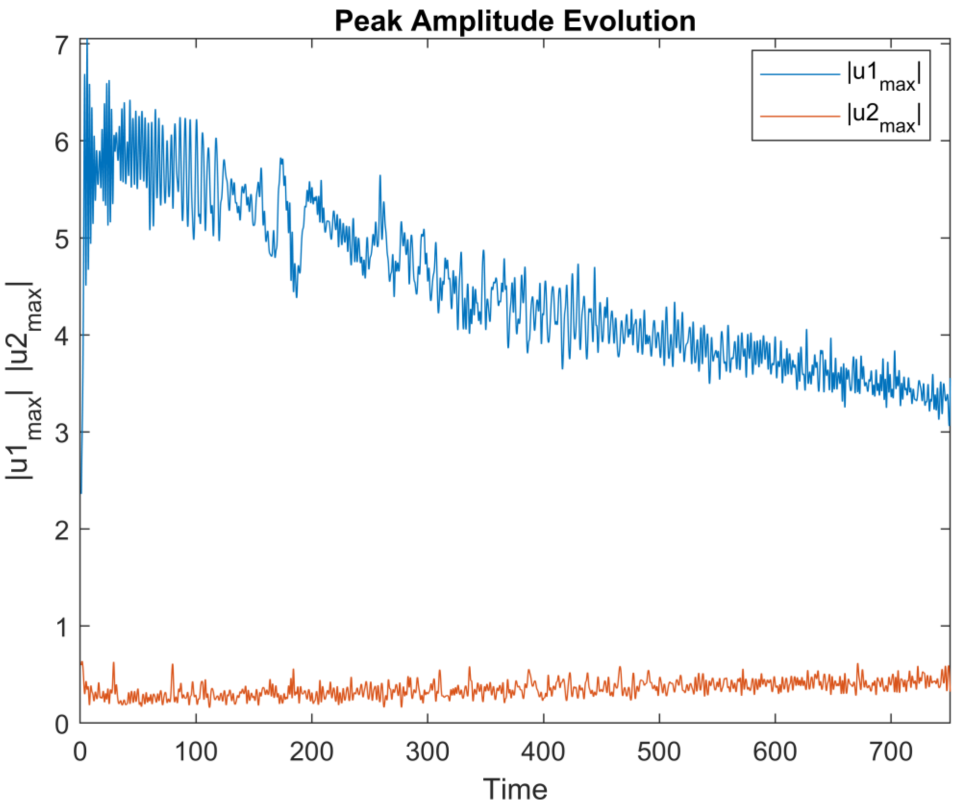

Figure 3.115 The peak amplitude evolution converging over time.

3.9 Fractional derivative α = 1.2

This section reviews curious dynamics for fractional derivatives of order α = 1.2.

3.9.1 u_data_a_1p2_mu_1p2_sym

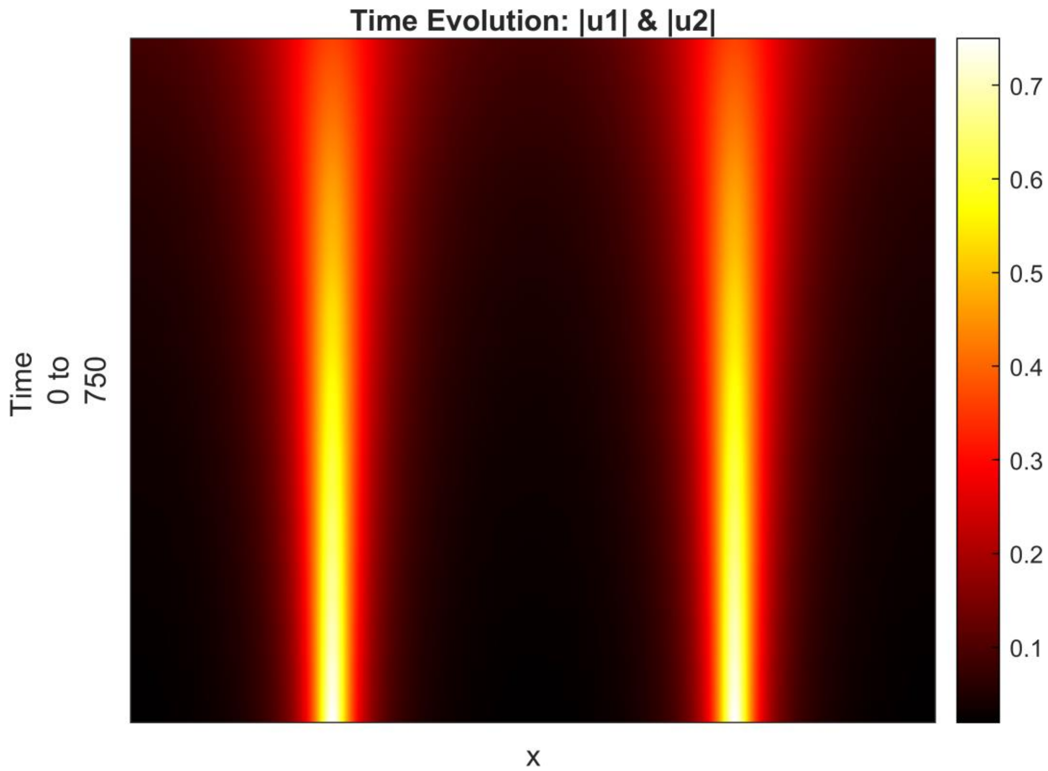

Figure 3.116 Symmetric, stable, but increasingly dispersed solutions.

In Figure 3.116 we present the results of a stable symmetric solution pair with the phase propagation constant μ = 1.2. We see little evidence of oscillations, but there is noticeable dispersion and amplitude decay as the solution evolves.

We confirm from the peak amplitude evolution in Figure 3.117 the solutions are symmetric, and stable as there is very little evidence of oscillations. The centre of mass evolution plot in Figure 3.117 confirms the stability of the oscillations but also indicates the dispersion in the solution corresponding to a positive slope as the experiment progresses. Considering the experiment time and the absence of high frequency oscillations, we conclude that despite the dispersion in the system as the solution evolves, u_1 and u_2 are stable soliton solutions.

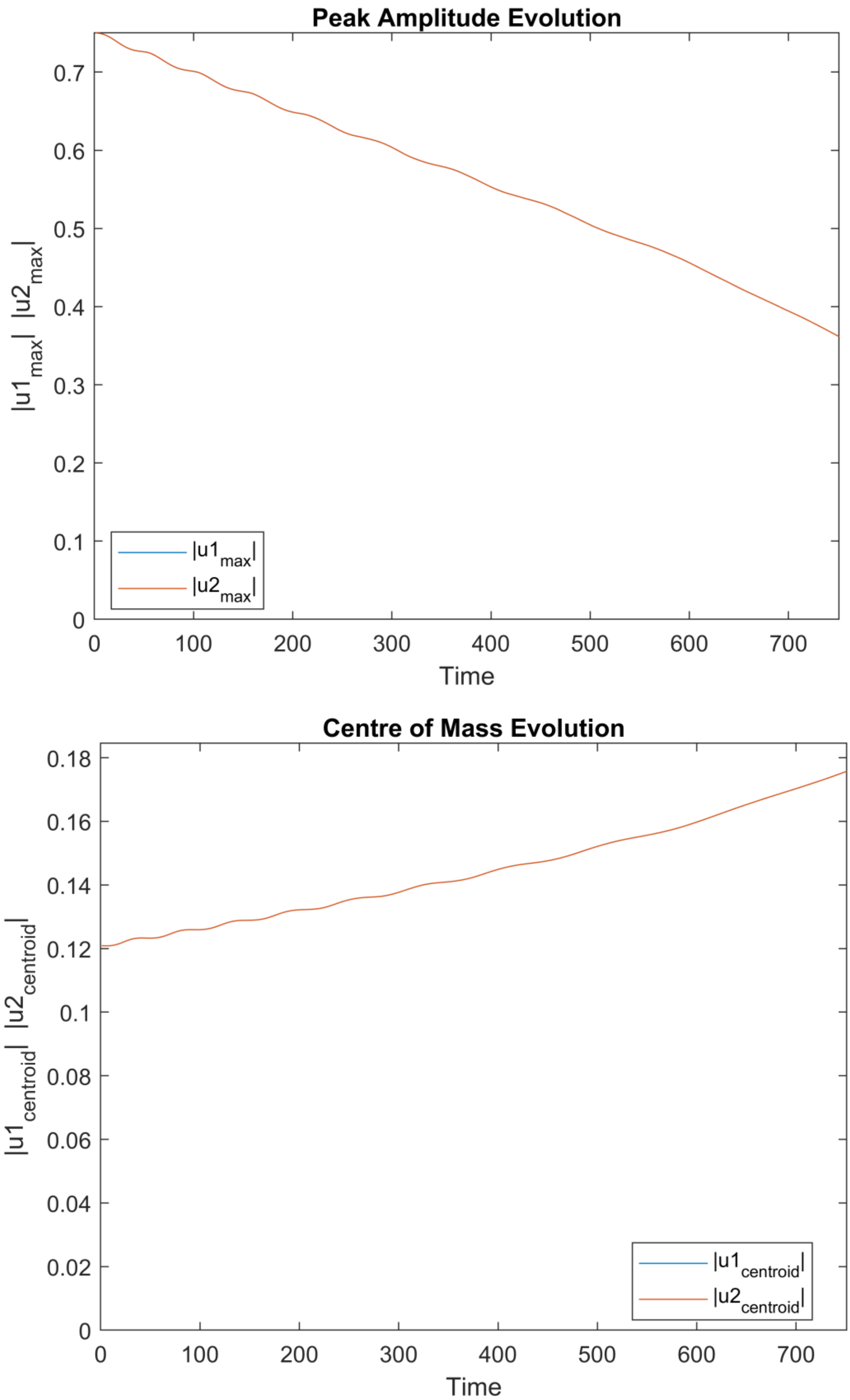

Figure 3.117 The peak amplitude evolution (top) shows stable, but gradually decaying solutions. The centre of mass (bottom) indicates the amount of dispersion as the solutions evolve.

3.9.2 u_data_a_1p2_mu_1p4_sym

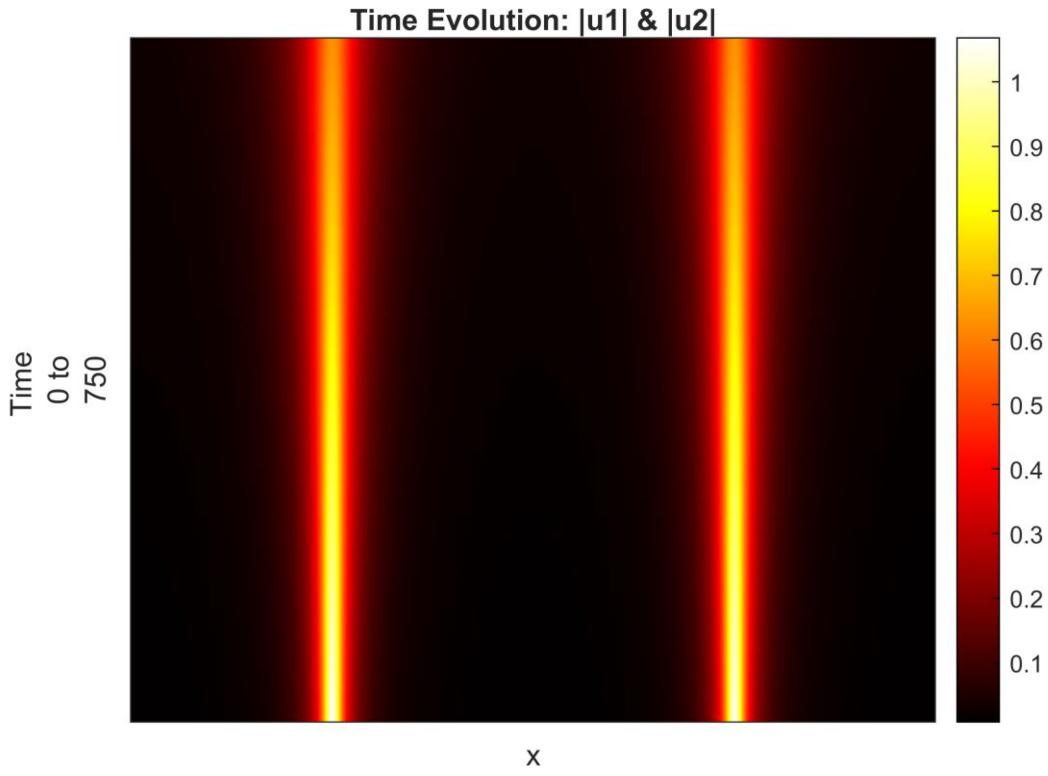

Figure 3.118 Heatmap of stable, symmetric solutions.

In Figure 3.118 we see a stable, symmetric solution pair corresponding to a fractional derivative of order $\alpha = 1.2$ and phase propagation constant $\mu = 1.4$. . The peak amplitude in Figure 3.119 reveals a decay in peak amplitude throughout the experiment, while the centre of mass evolution plot indicates minimal oscillations, and increased dispersion over time, confirming stability.

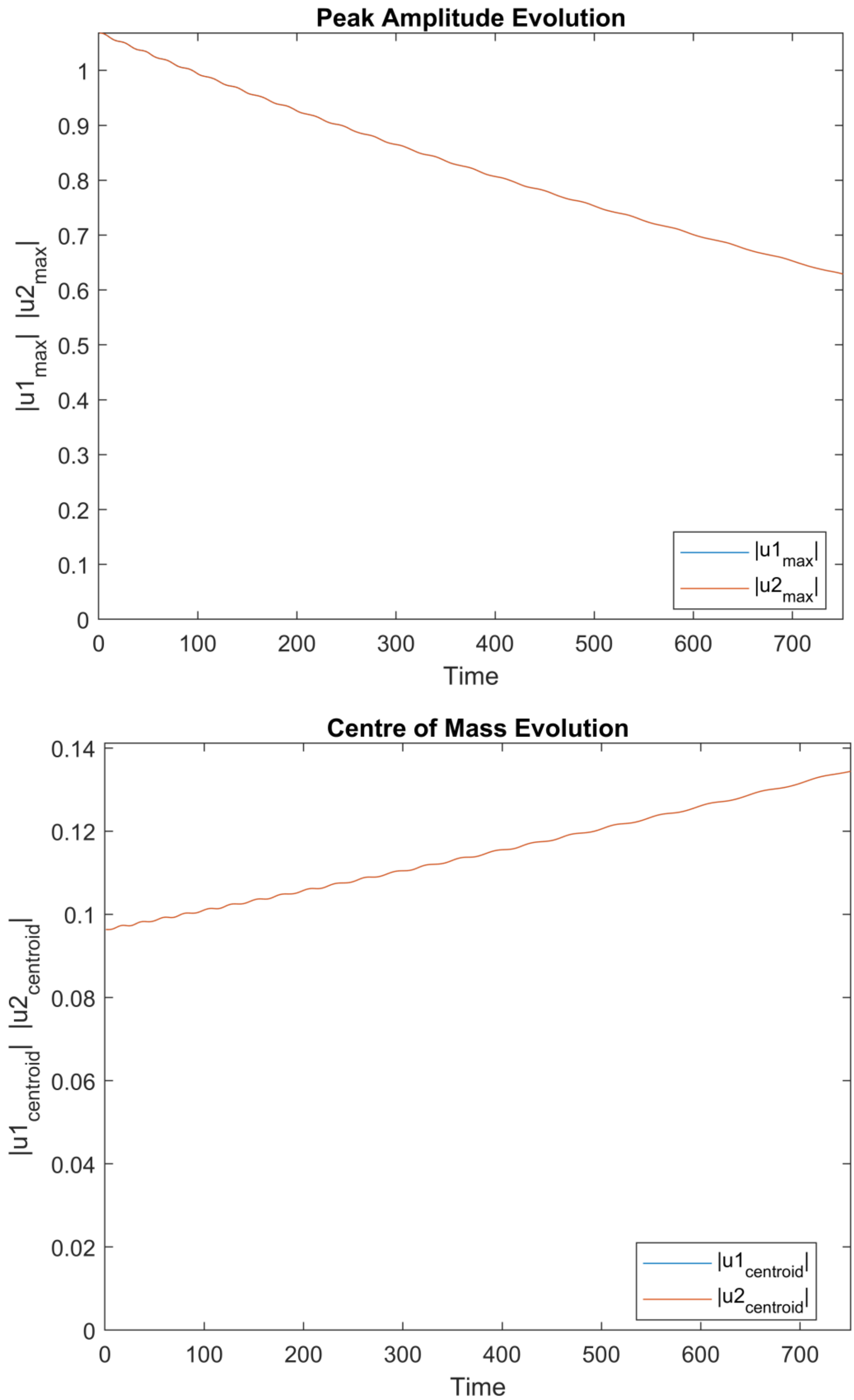

Figure 3.119 Peak amplitude evolution (top) and centre of mass evolution (bottom) of a stable symmetric solution pair.

3.9.3 u_data_a_1p2_mu_1p5_sym

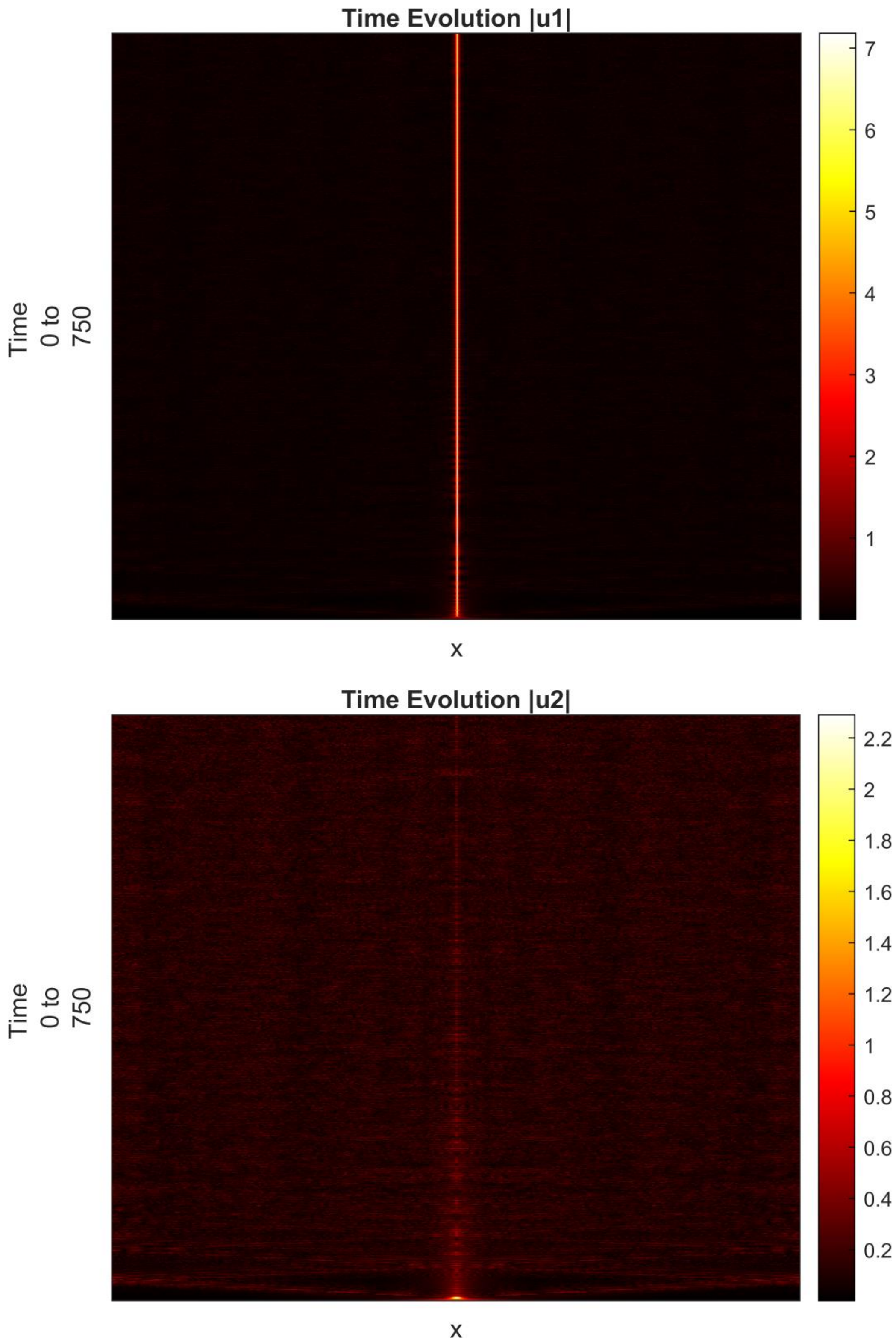

Figure 3.120 Asymmetry continues when the fractional derivative order α = 1.2

In Figure 3.120, when the fractional derivative order $\alpha = 1.2$ and the phase propagation $\mu = 1.5$, the solution returns to a stationary state yet remains asymmetric. We see the phase portrait in Figure 3.121 below, u_1 remains relatively stable with a peak amplitude ranging from approximately 5 to 6. We must remain aware of the need for caution when interpreting peak amplitude and phase of low amplitude values, as the data used to determine these factors may in fact be noise from dispersion effects, therefore we do not display u_2, as it would appear to be stable at a value of approximately 0.5, consistent with the average amplitude of the noise in the solution field.

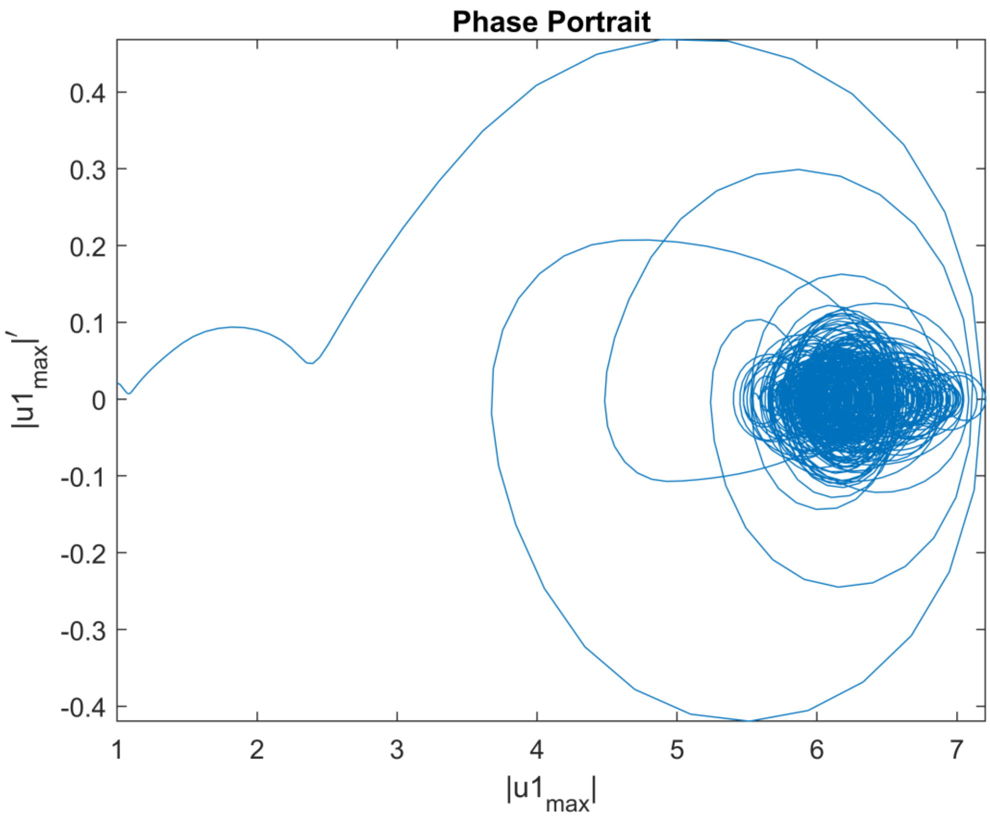

Figure 3.121 Phase portrait shows u_1 oscillates with an amplitude of approximately 6 for most of the experiment.

3.9.4 u_data_a_1p2_mu_1p6_asym

For fractional derivative of order α = 1.2 and phase propagation constant μ = 1.6 we see in Figure 3.122 the unstable asymmetric solution pair disperses immediately, creating visually appealing, symmetric diffraction patterns in the solution field.

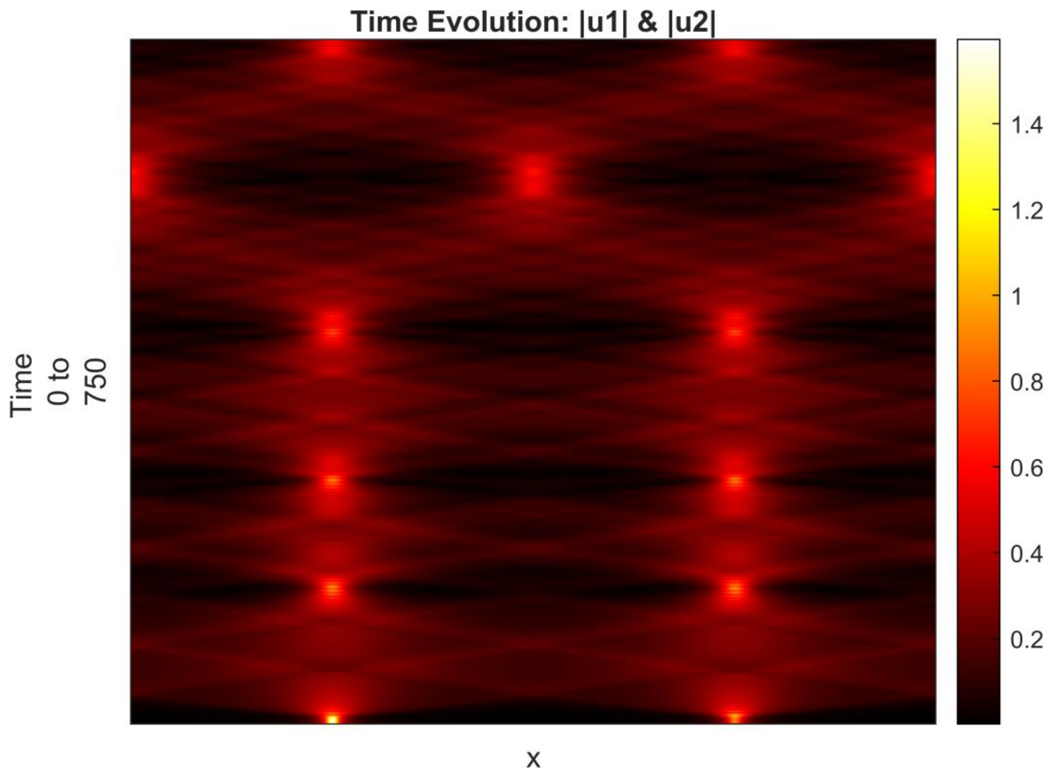

Figure 3.122 Heatmap of asymmetric solutions u_1 and u_2 with a phase propagation constant μ = 1.6, and fractional derivative order α = 1.2.

If we inspect the waterfall ED plot in Figure 3.123, we see four periodic peaks in the solution field before the solution disperses. Due to the periodic boundary conditions, we see a fifth pulse at the conclusion of the experiment.

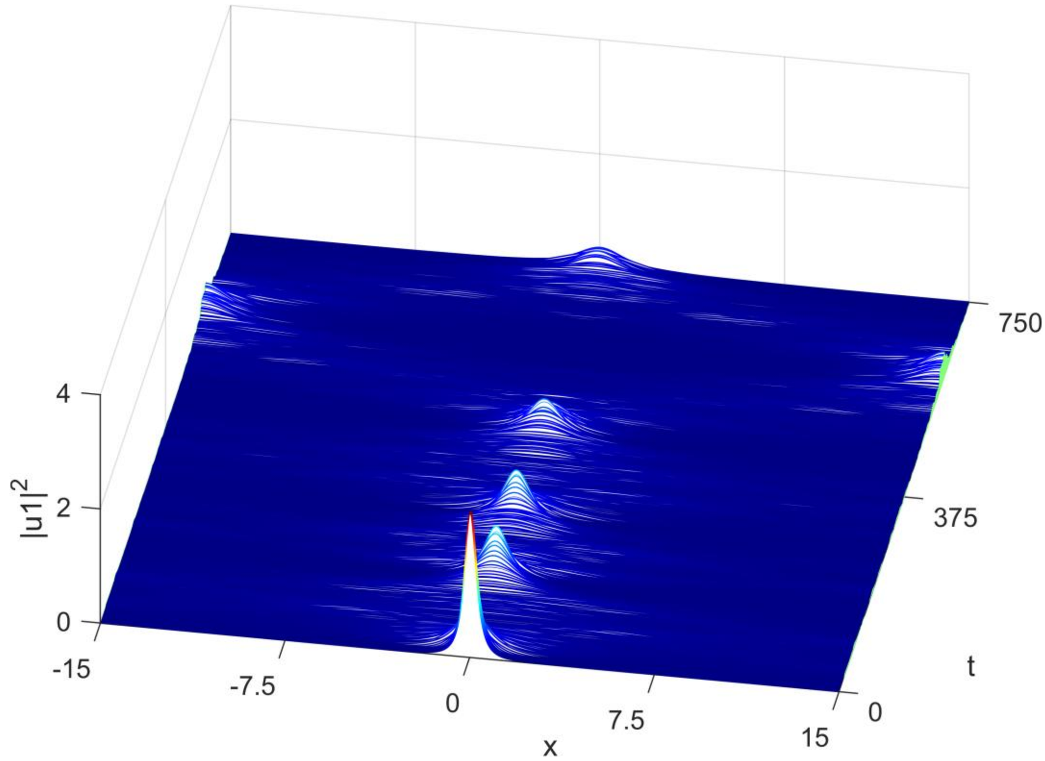

Figure 3.123 Asymmetric, unstable solution pair.

If we observe the following peak amplitude evolution and centre of mass evolution plots in Figure 3.124, we see these solutions are another example of group velocity propagating symmetrically, while remaining out of phase. The peak amplitude and centre of mass plots are a good example of the inverse relationship between peak amplitude and centre of mass.

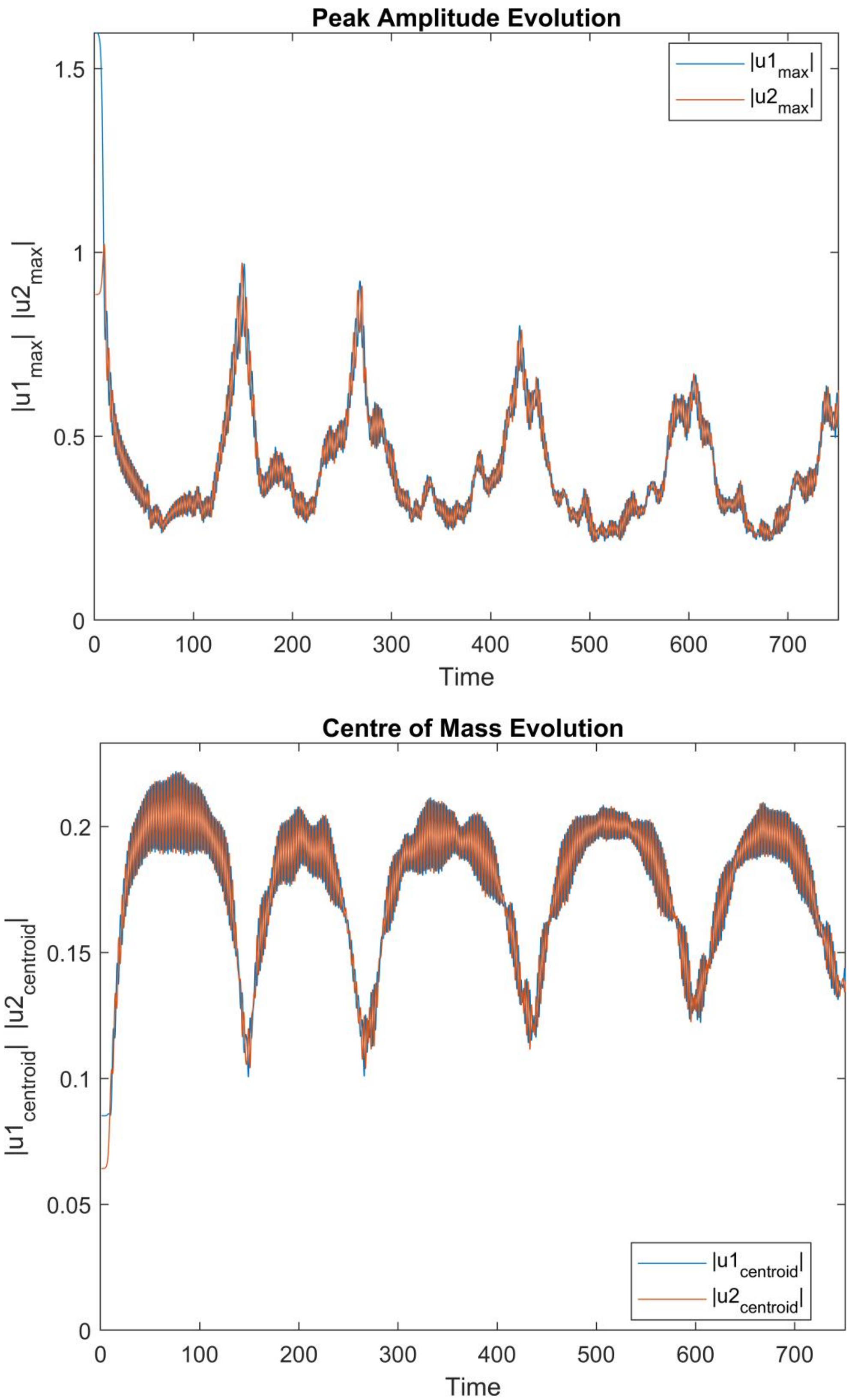

Figure 3.124 The peak amplitude evolution (top) and centre of mass evolution (bottom) show the solutions converging in symmetry. Both inner waves propagate symmetrically, while the surface waves remain asymmetric.

3.9.5 u_data_a_1p2_mu_1p8_sym

As the fractional derivative order α approaches one and the phase propagation constant $\mu = 1.8$, we see in Figure 3.125 the solution u_1 increases in amplitude and focus, whereas u_2 disperses immediately. We refer to the waterfall ED in Figure 3.125 to appreciate the focus of the stable solution u_1, as compared to its coupled solution u_2, which decays immediately.

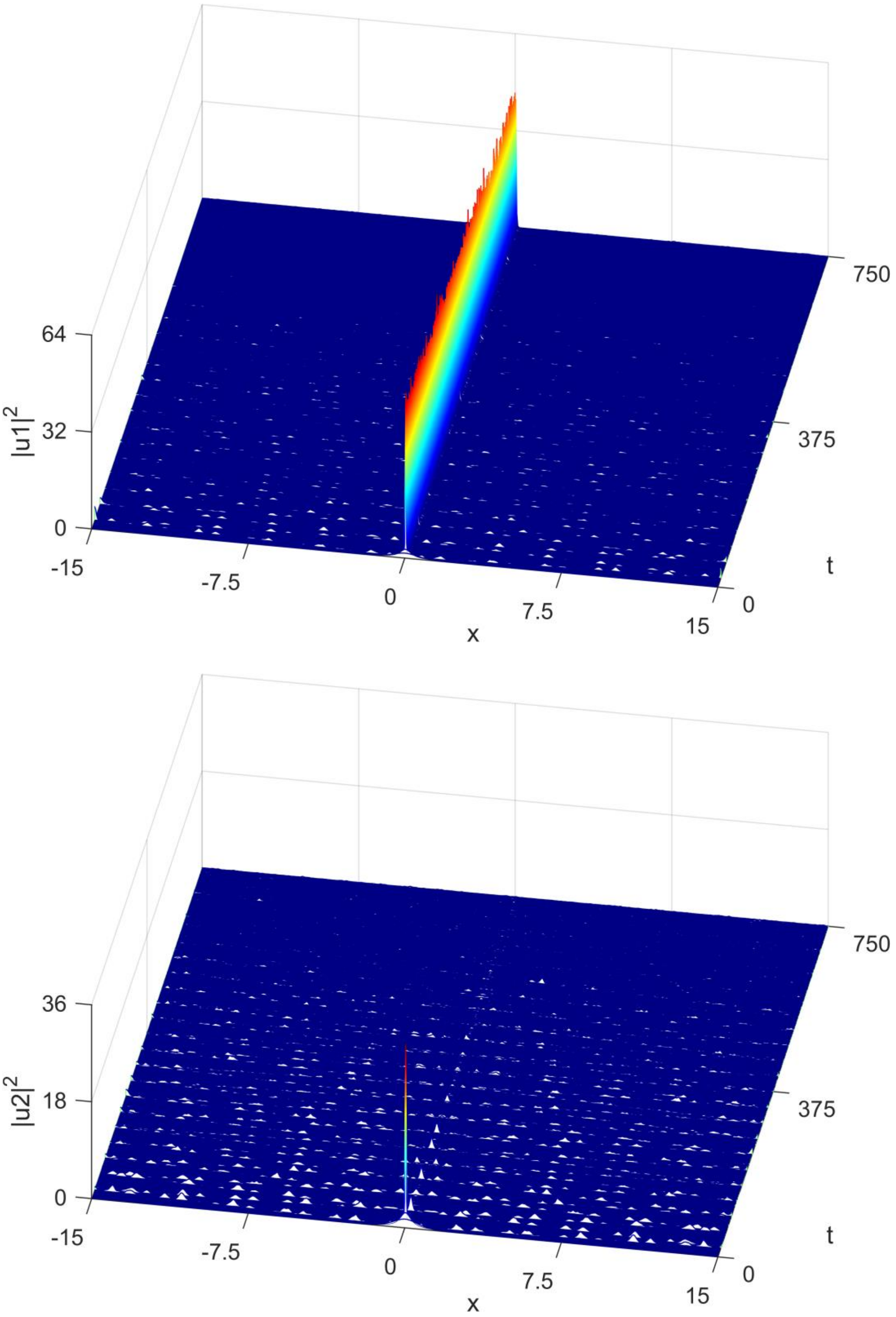

Figure 3.125 The ED shows u_1 is highly focussed, while u_2 decays to noise almost immediately, radiating both right and left of the solution field.

The phase portrait in Figure 3.126 shows u_1 to be reasonably stable when the peak amplitude is approximately 6.8, albeit with some variation in amplitude over time, consistent with oscillations.

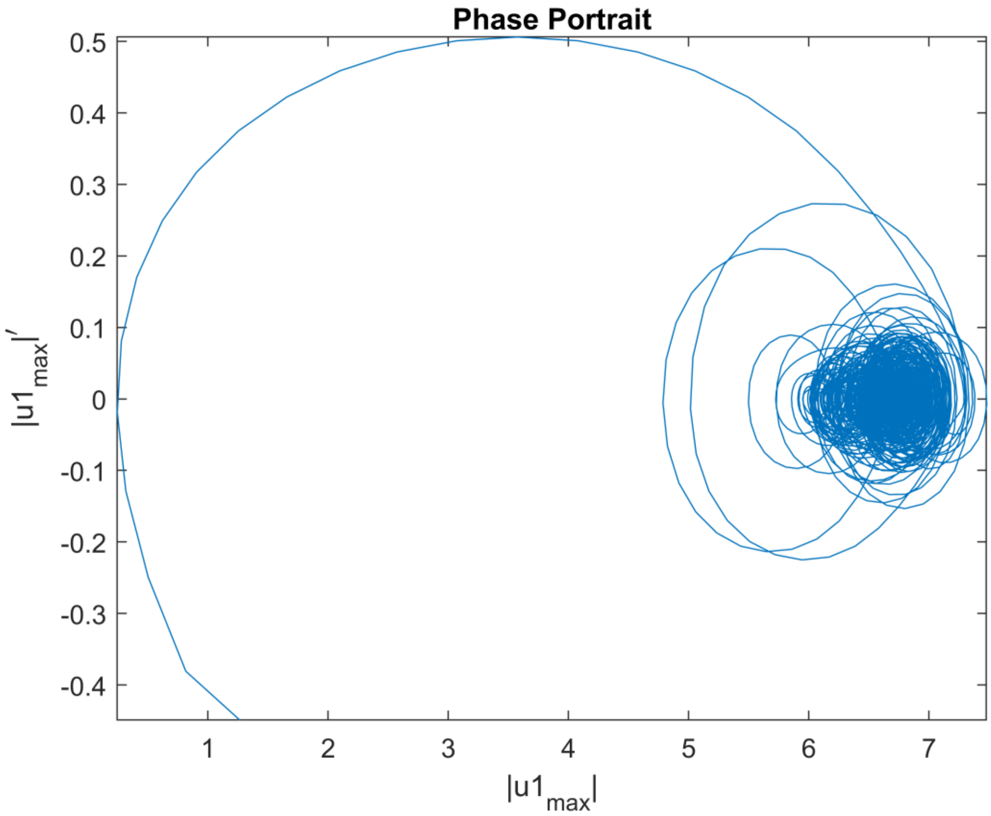

Figure 3.126 Phase portrait of peak amplitude shows u_1 to be reasonably stable when the peak amplitude is approximately 6.8.

3.9.6 u_data_a_1p2_mu_2p0_asym

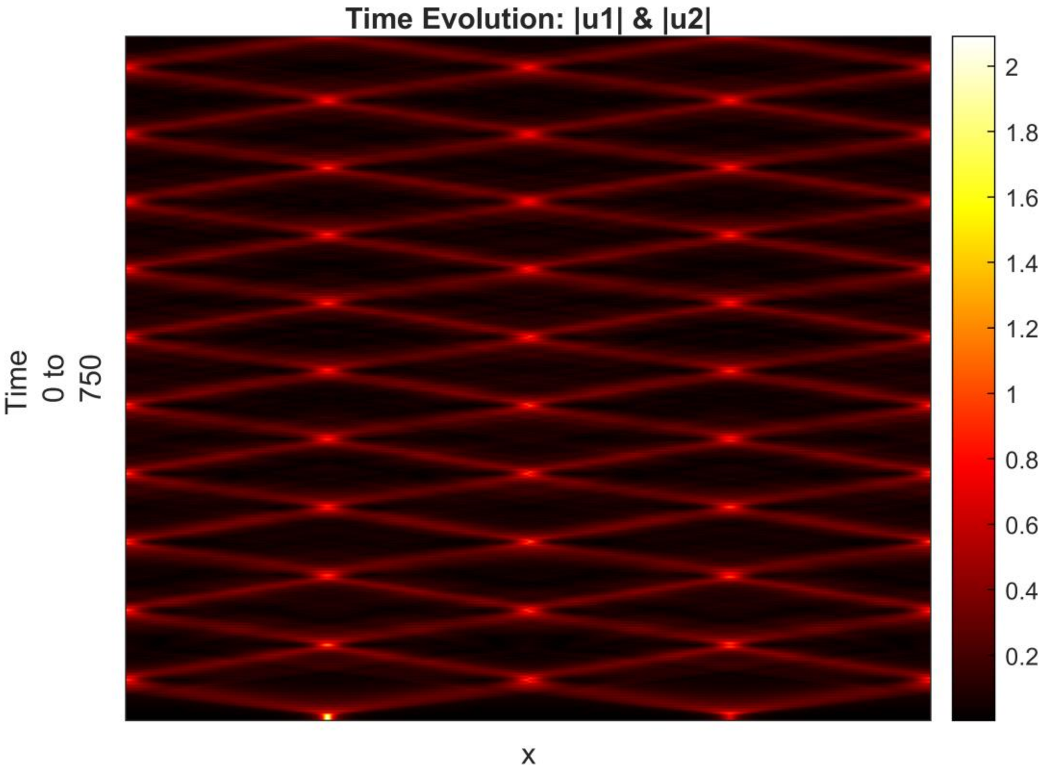

Figure 3.127 Unstable, asymmetric pair when α = 1.2.

For fractional derivative of order α = 1.2 and phase propagation constant μ = 2, we see in Figure 3.127 the unstable, asymmetric solutions u_1 and u_2 disperse immediately. As the dispersion combines with the periodic boundary conditions, we see appealing diffraction patterns throughout the solution field. Looking at the peak amplitude evolution and centre of mass evolution in Figure 3.128, we see evidence of the solutions approaching symmetry.

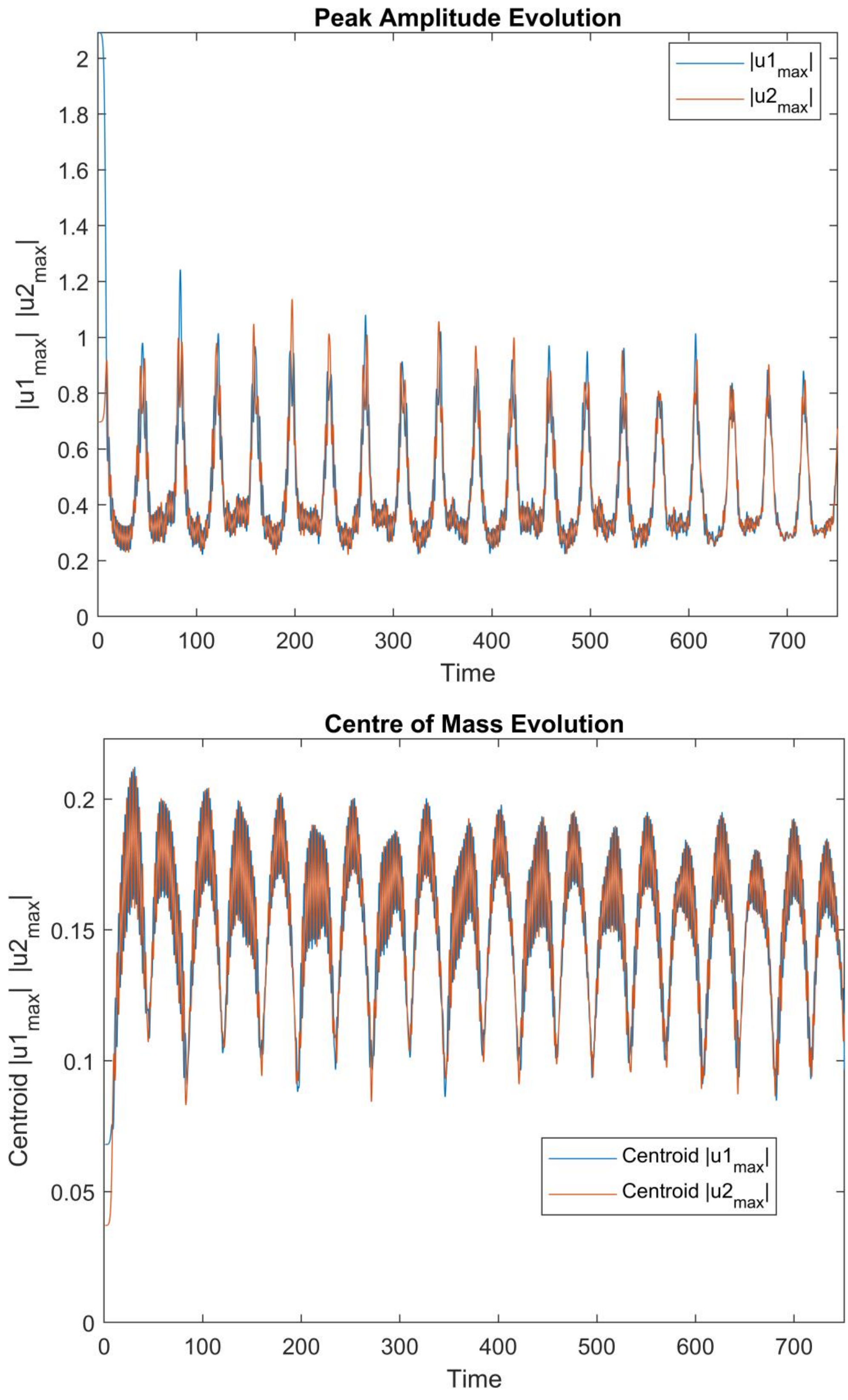

Figure 3.128 Peak amplitude evolution (top) and centre of mass evolution (bottom) show evidence of symmetric propagation of group velocity, while remaining out of phase.

3.9.7 u_data_a_1p2_mu_2p4_asym

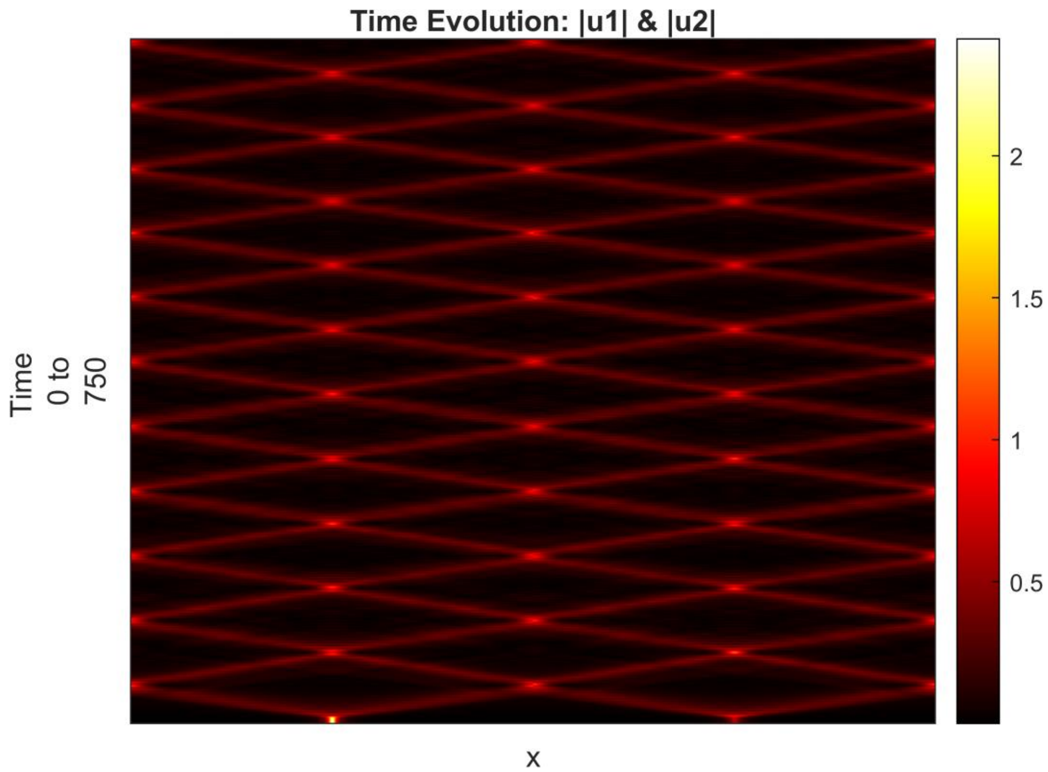

Figure 3.129 Unstable, asymmetric solution with interesting dispersion pattern.

When the fractional derivative order $\alpha = 1.2$ and the phase propagation constant $\mu = 2.4$ we observe in Figure 3.129 the results of unstable, asymmetric solutions dispersing early in the experiment. Due to the periodic boundary conditions, we see a periodic diffraction pattern in the solution field. Once again, if we observe the peak amplitude evolution and centre of mass evolution in Figure 3.130 below, we will see symmetric propagation of the group velocity and continued evolution out of phase.

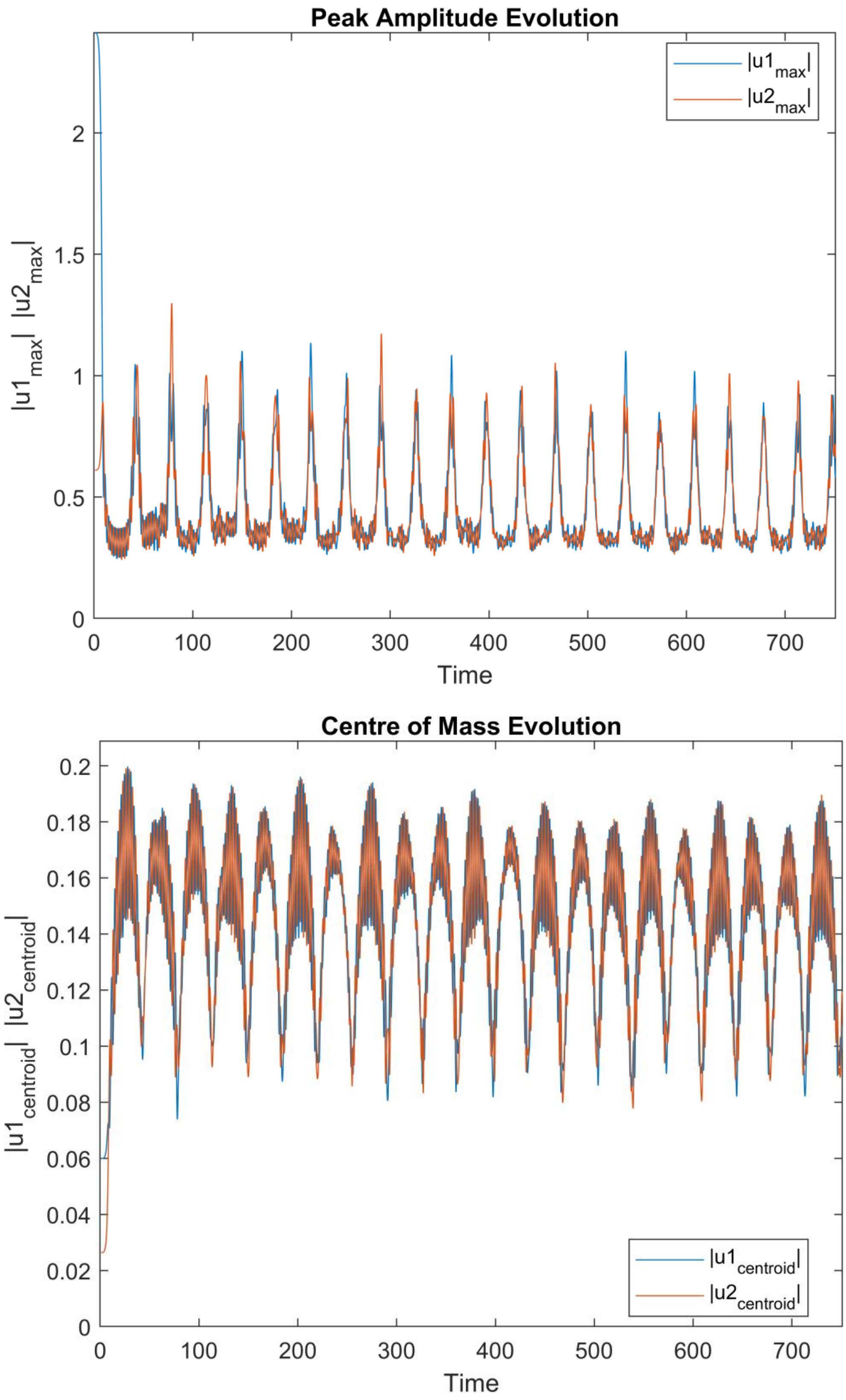

Figure 3.130 Peak amplitude evolution (top) and centre of mass evolution (bottom) show evidence of symmetry making conditions.

3.10 Bifurcation diagram: portion α = 1.2

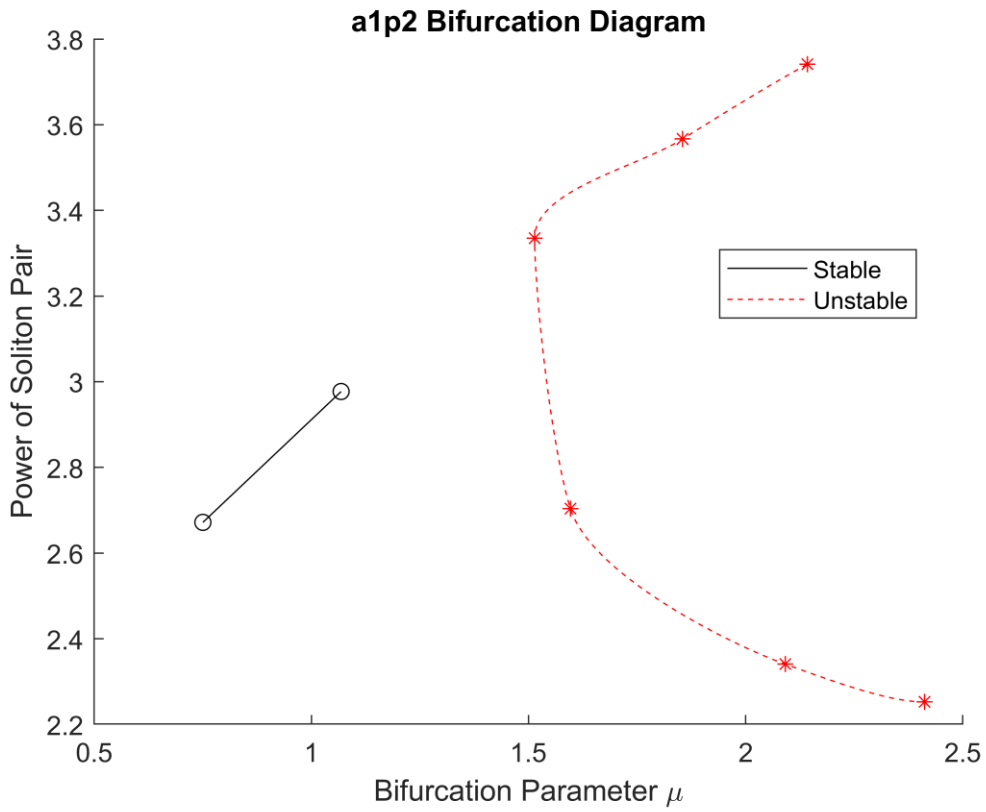

Figure 3.131 Bifurcation plot for α = 1.2 data.

Here we note in Figure 3.131 the stable bifurcation branch (black) corresponds to the average power to maximum amplitude ratio greater than 3, and the unstable branch (red) corresponds average power to peak amplitude ratio less than approximately 1.6.

Comparing the stable and unstable branches of the bifurcation plot with Table 3.3 below, we see stability corresponds to phase propagation values $\mu < 1.6$, and the unstable branch corresponds to phase propagation constants $\mu \geq 1.6$.

Table 3.3: Fractional value group α = 1.6

Data Pair	Stability	Abs. Max. Amplitude	Power
a_1p2_mu_1p2_sym	Stable	0.75010405	2.671736713
a_1p2_mu_1p4_sym	Stable	1.0684264	2.97717636
a_1p2_mu_1p6_asym	Unstable	1.5964785	2.703842224
a_1p2_mu_1p8_sym	Unstable	1.5139137	3.335051096
a_1p2_mu_2p0_asym	Unstable	2.0909423	2.340843955
a_1p2_mu_2p2_sym	Unstable	1.8548813	3.566778161
a_1p2_mu_2p4_asym	Unstable	2.4119801	2.252409669
a_1p2_mu_2p6_sym	Unstable	2.1421425	3.74140627

3.11 Fractional derivative α = 1.1

In this section we present various noteworthy and interesting dynamics for fractional derivatives of order α = 1.1.

3.11.1 u_data_a_1p1_mu_1p2_sym

In Figure 3.132 we see the symmetric solutions disperse, however, due to periodic boundary conditions we see an interesting pattern evolve in the solution field. This is the first of two examples (the second may be found in the following section 3.112 u_data_a_1p1_mu_1p2_sym) of a symmetric solution maintaining symmetry as the fractional derivative order α approaches 1: both symmetric solutions that evolve in this manner share a phase propagation constant μ = 1.2: generally when the fractional derivative order α = 1.6 symmetric solutions become asymmetric and non-stationary.

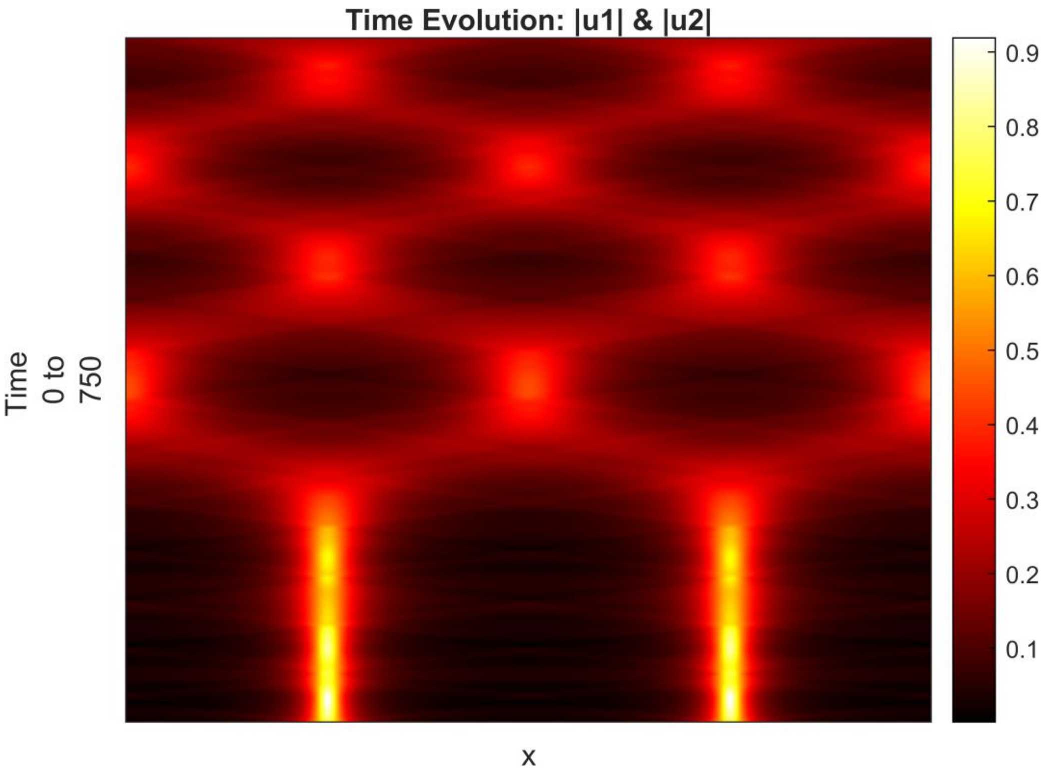

Figure 3.132 Symmetric dispersion pattern when fractional derivative order α = 1.1.

3.11.2 u_data_a_1p1_mu_1p2_sym

As the fractional derivative order decreases from $\alpha = 1.6$ to $\alpha = 1.1$ with the phase propagation constant $\mu = 1.2$ the solutions lose stability and increase dispersion until we observe the following periodic dynamics in Figure 3.133.

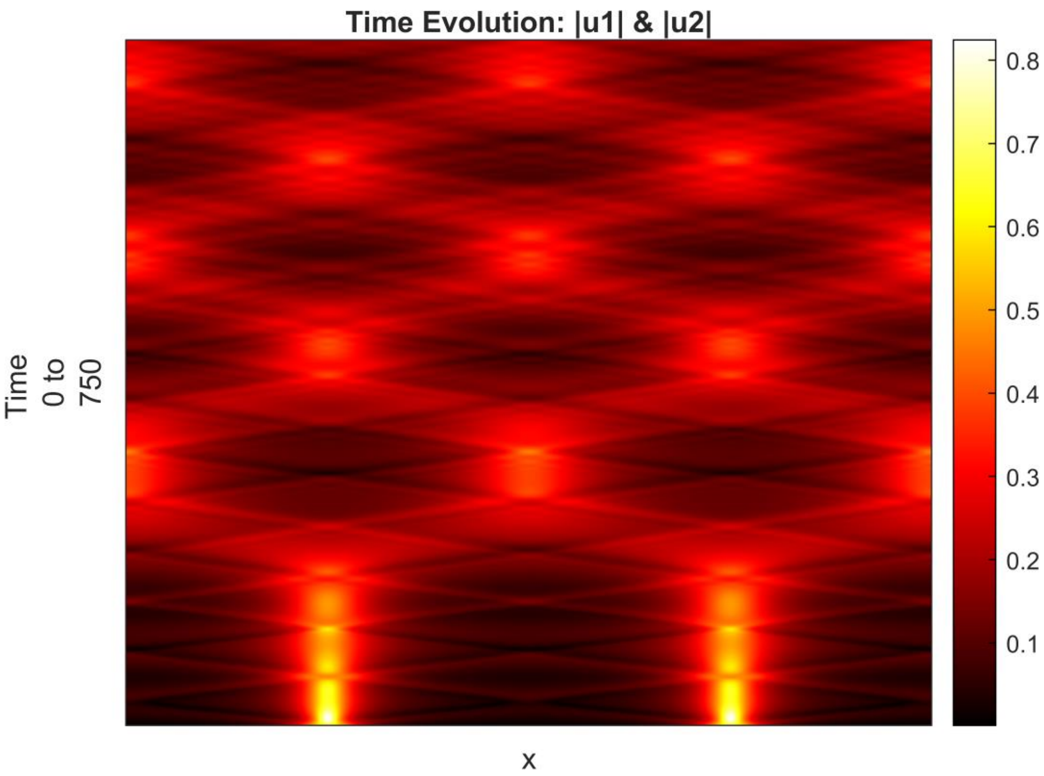

Figure 3.133 When the fractional derivative order $\alpha = 1.1$, the solution pair lose stability, but maintain symmetry. Here the solution resembles a cos(2t) sin(2x) surface.

When the fractional derivative order $\alpha = 1.1$, the solutions decay into what appears to be a cos(2t)sin(2x) surface, when the previous tile pattern occurs as in section 3.11.1. The waterfall ED in Figure 3.134 is included out of interest, to show how the solution quickly disperses from the initial conditions. This is an example of why periodic boundaries may be considered undesirable. This is also the first example of symmetric solutions maintaining symmetry as the fractional derivative order α approaches 1, instead of breaking symmetry and becoming highly focussed and non-stationary.

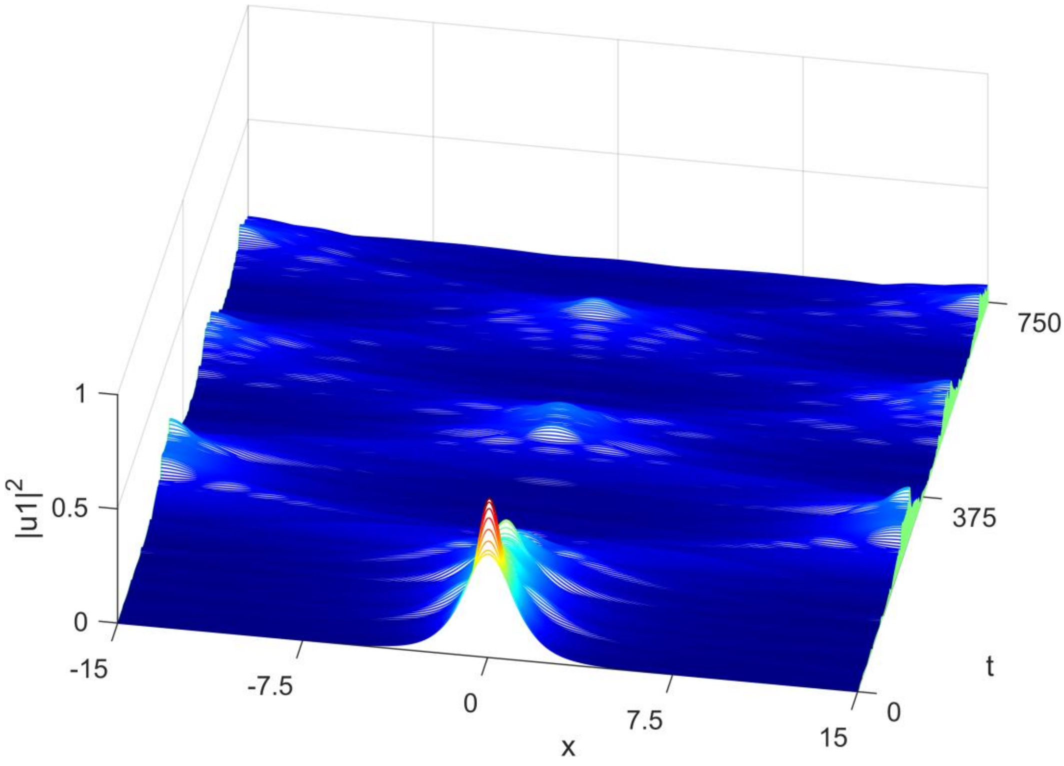

Figure 3.134 ED of the solution nicely demonstrates diffraction patterns from the regular boundary conditions.

3.11.3 u_data_a_1p1_mu_1p6_asym

When the fractional derivative order α = 1.1 and the phase propagation constant μ = 1.6, the solutions become highly asymmetric and focussed, visible in Figure 3.135. The solution u_2 decays immediately, whereas u_1 propagates as a highly focussed, oscillating, and decaying soliton throughout the experiment. We can see this behaviour in the ED waterfall plot in Figure 3.135 below.

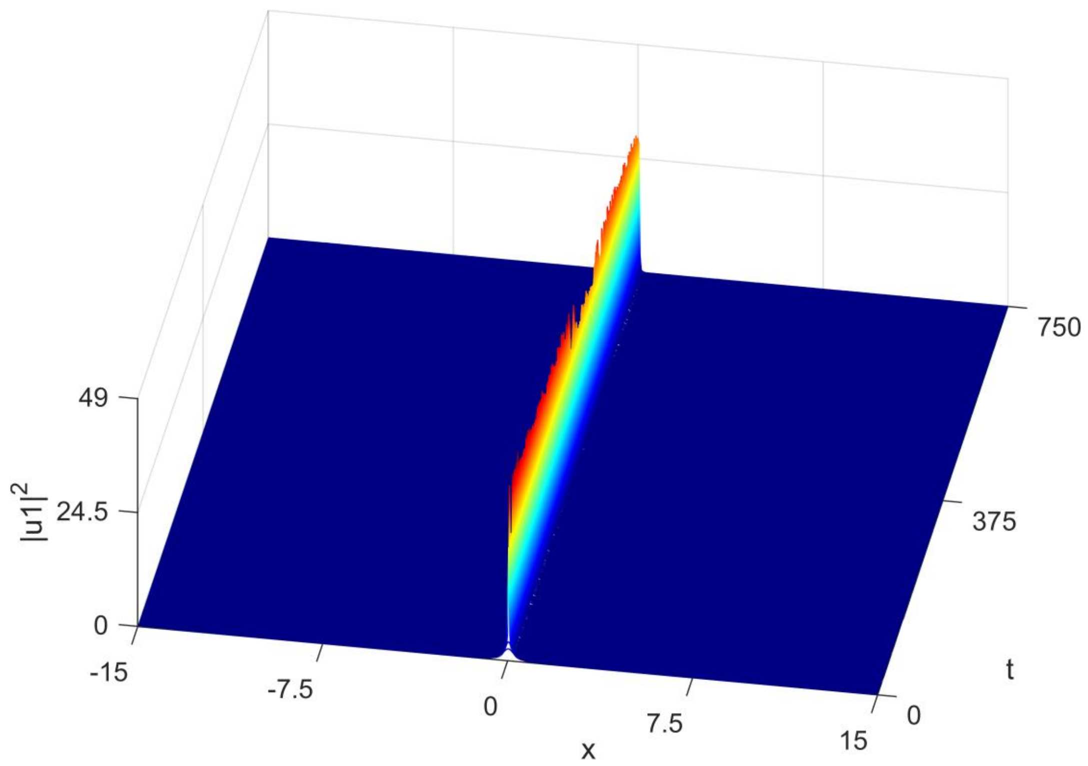

Figure 3.135 Waterfall ED displaying unstable, highly focussed, and asymmetric results when the fractional derivative order $\alpha = 1.1$.

3.11.4 u_data_a_1p1_mu_1p8_asym

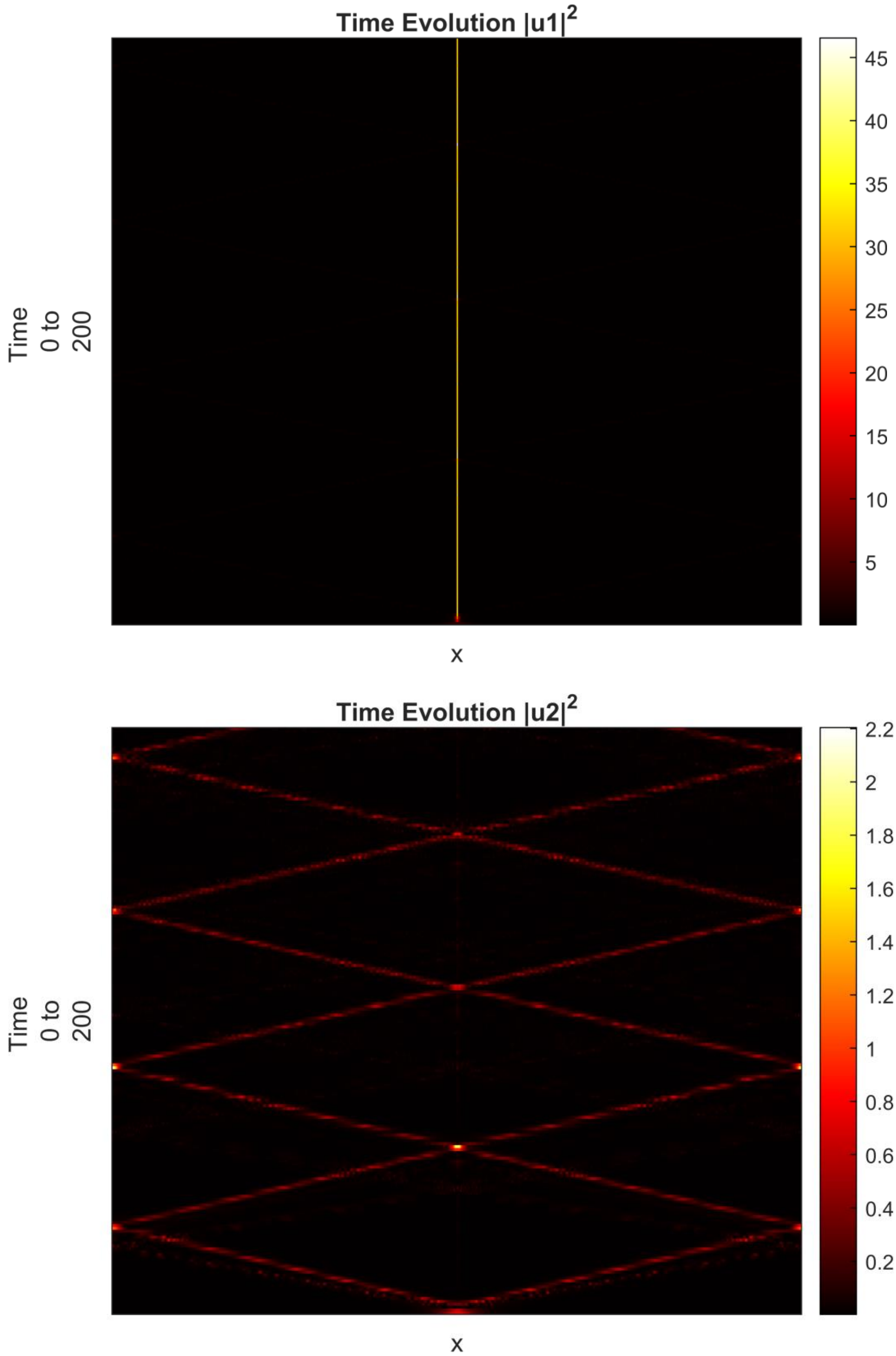

Figure 3.136 The heatmap shows the ED of u_1 and u_2.

Between fractional derivative order α = 1.3 and α = 1.1, and the phase propagation constant μ = 1.8, u_1 increases focus while u_2 immediately disperses. We see on the ED heatmap for 200t in Figure 3.136, u_1 has become focussed with a relatively high peak amplitude that appears to be stable. Alternatively in the ED waterfall plot for 750t in Figure 3.137, u_2 disperses immediately to the left and the right, until halfway through the experiment when radiative noise appears to propagate to the left only.

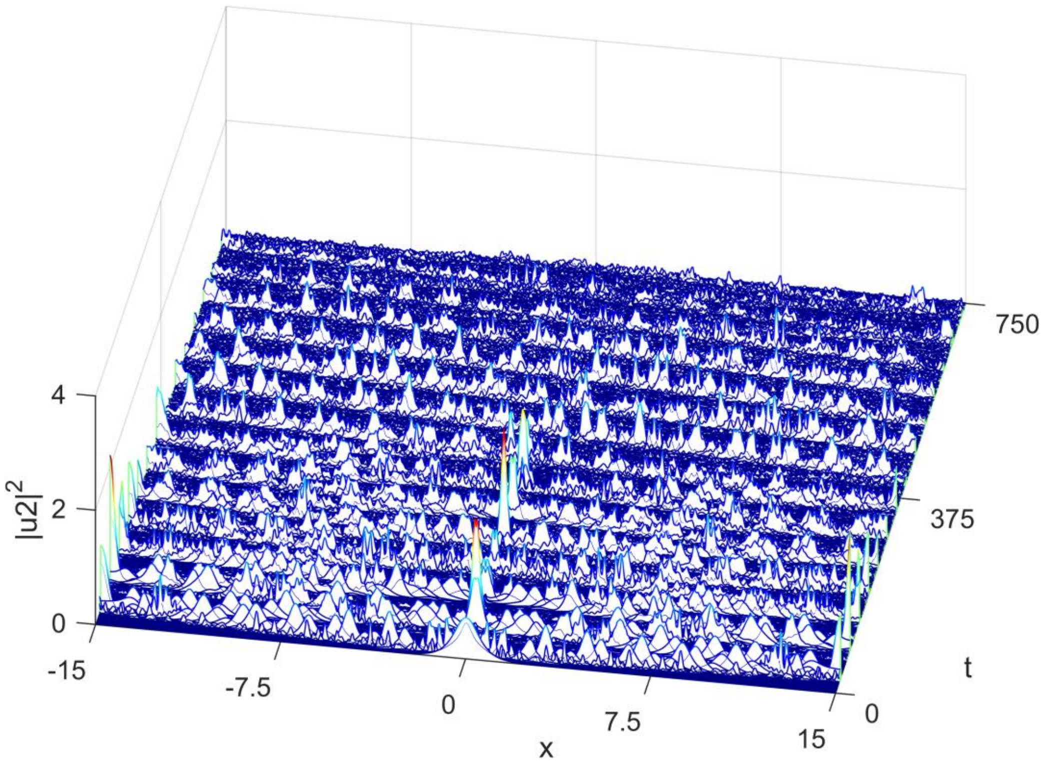

Figure 3.137 The ED waterfall plot of u_2 shows noise in the solution, and dispersion radiating to the left during the second half of the experiment.

3.11.5 u_data_a_1p1_mu_1p8_sym

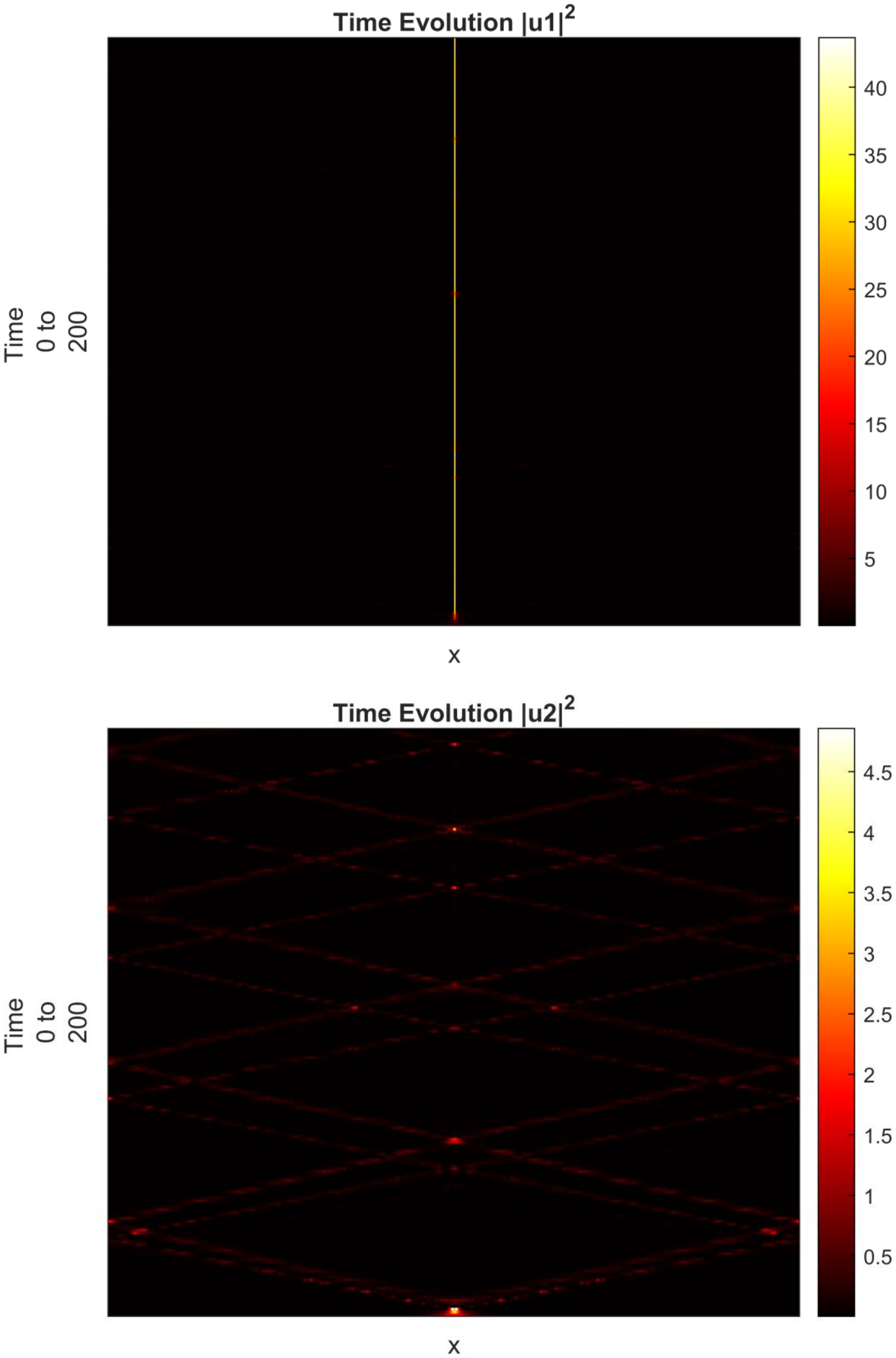

Figure 3.138 ED heatmap of u_1 and u_2 when the fractional derivative order α approaches 1.

In Figure 3.138, when the fractional derivative order $\alpha = 1.1$ and the phase propagation constant $\mu = 1.8$, we see the solution u_1 becomes highly focussed as u_2 disperses completely: u_1 appears to be stable. If we look at the phase portrait in Figure 3.139 below, we see u_1 oscillating around what appears to be an unstable sink, corresponding to a stable amplitude of approximately 6.3.

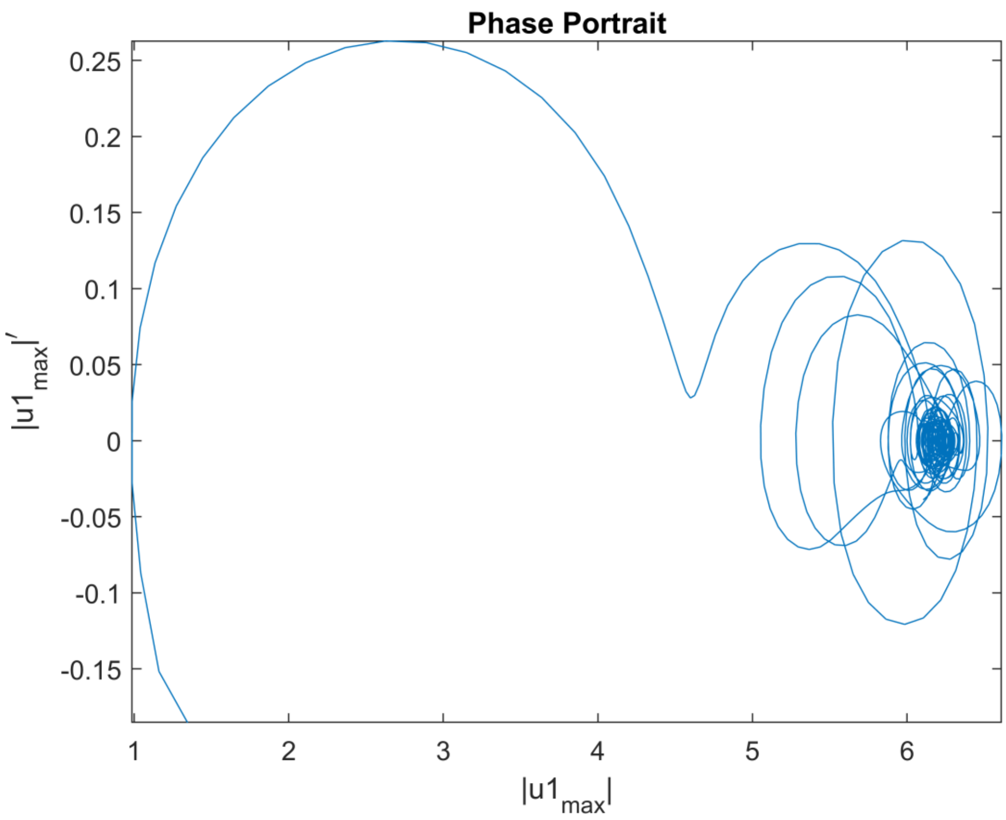

Figure 3.139 The phase portrait of u_1 shows an unstable sink when u_1 is approximately 6.3.

In the waterfall plot in Figure 3.140 below, we see u_1 and the contribution of u_2 as dispersion patterns in the solution field. Based on the ED heatmap in Figure 3.138, waterfall plot in Figure 3.140 and the phase portrait in Figure 3.139, u_1 appears to be highly focussed but stable.

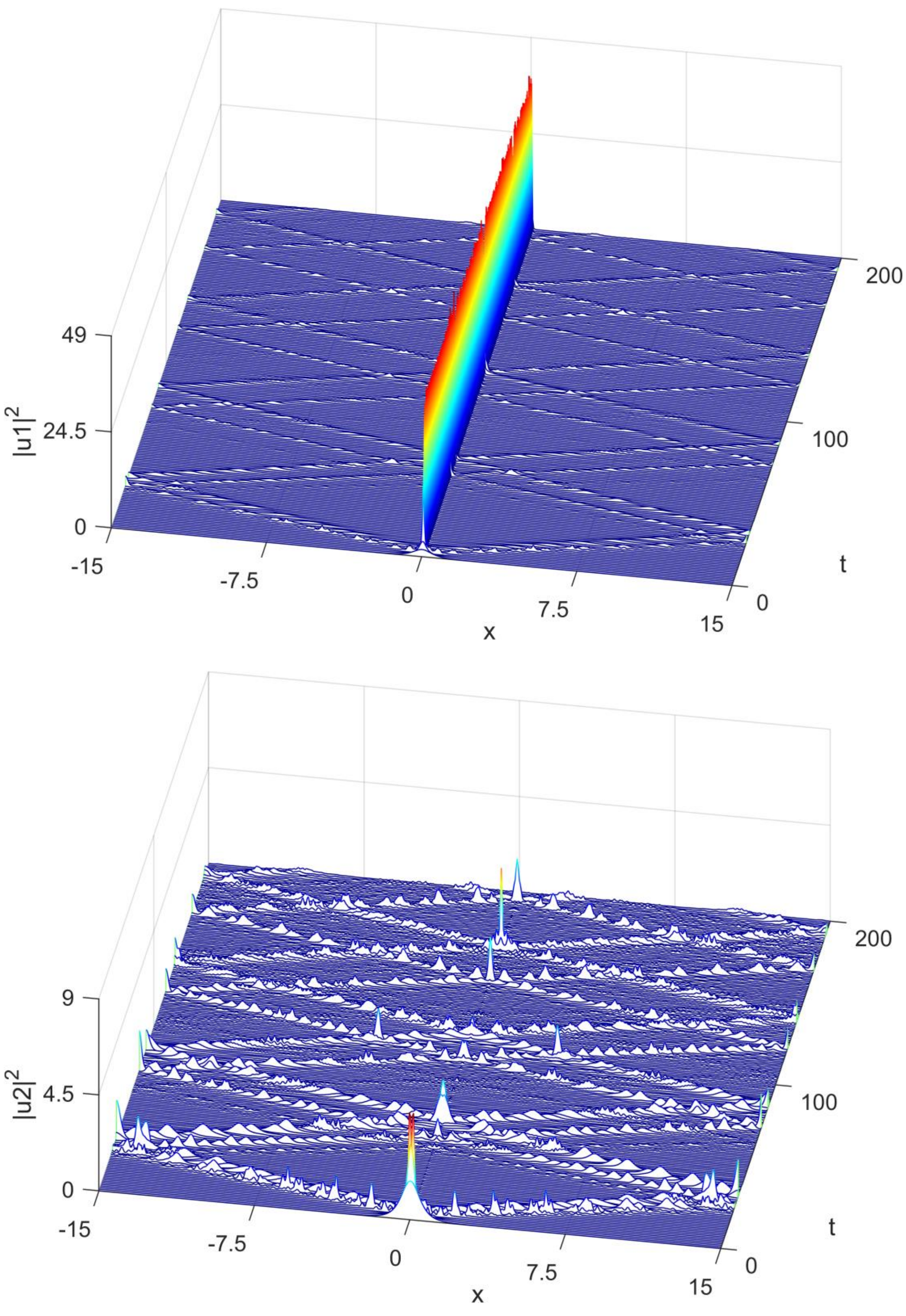

Figure 3.140 The waterfall ED plot illustrates the stability and focus of u_1, and the unusual dispersion pattern of u_2.

3.11.6 u_data_a_1p1_mu_1p8_asym

We see in Figure 3.141 below, as the fractional derivative order α decreases from 1.3 to 1.1 and when the phase propagation constant μ = 1.8, u_1 maintains shape and behaviour as a highly focussed soliton with substantial dispersion from initial conditions. The solution u_2 appears to disperse completely from the initial conditions.

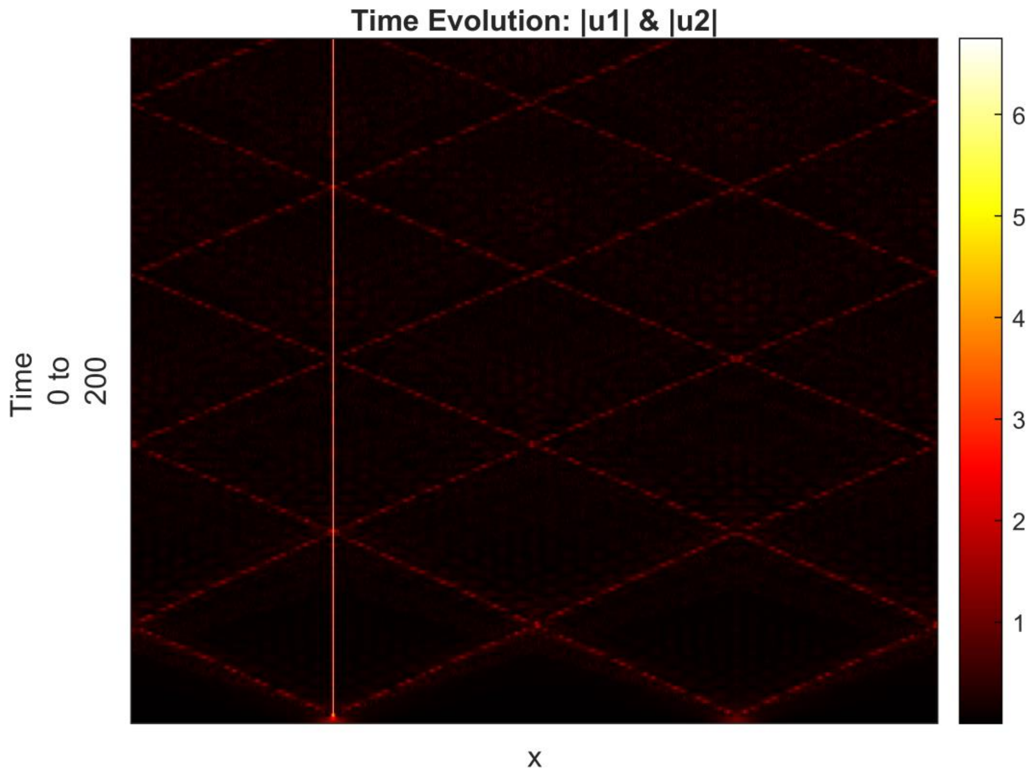

Figure 3.141 As the fractional derivative order α approaches 1, we continue to see highly asymmetric solutions, and well-defined dispersive losses, particularly in u_2.

In the phase portrait in Figure 3.142 below, we see u_1 appears stable as the peak amplitude phase oscillates around 6. We further support this conclusion with the waterfall plot in Figure 3.143, which shows little decay in peak amplitude over time, and minimal dispersion. The noise evident in the solution field of Figure 3.143 in the solution field equivalent to its coupled counterpart u_2.

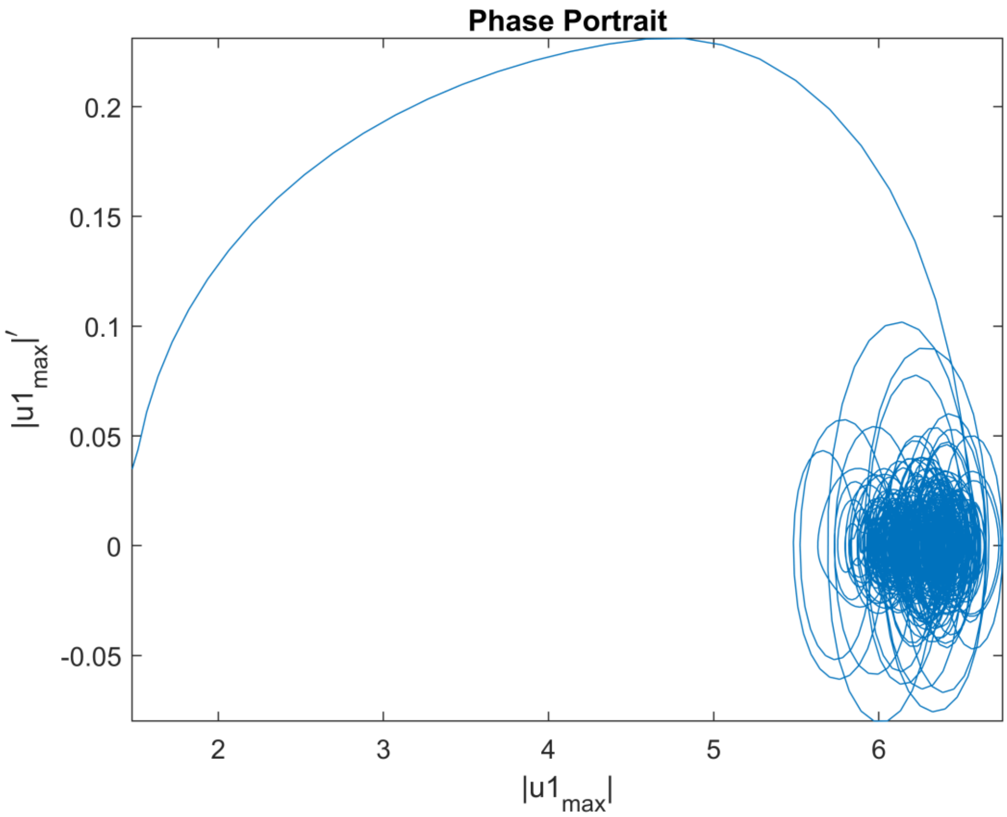

Figure 3.142 Despite initial losses, u_1 appears reasonably stable with a peak amplitude of approximately 6.3.

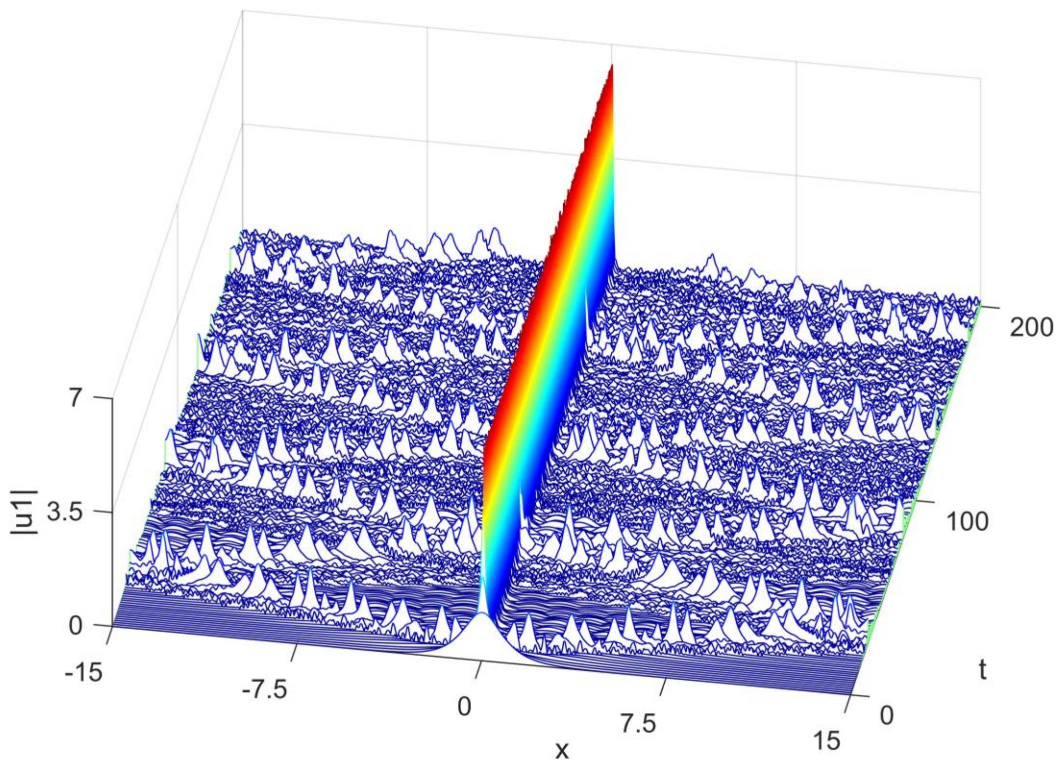

Figure 3.143 A focussed and stable solution, with dispersion effects.

3.11.7 u_data_a_1p1_mu_2_asym

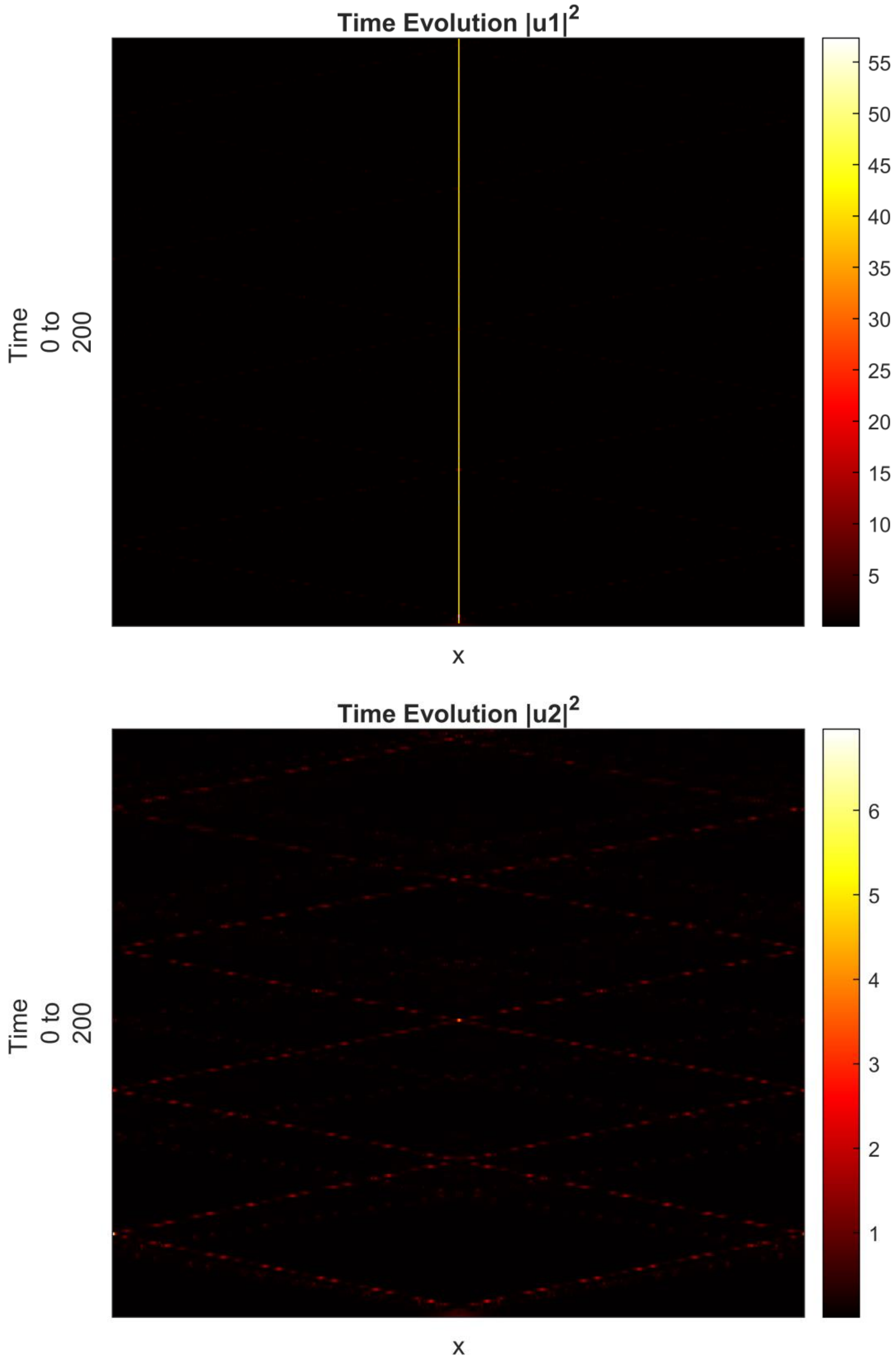

Figure 3.144 Heatmaps show u_1 becomes highly focussed and u_2 disperses completely to the left and right of the initial conditions.

As the fractional derivative order α approaches one the phase propagation constant μ = 2, we see in Figure 3.144 u_1 becomes highly focussed and reasonably stable throughout the duration of the experiment. From the heatmap in Figure 3.144 we see u_2 disperses immediately, whereas u_1 maintains a relatively large peak amplitude. Figure 3.145 confirms the stability of u_1 and shows the solutions converging on each other throughout the experiment.

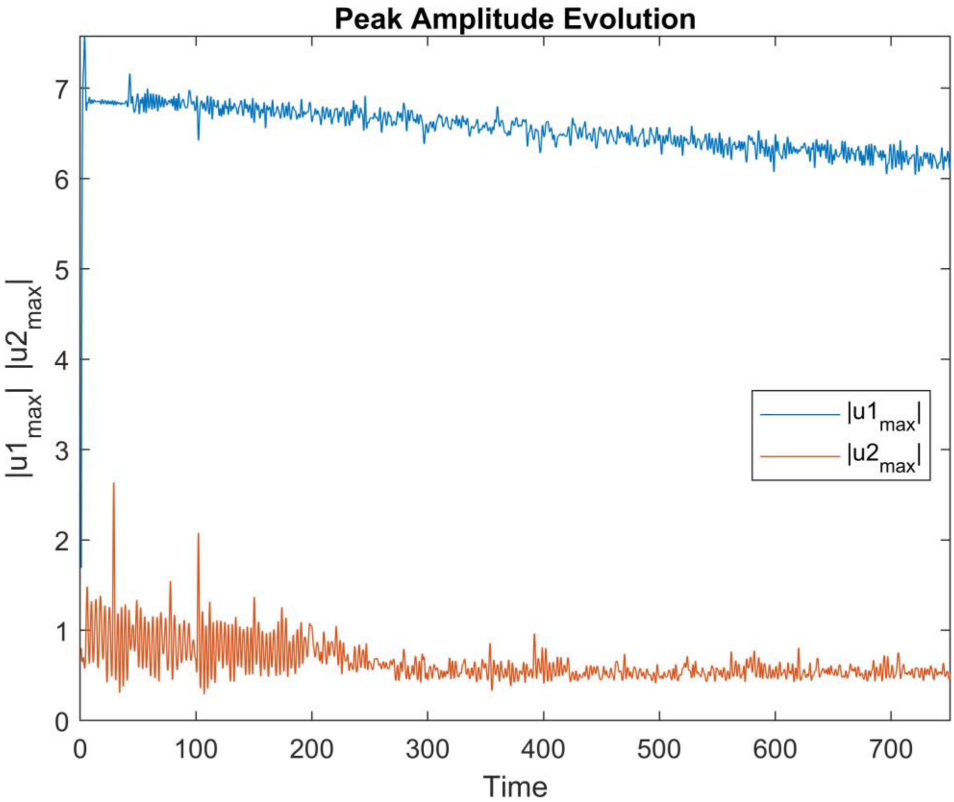

Figure 3.145 The peak amplitude evolution shows u_1 to be reasonably stable, whereas u_2 remains completely dispersed throughout the experiment.

3.11.8 u_data_a_1p1_mu_2p2_sym

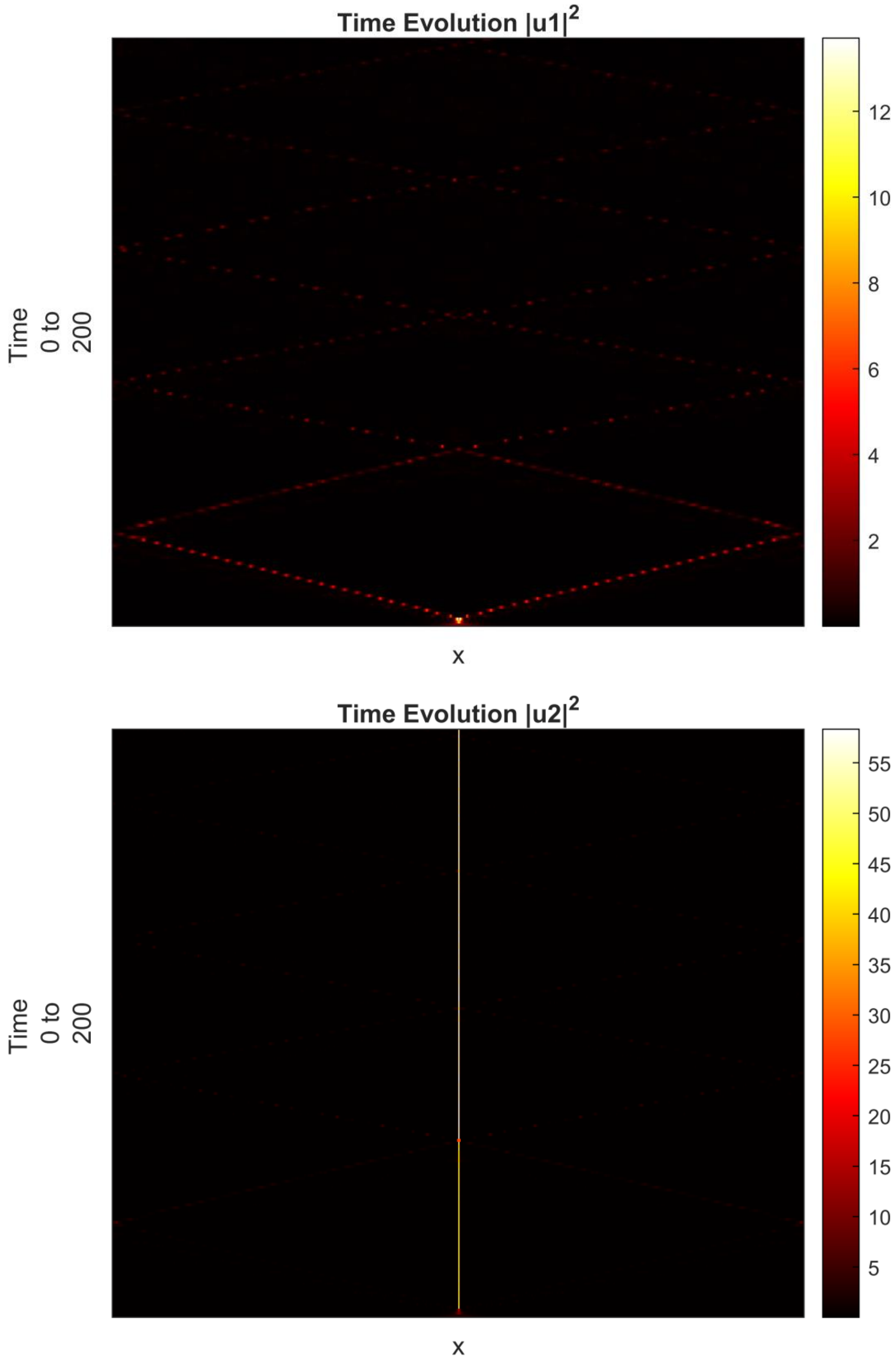

Figure 3.146 As the fractional derivative order α approaches 1, u_1 decays to noise, and u_2 becomes highly focussed.

From fractional derivative order $\alpha = 1.4$ to $\alpha = 1.1$ and the phase propagation constant $\mu = 2.2$, the solutions returned to stationary propagation through time as an asymmetric pair, however, in Figure 3.146, u_1 disperses immediately, and u_2 becomes focussed and stable. Observing the ED heatmap in Figure 3.146, we see u_1 disperse immediately to the left and right of the solution field while u_2 becomes highly focussed and appears stable and self-supporting.

The peak amplitude evolution in Figure 3.147 shows u_2 gradually decay, converging on u_1 throughout the experiment. Dispersion from the heatmap is corroborated when reviewing the centre of mass evolution, as the centre of mass increases throughout the experiment, indicating noise throughout the solution field.

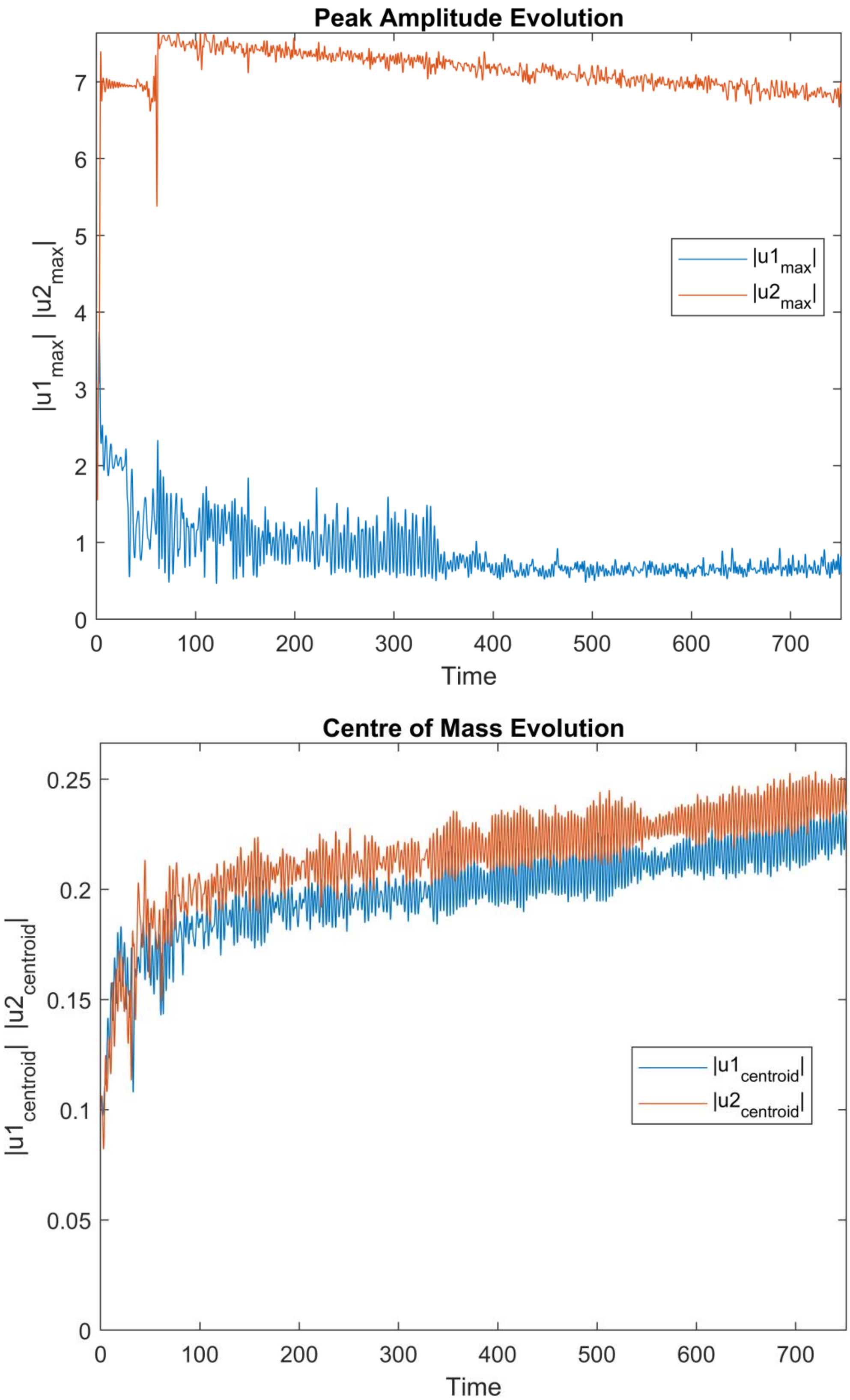

Figure 3.147 The peak amplitude evolution (top) shows the switch in symmetry between u_1 to u_2. The centre of mass evolution (bottom) shows increased dispersion over time.

3.11.9 u_data_a_1p1_mu_2p4_asym

As the fractional derivative order α decreases in value and the phase propagation constant $\mu = 2.4$, the solutions become more asymmetric and focussed, and we observe the following behaviour in Figure 3.148.

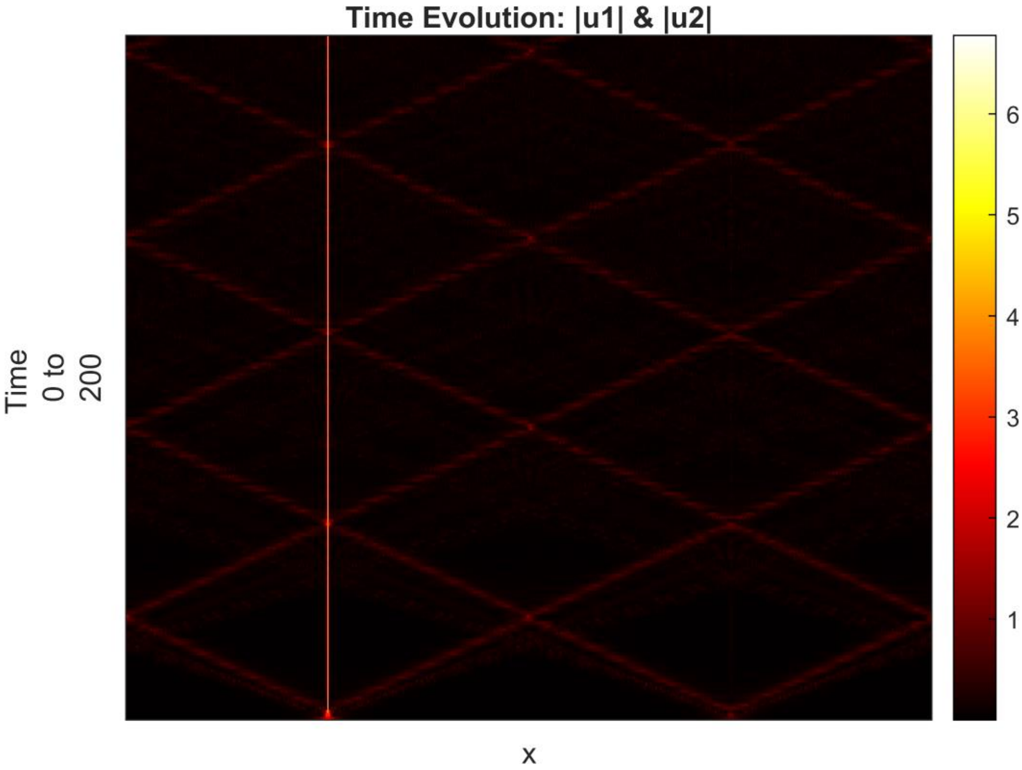

Figure 3.148 When the fractional derivative order α approaches 1, u_1 becomes highly focussed, while u_2 disperses completely.

Figure 3.148 shows dispersion in both solutions at the beginning of the experiment, however, considering the stability of u_1, we assume the persistent dispersion pattern in the u_1 solution field comes from the coupling with u_2. Conversely, there is little if any evidence of the u_1 coupling term in the u_2 solution which one would expect would appear as periodic pulses where the dispersive effect intersects in the centre of the solution field. As we investigate this potential expected phenomena in Figure 3.149, we see no evidence of symmetric pulses from the coupling of u_1 in the u_2 solution field.

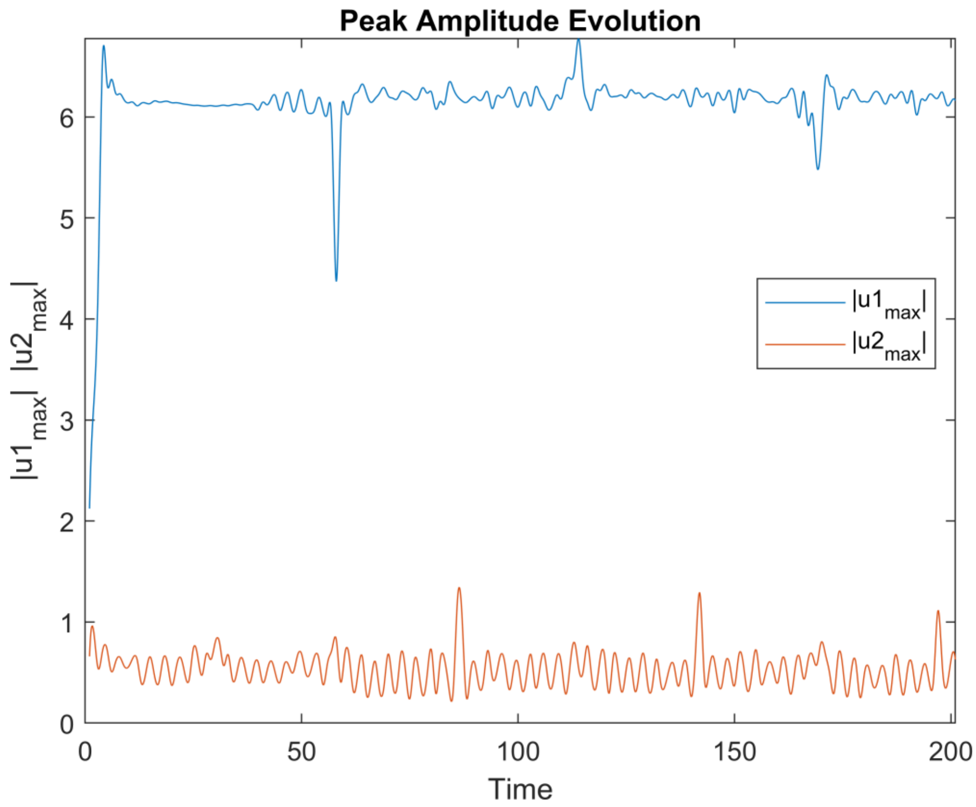

Figure 3.149 The peak amplitude plot shows u_1 to be reasonably stable while u_2 shows peaks corresponding to the dispersive waves meeting periodically at the boundary.

3.11.10 u_data_a_1p1_mu_2p4_asym

When the fractional derivative order α = 1.1, and phase propagation constant μ = 2.4, we see in Figure 3.150 below u_1 becomes highly focussed and reasonably stable, whereas u_2 radiates into noise. We observe noise in both solution fields with more easily discernible dispersion patterns. In this instance, u_2 has not dispersed completely, and may be seen propagating above background noise.

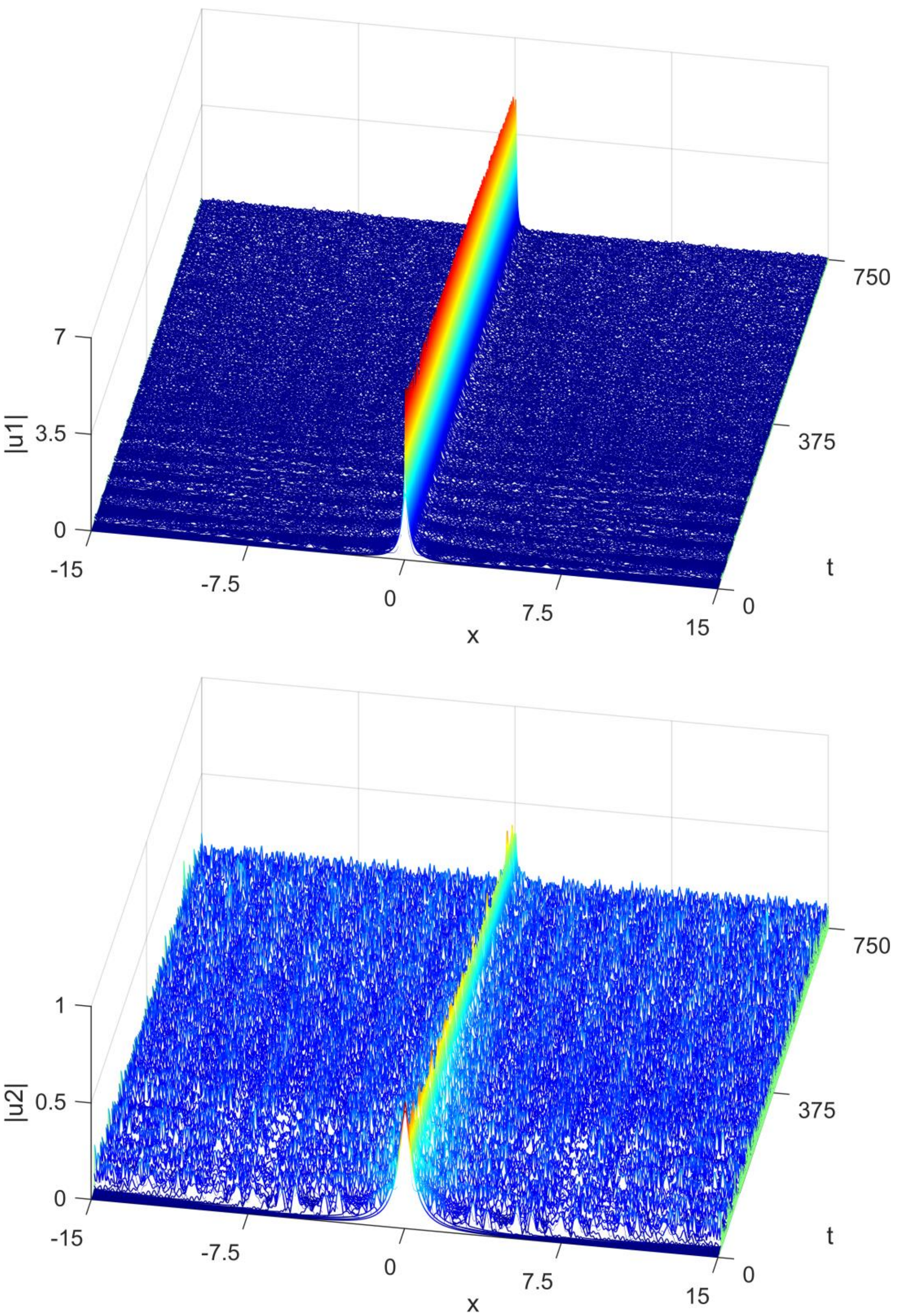

Figure 3.150 The waterfall plots show the extent of asymmetry, and the level of radiation in the solution fields.

3.11.11 u_data_a_1p1_mu_2p4_sym

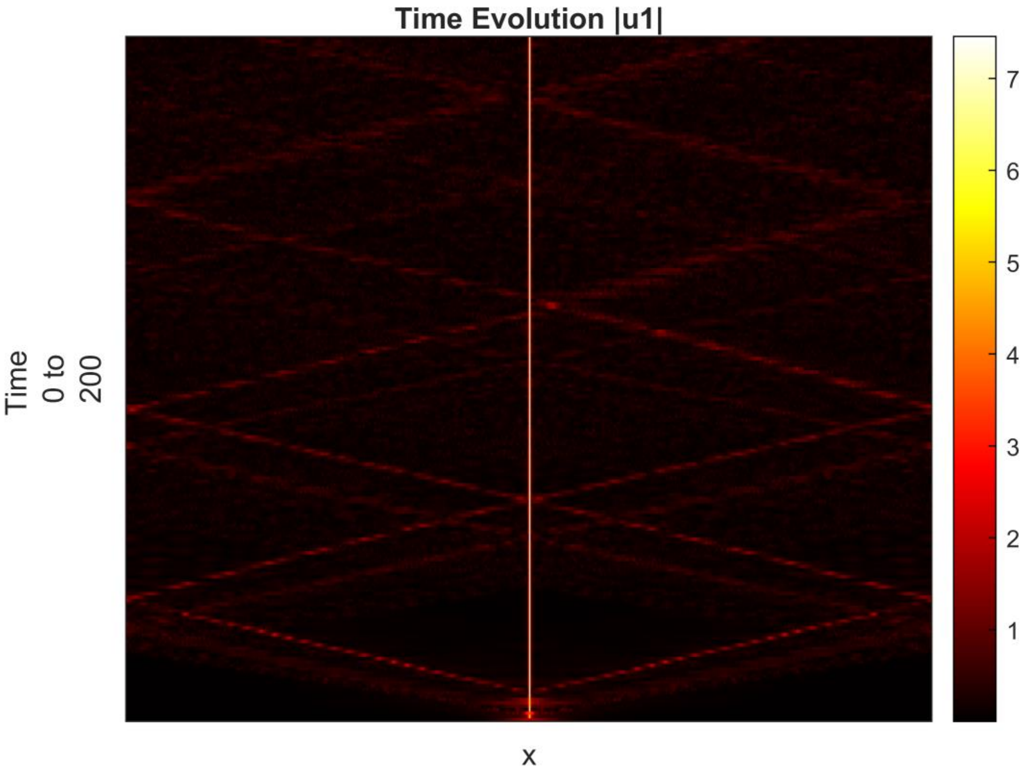

Figure 3.151 As the fractional derivative α approaches 1, u_1 becomes highly focussed, while u_2 decays to noise.

As the fractional derivative order α approaches 1 and the phase propagation constant μ = 2.4, we see in Figure 3.151 u_1 becomes focussed and shows signs of dispersive decay to the left and right of the solution at the beginning of the experiment. The solution u_2 decays to noise almost immediately after the initial conditions. Looking closely at the heatmap in Figure 3.151, after 100t, we see constructive and destructive interference where the diffraction pattern intersects near the centre of the solution field, alternating from the right of the solution to the left of the solution. Reviewing the following peak amplitude evolution plots in Figure 3.152, we observe u_1 converging on u_2, and the peak amplitude of dispersion from u_2 throughout the experiment.

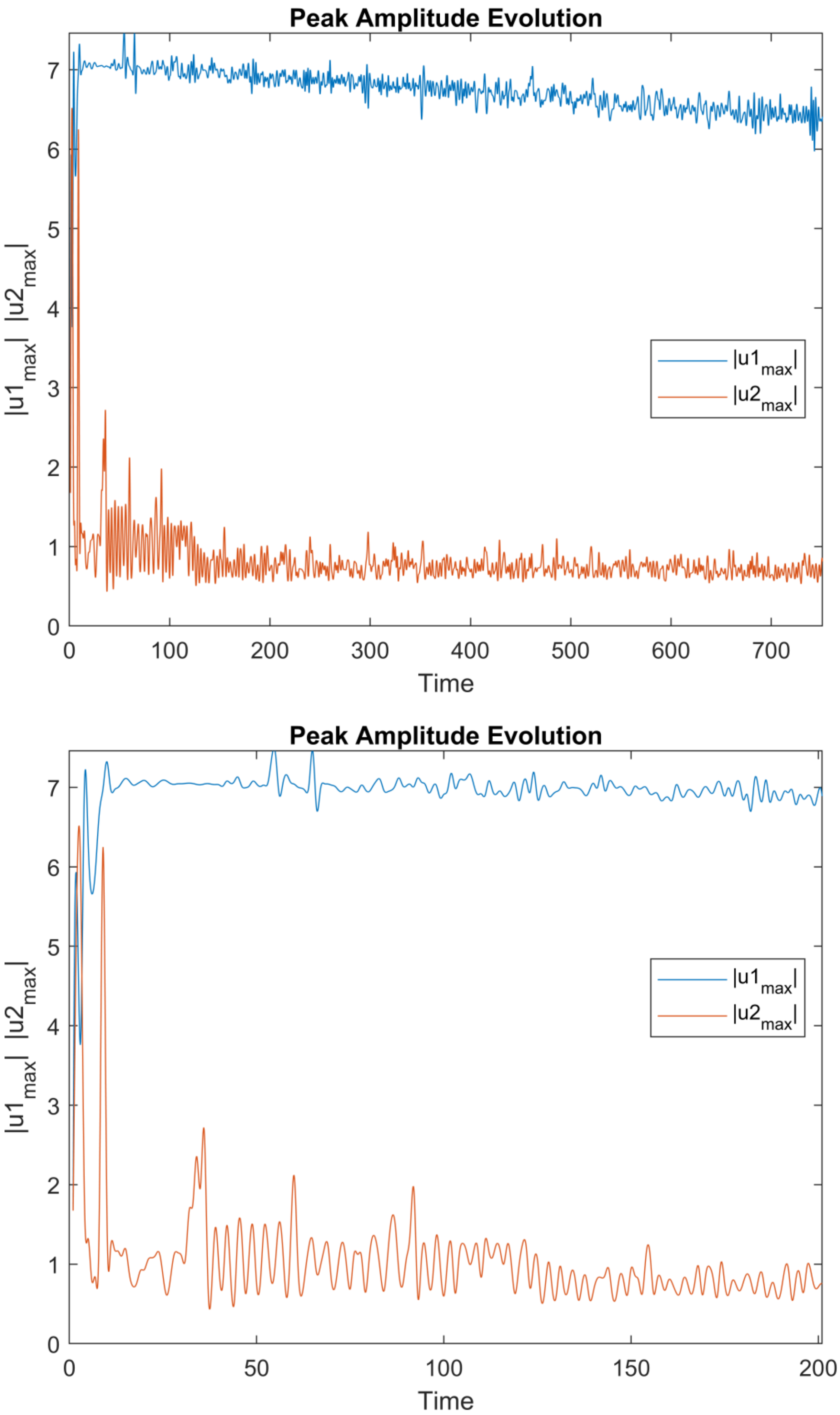

Figure 3.152 The peak amplitude of u_1 appears to be reasonably stable for 200t.

3.11.12 u_data_a_1p1_mu_2p4_sym

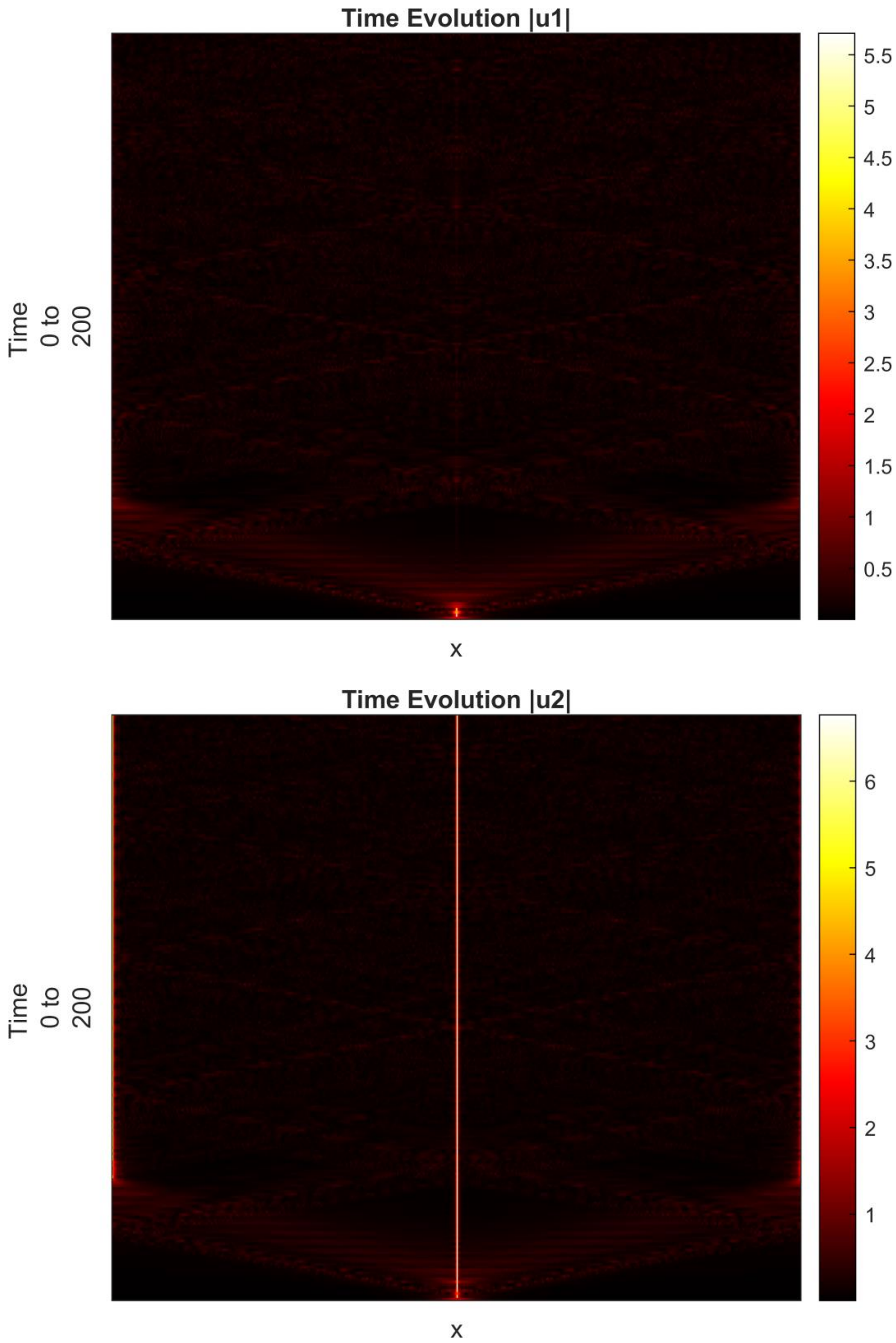

Figure 3.153 In this experiment u_2 becomes more focussed and stable.

As the fractional derivative order α approaches 1 and the phase propagation constant μ = 2.4, we see symmetry break early in the experiment, but for the second time from this dataset (where the fractional derivative order α = 1.1), we see u_2 become highly focussed, while u_1 disperses immediately into noise (the first example can be seen in Figure 3.146 in sub-section 3.11.8 u_data_a_1p1_mu_2p2_sym). If we observe the waterfall plot in Figure 3.154, we see unwanted effects of periodic boundary conditions: it appears the solution consists of two solitons in a single solution field, but this is simply the dispersive waves intersecting near the boundary rather than near the centre of the solution field at x = 0.

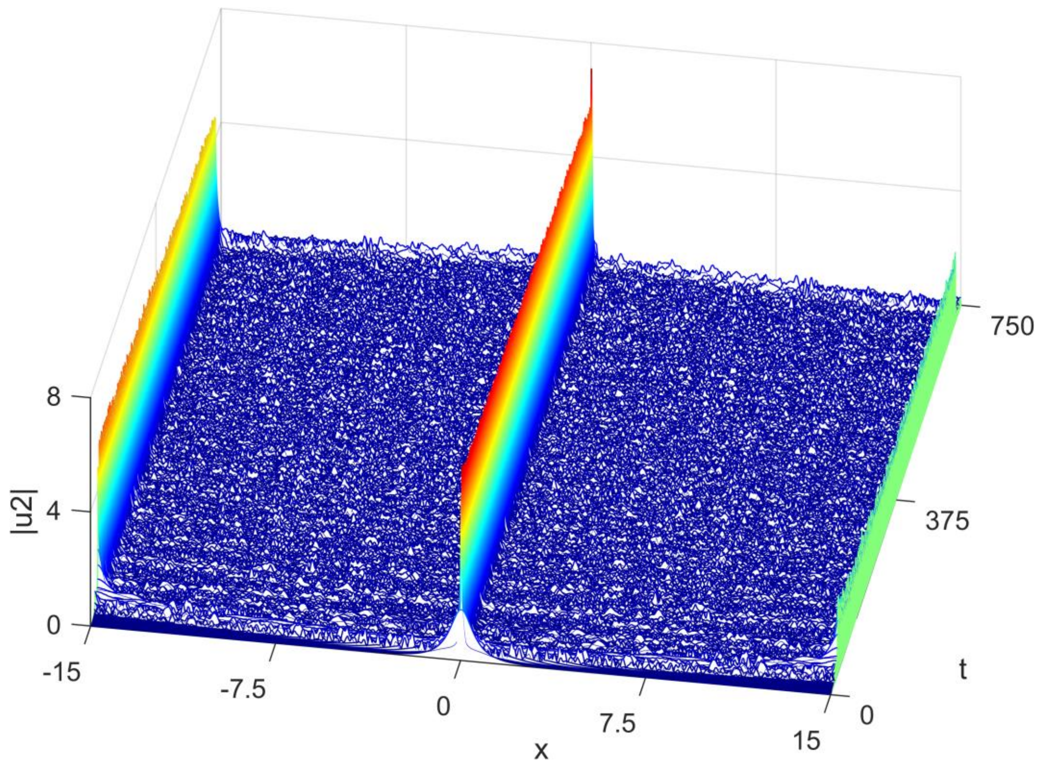

Figure 3.154 The waterfall plot shows undesirable edge effects more clearly.

Experimenting with the phenomenon of boundary effects, we adjust the solution field by increasing the value of the x-axis and therefore increasing the size of the solution field, we observe the following dispersive effects in Figure 3.155, Figure 3.156, and Figure 3.157.

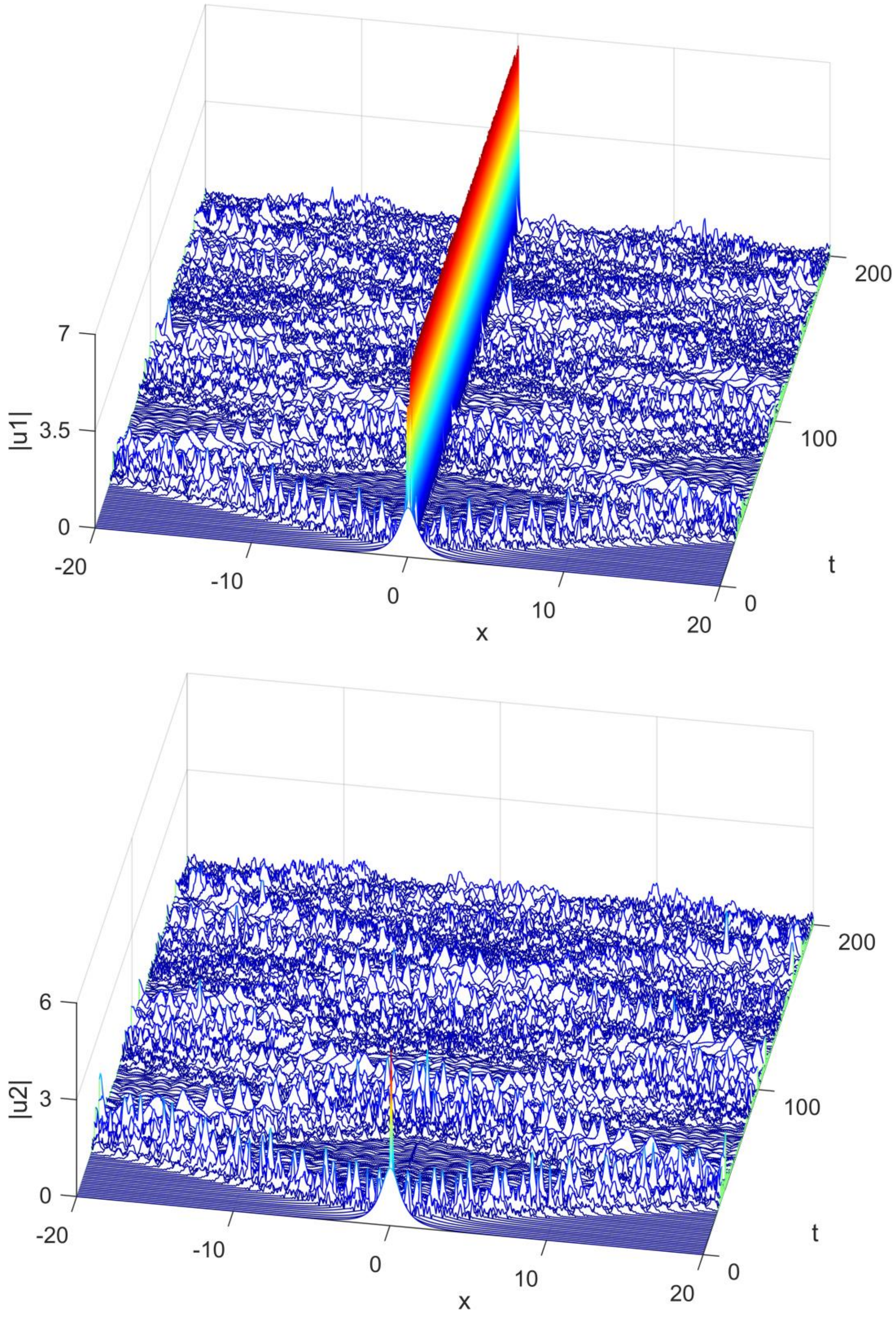

Figure 3.155 The focussed soliton shifts from u_2 to u_1 when the x-axis increases to 40.

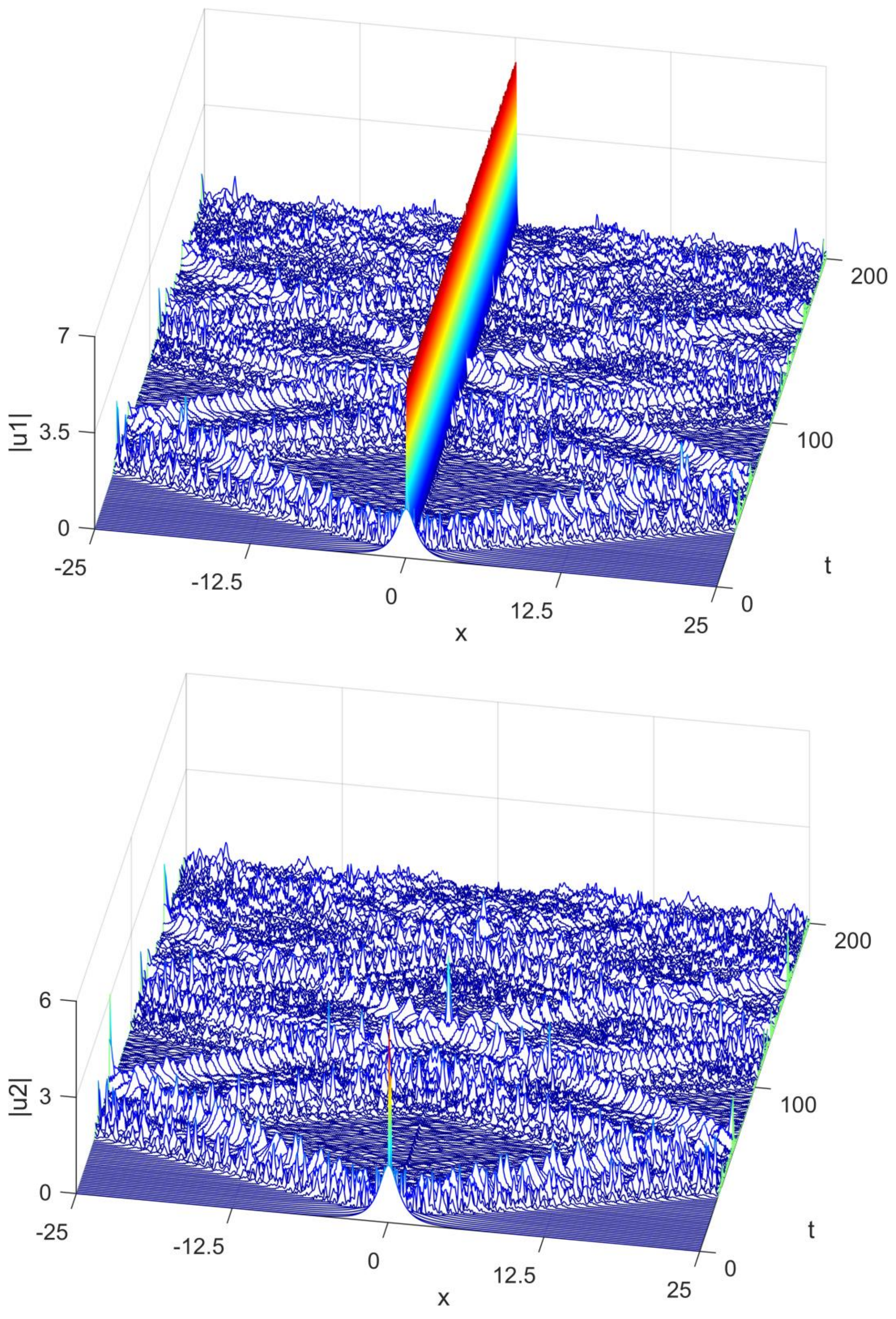

Figure 3.156 As the solution field increases, u_1 maintains focus and we see increased dispersion in the u_2 solution field when the x-axis increases to 50.

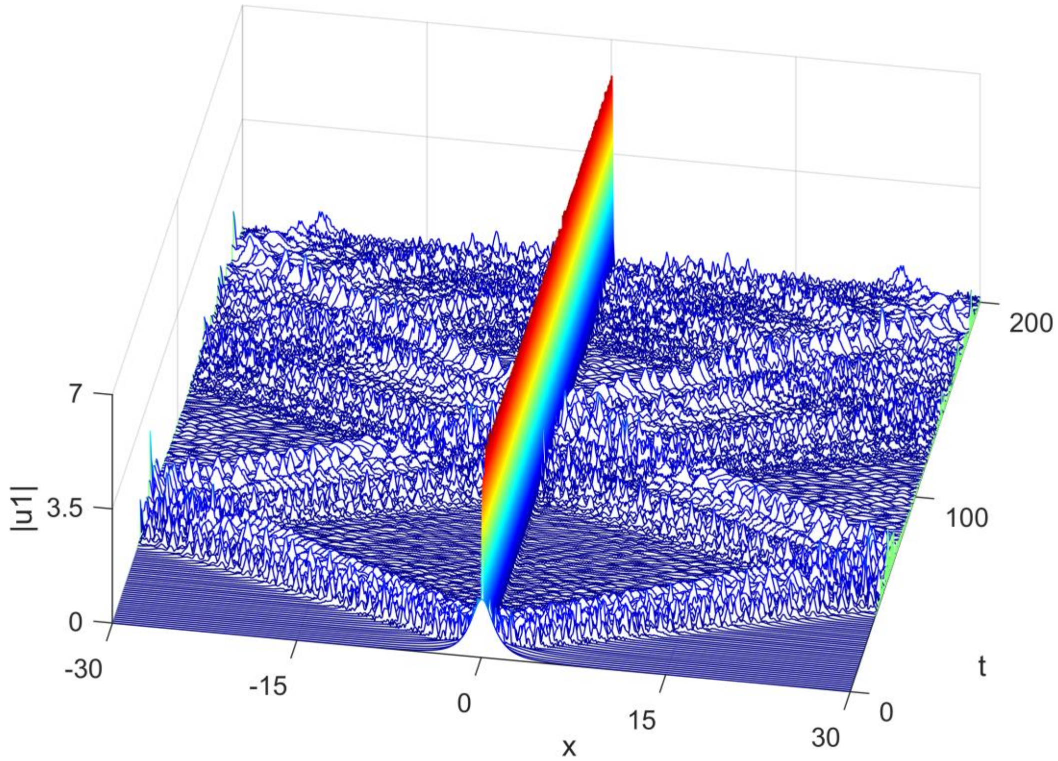

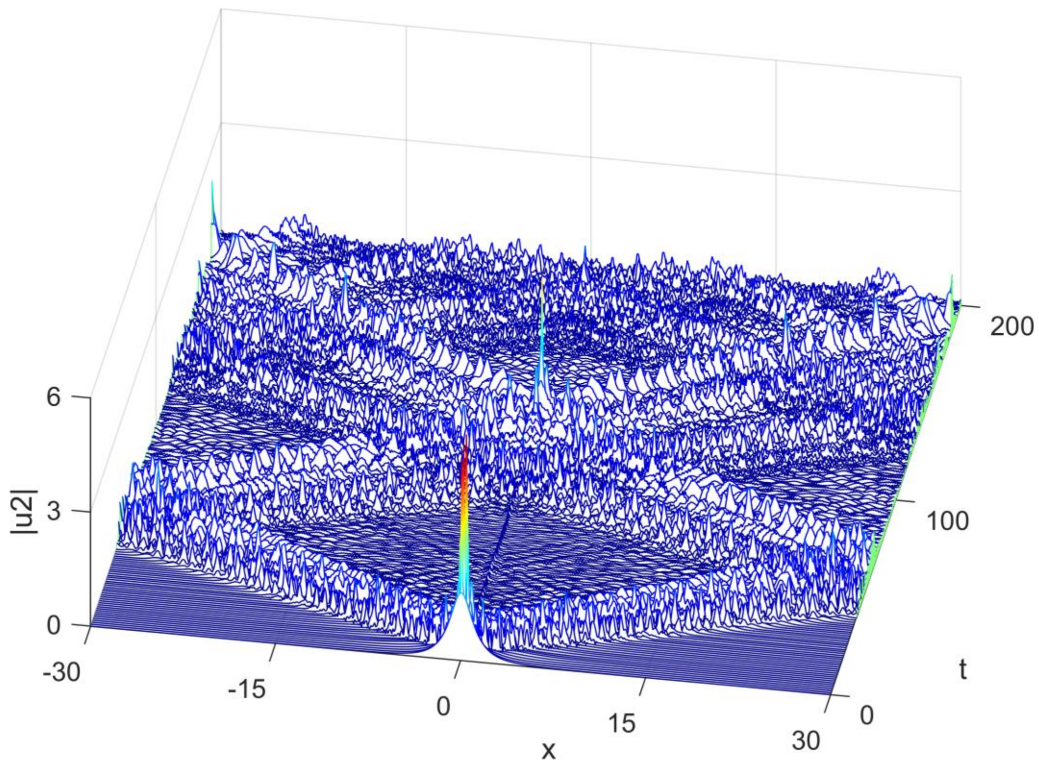

Figure 3.157 Noise in the solution field when the x-axis increases to 60.

As the solution field increases, the focussed soliton swaps symmetries from u_2 to u_1 (evident from Figure 3.155) and the noise in the solution field becomes more dispersed. However, the peak amplitude remained approximately the same for all experiments with this solution pair, maintaining a peak amplitude from approximately 6.5 to 5.5. When re-evaluating the data from the initial experiment when u_2 was focussed and stable (with the standard solution field width of x = 30), we see signs of numerical instability at the end of the experiment. Evidence of numerical instability may be seen in both Figure 3.154, and the peak amplitude plot in Figure 3.158 below at approximately 750t.

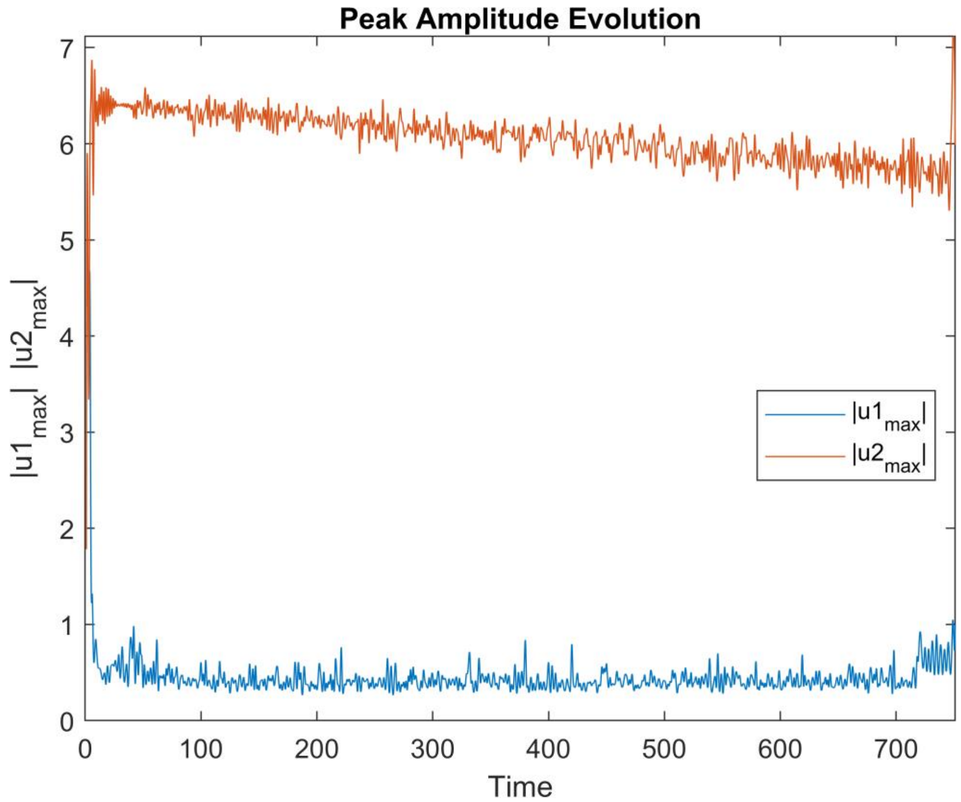

Figure 3.158 The peak amplitude evolution shows u_2 decaying until the solution 'blows up' at the end of the experiment.

3.11.13 u_data_a_1p1_mu_2p8_asym

As the fractional derivative order decreases and the phase propagation constant μ = 2.8, the solutions continue to remain highly focussed and asymmetric until u_2 disperses immediately, while u_1 becomes stable throughout the experiment, visible in Figure 3.159.

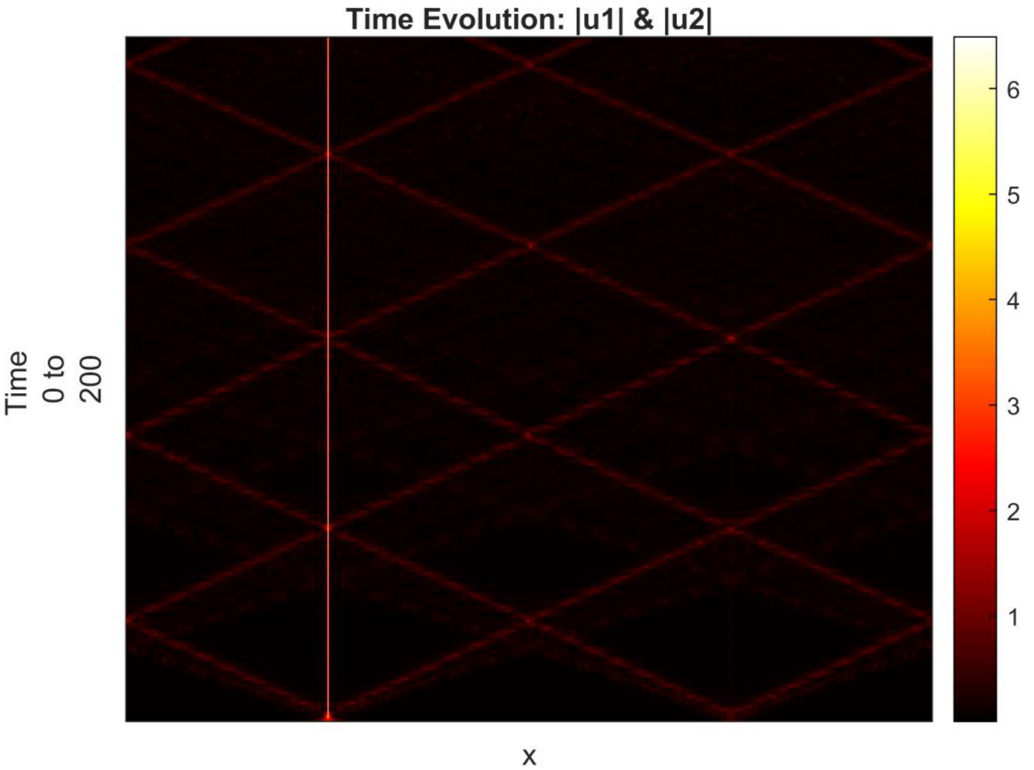

Figure 3.159 The heatmap of u_1 and u_2 show interesting dispersion patterns in the solution field. As α approaches 1, we see u_1 become highly focussed and stable, whereas u_2 disperses immediately.

If we look at the peak amplitude plot in Figure 3.160 and compare it to the heatmap in Figure 3.159, we see spikes in u_2 corresponding to the periodic intersection of dispersive waves early in the experiment ($t < 200$) due to periodic boundary conditions.

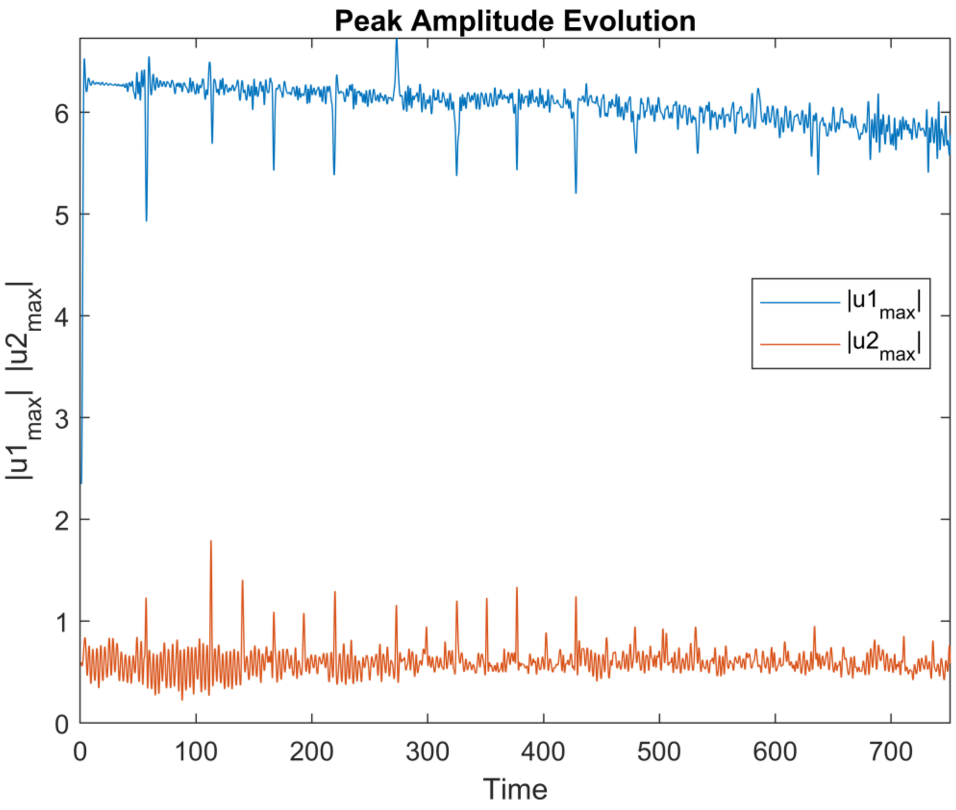

Figure 3.160 The peak amplitude evolution shows periodic, asymmetric peaks corresponding to edge effects and dispersion waves meeting in the centre of the solution field.

The peak amplitude evolution in Figure 3.160 above shows the diffraction in u_1 acts as destructive interference (lower amplitude values), while the diffraction acts as constructive interference (higher amplitude values) for u_2. The ED waterfall plots in Figure 3.161 indicates the level of dispersion in the solution field and provides indication of the focus and stability of u_1.

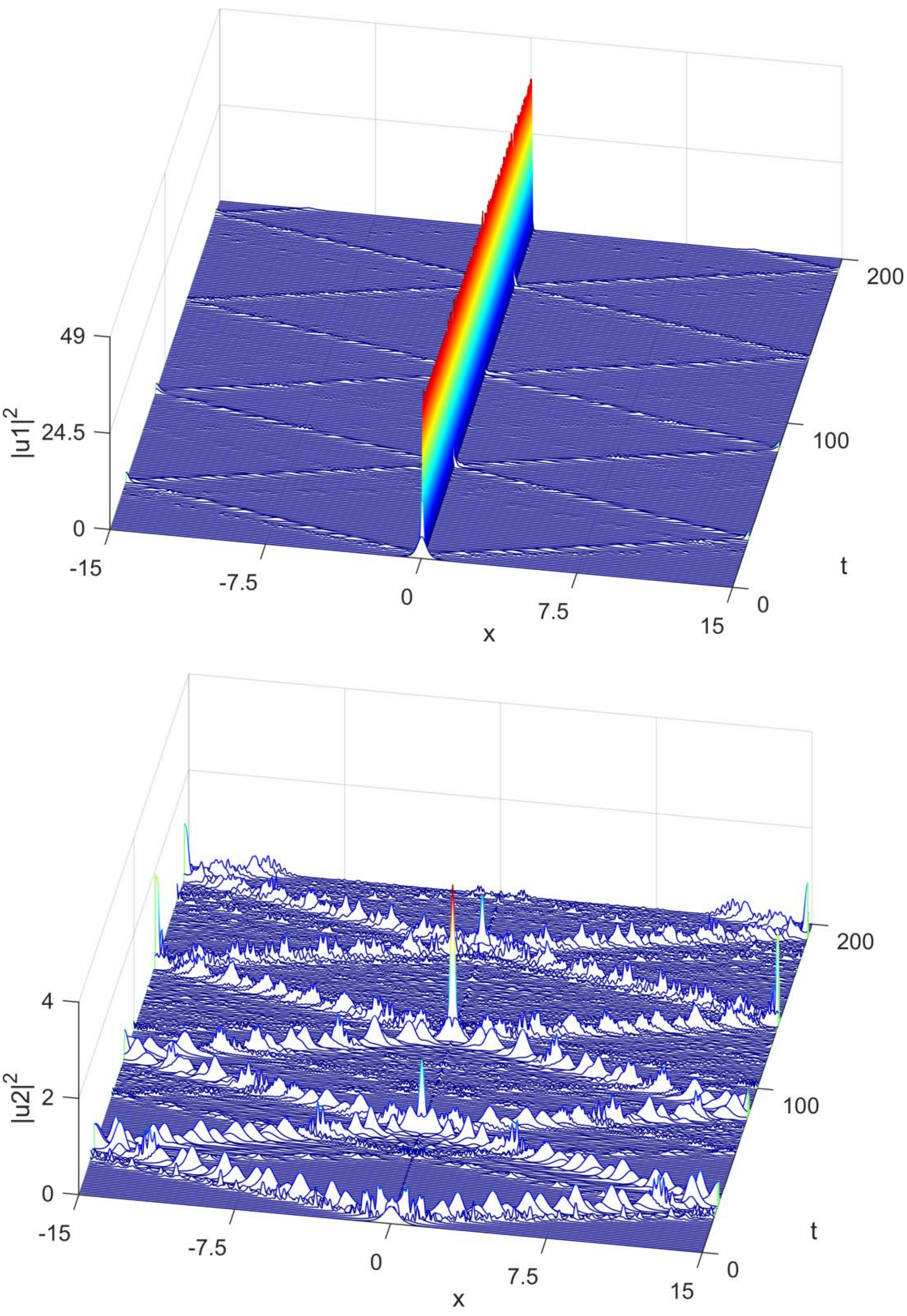

Figure 3.161 The waterfall ED reveals the stability and focus of u_1, and dispersion effects for u_2.

3.11.14 u_data_a_1p1_mu_2p8_sym

As the fractional derivative order α approaches 1 and the phase propagation constant μ = 2.8, u_1 continues to evolve as a highly focussed solution, and u_2 disperses immediately, leaving only the solution u_1 visible in Figure 3.162.

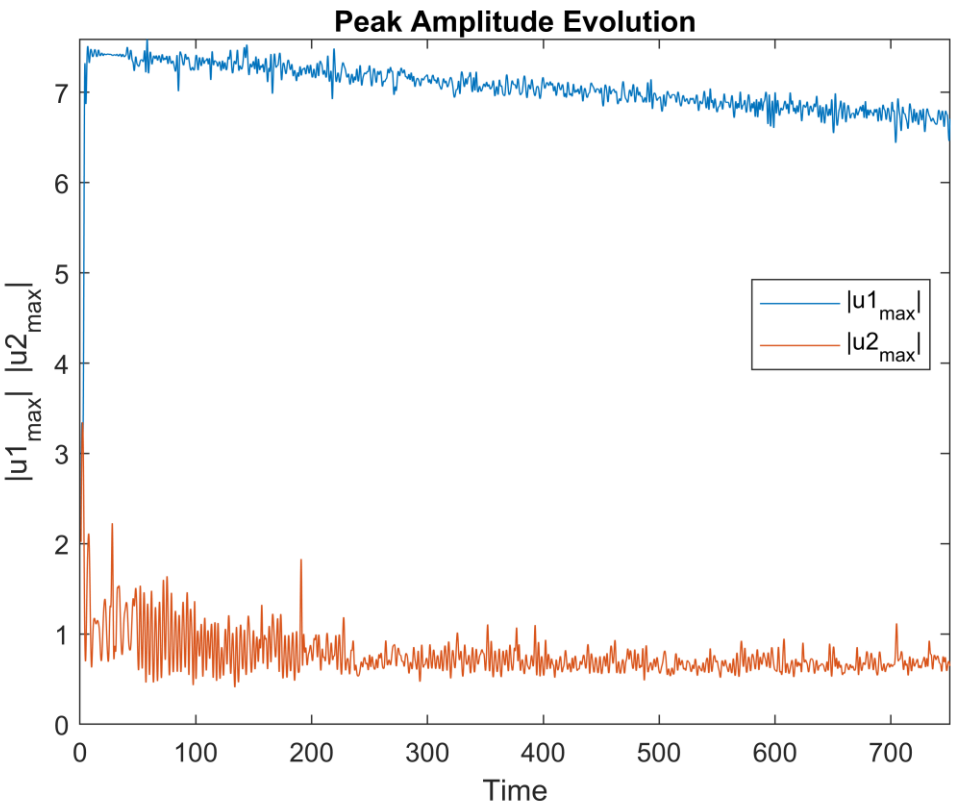

Figure 3.162 The peak amplitude evolution shows u_1 gradually converging on u_2 over time, whereas u_2 decays into noise.

The peak amplitude evolution plot Figure 3.162 shows u_1 decay slowly throughout the experiment, like other focussed, stable solutions. The ED waterfall plot in Figure 3.163 below illustrates the degree of focus and stability in u_1. Looking carefully in Figure 3.163, we can see the noise in the u_2 solution field appear as noise in the u_1 solution field.

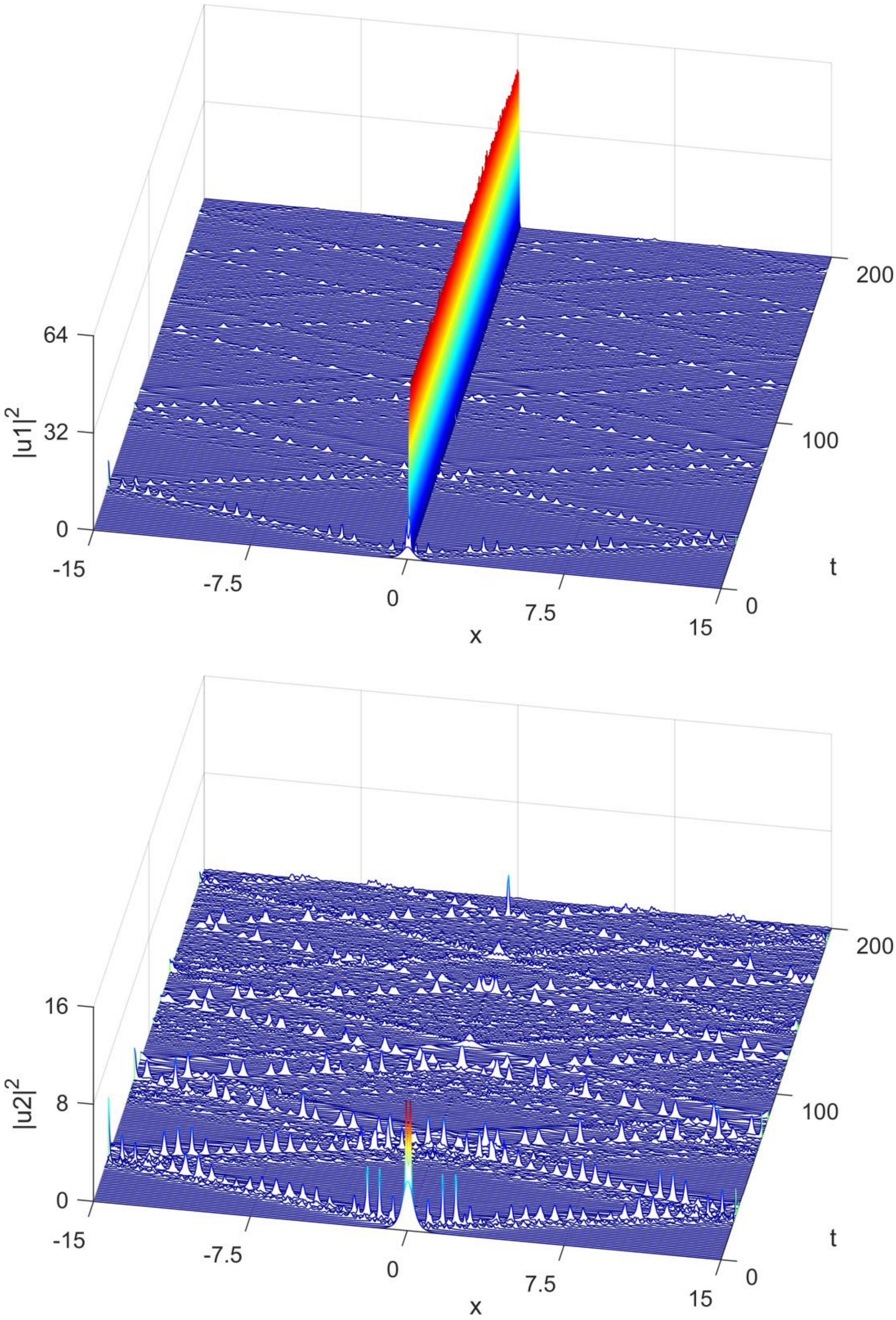

Figure 3.163 The ED waterfall plots details dispersion from u_2 and illustrate how highly focussed and stable u_1 becomes.

3.12 Bifurcation plot: all

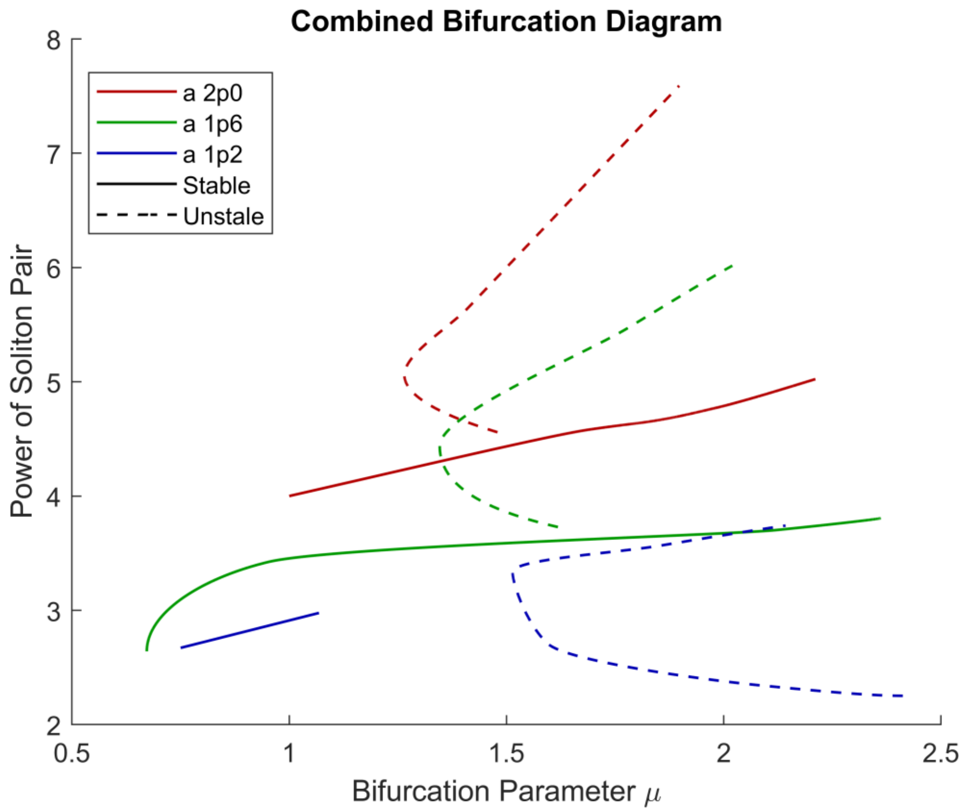

Figure 3.164 Combined bifurcation diagram for fractional derivative order α = 2 (red), 1.6 (green), and 1.2 (blue).

In Figure 3.164 we see the combined bifurcation plot. For the fractional derivative order α = 2, we have stability when the power to maximum amplitude ratio is approximately 3, and instability when the power to maximum amplitude ratio is approximately 3.8. For this set of data when α = 2, the unstable branch corresponds to symmetric solutions, whereas the stable branch corresponds to asymmetric solutions.

When the fractional derivative order α = 1.6, we have stability when the power to maximum amplitude ratio is approximately 2.7, and instability when the power to maximum amplitude ratio is approximately 2.9. When the phase propagation constant μ > 2.4 we see the unstable branch corresponds to symmetric solutions, whereas the stable branch corresponds to asymmetric solutions. This trend does not hold for $\mu < 2.4$. When $\mu < 1.4$, the solutions are stable, and for $1.4 < \mu < 2.4$, the solutions are unstable.

When the fractional derivative order $\alpha = 1.2$, we have stability when the power to maximum amplitude ratio is approximately 3, and instability when the power to maximum amplitude ratio is approximately 1.6. The stable branch corresponds to phase propagation values $\mu < 1.6$, and the unstable branch corresponds to $\mu \geq 1.6$.

CHAPTER 4 DISCUSSION

The data sets were grouped together to evaluate specific fractional derivatives of order α. The results focussed on determination of stability of the solution: that is, stable or unstable for each fractional derivative of order $\alpha = 2$, 1.6, and 1.2. The results of which determined each branch of the bifurcation plot.

Additionally, for each data pair, the fractional derivatives were evaluated at each tenth, for values $\alpha \in (1, 2]$. The MATLAB program output approximately twenty figures for each data set, for each fractional derivative order α. From the evaluated data, curious dynamics were presented here according to the fractional derivative order.

Changes in the fractional derivative order resulted in four main behaviours: stability optimisation, symmetry making or breaking, non-stationary solutions, and to a lesser extent, unstable bright / dark soliton pulses. We discuss the results here by groups sharing behavioural dynamics.

4.1 Stability optimisation

In some cases, we found fractional values of order α optimised stability for some solution pairs with a fractional order $\alpha = 1.6$ and 1.2. Stability optimisation occurred for symmetric solutions and can be seen in the sub-sections 3.4.1 u_data_a_1p6_mu_1p2_sym, 3.4.2 u_data_a_1p6_mu_1p4_sym, 3.9.1 u_data_a_1p2_mu_1p2_sym, and 3.9.2 u_data_a_1p2_mu_1p4_sym.

For each of the four solution pairs above, from $\alpha = 2$, to $\alpha = 1.6$, the results were symmetric, but highly oscillatory and dispersive. As $\alpha \to 1.6$, the frequency of peak amplitude oscillations decreased, while the solution evolved with some dispersion. To determine stability in these cases, rather than extending the experiment time, the solution could be optimised by changing the fractional value to limit energy losses in the wave equation by reducing the frequency of oscillations. Such solutions are note-worthy because these solitons would otherwise be dismissed as unstable solutions with conventional integer derivatives. Yet here, we have shown the solitons to be stable with fractional derivatives of order $\alpha = 1.6$, establishing a relationship between soliton stability and fractional derivative values for coupled NLSEs. This result is consistent with the assessment of soliton stability by Makhankov: determination of soliton stability requires some knowledge of the previous behaviour of the solution [44]. Fractional derivatives, by definition, tell us of the memory properties of the original problem, i.e., previous behaviour of the solution. Therefore, if we consider a soliton as a particle, these results may be indicative of particles 'remembering' a previously stable state and self-correcting their behaviour to maintain stability after perturbation.

4.2 Symmetry

One of the primary dynamics observed from the experiments included symmetry breaking boundaries for fractional values, and some evidence of symmetry making behaviour. Symmetry making was observed when stable, asymmetric solutions were provided enough experimental time to observe the frequencies of the solution pair converge on each other.

Symmetry breaking occurred for each symmetrical pair of solutions as $\alpha \to 1$, always prior to observation of non-stationary dynamics. We confirmed symmetry breaking with the peak amplitude and centre of mass amplitude plots, where this behaviour often occurred early in the experiment. Symmetric solutions generally broke symmetry before 50t, except in the cases where the phase propagation constant $\mu = 1.2$. In such cases, the solutions simultaneously dispersed, and because of the periodic boundary conditions, can be seen radiating in a similar fashion to cos(2t) sin(2x) diffraction patterns in the solution field.

4.2.1 Symmetry making

Solitons have been shown to converge experimentally in the past via numerical and physical experiments, however, previous merges we found occurred between stable, symmetric solitons [38, 66, 67]. Our research showed potentially novel symmetry making behaviour: both stable and unstable, asymmetric solutions tending to symmetric propagation.

Symmetry making behaviour occurred for the following eight sets of solutions in the following sections: 3.1.4 u_data_a_2p0_mu_2p0_asym, 3.1.6 u_data_a_2p0_mu_2p2_asym, 3.3.1 u_data_a_1p7_mu_2p8_asym, 3.4.6 u_data_a_1p6_mu_2p4_asym, 3.4.8 u_data_a_1p6_mu_2p8_asym, 3.9.4 u_data_a_1p2_mu_1p6_asym, 3.9.6 u_data_a_1p2_mu_2p0_asym, and 3.9.7 u_data_a_1p2_mu_2p4_asym.

Symmetry making behaviour was primarily seen in asymmetric solutions which were classified as stable. From this data, we saw the asymmetric solution pairs match their wavelength and group velocity, so the inner solutions began to oscillate symmetrically.

The peak amplitude evolution solutions converge and show signs of structural stability throughout the experiment, until numerical instability occurred.

In one instance, 3.3.1 u_data_a_1p7_mu_2p8_asym, the inner wave of both solutions converged, then the surface waves converged. In this example, the fractional derivative $\alpha = 1.7$ corresponds to symmetry making conditions and may be seen in Figure 3.29 and Figure 3.30. In the other cases where the inner wave, or group velocity converged, experiment time was insufficient to determine if the surface waves would eventually converge and approach stability. Generally, from the symmetry making data we showed the inner waves converged and began to propagate symmetrically, while the surface waves continued to oscillate out of phase.

Two asymmetric waves of unequal wavelength can be shown to propagate in and out of phase over time. However, from the data mentioned in this section, we see amplitude, wavelength, and phase of the two coupled solutions merging (changing amplitude, wavelength, frequency and phase from initial conditions), hence we conclude the potential for symmetry making conditions as a function of fractional derivative order α.

Symmetry making phenomena would be more significant if the initial conditions were asymmetric and unstable, and able to propagate without oscillations. This type of symmetry making behaviour would yield immediate benefits for physical optical networks with improved error-tolerance in optical communication, and may be an indication of particles having a ‘memory’ of their past. In any case, it is still interesting to see the behaviour and dynamics of stable asymmetric solutions approaching the behaviour of stable symmetric solutions. Given enough experiment time, or for a sufficiently defined fractional derivative order α, it may be possible to see unstable, asymmetric solutions converge throughout an experiment, and continue propagating as a self-supporting structure. If the solutions mentioned in this section are not representative of symmetry making, then perhaps such solutions represent a way to quantify mathematical stability: by examining the steady state of group velocity after convergence.

4.2.2 Symmetry breaking

Symmetry breaking behaviour occurred for most datasets as the fractional derivative order $\alpha \rightarrow 1$. For a fractional derivative order to be considered symmetry breaking, we must consider results from previously stable, symmetric solutions, since unstable solutions necessarily break symmetry and therefore propagate asymmetrically or disperse from initial conditions. Of the stable symmetric solutions, the following solution pairs are considered to have broken symmetry: 3.4.3 u_data_a_1p6_mu_1p5_sym, and 3.8.1 u_data_a_1p3_mu_1p4_sym. Additionally, it is useful to note symmetry was always broken prior to any solution becoming non-stationary: this behaviour occurred early in the experiment, usually less than 20t.

Of the unstable symmetric solutions to break symmetry, these consisted of solutions found in sections: 3.1.3 u_data_a_2_mu_1p8_sym, 3.1.5 u_data_a_2p0_mu_2p0_sym, 3.1.7 u_data_a_2p0_mu_2p2_sym, 3.4.5 u_data_a_1p6_mu_1p8_sym, 3.8.6 u_data_a_1p3_mu_1p8_sym, 3.8.9 u_data_a_1p3_mu_2p2_sym, and 3.8.12 u_data_a_1p3_mu_2p6_sym.

Each of the solution’s broke symmetry early in the experiment ($t < 20$) and continued to converge on each other throughout the rest of the experiment. After convergence, three of these solutions created unstable, dark / bright pulses 3.1.3 u_data_a_2_mu_1p8_sym, 3.1.5 u_data_a_2p0_mu_2p0_sym, and 3.1.7 u_data_a_2p0_mu_2p2_sym. Of these three sets of solutions, we note the dark / bright pulses after convergence correspond to derivatives of order $\alpha = 2$.

One asymmetric solution pair found in section 3.11.12 u_data_a_1p1_mu_2p4_sym were shown to switch focus as the width of the solution field changed. When the size of the spatial axis was increased, the solutions switched focus: u_2 was initially focussed and stable while u_1 dispersed, yet after increasing the boundaries, the solutions switched and u_1 became stable and focussed while u_2 dispersed.

4.3 Dark / Bright pulses

From the data we discovered two dark/bright soliton pulses in sections 3.1.5 u_data_a_2p0_mu_2p2_sym, and 3.4.3 u_data_a_1p6_mu_1p5_sym. Of these, one of the solutions produced this result for the fractional derivative of order $\alpha = 2$, while the other result occurred when the fractional derivative order $\alpha = 1.6$ respectively. The pulses appear after the previously stable initial conditions break symmetry, then converge throughout the remainder of the experiment. If the solutions converged, dark / bright pulses were often seen as a result.

While these solutions are not stable, stationary dark / bright solitons, we can see the dynamics leading up to the behaviour, and the switching properties of the pulses themselves.

4.4 Non-stationary dynamics

Nearly all solutions become non-stationary when the fractional derivative order $\alpha = 1.3$. Of these, all the solutions break symmetry if they are not already asymmetric, then continue as asymmetric solutions as the fractional derivative order α approaches 1. Furthermore, of the twenty-one non-stationary solutions, fourteen tended to propagate to the left of the solution field, while seven tended to the right. Taking the average fractional derivative order for non-stationary solutions, it seems the value $\alpha =$ 1.3 corresponds to non-stationary behaviour moving predominantly to the left of the solution field.

From this dataset non-stationary solutions are always asymmetric: usually u_1 becomes highly focussed whereas u_2 disperses completely. Evidence of self-supporting behaviour in u_2 after dispersion may be the result of coupling from u_1. Furthermore, non-stationary solutions result in highly focussed, and in some cases self-supporting propagation with exceptionally large amplitudes as compared to other data analysed here.

The details of the results are available in Table 4.1 below.

Table 4.1: Non-stationary Dynamics

Data	Fractional α Value	Direction
u_data_a_2_mu_1p5_sym	1.3	Right
u_data_a_2_mu_1p8_asym	1.4, 1.3	Left
u_data_a_2_mu_1p8_sym	1.4	Left
u_data_a_2_mu_2_asym	1.4, 1.3	Left
u_data_a_2p0_mu_2p0_sym	1.4	Right
u_data_a_2p0_mu_2p2_asym	1.4, 1.3	Left
u_data_a_2p0_mu_2p2_sym	1.4	Left
u_data_a_2p0_mu_2p4_asym	1.4, 1.3	Left
u_data_a_2p0_mu_2p4_sym	1.5, 1.4	Left
u_data_a_2p0_mu_2p8_asym	1.4	Right
u_data_a_2p0_mu_2p8_sym	1.5, 1.4	Left
u_data_a_1p6_mu_1p4_sym	1.3	Right
u_data_a_1p6_mu_1p8_asym	1.3	Right
u_data_a_1p6_mu_1p8_sym	1.3	Left
u_data_a_1p6_mu_2p4_asym	1.3	Left
u_data_a_1p6_mu_2p4_sym	1.4	Left
u_data_a_1p6_mu_2p8_asym	1.3	Right
u_data_a_1p6_mu_2p8_sym	1.4	Right
u_data_a_1p2_mu_1p8_sym	1.3	Left
u_data_a_1p2_mu_2p0_asym	1.3	Left
u_data_a_1p2_mu_2p6_sym	1.3	Left

4.5 Bifurcation diagrams

The data produced three bifurcation diagrams of the pitchfork type for different fractional derivative order groups $\alpha = 2$, 1.6, and 1.2. From these results available in Figure 3.164, we determined stability branches corresponded to solution symmetries for two of these groups: $\alpha = 2$, and 1.6.

For the dataset corresponding to fractional derivative order $\alpha = 2$, we found a stable branch corresponding to asymmetric solutions, and an unstable branch corresponding to symmetric solutions for each distinct phase propagation constant μ: the findings are consistent with other research in this area where stability branches are shown to correspond to solution symmetry [20, 36].

Taking a linear approximation for each branch, we calculated a power to peak amplitude ratio to determine stability limits. When the fractional derivative order $\alpha = 2$, we have a stable branch with power to maximum amplitude ratio of approximately 3.2, and an unstable branch when the power to maximum amplitude ratio is approximately 3.8. When the fractional derivative order $\alpha = 1.6$, we have a stable branch corresponding to power to maximum amplitude ratio of approximately 2.7, and an unstable branch when the power to maximum amplitude ratio is approximately 2.9. For the fractional derivative order $\alpha = 1.2$, we have a stable branch when the power to maximum amplitude ratio is approximately 3, and an unstable branch when the power to maximum amplitude ratio is approximately 1.6.

We note when the fractional derivative order $\alpha = 2$ and 1.6, the unstable branches have a steeper linearised slope as compared to the stable branches, whereas when the fractional derivative order $\alpha = 1.2$ the stable branch has the steeper slope than the unstable branch.

4.6 Evaluation techniques

To evaluate the stability of each experiment, the MATLAB programs produced heatmaps, waterfall plots, phase portraits and direction fields based on the peak amplitude value and centre of mass evolution for each solution u_1 and u_2. Furthermore, numerical data was collected to determine dispersion to assist with stability determination. From the collected plots, phase portraits and direction fields were not required to determine stability. The heatmap, waterfall plots, peak amplitude evolution and centre of mass evolution were sufficient to determine stability.

The results of the direction fields and phase portraits resemble chaotic, oscillating, nonlinear, unstable attractors. This makes sense, since we are using the peak amplitude value of coupled, oscillating solutions to calculate the plot data. Therefore, u_1 and u_2 are shown to behave in accordance with an unstable attractor: that would be the oscillating peak amplitude value of the coupled solution in our case. Our results are superficially consistent with chaotic systems [58-60], and to a lesser extent nonlinear oscillators [61, 62]. While the plots were unnecessary to determine stability for this project, perhaps future soliton analysis could benefit from appropriate statistical analysis of nonlinear, chaotic systems with plots such as these.

CHAPTER 5 CONCLUSIONS

The aim of this research set out to explore solitary wave solutions for coupled, NLSEs with fractional space derivatives of order $\alpha \in (1, 2]$. Experiments were run by decrementing the fractional derivative order α from 2 to 1.1 by tenths. The MATLAB programs calculated and output twenty-four plots for each data pair and calculated two tables of information designed to assist in the determination of stability. From the data, we selected noteworthy dynamics for consideration in this research paper.

5.1 Primary results

Examining the bifurcation diagrams, we found stable and unstable branches corresponding to asymmetric and symmetric solutions respectively when the fractional derivative order $\alpha = 2$, and 1.6. For $\alpha = 1.2$, the stable branch corresponds to phase propagation constant values $\mu < 1.6$ and consists exclusively of symmetric solutions. The unstable branch corresponds to $\mu \geq 1.6$ and consists of symmetric and asymmetric solutions. To produce the bifurcation diagram, we calculated soliton power and created bifurcation plots corresponding to fractional derivatives of order$\alpha = 2$, 1.6, 1.2. We found for fractional derivatives of order $\alpha = 2$, and 1.6, stable branches of the bifurcation plot corresponded to asymmetric solutions, while the unstable branches corresponded to their symmetric counterpart, consistent with similar symmetry breaking bifurcation results in fractional derivative research [20, 36, 38].

There is relatively little previous data or research in soliton stability analysis as a function of fractional derivative. Part of the problem researching this area of mathematics is compounded by the fact there exist numerous computational methods to approach NLSEs, and therein lie various approaches integrating fractional derivative values into the computational methods. For example, the Reisz fractional derivative ($\frac{\partial^{\alpha} u}{\partial |x|^{\alpha}}$) by the shifted Grünwald formulae restricts the fractional derivative value to the domain $\alpha \in (1, 2]$ which has been applied in similar research areas [20, 36, 57]. Other methods explore fractional derivatives outside of this domain [27, 31, 33, 35, 37]. What each method has in common, is the way in which the fractional values are calculated: showcasing the memory properties of fractional derivatives, and the need for numerical methods to solve them. This approach naturally lends itself to discrete computational methods, as the fractional derivative is defined in discrete terms: it also provides rigorous bounds the fractional value may take.

5.2 Stability assessment

Applying the shifted Grünwald approach to soliton research, we produced and captured heatmaps, waterfall plots, peak amplitude evolution, centre of mass evolution, phase portraits and direction fields for the wave solutions and corresponding energy density. While we found the resulting phase portraits and direction fields f were not necessary to determine stability, they did, however, imply the application to potentially help define solitons in the future, thereby providing a potential quantitative method to determine the stability of solitons. The reasoning here is the link between soliton evolution phase trajectories and nonlinear, oscillating, chaotic systems: this may open the door to a statistical approach to soliton analysis or may simply move the evaluation of soliton stability from a qualitative endeavour to a more quantitative process through methods employed in statistical analysis.

5.3 Symmetry boundaries

Looking closely at peak amplitude plots and scrutinising the symmetries between various solutions led to the discovery of symmetry breaking boundaries, and possibly more importantly the discovery of symmetry making boundaries. On four occasions, asymmetric solutions matched group velocities, so the inner wave solution began oscillating symmetrically (while the surface waves remained out of phase) until numerical instability occurred (these solutions are found in sections 3.1.4 u_data_a_2p0_mu_2p0_asym, 3.9.4 u_data_a_1p2_mu_1p6_asym, 3.9.6 u_data_a_1p2_mu_2p0_asym, and 3.9.7 u_data_a_1p2_mu_2p4_asym). On one occasion (in section 3.3.1 u_data_a_1p7_mu_2p8_asym), both group and phase velocity converged. If this phenomenon is not symmetry making, and is indicative of asymmetric stability, perhaps determining the steady state solution of group velocity of solutions is one way to quantify stability. Soliton stability boundaries are an important part of numerical mathematical research as the boundaries lead to a better understanding of diffusion equations in general. In terms of real-world applications, stability boundaries often represent physical properties of a medium which may be optimised to support the existence of a more stable propagating light pulse, and error tolerant optical communication applied in systems requiring less energy to produce, or fewer repeaters to maintain soliton pulse propagation. Therefore, the implication of symmetry making conditions and their applications cannot be understated [3, 5, 6, 10, 35, 42, 43, 56, 57, 65].

We also found non-stationary solitons for sufficiently low fractional derivative values of approximately $\alpha = 1.3$, which were often preceded by symmetry breaking behaviour in previously symmetric solutions. The non-stationary solutions were highly asymmetric, and mostly propagated to the left of the solution field. Furthermore, when symmetric solutions did break symmetry, we found the value of the peak amplitude of each solution continued to converge throughout the experiment, and in two of the stationary cases, convergence resulted in dark/bright soliton pulses (found in sections 3.1.5 u_data_a_2p0_mu_2p2_sym and 3.4.3 u_data_a_1p6_mu_1p5_sym).

5.4 Future research

Considering the breadth of NLSE research, and the relatively wide range of computational methods, coupled with the lack of a strict, rigorous definition of a soliton, and by extension, guidelines for what makes a soliton stable or unstable, NLSEs represent a very large area of fruitful mathematical research, with a lot of potential for continued development [21].

To begin with, a research priority should be the formulation of a strict definition for solitons, thereby creating a framework to determine soliton stability. As the NLSE field currently stands, stability is dependent on application, type of perturbation, and what we already know of the behaviour of the system. Strict mathematical guidelines for stability are required and would immediately benefit the area. Furthermore, numerical methods require transparency, and code should be published with results as part of the peer-review and publication process. When researching this area, it is assumed adequate numerical methods are universally employed, but this is impossible to know without making this type of data transparent.

There is potential to mathematically explore why stable, symmetric solutions break symmetry and become non-stationary when approaching fractional derivative order $\alpha = 1.3$. Since some solutions become non-stationary as the fractional derivative order

α =1.5, 1.4, or α =1.2, we cannot claim for there to be a 'magic fraction' to break symmetry, but we can certainly explore this mathematically with more rigour and determine the relationship between fractional derivative orders α and non-stationary solitons.

Additionally, we could explore the relationship between chaotic attractors and soliton solutions and determine if there are any further substantial links between NLSEs and stochastic, chaotic systems. Considering this project alone generated 6GB of data, it stands to reason that statistical methods could only serve to benefit soliton analysis: studying soliton stability through a statistical lens may yield results in terms of a strict definition of soliton stability for various NLSEs.

The next immediate area of research may simply be repeating this research with finer fractional derivative values, approaching symmetry making, breaking, and non-stationary behaviour with greater precision of derivative order to observe the evolution of the results. This may be solved by developing a program to iteratively process solution pairs in a loop of increasingly smaller changes in fractional derivative values: effectively nesting the programs used in this research in a loop. This type of approach would allow for the collection of results to observe solution behaviour as the fractional derivative order α changes over time. Generally, the NLSE field area would benefit from exploring how a wide variety of solutions behave with fractional derivatives for a range of NLSEs.

This research project set out to study solitary wave solutions for fractional, coupled NLSEs and find novel stability boundaries within the fractional derivative order. We found stable and unstable solitons corresponding to symmetry when α = 2 and 1.6, interesting symmetry breaking, non-stationary dynamics, bright / dark pulses, symmetry making dynamics, and a lot of potential for future research in this area including error-tolerant optical communication and the potential for particles to demonstrate memory and self-correcting behaviour.

REFERENCES

1. Berg ER. Acoustics: Encyclopaedia Britannica; 1998 [updated 20/08/2019]. Available from: https://www.britannica.com/science/acoustics.

2. Amador G, Colon K, Luna N, Mercado G, Pereira E, Suazo E. On solutions for linear and nonlinear Schrödinger equations with variable coefficients: A computational approach. Symmetry. 2016;8(38):2-16.

3. Copie F, Randoux S, Suret P. The physics of the one-dimensional nonlinear Schrödinger equation in fiber optics: Rogue waves, modulation instability and self-focusing phenomena. Reviews in Physics. 2020;5:1-17.

4. Jaradat EK, Alomari O, Abudayah M, Al-Faqih AM. An approximate analytical solution of the nonlinear Schrödinger equation with harmonic oscillator using Homotopy Perturbation Method and Laplace-Adomian Decomposition method. Advances in Mathematical Physics. 2018;2018:1-13.

5. Karachalios NI, Sánchez-Rey B, Kevrekidis PG, Cuevas J. Breathers for the discrete nonlinear Schrödinger equation with nonlinear hopping. Journal of Nonlinear Science. 2013;23(2):205-39.

6. Lakoba TI. Instability of the finite-difference split-step method applied to the nonlinear Schrödinger equation. I. Standing soliton. Numerical Methods for Partial Differential Equations. 2016;32(3):1002-23.

7. Oliari V, Agrell E, Alvarado A. Regular perturbation on the group-velocity dispersion parameter for nonlinear fibre-optical communications. Nature Communications. 2020;11(933):1-11.

8. Zeng L, Zeng J. One-dimensional gap solitons in quintic and cubic–quintic fractional nonlinear Schrödinger equations with a periodically modulated linear potential. Nonlinear Dynamics. 2019;98(2):985-95.

9. Liu X, Simpson G, Sulem C. Stability of solitary waves for a generalized derivative nonlinear Schrödinger equation. Journal of Nonlinear Science. 2013;23(4):557-83.

10. Marzuola JL, Raynor S, Simpson G. A system of ODEs for a perturbation of a minimal mass soliton. Journal of Nonlinear Science. 2010;20(4):425-61.

11. Li H, Guo Y. Numerical solution of coupled nonlinear Schrödinger equations on unbounded domains. Applied Mathematics Letters. 2020;104.

12. Antoine X, Bao W, Besse C. Computational methods for the dynamics of the nonlinear Schrödinger/Gross–Pitaevskii equations. Computer Physics Communications. 2013;184:2621-33.

13. Holmer J, Liu C. Blow-up for the 1d nonlinear Schrödinger equation with point nonlinearity I: Basic theory. Journal of Mathematical Analysis and Applications. 2020;483(1):1-20.

14. Tsitsas NL, Porfyrakis P, Frantzeskakis DJ. Modeling of ultrashort pulse propagation in lossy nonlinear metamaterials. Mathematical Methods in the Applied Sciences. 2018;41(3):952-8.

15. Cavalcanti MM, Corrêa WJ, Özsarı T, Sepúlveda M, Véjar-Asem R. Exponential stability for the nonlinear Schrödinger equation with locally distributed damping. Communications in Partial Differential Equations. 2020;45(9):1134-67.

16. Lin Z, Wang Z, Zeng C. Stability of traveling waves of nonlinear Schrödinger equation with nonzero condition at infinity. Archive for Rational Mechanics and Analysis. 2016;222(1):143-212.

17. Scott Russell J. Report on Waves. London: British Association for the Advancement of Science; 1845. Available from: https://books.google.com.au/books?hl=en&lr&id=994EAAAAYAAJ&oi=fnd&pg=PA1&dq=report+on+waves&ots=l8kZO7TZ9f&sig=bMKSs2_bDqUjskcueYpMokRVlc8#v=onepage&q=report%20on%20waves&f=false.

18. Bender CM. PT symmetry in quantum physics: From a mathematical curiosity to optical experiments. Europhysics News. 2016;47(2):17-20.

19. Serway RA, Moses CJ, Moyer CA. Modern Physics: Cengage Learning; 2004.

20. Li P, Li R, Dai C. Existence, symmetry breaking bifurcation and stability of two-dimensional optical solitons supported by fractional diffraction. Opt Express. 2021;29(3):3193-210.

21. Tao T. Why are solitons stable? Bulletin of the American Mathematical Society. 2008;46(1).

22. Baker MJ, Sutlief SG, editors. Green's Functions in Physics Version 12003.

23. Driben R, Malomed BA. Stability of solitons in parity-time-symmetric couplers. Optics Letters. 2011;36(22):4323-5.

24. Burns D. Gravity Visualized [Video]. You Tube: apbiolghs; 2012 [Available from: https://www.youtube.com/watch?v=MTY1Kje0yLg.

25. Cham J. Top 10 physics discoveries of the last 10 years. Nature Physics. 2015;11(10):799-.

26. IFT Webinars. Carl Bender (U.Washington) Unmasking PT Symmetry [Video]. YouTube; 2020 [cited 2021 June 21]. Available from: https://www.youtube.com/watch?v=93ndqT4nkrU.

27. Ortigueira MD, Tenreiro Machado JA. What is a fractional derivative? Journal of Computational Physics. 2015;293:4-13.

28. Wang S, Lim A. Thinking towards Motion Modeling: on High-order Derivatives of Displacement. arXiv: Classical Physics. 2019.

29. Gong C, Bao W, Tang G, Jiang Y, Liu J. Computational challenge of fractional differential equations and the potential solutions: A survey. Mathematical Problems in Engineering. 2015;2015:1-13.

30. Trefethen LN. Spectral Methods in MATLAB 2000. Available from: https://epubs.siam.org/doi/10.1137/1.9780898719598.

31. Sun H, Zhang Y, Baleanu D, Chen W, Chen Y. A new collection of real world applications of fractional calculus in science and engineering. Communications in Nonlinear Science and Numerical Simulation. 2018;64:18.

32. Inc M, Yusuf A, Isa Aliyu A, Baleanu D. Soliton solutions and stability analysis for some conformable nonlinear partial differential equations in mathematical physics. Optical and Quantum Electronics. 2018;50.

33. Atman KG, Şirin H. Nonlocal Phenomena in Quantum Mechanics with Fractional Calculus. Reports on Mathematical Physics. 2020;86(2):263-70.

34. Namias V. The fractional order Fourier transform and its application to quantum mechanics. Journal of the Institute of Mathematics and its Applications. 1980;25:14.

35. Bilal M, Ren J, Younas U. Stability analysis and optical soliton solutions to the nonlinear Schrödinger model with efficient computational techniques. Optical and Quantum Electronics. 2021;53.

36. Li P, Malomed BA, Mihalache D. Symmetry breaking of spatial Kerr solitons in fractional dimension. Chaos, Solitons & Fractals. 2020;132.

37. Fujioka J, Espinosa A, Rodríguez RF. Fractional optical solitons. Physics Letters A. 2010;374(9):1126-34.

38. Malomed BA. Optical Solitons and Vortices in Fractional Media: A Mini-Review of Recent Results. Photonics. 2021;8(9).

39. Wu G-Z, Yu L-J, Wang YY. Fractional optical solitons of the space-time fractional nonlinear Schrödinger equation. Optik. 2020;207.

40. Antoine X, Lorin E, Tang Q. A friendly review of absorbing boundary conditions and perfectly matched layers for classical and relativistic quantum waves equations. Molecular Physics. 2017;115(15-16):1861-79.

41. Christian JM, McDonald GS, Chamorro-Posada P. Helmholtz bright and boundary solitons. Journal of Physics A: Mathematical and Theoretical. 2007;40(7):1545-60.

42. Hu Y, Li H, Jiang Z. Efficient semi-implicit compact finite difference scheme for nonlinear Schrödinger equations on unbounded domain. Applied Numerical Mathematics. 2020;153:319-43.

43. Kevrekidis PG, Frantzeskakis DJ. Solitons in coupled nonlinear Schrödinger models: A survey of recent developments. Reviews in Physics. 2016;1:140-53.

44. Makhankov VG. Soliton Phenomenology. 1990;33.

45. Segur H. Solitons as approximate descriptions of physical phenomena. Rocky Mountain Journal of Mathematics. 1978;8.

46. Faou E, Gauckler L, Lubich C. Plane wave stability of the split-step Fourier method for the nonlinear Schrödinger equation. Forum of Mathematics, Sigma. 2014;2(e5):1-45.

47. Tsoy EN, Suyunov LA. Solitons of the generalized nonlinear Schrödinger equation. Physica D: Nonlinear Phenomena. 2020;414.

48. Palais R. The symmetries of solitons. Bulletin of the American Mathematical Society. 1997;34:4.

49. Purcell EM, Morin DJ. Electricity and Magnetism. 3 ed. Cambridge, United Kingdom: Cambridge University Press; 2013. 839 p.

50. Abdel-Gawad HI, Biswas A, Alshomrani AS, Belic M. Optical solitons and stability analysis with coupled nonlinear Schrödinger's equations having double external potentials. Results in Physics. 2019;15.

51. Li L, Cao Y, Zhi Y, Zhang J, Zou Y, Feng X, et al. Polarimetric parity-time symmetry in a photonic system. Light Sci Appl. 2020;9:169.

52. Li X, Zhang L, Zhang T. A new numerical scheme for the nonlinear Schrödinger equation with wave operator. Journal of Applied Mathematics and Computing. 2016;54(1-2):109-25.

53. Xiang R, Ling L, Lü X. Some novel solutions for the two-coupled nonlinear Schrödinger equations. Applied Mathematics Letters. 2017;68:163-70.

54. Charalampidis EG, Dawson JF, Cooper F, Khare A, Saxena A. Stability and response of trapped solitary wave solutions of coupled nonlinear Schrödinger equations in an external, PT- and supersymmetric potential. Journal of Physics A: Mathematical and Theoretical. 2020;53(45):455702-31.

55. Cooper F, Khare A, Comech A, Mihaila B, Dawson JF, Saxena A. Stability of exact solutions of the nonlinear Schrödinger equation in an external potential having supersymmetry and parity-time symmetry. Journal of Physics A: Mathematical and Theoretical. 2016;50(1):1-13.

56. de Oliveira GI, Rizzato FB. Nonlinear spatiotemporal stability of solitons against external perturbations. Chaos, Solitons & Fractals. 2006;28(5):1347-55.

57. Yang Q, Liu F, Turner I. Numerical methods for fractional partial differential equations with Riesz space fractional derivatives. Applied Mathematical Modelling. 2010;34(1):200-18.

58. Ban C, Cai G, Wei W, Peng S. Dynamic response and chaotic behavior of a controllable flexible robot. Nonlinear Dynamics. 2022;109(2):547-62.

59. Benkouider K, Bouden T, Sambas A, Lekouaghet B, Mohamed MA, Ibrahim Mohammed S, et al. A new 10-D hyperchaotic system with coexisting attractors and high fractal dimension: Its dynamical analysis, synchronization and circuit design. PLoS One. 2022;17(4):e0266053.

60. El Arem S. Nonlinear analysis, instability and routes to chaos of a cracked rotating shaft. Nonlinear Dynamics. 2019;96(1):667-83.

61. Negri M, Miraud D, Malavasi S. An analysis method of the vortex-induced vibrations of a tethered sphere. Meccanica. 2020;55(10):1949-74.

62. Wang J, Zhang J, Bai R, Yang X, Zhao Y. Nonlinear analysis of the locomotive traction system with rub-impact and nonlinear stiffness. Advances in Mechanical Engineering. 2018;10(12).

63. Makhankov VG. Soliton Stability. Soliton Phenomenology. Dordrecht: Springer Netherlands; 1990. p. 267-87.

64. Ferreira MFS. Dissipative Optical Solitons: An Introduction. In: Ferreira MFS, editor. Dissipative Optical Solitons. Cham: Springer International Publishing; 2022. p. 1-14.

65. Gao B, Zhang R-H, Huo J-Y, Ma C-Y, Han Y, Hou Q-R, et al. Generation and categories of solitons in various mode-locked fiber lasers. Optik. 2020;220.

66. Jang JK, Erkintalo M, Luo K, Oppo G-L, Coen S, Murdoch SG. Controlled merging and annihilation of localised dissipative structures in an AC-driven damped nonlinear Schrödinger system. New Journal of Physics. 2016;18(3).

67. Laurie J, Bortolozzo U, Nazarenko S, Residori S. One-dimensional optical wave turbulence: experiment and theory. 2012.

APPENDIX A

A1 Properties of the Reisz fractional derivative

This project requires discretisation of the Reisz fractional derivative ($\frac{\partial^\alpha u}{\partial|x|^\alpha}$) by the shifted Grünwald formulae where the fractional derivative order $\alpha \in (1, 2]$.

$$\left.\frac{d^\alpha u(x_i)}{dx^\alpha}\right|_0^x = \frac{1}{h^\alpha} \sum_{j=0}^{l+1} g_j u_{l-j+1} + O(H)\,, \text{LHS of } u(x_i),$$

$$\left.\frac{d^\alpha u(x_i)}{dx^\alpha}\right|_x^L = \frac{1}{h^\alpha} \sum_{j=0}^{N-l+1} g_j u_{l+j-1} + O(H)\,, \text{RHS of } u(x_i), \qquad (A.1)$$

where the coefficients are given as

$$g_0 = 1, g_j = (-1)^j \frac{\alpha(\alpha-1)\ldots(\alpha-j+1)}{j!}, \text{for } j \in \mathbb{N}.$$

Then the Reisz fractional diffusion equation reduces to the discretised system of ODEs:

$$\frac{du_l}{dt} \cong \frac{-K_\alpha}{2\cos(\frac{\pi\alpha}{2})h^\alpha}\left[\sum_{j=0}^{l+1} g_j u_{l-j+1} + \sum_{j=0}^{N-l+1} g_j u_{l+j-1}\right], \qquad (A.2)$$

where K_α is the dispersion coefficient, h is the space step, and in the application from the Yang, Liu, Turner paper, u is solute concentration [57].

A1.1 Check the shifted Grünwald approximation reduced to discretised ODE formulae

To confirm the Grünwald approximation is indeed appropriate for our discretisation experiments in MATLAB, we check that A.2 reduces to the discretised approximation for the second derivative when the fractional derivative order $\alpha = 2$.

Taking equation (A.2), we let $K_\alpha = 1$ and $\alpha = 2$, as follows:

$$\frac{du_l}{dt} \cong \frac{-1}{2\cos(\frac{\pi 2}{2})h^2}\left[\sum_{j=0}^{l+1} g_j u_{l-j+1} + \sum_{j=0}^{N-l+1} g_j u_{l+j-1}\right]$$

Since $\cos(n\pi) = (-1)^n, n \in \mathbb{Z}$,

$$\cong \frac{1}{2h^2}\left[\sum_{j=0}^{l+1} g_j u_{l-j+1} + \sum_{j=0}^{N-l+1} g_j u_{l+j-1}\right] \qquad (A.3)$$

Since we are given $g_0 = 1, g_j = (-1)^j \frac{\alpha(\alpha-1)\ldots(\alpha-j+1)}{j!}$, for $j \in \mathbb{N}$, we observe

$g_j = (-1)^j \frac{\alpha(\alpha-1)\ldots(\alpha-j+1)}{j!} \to 0$ when $\alpha = j - 1$. So, we are restricted in our summation up to $j = 3$.

Now we determine which discretised function values correspond to the coefficients g up to $j = 2$, where $j = 1, \ldots, N$. So, we restrict our summation to $j = 1, 2$, i.e., $N = 2$. By letting l=1, our summation limits change appropriately:

$$\sum_{j=0}^{l+1} g_j u_{l-j+1} + \sum_{j=0}^{N-l+1} g_j u_{l+j-1}$$

i.e.

$$\sum_{j=0}^{1+1} g_j u_{l-j+1} \to \sum_{j=0}^{2} g_j u_{2-j}$$

$$\sum_{j=0}^{N-l+1} g_j u_{l+j-1} \to \sum_{j=0}^{2-1+1} g_j u_{l+j-1} \to \sum_{j=0}^{2} g_j u_j \qquad (A.4)$$

To compare the Grünwald approximation of the second derivative to the discrete second derivative approximation, we determine the value of the second derivative of u at the lth position:

$$\frac{du_l}{dt} \cong \frac{1}{2h^2}\left[\sum_{j=0}^{l+1} g_j u_{l-j+1} + \sum_{j=0}^{N-l+1} g_j u_{l+j-1}\right]$$

$$= \frac{1}{2h^2}[g_0 u_{l+1} + g_0 u_{l-1} + g_1 u_l + g_1 u_l + g_2 u_{l-1} + g_2 u_{l+1}]. \qquad (A.5)$$

Substituting the values of the coefficients g_j yields:

$$\frac{du_l}{dt} \cong \frac{u_{l+1} + u_{l-1} - 2u_l - 2u_l + u_{l-1} + u_{l+1}}{2h^2}$$

$$\cong \frac{2u_{l+1} - 4u_l + 2u_{l-1}}{2h^2}$$

$$\cong \frac{u_{l+1} - 2u_l + u_{l-1}}{h^2}. \qquad (A.6)$$

So, we conclude the Grünwald approximation is an appropriate method for numerical NLSE experiments since it reduces to the second order, central difference approximation.

APPENDIX B

MATLAB code used to produce data are shown below. The script was run on MATLAB R2022b and consisted of a FFT script and a plotting program.

B1 FFT script

```
% The pseudospectral method for solving NLSEs
% iu1_t+(1/2)u1_{a}+|u1|^2*u1+u2=0
% iu2_t+(1/2)u2_{a}+|u2|^2*u2+u1=0

clear
clc
global tmax tdata dt L txt txp NN Mu1 Mu2

% Enter filename here
txt = "a_1p7_mu_2p8_asym_stable_1100t";
txp = "Portion a 1p6";  % Enter name of dataset

% Derivative Order
a = 1.7;                % a = (1, 2]

% Experiment length
tmax = 1100;             % ~750 - CPU runs out of memory ~1000

% Initialise variables and equations
% Solitons
load u1_data
load u2_data
u1=u1_data';
u2=u2_data';

ubdata = [];

% Space
L  = 30;                % Size of x-axis ~80
N  = length(u1(:, 1));  % u1 = N x 1
dx = L/N;               % dx >= 0.1322 for stability
x  = [-L/2:dx:L/2-dx]';

% Power Calculations
NN = sum(u1.^2 + u2.^2).*dx;
Mu1 = max(u1);
Mu2 = max(u2);

% Time
dt   = 0.001;            % ~ 0.01
nmax = round(tmax/dt);

% Wavenumbers
k  = [0:N/2-1 -N/2:-1]' * 2*pi/L;
k2 = abs(k).^a;

% FFT Data
```

```
tdata  = 0;
u1data = u1;
u2data = u2;

% FFT Integration
for nn = 1:nmax
    du11 = 1i * ((1/2) * ifft(-k2.*fft(u1)) + u1.*u1.*conj(u1) + u2);
    v1   = u1 + 0.5*du11*dt;
    du21 = 1i * ((1/2) * ifft(-k2.*fft(u2)) + u2.*u2.*conj(u2) + u1);
    v2   = u2 + 0.5*du21*dt;
    du12 = 1i * ((1/2) * ifft(-k2.*fft(v1)) + v1.*v1.*conj(v1) + v2);
    v1   = u1 + 0.5*du12*dt;
    du22 = 1i * ((1/2) * ifft(-k2.*fft(v2)) + v2.*v2.*conj(v2) + v1);
    v2   = u2 + 0.5*du22*dt;
    du13 = 1i * ((1/2) * ifft(-k2.*fft(v1)) + v1.*v1.*conj(v1) + v2);
    v1   = u1 +    du13*dt;
    du23 = 1i * ((1/2) * ifft(-k2.*fft(v2)) + v2.*v2.*conj(v2) + v1);
    v2   = u2 +    du23*dt;

    du14=1i*((1/2)*ifft(-k2.*fft(v1))+v1.*v1.*conj(v1)+v2);
    du24=1i*((1/2)*ifft(-k2.*fft(v2))+v2.*v2.*conj(v2)+v1);

    u1 = u1 + (du11 + 2*du12 + 2*du13 + du14)*dt/6;
    u2 = u2 + (du21 + 2*du22 + 2*du23 + du24)*dt/6;

    if mod (nn, round(nmax/tmax)) == 0
        u1data = [u1data u1];
        u2data = [u2data u2];
        tdata  = [tdata nn*dt];
    end

end

u1data = abs(u1data);
u2data = abs(u2data);

udata = [u1data' u2data']';        % For Plot function

if any(isinf(udata(:))) || any(isnan(udata(:))) == 1
    [r,c] = find (isnan(udata) | isinf(udata));
    Cinf= [ ,c];
    Newt = floor(dt*(min(Cinf)-1));
    disp(['Solution blew up! Set tmax to ', num2str(Newt), ' and try
again'])
    return
else
    Evol_Plot(udata)
    beep
end

% Stability Analysis
Evol_Stab(udata)
beep

% Bifurcation Data
Evol_BiFu(udata)
beep
```

B1.1 Plotting program

```
% Heatmap, Waterfall and Animation Function

% udata      space x time

function Evol_Plot(udata)

global tmax tdata L  txt

T  = size(udata, 2);
X  = size(udata, 1);
XX = 1:0.1:X;
a  = X/2;
e  = L/2;
xx = -e:L/(a-1):e;

% Decompose cdata into u(real), v(real)
u1 = udata(1:a,   1:T)';        % u1
u2 = udata(a+1:X, 1:T)';        % u2
uc = [u1 u2];

% Axis scaling
cc = ceil(abs(max(u1, [], 'all')));
dd = ceil(abs(max(u2, [], 'all')));
c2 = cc^2;
d2 = dd^2;
ee = max(c2, d2);

% Heatmap Plots
figure(1)                % Plot coupled equations
H1 = heatmap (uc , Title = 'Time Evolution: |u1| & |u2|', XLabel = 'x',
YLabel = [{'Time ', '0 to' num2str(tmax)}], Colormap = hot,
GridVisible='off');
% Removes categories from heatmap
HA = gca;
HA.XDisplayLabels = nan(size(HA.XDisplayData));
HA.YDisplayLabels = nan(size(HA.YDisplayData));
HA.NodeChildren(3).YDir='normal';     % Flips y-axis
H1T = strcat ('H_u1u2_', txt, '.png');
exportgraphics(HA, H1T,'Resolution',600)

figure(2)           % Plot u1
H2 = heatmap (u1, Title = 'Time Evolution |u1|', XLabel = 'x', YLabel =
[{'Time ','0 to' num2str(tmax)}], Colormap = hot, GridVisible='off');
HB = gca;
HB.XDisplayLabels = nan(size(HB.XDisplayData));
HB.YDisplayLabels = nan(size(HB.YDisplayData));
HB.NodeChildren(3).YDir='normal';     % Flips y-axis
H2T = strcat ('H_u1_', txt, '.png');
exportgraphics(HB, H2T,'Resolution',600)

figure(3)          % Plot u2
H3 = heatmap (u2, Title = 'Time Evolution |u2|', XLabel = 'x', YLabel =
[{'Time ','0 to' num2str(tmax)}], Colormap = hot, GridVisible='off');
HC = gca;
HC.XDisplayLabels = nan(size(HC.XDisplayData));
HC.YDisplayLabels = nan(size(HC.YDisplayData));
HC.NodeChildren(3).YDir='normal';     % Flips y-axis
```

```
H3T = strcat ('H_u2_', txt, '.png');
exportgraphics(HC, H3T,'Resolution',600)

figure(4)          % Plot u1^2
H4 = heatmap (u1.^2, Title = 'Time Evolution |u1|{^2}', XLabel = 'x',
YLabel = [{'Time ','0 to' num2str(tmax)}], Colormap = hot,
GridVisible='off');
HD = gca;
HD.XDisplayLabels = nan(size(HD.XDisplayData));
HD.YDisplayLabels = nan(size(HD.YDisplayData));
HD.NodeChildren(3).YDir='normal';     % Flips y-axis
H4T = strcat ('H_u1^2_', txt, '.png');
exportgraphics(HD, H4T,'Resolution',600)

% Plot u2^2
figure(5)
H5 = heatmap (u2.^2, Title = 'Time Evolution |u2|{^2}', XLabel = 'x',
YLabel = [{'Time ','0 to' num2str(tmax)}], Colormap = hot,
GridVisible='off');
HE = gca;
HE.XDisplayLabels = nan(size(HE.XDisplayData));
HE.YDisplayLabels = nan(size(HE.YDisplayData));
HE.NodeChildren(3).YDir='normal';     % Flips y-axis
H5T = strcat ('H_u2^2_', txt, '.png');
exportgraphics(HE, H5T,'Resolution',600)


% Waterfall Plots
% Plots u1 and u2
figure (6)
W1 = waterfall ([xx xx], tdata, uc.^2);
colormap jet
shading interp
view (10,60)
xlabel ('x')
ylabel ('t')
zlabel ('u1{^2}  u2{^2}')
axis ([-e, e, 0, tmax, 0,  ee])
grid on
set (gca, 'xtick', [-e, -e/2, 0, e/2, e])
set (gca, 'ytick', [0, tmax/2, tmax])
set (gca, 'ztick', [0, (ee)/2, ee])
W1T = strcat ('W_u1u2_', txt, '.png');
exportgraphics(gca, W1T,'Resolution',600)

% Plot u1
figure (7)
W2 = waterfall (xx, tdata, abs(u1));
colormap jet
shading interp
view (10,60)
xlabel ('x')
ylabel ('t')
zlabel ('|u1|')
axis ([-e, e, 0, tmax, 0, cc])
grid on
set (gca, 'xtick', [-e -e/2 0 e/2 e])
set (gca, 'ytick', [0 tmax/2 tmax])
set (gca, 'ztick', [0 cc/2 cc])
```

```
W2T = strcat ('W_u1_', txt, '.png');
exportgraphics(gca, W2T,'Resolution',600)

% Plot u2
figure (8)
W3 = waterfall (xx, tdata, abs(u2));
colormap jet
shading interp
view (10,60)
xlabel ('x')
ylabel ('t')
zlabel ('|u2|')
axis ([-e, e, 0, tmax, 0, dd])
grid on
set (gca, 'xtick', [-e -e/2 0 e/2 e])
set (gca, 'ytick', [0 tmax/2 tmax])
set (gca, 'ztick', [0 dd/2 dd])
W3T = strcat ('W_u2_', txt, '.png');
exportgraphics(gca, W3T,'Resolution',600)

% Plotting |u1|^2
figure (9)
W4 = waterfall (xx, tdata, abs((u1).^2));
colormap jet
shading interp
view (10,60)
xlabel ('x')
ylabel ('t')
zlabel ('|u1|{^2}')
axis ([-e 0 tmax 0 c2])
grid on
set (gca, 'xtick', [-e, -e/2 0 e/2 e])
set (gca, 'ytick', [0 tmax/2 tmax])
set (gca, 'ztick', [0 c2/2 c2])
W4T = strcat ('W_u1^2_', txt, '.png');
exportgraphics(gca, W4T,'Resolution',600)

% Plotting |u2|^2
figure (10)
W5 = waterfall (xx, tdata, abs((u2).^2));
colormap jet
shading interp
view (10,60)
xlabel ('x')
ylabel ('t')
zlabel ('|u2|{^2}')
axis ([-L/2 L/2 0 tmax 0 d2])
grid on
set (gca, 'xtick', [-e -e/2 0 e/2 e])
set (gca, 'ytick', [0 tmax/2 tmax])
set (gca, 'ztick', [0 d2/2 d2])
W5T = strcat ('W_u2^2_', txt, '.png');
exportgraphics(gca, W5T,'Resolution',600)

%{
% Drawnow Plot
prompt = 'Run animation? Y/N? ';
pp = input(prompt, 's');
if  pp == 'y'
```

```
    for j = 1:T
        figure(7)
        plot(xx, u1(j, :), xx, u2(j, :))
        hold off; axis([-e min(udata(:)) max(udata(:))]);
        legend('|u1|', '|u2|')
        title ('|u1(z,t)|, |v2(z,t)|'); xlabel ('z');
        drawnow
    end
else
end
%}
```

B1.2 Stability analysis

```
% Plots used to determine stability

function Evol_Stab(udata)

global txt dt

T = size(udata, 2);
TT = 1:T;

X = size(udata, 1);
a = X/2;

% Decompose udata into u1, u2
u1 = udata(1:a,   1:T);        % u1
u2 = udata(a+1:X, 1:T);        % u2

% Max amplitudes
U1 = max(u1);
U2 = max(u2);
TM = max(max(U1, U2));

% Soliton centre of mass
C1 = mean(u1);
C2 = mean(u2);
C3 = gradient(C1);
C4 = gradient(C2);
MM = max(max(C1, C2));

XX = 1:0.1:length(U1);

% Interpolated gradients
P1 = interp1(U1, XX, "spline");
P2 = gradient(P1);
P3 = gradient(U1);
m1 = interp1(C1, XX, "spline");
m2 = interp1(C2, XX, "spline");
M1 = gradient(m1);
M2 = gradient(m2);

Q1 = interp1(U2, XX, 'spline');
Q2 = gradient(Q1);
```

```
Q3 = gradient(U2);

[X1 Y1] = meshgrid(U1(1:15:end), U2(1:15:end));
[X3 Y3] = meshgrid(P3(1:15:end), Q3(1:15:end));

[X2 Y2] = meshgrid(C1(1:15:end), C2(1:15:end));
[X4 Y4] = meshgrid(C3(1:15:end), C4(1:15:end));


% Peak Amplitude Evolution
figure(11)
plot(XX, P1, XX, Q1)
xlabel ('Time')
ylabel ('|u1_{max}|  |u2_{max}|')
title ('Peak Amplitude Evolution')
legend ('|u1_{max}|', '|u2_{max}|', 'location', 'best')
axis ([0, T, 0, TM])
P1T = strcat ('Amplitude_u_', txt, '.png');
exportgraphics(gca, P1T,'Resolution',600)

figure(12)
plot(XX, m1, XX, m2)
xlabel ('Time')
ylabel ('|u1_{centroid}|  |u2_{centroid}|')
title ('Centre of Mass Evolution')
legend ('|u1_{centroid}|', '|u2_{centroid}|', 'location', 'best')
axis ([0, T, 0, MM*(1.05)])
P2T = strcat ('Centroid_u_', txt, '.png');
exportgraphics(gca, P2T,'Resolution',600)

% Phase Portraits

figure(13)
plot(Q2, P2)
xlabel ('|u2_{max}|^{\prime}')
ylabel ('|u1_{max}|^{\prime}')
title ('Peak Amplitude Phase Portrait')
axis tight
P3T = strcat ('Amplitude Phase_u_', txt, '.png');
exportgraphics(gca, P3T,'Resolution',600)

figure(14)
plot(P1, P2)
xlabel ('|u1_{max}|')
ylabel ('|u1_{max}|^{\prime}')
title ('Peak Amplitude Phase Portrait')
axis tight
P3T = strcat ('Amplitude Phase_u1_', txt, '.png');
exportgraphics(gca, P3T,'Resolution',600)

figure(15)
plot(Q1, Q2)
xlabel ('|u2_{max}|')
ylabel ('|u2_{max}|^{\prime}')
title ('Peak Amplitude Phase Portrait')
axis tight
P4T = strcat ('Amplitude Phase_u2_', txt, '.png');
exportgraphics(gca, P4T,'Resolution',600)
```

```
figure(16)
plot(M2, M1)
xlabel ('|u2_{centroid}|^{\prime}')
ylabel ('|u1_{centroid}|^{\prime}')
title ('Centre of Mass Phase Portrait')
axis tight
P5T = strcat ('Centroid Phase_u_', txt, '.png');
exportgraphics(gca, P5T,'Resolution',600)

figure(17)
plot(m1, M1)
xlabel ('|u1_{centroid}|')
ylabel ('|u1_{centroid}|^{\prime}')
title ('Centre of Mass Phase Portrait')
axis tight
P5T = strcat ('Centroid Phase_u1_', txt, '.png');
exportgraphics(gca, P5T,'Resolution',600)

figure(18)
plot(m2, M2)
xlabel ('|u2_{centroid}|')
ylabel ('|u2_{centroid}|^{\prime}')
title ('Centre of Mass Phase Portrait')
axis tight
P6T = strcat ('Centroid Phase_u2_', txt, '.png');
exportgraphics(gca, P6T,'Resolution',600)

% Direction Fields
figure(19)
quiver(X1, X3)
xlabel ('|u1_{max}|')
ylabel ('|u1_{max}|^{\prime}')
title ('Peak Amplitude Direction Field')
axis tight
P7T = strcat ('u1 Amplitude Direction Field_', txt, '.png');
exportgraphics(gca, P7T,'Resolution',600)

figure(20)
quiver(X2, X4)
xlabel ('|u1_{centroid}|')
ylabel ('|u1_{centroid}|^{\prime}')
title ('Centre of Mass Direction Field')
axis tight
P8T = strcat ('u1 Centroid Direction Field_', txt, '.png');
exportgraphics(gca, P8T,'Resolution',600)

figure(21)
quiver(Y1, Y3)
xlabel ('|u2_{max}|')
ylabel ('|u2_{max}|^{\prime}')
title ('Peak Amplitude Direction Field')
axis tight
P9T = strcat ('u2 Amplitude Direction Field_', txt, '.png');
exportgraphics(gca, P9T,'Resolution',600)

figure(22)
quiver(Y2, Y4)
xlabel ('|u2_{centroid}|')
ylabel ('|u2_{centroid}|^{\prime}')
```

```
title ('Centre of Mass Direction Field')
axis tight
P10T = strcat ('u2 Centroid Direction Field_', txt, '.png');
exportgraphics(gca, P10T,'Resolution',600)

figure(23)
quiver(Q1, P1, Q2, P2)
xlabel ('|u2_{max}|')
ylabel ('|u1_{max}|')
title ('Peak Amplitude Direction Field')
axis tight
P11T = strcat ('Amplitude Direction Field_', txt, '.png');
exportgraphics(gca, P11T,'Resolution',600)

figure(24)
quiver(m2, m1, M2, M1)
xlabel ('|u2_{centroid}|')
ylabel ('|u1_{centroid}|')
title ('Centre of Mass Direction Field')
axis tight
P12T = strcat ('Centroid Direction Field_', txt, '.png');
exportgraphics(gca, P12T,'Resolution',600)
```

B1.3 Bifurcation collation

```
% Plot Bifurcation Data

function Evol_BiFu(udata)

global txp Unstable_a_ tmax L dt dx txt u1 u2 NN a Mu1 Mu2

% Create ubU for each new portion P
ubUP = [0 0];
ubSP = [0 0];

T = size(udata, 2);
X = size(udata,1);
a = X/2;
e = L/2;
xx = -e:L/(a-1):e;
tt = 0:dt:tmax;

u1 = udata(1:a,   1:T);        % u1
u2 = udata(a+1:X, 1:T);        % u2

M1 = max(u1);
M2 = max(u2);

C1 = mean(M1);
C2 = mean(M2);

RM1 = rms(M1);
RM2 = rms(M2);

disp('Calculated Dispersion is:')
```

```
Dp1 = abs(sqrt(C1^2 - RM1^2))
Dp2 = abs(sqrt(C2^2 - RM2^2))

prompt = 'Is the solution stable? Y/N? ';
pp = input(prompt, 's');

% Bifurcation Data
if  pp == 'y'
    if Mu1 > Mu2 == 1
        Mxu = Mu1;
    else
        Mxu = Mu2;
    end
    ubS =[Mxu NN];

    save Stable_a_ ubS '-append' '-ascii'
    SS = ' Stable';
else
    if Mu1 > Mu2 == 1;
        Mxu = Mu1;
    else
        Mxu = Mu2;
    end
    ubU = [Mxu NN];
    save Unstable_a_ ubU '-append' '-ascii'
    SS = ' Unstable';
end


% Experiment Data Collection

nms = {'Data Pair' 'u1 Max. Amp.' 'u2 Max. Amp.' 'u1 RMS', 'u2 RMS', 'u1
Ar. Mean', 'u2 Ar. Mean', 'u1 Dispersion', 'u2 Dispersion'};
DT = [txt Mu1 Mu2 RM1 RM2 C1 C2 Dp1 Dp2];
S1T = strcat (txp, ' Stability Data.xls');
writecell(nms, S1T)
writematrix(DT, S1T, 'WriteMode', 'append')

Nms = {'Data Pair' 'Stability' 'Abs. Max. Amp.' 'Power' 'u1 Ar. Mean', 'u2
Ar. Mean', 'u1 RMS', 'u2 RMS', 'u1 Dispersion', 'u2 Dispersion'};
Stb = {txt SS Mxu NN C1 C2 RM1 RM2 Dp1 Dp2};
S2T = strcat (txp, ' All Data.xls');
writecell(Nms, S2T)
writecell(Stb, S2T, 'WriteMode', 'append')

beep
prompt = 'Is this the end of dataset? Y/N? ';
pp = input(prompt, 's');

% Bifurcation Plot
if  pp == 'y'
    load Stable_a_;
    load Unstable_a_;
    ubUP = Unstable_a_;
    ubU = sort(Unstable_a_);
    ubS = sort(Stable_a_);

    HUP = ubU(:, 1)';
    NUP = ubU(:, 2)';
```

```
    HSP = ubS(:, 1)';
    NSP = ubS(:, 2)';

    figure (25)
    plot(HSP, NSP, 'ko-', HUP, NUP, 'r*--');
    xlabel 'Bifurcation Parameter {\mu}';
    ylabel 'Power of Soliton Pair';
    title (txp, ' Bifurcation Diagram');
    legend ('Stable', 'Unstable', 'Location', 'best');
    B1T = strcat ('Bifurcation Diagram_', txp, '.png');
    exportgraphics(gcf,B1T,'Resolution',600)
    disp ('All Done! Prepare Stable and Unstable data for Evol_Merge')
else
    beep
    disp ('All Done, load new u1_data, u2_data, and change filename')
end
```

B2 Merged bifurcation plot

```
% Merge and Plot Fractional Data
clear
clc

load Stable_a_2p0;
load Unstable_a_2p0;

load Stable_a_1p6
load Unstable_a_1p6

load Stable_a_1p2
load Unstable_a_1p2

A2p0S = sort([Stable_a_2p0], 2);
A2p0S1 = A2p0S(:, 1);
A2p0S2 = A2p0S(:, 2);

A1p6S = [Stable_a_1p6];
A1p6S1 = A1p6S(:, 1);
A1p6S2 = A1p6S(:, 2);

A1p2S = [Stable_a_1p2];
A1p2S1 = A1p2S(:, 1);
A1p2S2 = A1p2S(:, 2);

A2p0U = [Unstable_a_2p0];
A2p0U1 = A2p0U(:, 1);
A2p0U2 = A2p0U(:, 2);

A1p6U = [Unstable_a_1p6];
A1p6U1 = A1p6U(:, 1);
A1p6U2 = A1p6U(:, 2);

A1p2U = [Unstable_a_1p2];
A1p2U1 = A1p2U(:, 1);
```

```
A1p2U2 = A1p2U(:, 2);

HA2p0U = interp1(A2p0U(:, 1), 1:0.001:length(A2p0U(:, 1)), 'pchip')';
NA2p0U = interp1(A2p0U(:, 2), 1:0.001:length(A2p0U(:, 2)), 'pchip')';

HA2p0S = interp1(A2p0S(:, 1), 1:0.001:length(A2p0S(:, 1)), 'pchip')';
NA2p0S = interp1(A2p0S(:, 2), 1:0.001:length(A2p0S(:, 2)), 'pchip')';

HA1p6U = interp1(A1p6U(:, 1), 1:0.001:length(A1p6U(:, 1)), 'pchip')';
NA1p6U = interp1(A1p6U(:, 2), 1:0.001:length(A1p6U(:, 2)), 'pchip')';

HA1p6S = interp1(A1p6S(:, 1), 1:0.001:length(A1p6S(:, 1)), 'pchip')';
NA1p6S = interp1(A1p6S(:, 2), 1:0.001:length(A1p6S(:, 2)), 'pchip')';

HA1p2U = interp1(A1p2U(:, 1), 1:0.001:length(A1p2U(:, 1)), 'pchip')';
NA1p2U = interp1(A1p2U(:, 2), 1:0.001:length(A1p2U(:, 2)), 'pchip')';

HA1p2S = interp1(A1p2S(:, 1), 1:0.001:length(A1p2S(:, 1)), 'pchip')';
NA1p2S = interp1(A1p2S(:, 2), 1:0.001:length(A1p2S(:, 2)), 'pchip')';

figure (26)
hold on
plot(HA2p0S, NA2p0S, '-', HA2p0U, NA2p0U, '--', 'color', [0.7 0 0],
'LineWidth',1);
plot(HA1p6S, NA1p6S, '-', HA1p6U, NA1p6U, '--', 'color', [0 0.6 0],
'LineWidth',1);
plot(HA1p2S, NA1p2S, '-', HA1p2U, NA1p2U, '--', 'color', [0 0 0.7],
'LineWidth',1);
xlabel 'Bifurcation Parameter {\mu}';
ylabel 'Power of Soliton Pair';
title ('Combined Bifurcation Diagram');
qw{1} = plot(nan, 'color', [0.7 0 0], 'LineWidth',1);
qw{2} = plot(nan, 'color', [0 0.6 0], 'LineWidth',1);
qw{3} = plot(nan, 'color', [0 0 0.7], 'LineWidth',1);
qw{4} = plot(nan, 'k-', 'LineWidth',1);
qw{5} = plot(nan, 'k--', 'LineWidth',1);
legend([qw{:}], {'a 2p0','a 1p6','a 1p2', 'Stable', 'Unstable'},
'location', 'best')
hold off
B1T = strcat ('Combined Bifurcation Diagram.png');
exportgraphics(gcf,B1T,'Resolution',600)

figure (27)
hold on
plot(HA2p0S, NA2p0S, 'k-', HA2p0U, NA2p0U, 'r--');
plot(A2p0S1, A2p0S2,'ko', A2p0U1, A2p0U2, 'r*');
xlabel 'Bifurcation Parameter {\mu}';
ylabel 'Power of Soliton Pair';
title ('a2p0 Bifurcation Diagram');
legend ('Stable', 'Unstable', 'Location', 'best');
hold off
B1T = strcat ('a2p0 Bifurcation Diagram','.png');
exportgraphics(gcf,B1T,'Resolution',600)

figure (28)
hold on
plot(HA1p6S, NA1p6S, 'k-', HA1p6U, NA1p6U, 'r--');
plot(A1p6S1, A1p6S2,'ko', A1p6U1, A1p6U2, 'r*')
xlabel 'Bifurcation Parameter {\mu}';
```

```
ylabel 'Power of Soliton Pair';
title ('a1p6 Bifurcation Diagram');
legend ('Stable', 'Unstable', 'Location', 'best');
hold off
B1T = strcat ('a1p6 Bifurcation Diagram', '.png');
exportgraphics(gcf,B1T,'Resolution',600)

figure (29)
hold on
plot(HA1p2S, NA1p2S, 'k-', HA1p2U, NA1p2U, 'r--');
plot(A1p2S1, A1p2S2,'ko', A1p2U1, A1p2U2, 'r*')
xlabel 'Bifurcation Parameter {\mu}';
ylabel 'Power of Soliton Pair';
title ('a1p2 Bifurcation Diagram');
legend ('Stable', 'Unstable', 'Location', 'best');
hold off
B1T = strcat ('a1p2 Bifurcation Diagram', '.png');
exportgraphics(gcf,B1T,'Resolution',600)
```